Battery Performance Characterisation for Stand-Alone Photovoltaic Systems

C J de V PURCELL, BSc (Chem), UCT

Energy for Development Research Centre
Energy Research Institute, University of Cape Town

September 1991

DECLARATION

I declare that this dissertation is my own original work. It is being submitted in partial fulfilment for the degree of Master of Science in Applied Science at the University of Cape Town. It has not been submitted before for any degree or examination at any university.

Signed by candidate

Signature Removed

....

C J de V PURCELL

16 September 1991

ABSTRACT

One of the main factors limiting optimisation of PV system designs over the life of the system has been the lack of battery test data appropriate to PV applications. The main objective of this study was to determine accurate empirical data for locally available lead-acid batteries which could be used in photovoltaic systems and to present this data in a format directly applicable to PV system designers.

The study included (i) a review of battery performance regimes typical of PV systems; (ii) a literature review of lead-acid battery performance and reactions important to PV applications, battery electrical models, battery life models, a review of specialist PV battery designs and the interaction of battery and voltage regulator in PV systems; (iii) a review of testing and research literature, and the design of a suite of experimental procedures suitable for characterising batteries under PV operating regimes; (iv) the design and construction of a specialised battery test-unit to automatically perform tests and capture data; (v) selection, testing and characterisation of five generic types of batteries which could be used in local PV applications.

The five types of lead-acid battery were:

1) conventional calcium alloy positive and negative grids, flat plate, flooded electrolyte, vented casing;
2) low antimony alloy positive grid, conventional calcium negative grid, flat plate, flooded electrolyte, vented casing;
3) low antimony alloy positive grid, heat treated calcium negative grid, flat plate, immobilised absorbed electrolyte, sealed casing with O_2 cycle gas recombination;
4) antimony alloy positive and negative grids, flat plate, flooded electrolyte, vented casing;
5) antimony alloy positive and negative grids, tubular plate, flooded electrolyte, vented casing.

Selenium grid alloy cells and gelled electrolyte batteries were not represented amongst the batteries tested, owing to problems of availability or cost.

Performance data presented at the temperatures and low currents typical of PV applications include discharge and capacity curves, charge curves and charge efficiency curves. Performance under PV cycling regimes is analysed. Life cycle estimates and associated battery life cycle costs are tabulated, with discussion of special considerations when selecting these batteries for a PV application. The battery data generated has also been incorporated in a database battery model in a PV system simulation package, PVPRO, for improved battery performance modelling.

ACKNOWLEDGEMENTS

I would like to thank the following people and organisations for their contributions to this research project:

- Dr Anton Eberhard and Bill Cowan for their guidance and supervision at various stages of this dissertation,

- the organisations in the battery and photovoltaic industries that so readily made their equipment available for testing,

- colleagues at the Energy for Development Research Centre for their persistent encouragement and interest,

- Susan, especially, for her patience and understanding during this time.

TABLE OF CONTENTS

LIST OF FIGURES

LIST OF TABLES

CHAPTER 1

INTRODUCTION

1.1 RATIONALE

Most stand-alone photovoltaic (PV) systems incorporate a form of energy storage, since many applications require power when sufficient solar energy is not immediately available. Energy storage increases power availability. In photovoltaic systems, energy storage is most commonly provided by electrochemical batteries. In certain applications the collected energy may be stored in other forms (for example, pumped water may be stored in a reservoir); or storage may be avoided altogether, as in the case of grid-connected PV systems; but in the majority of installations the electrochemical battery is an integral component of stand-alone PV systems.

Photovoltaic technology is inherently reliable, but battery storage is subject to many factors which can adversely affect battery lifetime and hence reduce the reliability and increase the costs of energy available from a photovoltaic system with battery storage.

When photovoltaic systems are used to power critical loads in remote locations (such as telecommunications repeater stations) it is usual practice to oversize the PV array and the battery capacity in relation to the load, in order to assure high availability and reliability. Such oversizing reduces the cycling demands placed upon the battery, and reliable battery performance can be expected.

Increasingly, however, small photovoltaic systems are used in underdeveloped areas, remote from the grid, to supply electrical power for a variety of purposes including domestic lighting, television and other appliances, vaccine refrigeration and water pumping. In some of these applications the load is critical (such as vaccine refrigeration); but in many cases it is desirable to economise as far as possible on system costs while still providing for an acceptable level of power availability. This leads to the design of minimally sized systems which are intended to provide adequate power availability with mimimum surplus

generating capacity. The aim is to reduce energy costs and to make PV power as affordable as possible.

Research at the EDRC has shown that there is considerable scope for making photovoltaic power more affordable through accurate design techniques, new sizing methods, improved treatment of solar radiation data and reliable system component characterisation data. At this stage, one of the main factors inhibiting the optimisation of PV system design has been the lack of battery performance data appropriate to PV applications.

Battery performance is particularly significant in the design of minimally sized PV systems, in which cycling demands on the battery may be greater, and in which there is less latitude for maintaining a suitable battery environment through a range of operating conditions. There can be strong (and unanticipated) effects on energy supply costs if batteries fail before they are expected to do so, especially in cost-cutting system configurations. The people bearing these unforeseen costs are frequently those least able to afford the consequences of design mistakes.

It is reported internationally that batteries stand out as a weak link in the reliability of stand-alone PV systems, especially in developing country applications. Many of the problems are attributable to unsuitable selection of batteries, unsuitable regulation of battery cycling or to inadequate adaptation of operating parameters to local environmental conditions. Battery regulators are reported as a further weak link. Faulty or unsuitable regulation contributes to premature battery failure.

Lead-acid batteries, which are nearly always the choice in PV systems, are a well established technology. However lead-acid battery behaviour is extremely complex and varies in significant ways according to battery design, battery history and operating conditions. Consultation with local producers and suppliers of batteries has shown there is a serious lack of available information about battery performance characteristics relevant to PV system applications, while local PV system designers and suppliers experience uncertainties in making decisions about what batteries to select, how they should be regulated and how long they can be expected to last. International research in batteries for PV applications has been sproradic and does not yet provide the required information, although useful methods are being developed. These factors led to the present project, which

aimed to develop test equipment, test methods and obtain empirical battery performance data relevant to battery operation in photovoltaic systems.

1.2 OBJECTIVES

The main objective of this study was to determine accurate empirical data for locally available batteries which could be used in photovoltaic systems, and to present this data in a format directly applicable to PV system designers.

Secondly, the experimental battery data and gains made in understanding battery performance were intended to contribute to the accuracy of PV system simulation methods being developed at EDRC. PV system simulation tools provide an effective way of evaluating and optimising system design options. Modelling battery behaviour is a vital but presently problematic component in simulating PV systems with battery storage.

These aims entailed the design, development and construction of specialised test equipment to collect empirical battery data relevant to photovoltaic applications. A microcomputer-controlled battery test-rig was developed which is capable of variable charge and load cycling, automated data capture and PV emulation.

The unit consists of a 3kW (50A, 60V) programmable power supply and a 1.8kW (30A, 60V) programmable electronic load, both constructed in house. The power electronics is controlled through analog-digital converters by customised software on the microcomputer. The software monitors the battery voltage, current, temperature, ampere-hours and watt-hours removed and returned. The computer switches the battery from charge to discharge at the appropriate times. The computer also monitors the battery for out-of-limit alarm conditions and automatically terminates the test if these conditions are exceeded. The parameters are measured once a minute, and the accumulated data are stored on disk at user-specified time intervals. The software allows tabular or graphical display of any of the accumulated battery parameters.

The test software supports conventional battery testing as well as PV system emulation. Solar irradiation data, characteristic PV curves and load data are input,

and the software-controlled power supply is able to emulate the PV array to determine and display the battery and array operating points.

A temperature-controlled water bath enables battery temperature to be controlled.

Design of this equipment and development of appropriate testing procedures were major interim objectives of this project.

Battery theory and research literature has been extensively reviewed from the viewpoint of understanding battery behaviour in PV systems. Theory and existing research are presented to provide background for the concerns and test methods used in the present study. Existing models of battery performance are discussed.

Batteries in stand-alone PV systems are generally subject to particular operating conditions such as low charging currents and variable depths of discharge. In the light of such requirements and theories of battery performance, innovative designs for specialist PV-compatible batteries are described. Methods of battery charge regulation, which should be adapted to battery performance characteristics and operating conditions, are assessed.

The review of battery theory is selective, and is described mainly at the phenomenological level. This review is essential for understanding major mechanisms which determine battery behaviour.

Prior to data collection, the literature on testing methods was extensively searched to establish suitable experimental techniques for particular batteries.

A short and elegant method of determining charge curves was developed. This method entails periodically and incrementally varying the battery charging current over a suitable range, and maintaining the incremented current till the battery charge voltage stabilises. The stabilised voltage is taken as one point on the charge curve and points of constant current can be combined to form the charging curve.

Instantaneous charging efficiencies were determined by monitoring gassing rates, and quasi-constant current charging curves were generated by correcting the

experimental charging curves for the charging inefficiencies indicated by the gassing curves.

Good agreement with conventional constant current charging curves has been obtained. The innovative method permitted the collection of battery charging data in a range of low charging currents applicable to PV operating conditions. Such data are rarely available from battery manufacturers and would take an impractically long time to collect by conventional constant current charging methods.

Other experiments conducted on the selected batteries included discharge tests and capacity determination at various temperatures. Cycling tests developed by Sandia National Laboratories were used to charge/discharge the batteries in typical PV system state-of-charge regimes and these tests provided comparative information on charge acceptance rates and overcharge requirements. Temporary and reversible capacity losses caused by stratification, and permanent capacity losses leading to battery failure, were also monitored. Energy efficiencies in the cycling regime were measured.

1.3 CONSTRAINTS

The aims of the study required entering an area where there is little accumulated local knowledge. The empirical aims required the design and construction of suitable test equipment. Distinct phases of the research were: (i) searching for relevant literature on battery theory, modelling and test methods, (ii) selecting appropriate theory and methods, (iii) designing and constructing suitable test equipment, (iv) conducting selected tests on a variety of batteries and (v) analysing and interpreting the results and indications of the tests. Parallel activities included feeding provisional findings to co-workers developing PV system simulation and sizing models, and comparing test data with simulation results.

Because each of the major phases was time consuming, an overall constraint on the scope of the project was set by time limitations.

In particular, time constraints limited the battery tests to short-term characterisation tests (at various battery temperatures). Short duration cycling tests were conducted to assess electrical, chemical and physical equilibrium stabilities under defined cycle conditions, but long duration life cycle tests were not practicable. Budget constraints necessitated in-house design and construction of a single test rig. This took time and the single rig restricted testing to one battery at a time. Since relevant battery tests can take several days per test, it was necessary to select a limited number of batteries for testing, representing major types of battery available locally, and it was not possible to repeat tests on several batteries of the same type to establish statistical variations in tested characteristics. Tests were only repeated where ambiguous or unexpected results were observed. These constraints limited the scope and statistical representativeness of the empirical data obtained.

Although the batteries tested and the scope of the tests have been limited by time, it has been valuable to obtain empirical data for key types of batteries which has not previously been available and which will assist PV designers. Combining the empirical findings with an attempt to understand observed behaviour in the light of battery theory has contributed to a greater degree of understanding of parameters which affect battery choice and cycle regulation in PV systems.

1.4 REPORT OUTLINE

The outline of the report is as follows:

CHAPTER 2: An introduction to the components of stand-alone photovoltaic systems with battery storage; a technical and economic comparison of two typical system sizing approaches; the determination of typical battery charge operating regimes based on the two system sizing approaches presented.

CHAPTER 3: A literature review of theory and research of lead-acid batteries; a review of lead-acid battery models suitable for PV systems; a review of design trends for specialist PV batteries; a review of voltage regulator operating modes and charge and load shed regulator requirements.

CHAPTER 4: A literature review of PV battery testing; a review of battery data widely available and data quality; test equipment requirements and equipment sizing.

CHAPTER 5: Experimental equipment design; electronic design of programmable load and power supply; computer interface to power electronics; software design and description; battery temperature control and measurement.

CHAPTER 6: Description of batteries selected for testing; detailed description of the test procedures followed; explanation of the format in which test results are presented.

CHAPTER 7: Test results of the five batteries selected; comparative discussion of the results.

CHAPTER 8: Conclusions.

CHAPTER 2

PHOTOVOLTAIC SYSTEMS WITH BATTERY STORAGE

2.1 COMPONENTS OF A STAND-ALONE PV SYSTEM

A typical stand-alone photovoltaic system (SAPV) consists of photovoltaic (PV) panels for conversion of solar radiation to DC electricity, batteries for DC energy storage, battery regulation equipment, and high efficiency DC loads. An inverter converts direct current power to alternating current if AC appliances are used.

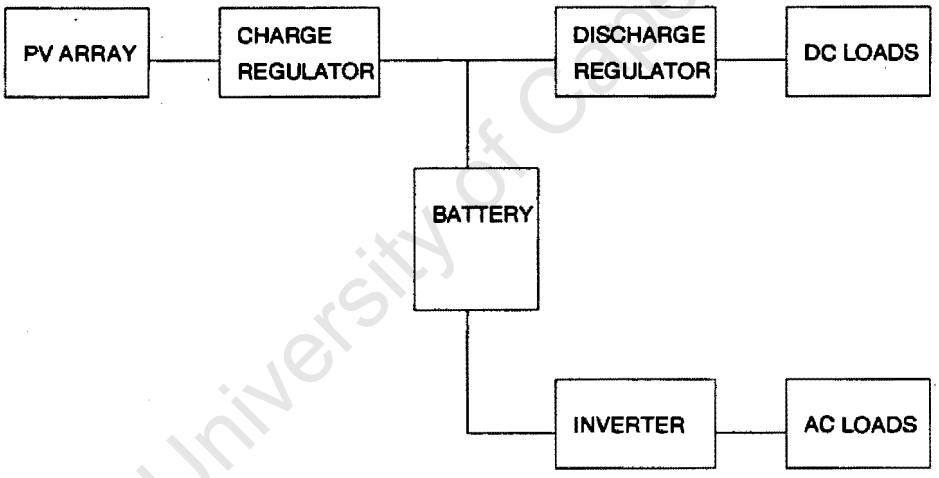

Figure 2.1 Components of a stand-alone PV system with battery storage: PV array, charge regulator, battery, discharge regulator, DC load, optional inverter and AC load.

The main components are examined individually to facilitate more detailed discussion in later chapters.

2.1.1 Photovoltaic Panel Output

The PV cell is the basic building block of the PV panel. The PV cell is a semi-conductor device which converts solar energy directly into electrical energy by the photovoltaic effect[1]. PV cells are connected in series and in parallel arrangements to form integrated modules or panels which provide the desired electrical output characteristics. Panels can be combined in series and parallel to form PV arrays, which provide higher electrical power than the same single panels. For the PV system designer, the PV panel is the basic building block of the PV array. Panels come in a range of sizes, and the output of the panel is affected by solar irradiance and the temperature of the cells. Figure 2.2 shows the output characteristics of a small panel at various irradiance intensities and a cell junction temperature of 25°C.

The power delivered by the panel is the product of the current and voltage on the I-V curve. At open circuit voltage, V_{oc}, the panel power falls to zero as no current flows, and at short circuit the panel voltage falls to zero, but the current reaches a maximum, I_{sc}. Somewhere between these point the output power is maximised at P_{max}, where the voltage and current are given by V_{mp} and I_{mp}.

The effect of cell temperature on output is shown in Figure 2.3. It is common for increased temperatures to produce lower efficiencies in semiconductor devices. In the case of crystalline PV modules, the primary effect of increasing cell temperature is to depress output voltages. The relationship is nearly linear for the operating temperature range of non-concentrating modules.

The power rating of a panel is specified for a defined cell junction temperature and irradiance, usually 1000Wm^{-2} and 25°C. The rated power is the maximum power, P_{max}, in the defined state, expressed in peak watts, W_p.

[1] There is abundant literature describing the photovoltaic effect, and how PV cells operate (for example SERI,1984). The discussion here is limited to PV output characteristics.

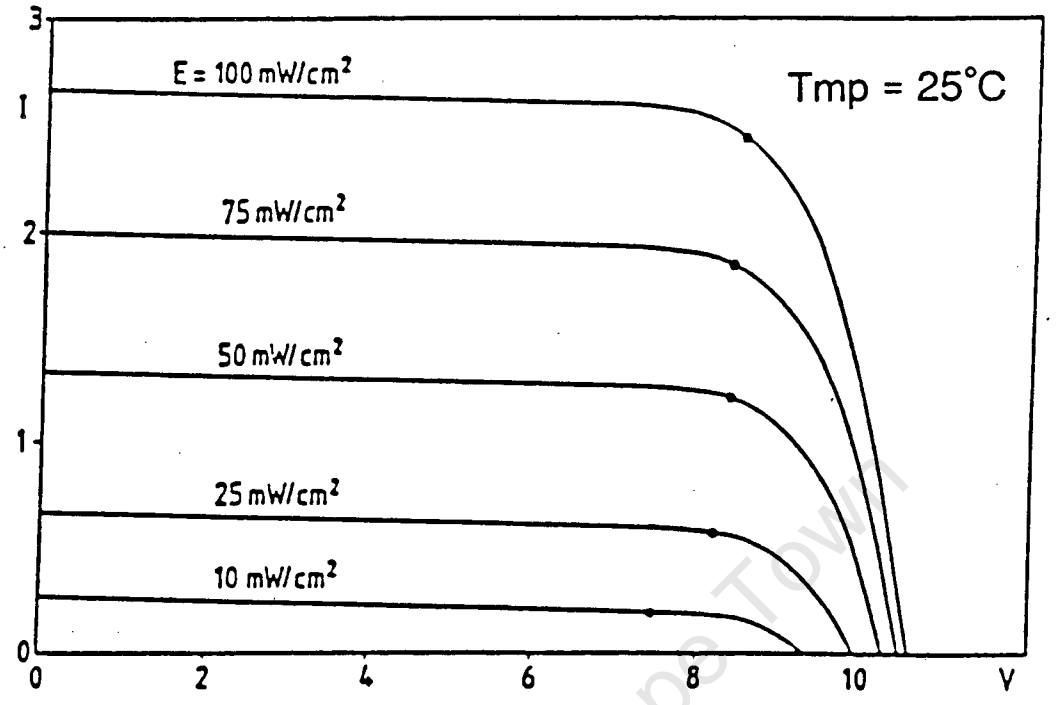

Figure 2.2 I-V characteristics of a crystalline silicon PV module as a function of irradiance; cell temperature 25°C.

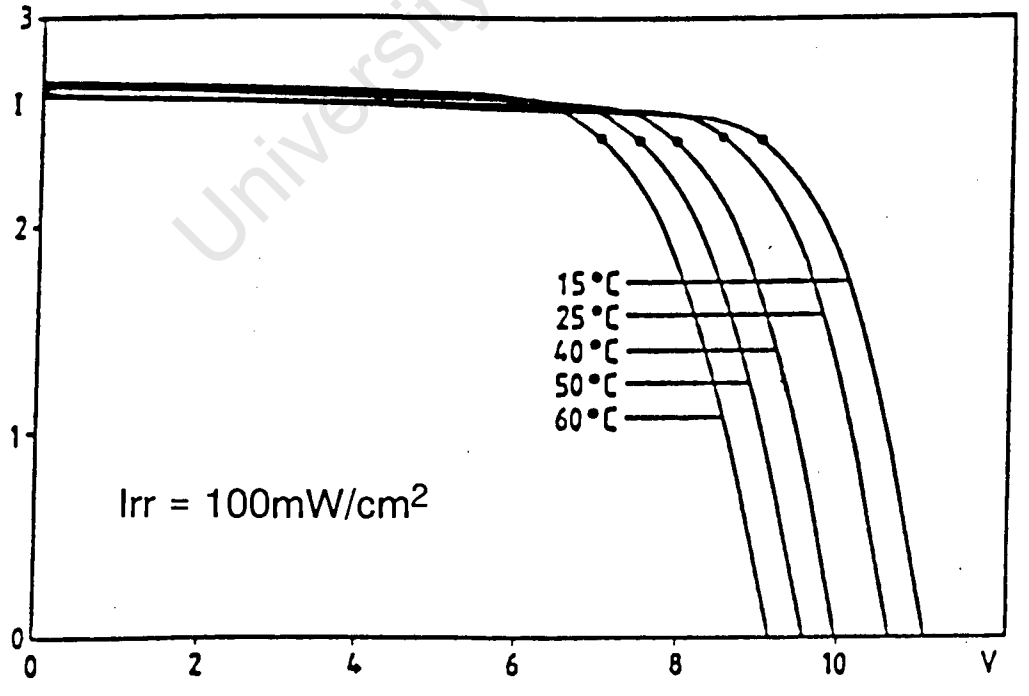

Figure 2.3 Effect of temperature on I-V curve at 1000Wm^{-2}.

2.1.2 Battery

Batteries are used to store the PV energy for times when energy is not directly available from the panels. Energy can be stored during the day for night use, during sunny days to provide reserve for cloudy days, during peak solar seasons for poorer seasons, or even during the day for more intense use later that day. The result of battery storage is that system sizes can be optimised since the PV panel no longer needs to provide the peak energy demand. However, together with the gains come losses. Battery energy storage necessitates some efficiency losses, and only 75%-85% of energy stored is retrieved (for lead-acid batteries).

The size of the battery is described by the amount of electrical energy , in ampere-hours (Ah) or watt-hours (Wh), that can be delivered in a specified time. The most commonly used basis is Ah at the 10 hour rate for automotive and electric vehicle batteries. A battery rated as 90 Ah capacity at the 10 hour rate (C_{10}) will be able to deliver approximately 9A of current for 10 hours. At higher discharge rates the battery will provide less than 90Ah, while at lower discharge rates than 9A the battery will deliver more than 90Ah. The state-of-charge (SOC) of a battery is a percentage indicating the fullness of the battery. SOC is often referenced to the C_{10} capacity. (Capacity, SOC, efficiency and other characteristics are discussed in detail in following chapters.)

Most batteries used in PV systems are the lead-acid variety. There are several other candidates, namely Nickel-Cadmium (Ni-Cd), Nickel-Iron (Ni-Fe), Iron-Air (Fe-O_2), and Sodium-Sulphur (Na-S). Most of these batteries are simply too expensive as the batteries are still in the development stage, or are not sufficiently broadly used to bring elasticity to the prices. Some are plagued by low efficiencies, requirements for complex thermal control or difficult manufacturing processes (Rand,1984:721). The lead acid battery, although complex, is well understood, and although toxic can be recycled. The battery is relatively cheap, and depending on the battery design and operating conditions can last from two to fifteen years in typical PV installations. (Battery designs are discussed in detail in Section 3.5). So far the projected cost reductions of alternatives have not been realised.

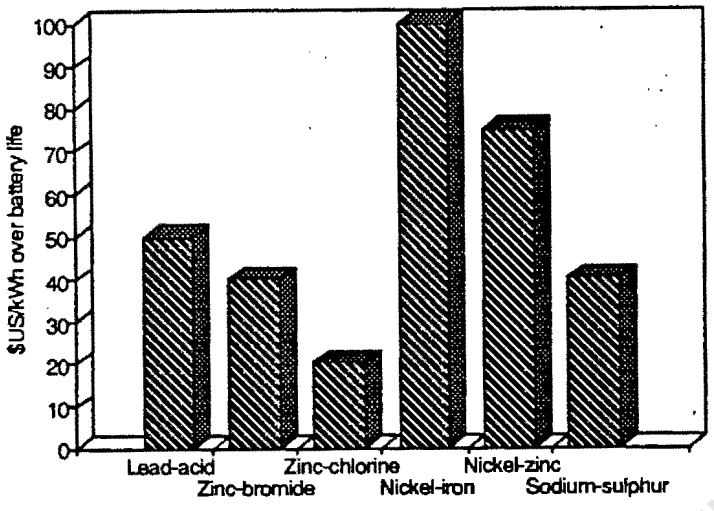

Figure 2.4 Projected energy cost for various batteries in USA. (Source: Rand,1984).

The principal limitation of the lead-acid battery is the strict operating regime required for long life, which gives rise to the need for battery regulation equipment in the PV system. Lead-acid batteries may be damaged if they are overcharged, if they are fully-discharged, or if they remain in a discharged state for long periods. (Failure modes and other aspects of lead-acid batteries are discussed in Section 3.11.)

2.1.3 Regulator

The two main regulator functions are prevention of battery overcharge and prevention of over-discharge.

Overcharge protection, or charge regulation, is accomplished by controlling or limiting the current flowing into the battery.

Over-discharge protection requires disconnection of the load before the battery becomes discharged. The disconnection is called load-shedding, and is easily accomplished when the load appliances are not connected directly to the battery, but rather via the regulator.

The merits of various charge/discharge regulation methods, load-shedding detection and other issues are discussed in detail in Section 3.14.

2.1.4 Inverters

Inverters are used only in PV systems that require AC loads. If efficient DC loads are available it is usually better to use them, as the efficiency losses associated with inverters can be considerable if they are not operated at nearly full capacity. The capacity of an inverter is measured in Volt-amperes (VA).

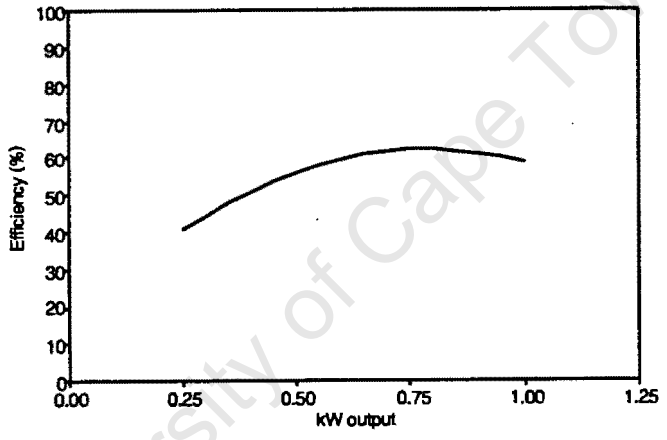

Figure 2.5 Efficiency vs power output for a 1kVA non-sinusoidal inverter with resistive loads. (Source: Bower,1988).

From the point of view of battery operation, typical inverter characteristics as a load are high currents, direct connection to the battery and pulsing of the battery.

For example, a 500VA inverter producing 350W output at 60% efficiency will draw 48A from a 12V battery. Many inverters have their own independent load-shed detectors, and are not wired through the regulator. If DC and AC loads are used together, they will not load-shed simultaneously. There may be some unpredictable interaction between the two load-shed devices. Additionally, some inverters "pulse" the battery during operation; they alternately charge and discharge current into the battery at twice the AC frequency (Williams,1989). This could affect battery performance (Cataldo,1978).

2.2 BATTERY OPERATING REGIMES IN PV SYSTEMS

It is useful at this stage to describe the range of operating conditions that batteries experience in typical PV systems. These are illustrated by example, using two systems that describe battery characteristics typical of PV installations.

1. A typical small system as would be supplied by a major panel manufacturer. The system sizing has been obtained using the manufacturer's design software. Such systems are usually sized for a specific site by considering site-specific weather data and patterns.

2. A low cost modular system for household lighting. Such systems are often sold in standard sizes and are not optimised for any particular location. They are available off-the-shelf, for use in any South African site.

For the purposes of comparison, the systems are scaled to provide the same design load, taken as 200Wh/day DC nighttime load in Nelspruit, Eastern Transvaal, South Africa.

2.2.1 System Sizing

System 1 was sized using the ARCO Solar (1982) programme, "SASY-B". The load was set at 1kWh/day, with the system required to provide power for up to five consecutive sunless days (5 days of autonomy). The system sizing results in a requirement for a 325W_p array and 540Ah deep cycle batteries at a nominal system voltage of 12V. The sizing programme intimates that the batteries will be fully charged at the end of each month. Scaling the system for a 200Wh/day load yields a panel power of 65W_p and battery capacity 108Ah at 12V.

System 2, as a commercial package, is of a set size. The standard package that is purchased comes complete with one 20W_p panel, and two 15W high efficiency DC lights. No charge regulator is provided, but protection against over-discharging the battery is included. Daily load consumption is possibly 100Wh/day (determined by the time the lights are used, say 3 and a bit hours a day, times 30W). No battery is supplied or specified. Most users purchase the cheapest

battery available, say a 100Ah "car battery"[2]. The system is relatively low cost, in terms of capital outlay. Notionally scaling the system for a 200Wh/day load would result in a $40W_p$ panel and 200Ah "car" battery.

2.2.2 System Simulation

The dynamic system parameters relevant to battery performance are shown for both systems. These have been generated using PV simulation software developed by Geerdts (1990). For the purposes of the present illustrations, generic PV and battery models incorporated in this programme have been used. (The role of this project in providing data for improved battery models is discussed in Chapter 8). In simulating a typical years performance for each system, weather data for Nelspruit was employed, with the PV array in each case tilted at an angle of 25 degrees.

System 1

Figure 2.6 shows how the battery state-of charge (SOC) cycles between 98% and 85% throughout the year. The impact on cycle depth of seasonal variation in the weather patterns is negligible. The daily overcharge (net current into the battery that does not increase the state-of-charge) is however very seasonal, with the regulator set at 14.2V. The maximum daily charging current into the battery is not strongly affected by the seasons. It is interesting that the maximum current is 4A/100Ah of installed battery capacity. The maximum array output is 4.3A/100Ah at the maximum power point under standard conditions. The charging current into the battery is low; nearly 99% of the time that the battery is charging the current is lower than 3A/100Ah, or 3% of C_{10} capacity. (In non-PV applications, typical starting charging rates for deep-cycle batteries vary from 15% of C_{10} to 7% of C_{10}, depending on the initial SOC, and finish at 3% of C_{10} when the battery is fully charged (Vinal,1955:264).

[2] A common choice in these circumstances is the Willard 774 "Leisure Pack", readily identified by its handles. Alternatively any battery to hand may be used, typically a car battery.

System 2

By comparison, Figure 2.7 shows that System 2 would have a maximum array output of only 1.25A/100Ah or 1.25% of C_{10}. The charging current is less than .7% of C_{10} for 98% of the time that the battery is charging, which is extremely low. The battery cycles through about 5% of C_{10} capacity on a daily basis. Superimposed on this is an SOC variation throughout the year that is strongly affected by seasonal weather patterns, ranging between 100% SOC (summer) to 80% (winter). For one third of the year the simulation indicates that the battery would never be fully charged, and would cycle in a partial state-of-charge. The daily overcharge is similarly affected by seasonal variation.

2.2.3 Costing

Renewable energy systems are usually costed over twenty years, the projected useful life. For PV systems there are two major cost components, the initial capital expenditure for the array, regulator, battery and perhaps some appliances; and the operating costs for battery maintenance, and battery and regulator replacement. Money to be spent in the future is discounted to the present value using methods described in the Appendix B1. Cost comparisons can be made using the present value of money, and on this basis the life-cycle costs (LCC) of the project can be projected. The unit energy cost is the levelised life-cycle cost (LLCC) divided by the total amount of energy generated over the life of the project.

The life cycle costs of the two systems show that the systems are fundamentally different. System 1 has high capital outlay of 67% of the total LCC, with low operating proportion mainly due to the forecast 10 year battery life expected for the high quality batteries selected, operating in a narrow cycling regime. The unit energy cost is 337c/kWh. System 2, while demanding only 40% of the forecast LCC as capital outlay, is intensive in operating costs particularly due to the short (three year) life expectancy of the low cost battery. The unit energy cost is 416c/kWh. These are shown graphically in Figures 2.8 and 2.9. Costing and assumptions are shown in Appendix B2.

The battery lifetimes used above are based on cycle life expectancy for cycling in fixed regimes. For tubular batteries 4000 cycles at 20% DOD is standard, and for automotive types 900 cycles at 5% would be typical. In practice, forecast battery life is strongly influenced by the operating conditions as well as DOD. The effects on LLCC and maintenance costs can be severe. To illustrate the impact of varying assumptions for battery lifetime, adjusted LLCC costs are shown in Figures 2.8 and 2.9.

In System 1, it is unlikely that battery life will be less than five years if conditions are moderate and the battery reaches full charge at the top of the cycle. The energy cost would increase by 21% to 410c/kWh for five year life. If battery life were optimistically 15 years the energy cost would drop by 10% to 300c/kWh.

The battery in System 2 could conceivably last three years, perhaps two years (550c/kWh), or even only one year (916c/kWh) if the user selected the "wrong" battery incapable of dealing with prolonged partial SOC operation. Energy cost increases very steeply if the battery life is under two years, and doubles if life is only one year. System 2 is more sensitive to errors in battery life estimate than System 1.

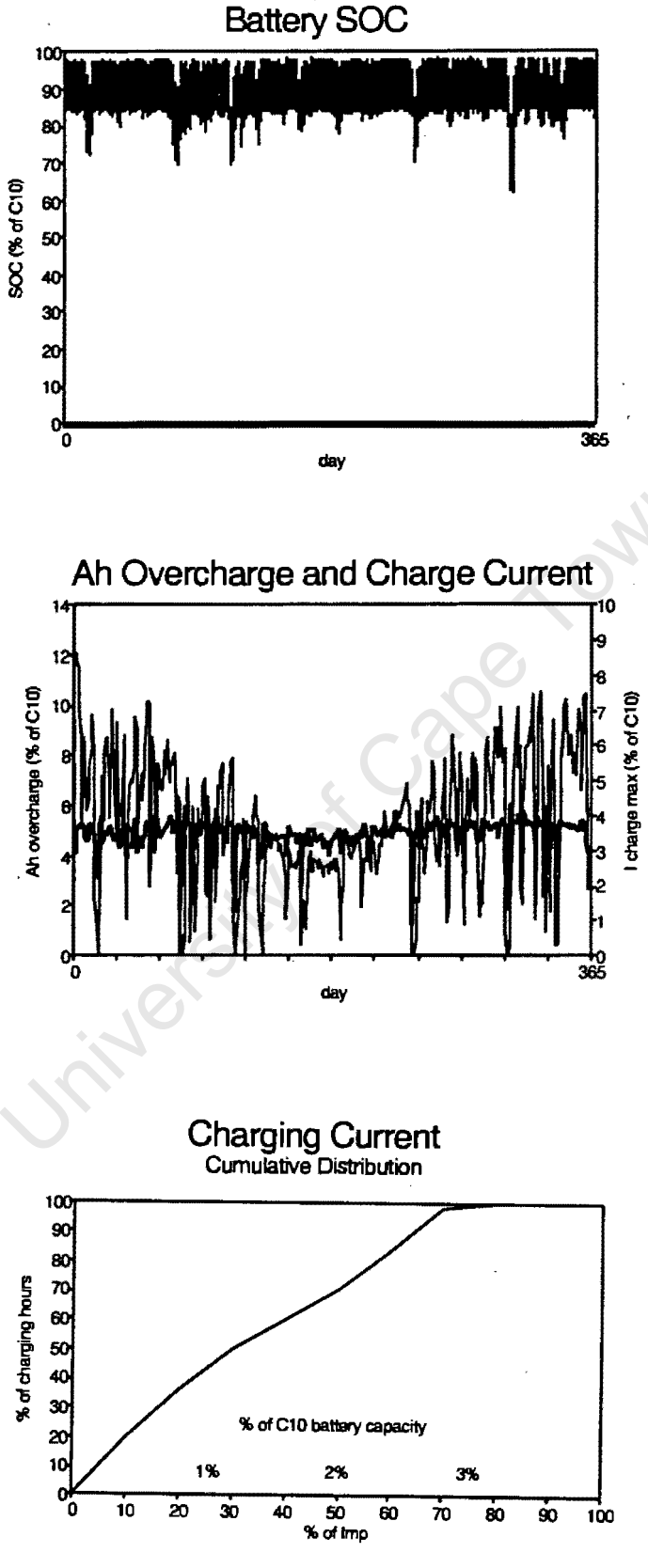

Figure 2.6 Operating conditions for System 1, supplier system.

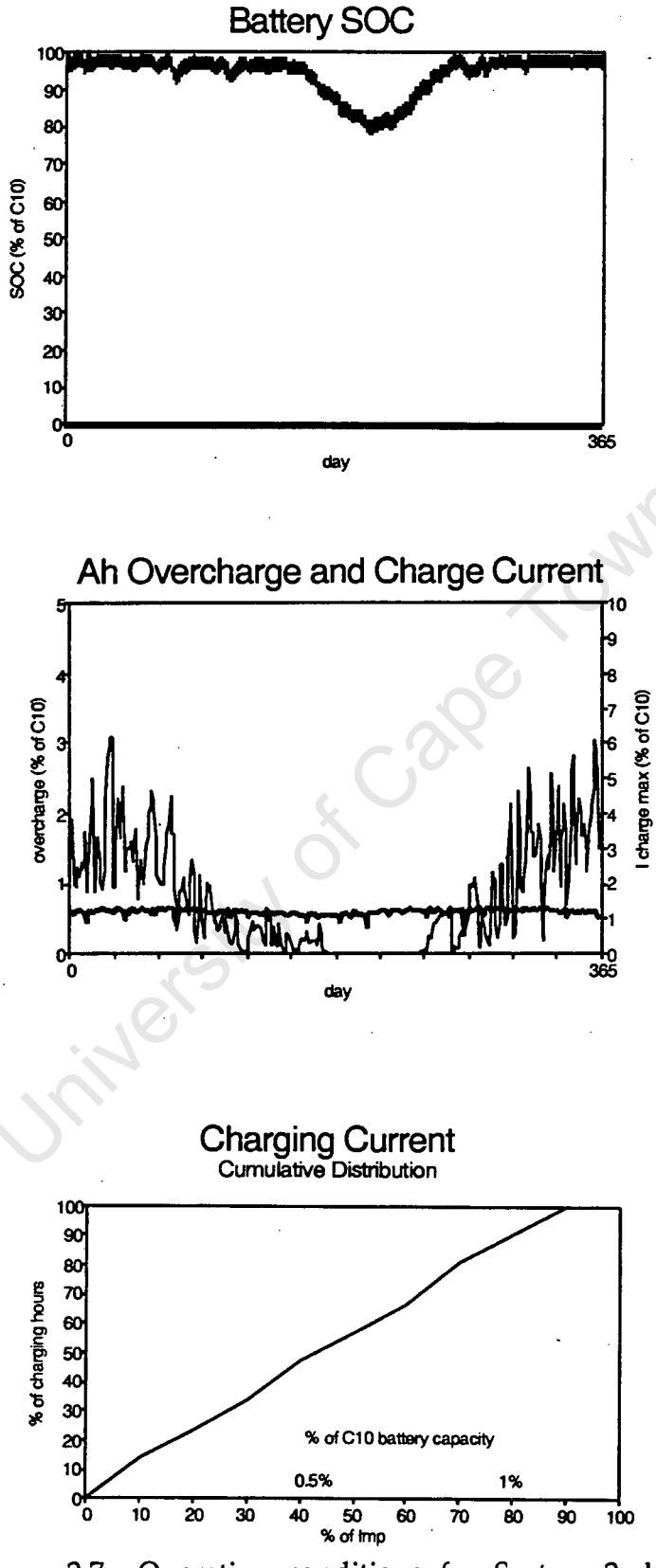

Figure 2.7 Operating conditions for System 2, low cost modular system.

Typical Supplier PV System
Life-cycle costs

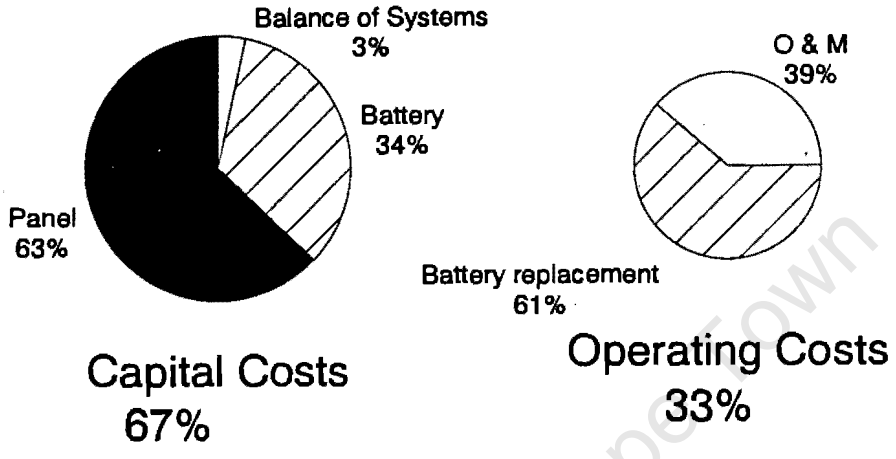

Unit Energy cost=337c/kWh (R1990)

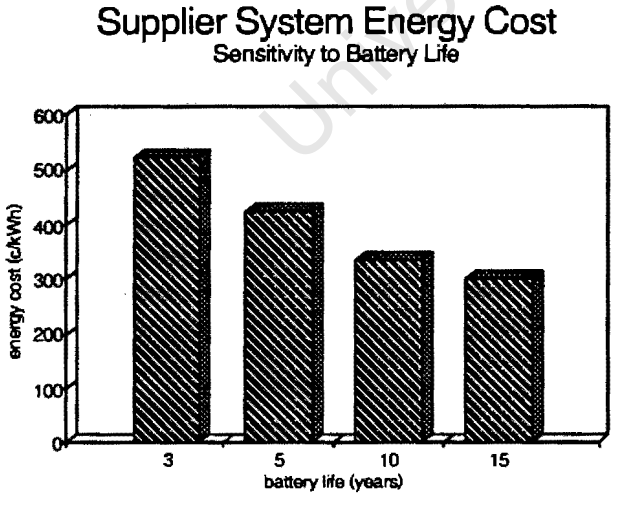

Base Case Assumptions	
Interest rate	5%
System life	20 years
Battery life	10 years
O&M costs	10% battery costs
Array size	325W_p
Battery size	540Ah, 12V
Daily load	1000Wh/day
Array cost (R20/W_p)	R6500
Battery cost	R3488

All prices R1990

Figure 2.8 Life cycle costs for System 1, supplier system.

Typical Low-cost PV System
Life-cycle costs

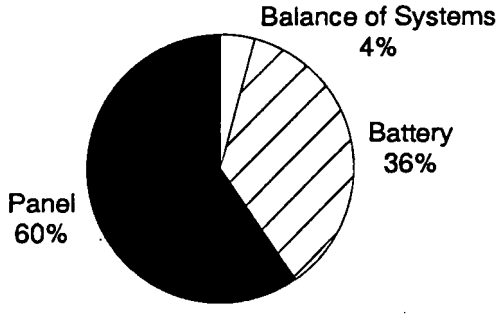

Capital Costs
40%

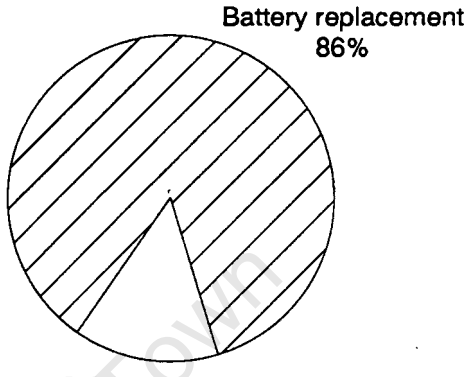

Operating Costs
60%

Unit Energy cost=416c/kWh (R1990)

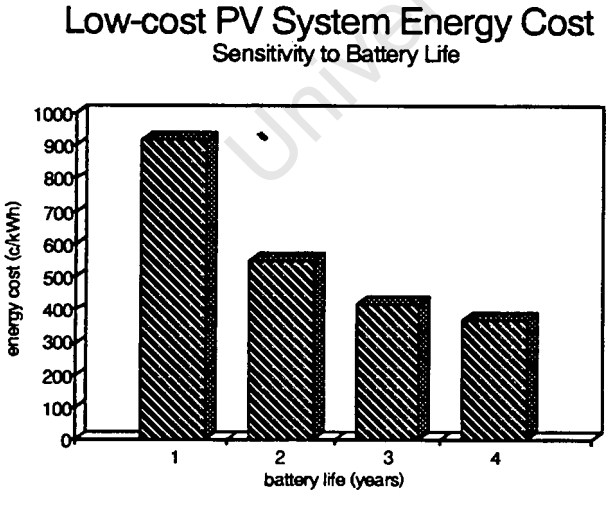

Base Case Assumptions	
Interest rate	5%
System life	20 years
Battery life	3 years
O&M costs	10% battery costs
Array size	40W_p
Battery size	200Ah, 12V
Daily load	200Wh/day
Array cost (R20/W_p)	R800
Battery cost	R500

All prices R1990

Figure 2.9 Life cycle costs for System 2, low cost modular system.

2.3 CONCLUSIONS

This chapter has introduced the basics components in a stand-alone PV system; PV panel, battery, regulator, and the inverter.

Two typical systems were analysed to illustrate some important points about PV systems in general, and about systems of supposedly similar capacities installed at any one site:

- Different panel/battery configurations are available which can provide energy for the application.

- Battery SOC profiles can be substantially different, depending on the panel/battery configuration of the installation.

- Some PV installations may require the battery to operate in a partial state-of-charge for several months before it can be completely recharged. This is usually the result of matching large batteries with small arrays.

- Charging currents in PV systems are relatively low, varying from 1% C_{10} to 5% C_{10}, but not normally higher. They can be regularly lower than this.

- Minimising the installed cost of a system does not necessarily lead to minimised operating costs. Conversely, minimising operating costs probably requires higher installed costs.

- Operating costs are affected by the type of battery selected, and its lifetime. The battery should be suited to the prevalent operating regimes, such as SOC profile, Ah overcharge and charging currents.

- Over-estimating the cycle life of a battery during system sizing strongly affects the effective LLCC and energy costs when the battery life is not realised. This is particularly pertinent to systems that tend to have high operating costs.

This research focuses on the battery in the PV system, in particular the performance under the typical operating regimes of PV systems. Emphasis is on gathering empirical performance data relevant to PV operation. This data is to be used

- to provide battery data useful for PV system designers
- for complementing and for quality checking of the manufacturer's data where it is provided
- to study behaviour of specific batteries under various states of charge and operating regimes
- to provide data suitable for computer simulation of batteries in PV systems.

Chapter 3

THE LEAD-ACID BATTERY

This chapter describes the physical, chemical and electrical aspects of the lead-acid battery.

Sections 3.1 to 3.4 are concerned with the history, basic chemical operation of the battery, cell design and construction and electrical characteristics.

Section 3.5 describes the requirements and designs of conventional battery types.

A more detailed electro-chemical discussion in Section 3.6 extracts from the literature the most important micro-processes and side reactions, including mechanisms of failure of the active mass and grid corrosion processes. Polarisation and overpotential in Section 3.7 describe the mechanisms and effects of gas evolution during battery charging. Section 3.8 describes the macro-processes, particularly stratification and gassing related issues. Section 3.9 presents some discussion on methods of reducing water loss in lead-acid batteries.

Though these detailed sections are primarily of interest to battery modellers, they provide invaluable insight into the operation and life limiting processes.

Section 3.10 describes electrical characterisation battery models suitable for PV applications.

Failure modes of lead-acid batteries are presented in Section 3.11.

Battery life models are discussed in Section 3.12.

Section 3.13 illustrates battery design options available, and shows how these are configured together to meet the requirements of modern photovoltaic batteries.

Section 3.14 describes voltage regulators in PV systems as they apply to the battery and battery operating environment.

3.1 HISTORY

Planté, in 1859, passed current through two lead plates separated by rubber strips, and submersed in dilute H_2SO_4. After a short time, a 2V cell was formed. The interesting characteristic of this cell was its reversibility. The cell could accumulate charge by conversion of electrical energy into chemical energy, and could transform the chemical energy to electrical in the reverse process.

The early lead-acid battery required several cycles to realise full capacity. This formation process required the conversion of the lead sheets into a porous active material, PbO_2 on the positive and spongy lead on the negative electrodes.

The specific energy of the Planté cell was low, but it was shown that there was a linear relationship between electrode surface area and capacity. In 1880 Faure developed the method of covering the lead plates with powdered lead oxides made up as pastes a mixture of lead oxides, H_2SO_4 and water. The spongy nature of these pastes results in the electrolyte diffusing through the pores and coming into contact with a greater area of the active material.

The active material has no rigid structure, and the positive material is a relatively poor conductor. Swan developed the method of mounting the active mass on lead grids to maintain shape and to conduct current evenly through the active material. Sellon introduced antimony as an alloy into the grid to increase mechanical strength. The paste was then pressed onto the grid lattice, forming plates. The flat plate grid is still used for both positive and negative plates. The early cells had a cycle life of 300 charge/discharge cycles before failure, usually by shedding of the positive material.

The development of the Ni-Fe tubular cell by Edison had spin-offs for the lead-acid battery. The tubular plate design was applied to the positive plates of the lead-acid cell. The tubular plate consists of a series of spines surrounded by glass fabric tubing, forming an annulus which contains the active material. The spines enhance current flow through the active material. Cycle life was improved to 1500 cycles.

From 1880, development in cell design was enhanced by a new range of applications. Initially lead-acid batteries were used in power stations, followed by traction and electric vehicle (EV) applications, submarines, railway lighting and electronic equipment.

The breakthrough came with the boom in the automobile industry. The batteries were used for vehicle lights, then later for starting the engine as well. The SLI (starting, lighting, ignition) battery had arrived.

Fundamental research into the processes occurring in the lead-acid battery began when Gladstone and Tribe (1882) detected lead sulphate, PbSO4, at both electrodes of a discharged cell. The "double sulphate theory" was evolved.

The lead-acid battery is described as a dynamic system, in which processes are always in progress regardless of whether the battery is idle or at work. Pavlov (1984) writes

> "...to understand these processes, it is necessary to differentiate between them and to have knowledge of conditions under which a given process is initiated, becomes dominant, or as a result of their own actions become suppressed so a new process is promoted. It is considered that elucidation of the complex array of chemical, physical, electrochemical, semiconductive and crystallisation phenomena that take place in the electrolytic solution, the electrode porous mass and the solid active material itself will assist attempts to increase power, energy, reliability and life of lead-acid batteries."

Today, the lead-acid battery is relatively well understood. There is considerable literature available on its origin, operation, and design. It is beyond the scope of this thesis to regurgitate this, and only relevant phenomena are discussed. Background information is available in the battery encyclopedias, Vinal (1955), Smith (1964), Bode (1977), Mantell (1970). Detailed electrochemistry data is widely published. Pavlov (1984) is particularly recommended.

3.2 BASICS: HOW A LEAD-ACID BATTERY WORKS

Lead-acid battery electrochemical operation is the same regardless of the method of construction.

A cell consists of positive and negative electrodes and an electrolyte. When the cell is fully charged, the positive electrode consists of lead dioxide (PbO_2), the negative electrode of lead (Pb), and the electrolyte of dilute sulphuric acid (H_2SO_4).

During discharge of the cell, lead dioxide is reduced to lead sulphate ($PbSO_4$) at the positive electrode, while metallic lead is oxidised to lead sulphate at the negative electrode: the "double sulphate theory". The sulphate is formed from dissociated sulphuric acid. The acid becomes more dilute the longer the process continues.

During charging the process is reversed, and the lead sulphate on the positive and negative electrodes is converted to lead dioxide and spongy lead respectively. The sulphate that is released combines with water in the electrolyte to reform sulphuric acid. When the cell can no longer accept charge, the voltage rises, and the excess charge is consumed in H_2 and O_2 gas evolution.

The half cell reactions and the overall cell reaction can be summarised as:

Positive: $PbO_2 + 2H^+ + H_2SO_4 + 2e^- \rightharpoonup PbSO_4 + 2H_20$

Negative: $Pb + H_2SO_4 \rightharpoonup PbSO_4 + 2H^+ + 2e^-$

Overall: $Pb + PbO_2 + 2H_2SO_4 \rightharpoonup 2PbSO_4 + 2H_20$

The rated voltage under open circuit conditions is

$\Delta E_e = 2.040V.$

3.3 CELL DESIGN AND CONSTRUCTION

3.3.1 The Ideal Cell

The ideal cell specific energy is expressed in watt-hours per kilogram of reactants (Wh/kg). The theoretical weight contributions of the reactants are:

$$207.2g\ Pb + 239.2g\ PbO_2 + 196g\ H_2SO_4 = 642.4\ g$$

According to Faraday's law 642.4g of reactants provide 2 moles of electrons, equal to:

$$2 * 96500\ coulombs = 193000\ coulombs = 53.61Ah$$

This is equivalent to:

3.865 gram/Ah of negative active material (Pb)
4.462 gram/Ah of positive active material (PbO_2)
3.666 gram/Ah of concentrated sulphuric acid (H_2SO_4)
(equivalent to 8.46cc of 1.260 SG H_2SO_4/Ah)

for a total reacted active mass of
11.99 g/Ah, yielding 83.4 Ah/kg or 170.2 Wh/kg for the cell

The theoretical specific energy is not realised in practice. Practically, the specific energy of the active material varies from 32Wh/kg (64g/Ah) to 10Wh/kg, depending on the battery design (Pavlov,1984:203). To transform the basic lead-acid cell into a practical power source several modifications must be met.

3.3.2 Cell Components

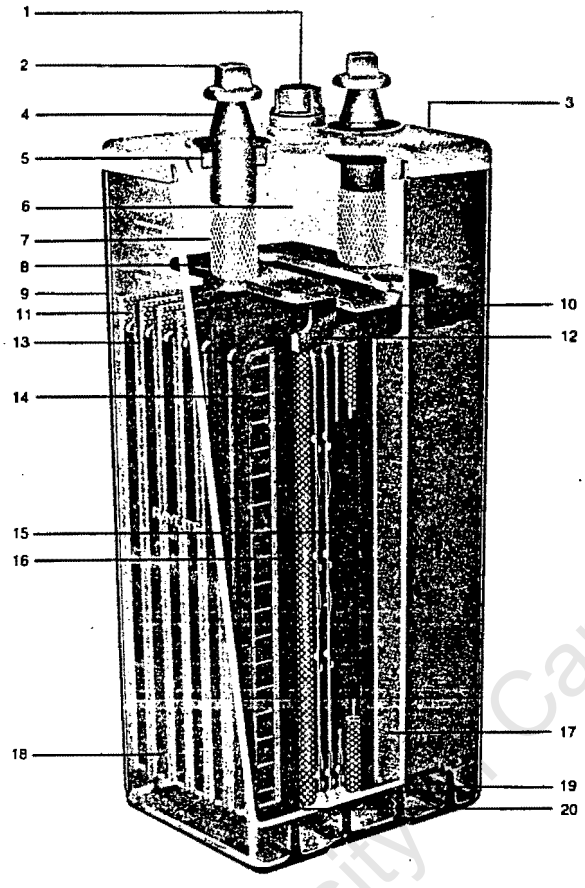

1. Vent plug
2. Lead-coated brass bolt
3. Cover
4. Terminal post
5. Post/Cover seal
6. Large headroom.
   Reduces need for topping up. Ideal for solar applications.
7. Terminal post sleeve prevents loose material from post reaching plate.
8. Positive group bar submerged. Avoids flaking.
9. Container
10. Separator guard
11. Perforated separator
12. Positive plate (tubular)
13. Separator
14. Negative grid
15. Positive spines.
    Spines are not in direct contact with electrolyte – minimises corrosion
16. P G Tube
    Tube holding active material reduces sedimentation
17. Negative plate (end)
18. Edge of plates insulated. No shorts.
19. Rib
20. Bottom bar

Figure 3.1 Construction of a modern standby cell. (Source: Raylite standby battery literature)

The positive active masses are porous, and part of the mass must act as a conductive skeleton to carry the products, reactants and current to each point of the active mass. The remainder is used for electrochemical conversion. The active section of the active mass varies from 35% to 55%. The acid resistant grid supporting the active masses adds further to the weight.

The positive and negative plates are separated by micro-porous separators.

The acid concentration used is usually 35% by weight (1.260 SG). The conductivity is high, and the freezing point is low. The grids are resilient to corrosive attack by the acid. On completion of discharge, excess electrolyte must remain for electrical conductivity during the beginning of charge and end of discharge.

The active block is formed by the positive and negative plates and the separator, together with the electrolyte in the pores. An electrolyte reservoir located above the active block enhances H_2SO_4 availability, as the H_2SO_4 in the active block is restricted. During discharge the acid moves from the reservoir to the active block, and the weight of the active block is increased by the formation of $PbSO_4$. During charge, H_2SO_4 is generated and flows back to the reservoir.

The positive and negative plates are connected into cells, with external terminal posts.

Water decomposition occurs at the end of charging. The evolved H_2 and O_2 is vented through vent caps. The water that is lost through gassing is replaced by removing the vent caps and adding water as required. The cells are mounted in a container with a cover, and adjacent cells are joined with through-the-wall connectors. The active block rests on an element rest. Active mass which is shed is contained in the sediment space under the active block.

3.3.3 Design of the Active Block

The amount of active material theoretically required for reaction is determined by Faraday's law. Practical requirements can be achieved by applying utilisation coefficients taking into account limitations in the processes.

a) Electrolyte

In theory 3.666g of H_2SO_4 is required for 1Ah of current. The real requirement depends on the ampere-capacity, the range of H_2SO_4 concentration during charge and discharge, and the degree to which electrolyte in the upper and lower reservoirs participates in the reactions.

The range of SG's normally used in the various applications is shown in Figure 3.2. The smaller the range the more electrolyte is required for a particular application. The effect of electrolyte concentration on resistivity ($\Omega.cm^{-1}$) is shown in Figure 3.3. SLI batteries are designed for high discharge current, and therefore require low resistivity during normal operating conditions. In traction batteries, there is a trade-off between volume (specific energy of the battery) and low

resistivity. Standby batteries are not specific energy limited, and can operate at relatively low SG's.

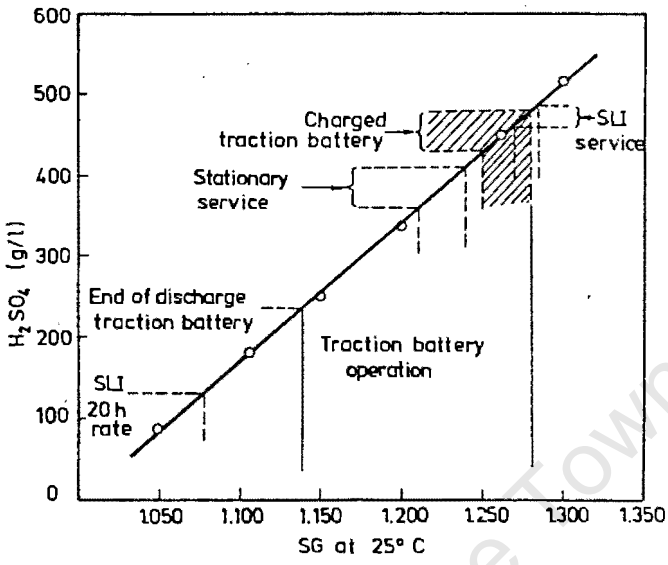

Figure 3.2 Concentration of H_2SO_4 at 25°C over the range used in different batteries. (Source: Pavlov,1984;fig 171).

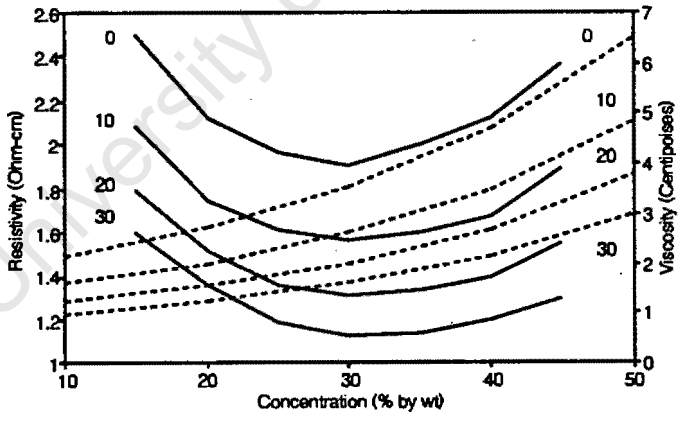

Figure 3.3 Effect of H_2SO_4 concentration and temperature on resistivity and viscosity. Resistivity is represented by the solid line, viscosity by the broken line. Temperature is in degrees celsius. (Source: Vinal,1955;Tables 15, 19)

Most of the electrolyte is located between the active block and the upper and lower reservoirs. The transfer of H_2SO_4 from the lower reservoir to the active block is slow, and only about 10-20% utilisation of this electrolyte is achieved

(Pavlov,1984:355). The slow transfer process is largely due to the viscosity of the electrolyte, which increases approximately linearly with concentration.

Within the active block, the electrolyte is located in the pores of the plates and the separators, and in the spaces between the positive and negative plates. The reactions below

Positive: $4H^+ + PbO_2 + 2e^- + SO_4^{2-} \rightleftharpoons PbSO_4 + H_2O$

Negative: $Pb + SO_4^{2-} \rightleftharpoons PbSO_4 + 2e^-$

show that the mass of electrolyte participating during discharge at the positive plate is greater than at the negative. The water evolved at the positive plate dilutes the neighbouring H_2SO_4. The volume of the positive electrolyte space must be greater than for the negative. This is another point indicating the limiting role of the positive plate.

b) Positive and negative active material

3.865g of Pb and 4.462g of PbO_2 are required for 1Ah of electricity. The actual amount required will depend on the utilisation coefficient, which in turn depends on the active mass porosity and micro-structure, plate thickness, and charge/discharge conditions. Pavlov (1984:357) has determined that the average active mass utilisation of the negative plate is 0.32 and for the positive is 0.34 for traction cells in service. These cells have cycle-life of 1500 cycles. Increasing the utilisation coefficients to 0.44 will decrease cycle-life to 300-500 cycles.

The number of negative plates is usually greater than the positive by one, and the utilisation coefficient is reduced by the outer surfaces of the outer negative plates not participating in the reaction. The outer negative plates have utilisation coefficients of 0.28. The active mass/plate ratio and grid/plate ratio are useful for determining the mechanical stresses and mass changes likely during cycling. These are tabulated below for the positive and negative plates of traction cells.

Table 3.1 Positive and negative active material characteristics of traction cells. (Source: Pavlov,1984; Tables 23 and 24)

	Weight (grams)			Active mass utilisation coefficient	Active mass/ plate ratio	Grid/ plate ratio
	plate	grid	active mass			
Negative	1050	390	660	0.32	0.63	0.37
Positive	1400	600	800	0.34	0.57	0.43

c] Plate design

Two plate designs predominate. Flat pasted plate designs are conventionally used for the negative electrodes, while the positive plate may be either the flat plate or tubular plate design.

Flat pasted plate design

The grid of the flat plate design consists of a planar conductive network of lead alloy for supporting the active mass, and for facilitating good electrical conduction throughout the plate. The active mass is "pasted" onto both sides of the grid.

The effect of positive plate thickness on performance is mainly related to the access of H_2SO_4 into the active mass. Figure 3.4 shows that at low discharge current rates the flat plate capacity is more dependant on thickness than at high currents. The advantages of thin plates with large area can be demonstrated by comparing two cells with the same volume of active mass, one with two 2.4mm thick plates and the other with one 4.8mm thick plate. Discharged over 30 hours, the 2.4mm plates deliver 2*70Ah=140Ah, while the 4.8mm plate delivers 120Ah. The effect of plate area on capacity is also a function of discharge rate.

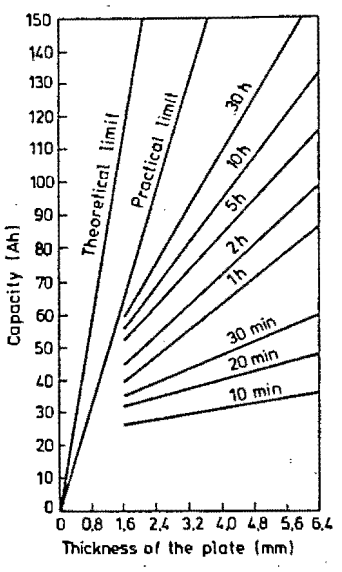

Figure 3.4 Capacity vs plate thickness at different discharge rates. (Source: Vinal,1955:fig 63)

Vinal has shown that when both positive and negative plates are increased by the same thickness, the negative plate shows a greater rise in capacity.

Tubular plate design.

In tubular cells spines replace the conventional grid. The spines are located at the centre of the tubes, made from braided acid-resistant glass wool. The active material is contained between the wall of each tube and the central spine.

The principle of tubular design is that shedding of the active mass does not occur as the active mass is held by the tube. The capacity of the tubular plate depends on the diameter of the tube. At low discharge rates a 9mm tube yields the optimum capacity (Figure 3.5), though tube diameters are usually 8-8.4mm with an active mass thickness of 2-2.22mm.

The tube dimensions affect the corrosion process, as the spine is enclosed by a layer of active material which protects it from corrosion. Figure 3.6 shows how cycle life increases with tube diameter under deep discharge conditions. The approximate cycle life relationship between tubular and flat plate cells of the same specific energy is shown in Figure 3.7.

A disadvantage of the tubular plate is the cost, due of the labour intensive technology, and the low utilisation coefficients usually achieved. At high current drains the increased current density at the active mass/spine interface may cause local heating and cracking of the corrosion layer.

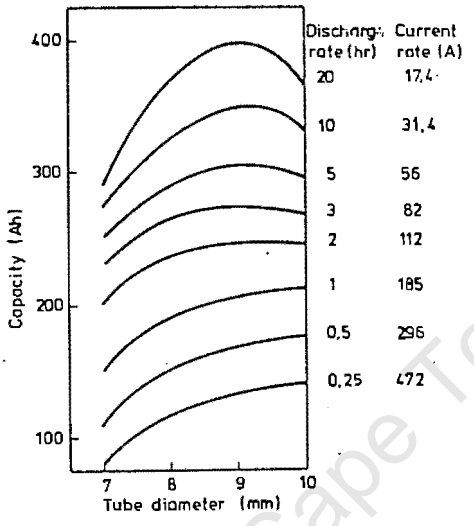

Figure 3.5 Capacity vs tube diameter at different discharge rates.
(Source: Pavlov,1984:fig.174)

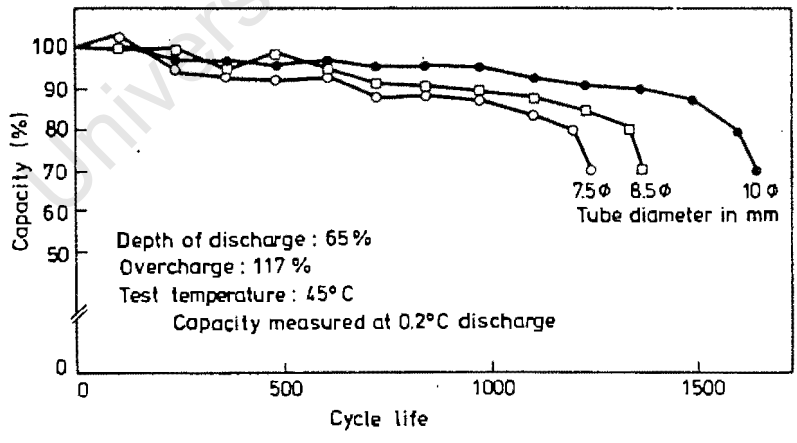

Figure 3.6 Capacity vs cycle life of tubular batteries.
(Source: Pavlov,1984:fig.176)

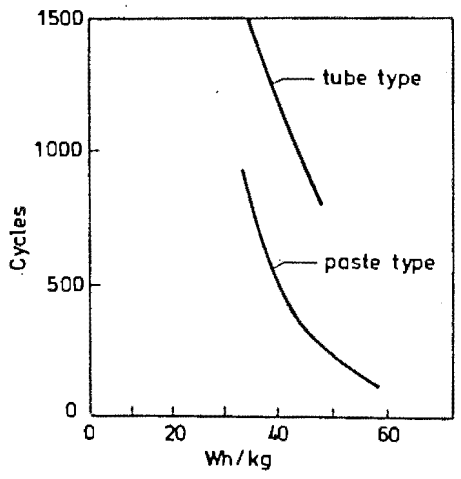

Figure 3.7 Relationship between cycle life and specific energy of tubular and pasted plate designs. (Source: Pavlov,1984:fig.177)

d) Active block dimensions

In large cells the transport of H_2SO_4 between the active block and the reservoirs has a marked effect on cell capacity at high discharge rates. During discharge an acid concentration gradient is established over the height of the cell. The SG decreases from the bottom to the top of the block, and the effect is enhanced during deep discharges. This effect is known as acid stratification. (See Section 3.8.1.)

The path of the sulphuric acid flows tending to equalise the concentration gradients depend strongly on the design of the active block. Pavlov (1984:362) suggests that there is considerable scope for investigating active block designs with a view to improving active mass utilisation coefficients.

3.4 ELECTRICAL CHARACTERISTICS

3.4.1 Open Circuit Voltage and SG

The open circuit voltage of a cell depends on the electrolyte concentration and its temperature, as described by the Nernst equation.

$$\Delta E_e = \Delta E_e^o + \frac{2RT}{nF}\ln\left(\frac{{}^{a}H_2SO_4}{{}^{a}H_2O}\right)$$

where

ΔE_o = 2.040V

R = gas constant (8.31441 J K^{-1} mol^{-1})

n = number of reacting electrons (2)

F = Faraday constant (9.648 x 10^4 C mol^{-1})

T = temperature (K)

The measured temperature effect has been shown to be 0.00136V/°C, compared with the theoretically calculated value of 0.00135V/°C (Vinal,1955:194).

Open circuit voltage is often used as an approximation of the state of charge (SOC) of the cell. The relationship is given in Figure 3.8.

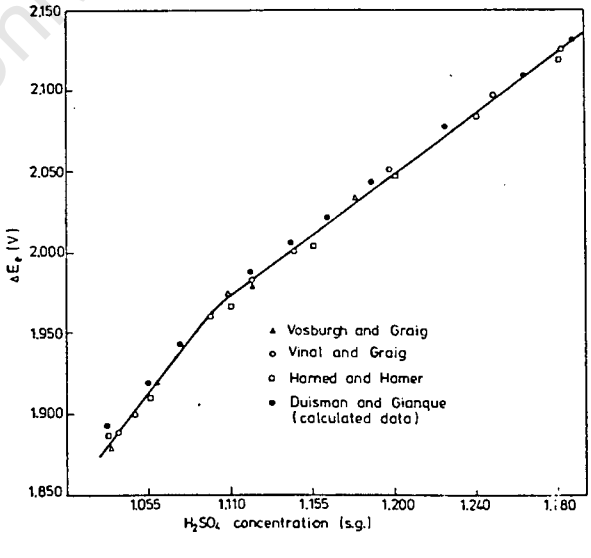

Figure 3.8 Experimentally determined and calculated dependence of cell voltage on H_2SO_4 concentration. (Source: Vinal,1955:Table 39)

Limitations of voltage and SG as SOC indicators.

Voltage is approximately a linear function of concentration of the electrolyte in contact with the active material.

SOC is a linear function of the average electrolyte concentration in the cell, by nature of the stoichiometry of the reactions.

The measured SG is a measure of the bulk electrolyte concentration. Only after the cell has stood in open circuit for several hours will the bulk fluid and average fluid concentrations be equal. Only then will SG be an accurate indicator of SOC, and only then will voltage be a reasonably accurate indicator of SG. (Fluid concentration gradients are discussed in more detail in Sections 3.3.3(d) and 3.6.2.)

3.4.2 Capacity

The capacity of a cell during discharge (C_d) is determined by the amount of electricity that can be delivered by the cell at constant current (I_d) till the cut-off voltage is reached. The cut-off voltage represents a certain active mass utilisation coefficient.

$$C_d = I_d\, t_d$$

where t_d is the time to reach the cut-off voltage (see Section 3.3.3(d)). Figure 3.9 shows the relationship between capacity and discharge current. Standards have been introduced to compare different batteries. Most standards require the capacity to be determined by discharge with a current at which the battery reaches the cut-off voltage at 20°C after 20 hours. The capacity is referred to as C_{20}, and is known as the rated capacity. The current is also referred to as C_{20}, or as the 20 hour rate. Manufacturers normally recommend restrictions on the depth of discharge, mainly to preserve the electrical contact between the active mass and the grid.

Different types of batteries are rated at different discharge rates, but the 10 or 20 hour rates are most common.

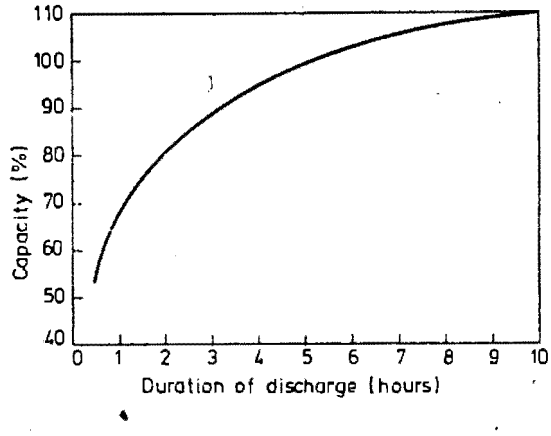

Figure 3.9 Relationship between capacity and discharge current.

Capacity is affected by the following factors:

i) Temperature: Capacity decreases with decreasing temperature. One percent per degree Celsius is a well quoted factor (Vinal,1955:220). Temperature enhances the electrolyte mobility.

ii) Aging: After an initial increase of 10% over the first few cycles, capacity decreases with aging of the battery, and the battery is usually assumed useless when the capacity has fallen to 80% of the rated capacity.

iii) Rate of discharge: Increasing the rate of discharge decreases the instantaneous capacity. (See Section 3.4.3(a))

iv) Previous discharge: The capacity is affected by the immediately preceding discharges. The hysteresis effect shows that capacity is decreased if preceded by a higher current, and is increased if preceded by a lower current (Vinal,1955:228). Capacity is increased by intermittent discharge, but the increase is less than 10% except for discharge rates shorter than about 5 hours.

v) Electrolyte concentration: Capacity increases with an increase in electrolyte concentration (Vinal,1955:222). Increased concentration increases the potential of the cell, decreases the electrolyte resistance, but increases the viscosity (decreases mobility). Electrolyte diffusion is also concentration related.

3.4.3 Voltage During Operation

Because the electrochemical process in the battery is not fully reversible, the voltage during discharge must be less than the open circuit voltage, and the voltage during charge greater than the open circuit voltage. The voltage of the cell depends on the magnitude and direction of the current, and the cell temperature (and SOC of course).

The discharge voltage, V_d, of the cell is given by

$$V_d = V_r + r_d I_d, \quad I_d < 0$$

and the charge voltage, V_{ch}, by

$$V_{ch} = V_r + r_{ch} I_{ch}, \quad I_{ch} > 0$$

where r_{ch} and r_d are the (apparent and non-constant) internal resistances during charge and discharge, and I_{ch} and I_d are the corresponding currents. V_r is the rest voltage.

a) Discharge curves

Figure 3.10 shows the discharge curves for a 12V 90Ah SLI battery for different discharge currents at 20°C. After a given time voltage begins to decrease rapidly. This is caused by an increase in internal resistance due to: dilution of the electrolyte (and drop in conductivity) and interference by physical processes in the ion flow (observed as an increase in concentration and resistance overpotentials, see Section 3.7.1).

Since deep discharges have an adverse effect on battery performance, a limit is set for the end-of-discharge voltage, and is termed the cut-off voltage. This is typically 1.75V per cell for discharges longer than 20 hours. The mean discharge voltage ($V_{d,mean}$) is shown in the Figure 3.10. This is necessary for calculating the energy and power characteristics of the battery.

The discharge current is often represented as a function of the capacity, eg. the discharge current resulting in the cut-off voltage after 20 hours is the "20 hour rate" (C_{20}). A lower current might be referred to as $0.05C_{20}$. Charging current is referred to the same basis, eg. C_{20}.

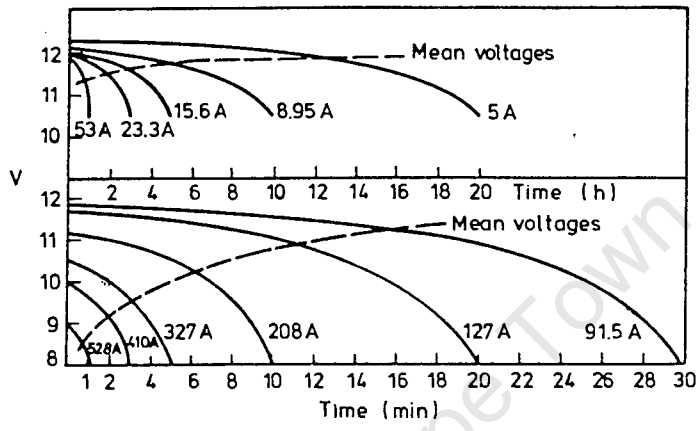

Figure 3.10 Standard discharge curves for a 12V 90Ah SLI battery. Temperature = 20°C. (Source: Pavlov,1984:fig.60)

b) Self-discharge

The self-discharge of the battery increases with temperature, age of the battery, and the amount of antimony in the grid. Self-discharge consumes water. The rate of self-discharge is usually measured as a percentage loss in capacity per month, or drop in SG per month. The SG is measured after the electrolyte has been restored (topped up).

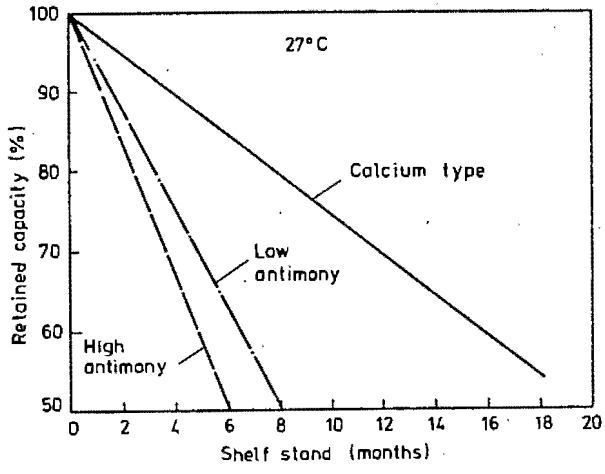

Figure 3.11 SLI battery retained capacity during open circuit storage. (Source: Pavlov,1984:fig 66).

The self-discharge rate of lead-calcium grid cells is considerably lower than for the other grid alloy types. The higher the antimony content of the grid alloy the greater the self-discharge rate.

c) Charging curves

During cell charging the voltage is greater than the open circuit voltage of the cell. The charging curve can be divided into three main regions, which are particularly clear during constant current charging.

Efficient charge stage - The main reaction is the conversion of $PbSO_4$ to PbO_2. Charging is nearly 100% efficient. This stage lasts till SOC reaches about 70%, when the voltage reaches 2.3V per cell.

Mixed stage - Water decomposition reactions begin to occur along with the charge accumulation reaction. The voltage rises sharply, and the rate of cell heating increases. Charge acceptance is reduced as current is increasingly consumed by gassing.

Gas evolution stage - charge acceptance is complete, water decomposition and gassing are the predominant reactions. The cell voltage tapers, and the total charging current is used for gas evolution. Cell heating is increased further (Calder,1985).

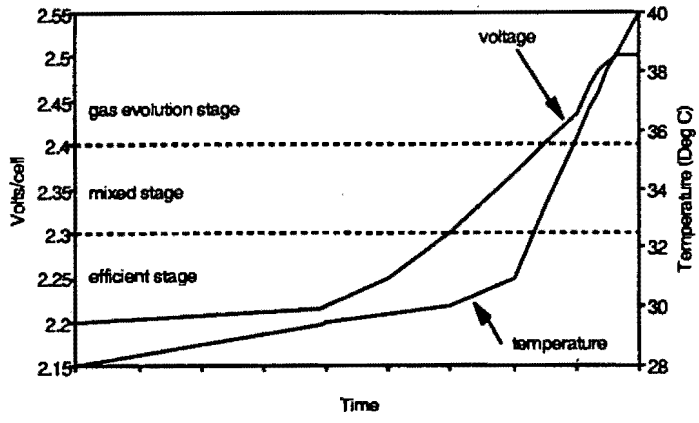

Figure 3.12 Three charging regimes during constant current charging, showing voltage and temperature vs time.

Charging at constant currents may not be the most effective way to charge the battery. High or low rates of charge at the wrong time can cause damage to the battery. The basic principle to be followed is, charge at maximum admissible current during the efficient charge stage, and optimum current during the mixed stage.

The main parameters describing the charge regimes are:

- initial and final voltages
- initial gas evolution voltage
- charging current during the efficient stage
- current at the beginning of the mixed stage
- finishing charge current
- SOC during efficient stage
- upper temperature limit.

Both temperature and aging decrease the voltage at which the battery begins to gas, and therefore the finishing voltage should be decreased to compensate for this effect. Increased temperature improves charge acceptance during the efficient stage, and the current can be increased to take advantage of this. Excessive temperatures may result in earlier onset of the mixed stage. Cooler temperatures require both higher finishing voltage and slower charging during the efficient stage. Aging of the battery is likely to cause increased internal resistance during the efficient stage.

d) Ampere-hour efficiency

During the mixed charging stage, some of the charging current is consumed by water electrolysis. Clearly battery charging is therefore not one hundred percent efficient. The Ah efficiency is defined as:

$$Ah\eta = \textit{effective Ah input / total Ah input}$$

Ampere-hour efficiencies are typically around 90% or greater for deep cycling. Recharging the battery from shallow DOD will result in lower efficiencies.

3.4.4 Charging Methods

Charging methods have generally been developed with the specific aims of:

- minimising charging times, particularly for traction batteries.
- minimising gassing for standby and SLI cells

Constant current charging - The current must be low enough not to cause excessive heating during the mixed and gassing stages. As a result, the charging time is long. A variation, the multi-step current charge, aims to reduce the charging time and increase efficiency. In a method proposed by Smith (1964), the initial current during the efficient charging stage is about 20-40% of the rated Ah capacity of the battery, and is reduced by half each time the voltage reaches 2.4V/cell. There are many variations of the multi-step method.

Constant voltage - The voltage limits the current in the final stages of charge, but the initial current may be large, unless the initial DOD is low as for an SLI battery. For deep discharge applications the initial current may exceed the recommended charging current, and the cost of equipment to satisfy the initial current consumption will be prohibitive. This method is most suitable for float charging of SLI and standby cells.

Controlled current-voltage - Charging is carried out under constant current conditions during the efficient stage, followed by constant voltage charging (2.4V per cell) for the remaining duration of the charge. The current decreases exponentially during this stage as illustrated in Figure 3.13. Charging is complete

when the current has fallen to 1A/100Ah. The actual finishing voltage will depend the initial DOD and temperature. At higher temperatures the current will be higher at the same finishing voltage. The controlled current enables use of smaller and less costly chargers.

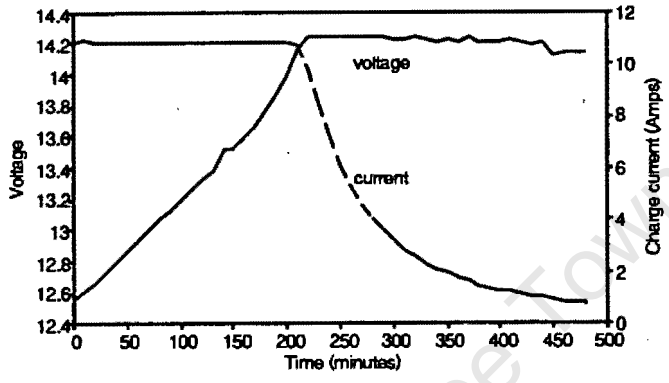

Figure 3.13 Charge under controlled current-voltage conditions for a 100Ah 12V battery. (Source: Experimental data)

PV charging regimes - In terrestrial PV systems, constant current charging over any length of time is virtually impossible due to irradiance and load variations. Currents are usually lower than traction battery charging regimes, and are usually voltage controlled at the end-of-charge by the voltage regulator.

3.4.5 Equalising Charge and Defined Charge State

A clear cut point which defines the end of charge does not exist. Furthermore, the individual cells are not always in an equally charged state. To avoid charge mismatch and to prolong the life of the battery, manufacturers recommend an equalising charge at least once a month for deep-cycle batteries. This usually involves prolonging the mixed charge stage, and charging at the recommended finishing current till the voltage and SG of the cells in the battery do not change over a two hour period. The SG and voltage can only be used as indicators of the end of charge if the electrolyte levels have been corrected by water addition.

Before capacity tests are determined the battery must be in a defined state. Usually a current of five percent of C_5 is passed through the battery till the voltage and SG values do not change over a three hour period. This is similar to equalise charging.

3.4.6 Energy and Energy Efficiency

The instantaneous energy transferred to the battery during charge (E_{ch}) or delivered during discharge (E_d) under constant current conditions is given by

$$E_{ch} = V_{ch} I_{ch}$$

$$E_d = V_d I_d$$

The energy delivered by the battery during discharge is the sum of the instantaneous energies. The relationship between energy and discharge current from full charge to 100% DOD is given in Figure 3.14.

The energy transferred to the cell during controlled charge depends on both the charging current and the finishing voltage. Figure 3.15 shows the energy requirements for the same cell from a fully discharged state, at different charge rates and finishing voltages. At low charging currents the energy requirements are low. At high currents and low finishing voltage the energy is moderate, and at high finishing voltages the energy input requirements are higher.

Energy is usually measured in watt-hours (Wh).

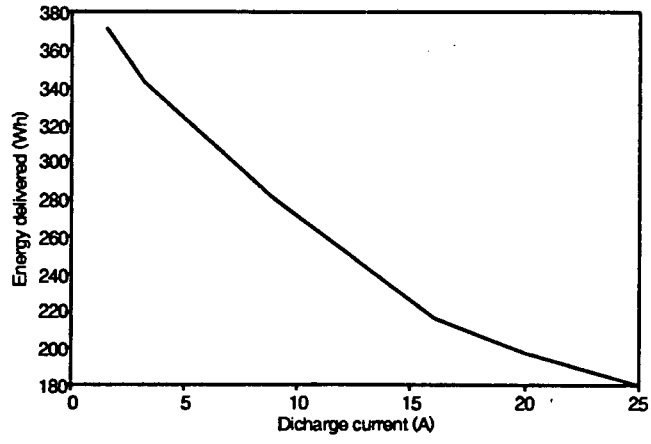

Figure 3.14 Relationship between energy and discharge current for 4V 100Ah cell to complete discharge.

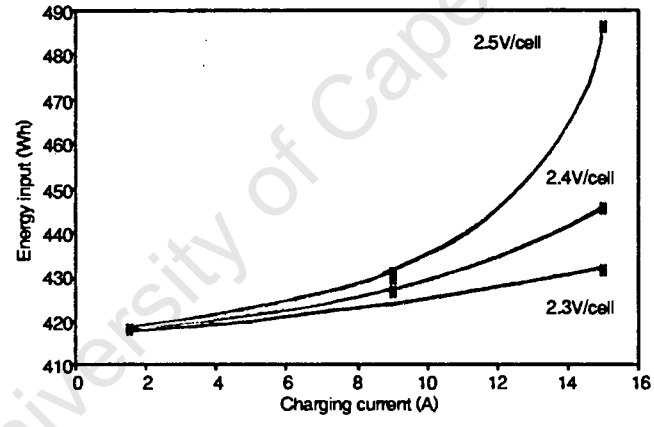

Figure 3.15 Relationship between charging energy and controlled current-voltage charging parameters.

Energy efficiency

The energy efficiency is defined as the total energy output during one discharge cycle, divided by the energy input during the charge cycle that returns the battery to its original state of charge.

Firstly, energy efficiency is highest when discharge and charge currents are low, and during deep cycling. The energy efficiency is directly affected by the Ah efficiency, which is determined by the charge parameters. Energy efficiency is

more strongly affected by inefficient charging than Ah efficiency, as the voltage during the gassing stage rises sharply as well. During shallow cycling a greater percentage of the charging time is spent in the gassing region.

The watt-hour efficiency for deep-cycling is typically in the region of 85% at low currents, but can drop to 75% at higher currents. For shallow cycling in the 10-20% DOD region at low currents, the energy efficiency is typically 95% dropping as low as 50% at higher currents and finishing voltages.

3.4.7 Cycle Life

The service life of a battery is rated on the basis of the charge/discharge cycles obtained during laboratory bench tests. Most conventions specify cycle life as the number of cycles a battery attains at the specified DOD before its capacity is reduced by wear and aging to 80% of the rated value. Some manufacturers, however, specify cycle life as the number of cycles to 50% loss of capacity.

A typical battery life decay curve has been shown in Figure 3.6. After 20% loss in capacity, further degradation is usually rapid, so it makes only a slight difference to cycle life whether the end of life is taken to occur at 80% or 50% of capacity.

Battery cycle life as a function of depth of cycling is most often portrayed as a straight line on a semi-logarithmic graph. Curves for various lead-acid types tend to conform with this assumption (Figure 3.16). The different slopes of the curves indicate various modes of wear or failure for the battery designs. The various modes of failure are outlined in Section 3.11.

Some manufacturers represent cycle life as a straight line on a log-log curve (Delco,1979), which gives very high cycle life for low DOD if data extrapolation is used. Only the semi-log model is theoretically supported, and only in the range 10%-80% DOD. The issues are taken up in Section 3.12.

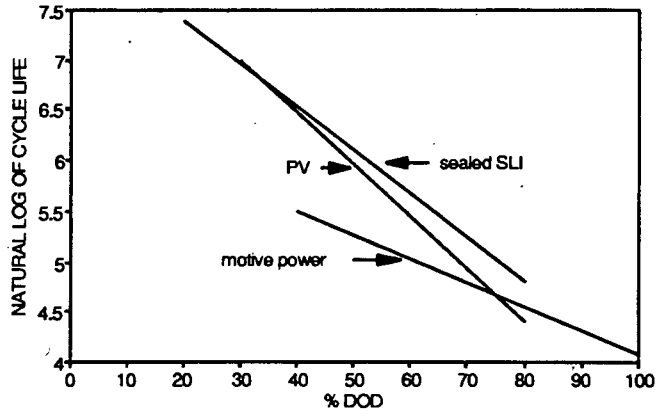

Figure 3.16 Cycle life vs DOD for various battery designs. (Sources: Sieger,1981; Delco,1979)

The actual life of the battery may be longer or shorter than the laboratory tests. Other life-limiting factors may come into effect. Sieger (1981) finds that cycle life also depends strongly on the frequency of cycling. Using 2, 5, and 10 cycles per week, cycle life logarithmically depends on the frequency. He attributes this mainly to the self-discharge process.

Bechtel National (1980) find a strong dependence of cycle life on temperature. If the battery is used within normal temperature ranges (20-40°C), at low rates of discharge in the absence of deep discharge it will last longer.

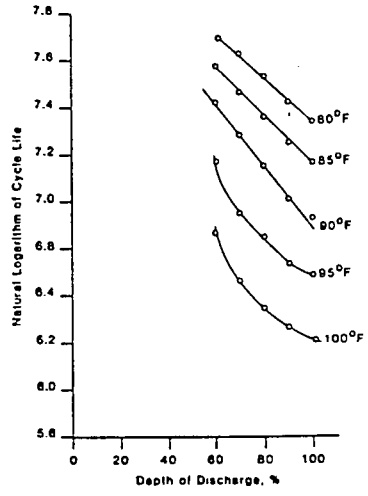

Figure 3.17 Dependence of cycle life on temperature, lead-acid motive power cell. (Source: Sieger,1981)

If current drain is heavy, operating temperature high or the electrolyte is affected by impurities then life will be reduced.

3.5 BATTERY TYPES

This section introduces the common types of battery, and shows by example how subtleties in cell design can affect the battery characteristics.

3.5.1 Starting, Lighting, Ignition (SLI) Batteries

SLI or starter batteries are used for starting the motor vehicle, for lighting and for ignition of the spark plugs. After the engine has started the basic energy requirements are met by the generator. During conditions of heavy energy demand, the battery covers the shortfall.

Use patterns affect the battery. In private vehicles the battery is subjected to substantial idle periods. In taxis and urban driving stop-start conditions the battery is often deep-cycled. In touring the battery is often overcharged.

a) Basic parameters affecting cell design.

Power

The primary requirement of SLI batteries is to provide high power for short intervals to start the motor. High power is achieved by high current flows, typically 300A for a 100Ah battery.

Power can be increased by:

- decreasing plate thickness (typically neg=1-1.5mm, pos=1.3-1.8mm) and increasing the number of plates
- introduction of radial grids
- reduction of the inter plate distance
- use of thin micro-porous separators
- increase in cross-section and reduction in length of inter-cell connectors.

Capacity

The full capacity of the SLI battery is not used, normally 1% of C_{20}, and at most 50% of C_{20}.

Cycle life

SLI batteries are designed to deliver high currents for short time duration, and immediately be recharged. They are not designed for deep charge/discharge cycling, but can generally withstand overcharge or corrosion of the positive grid. During cycling the active mass is subjected to heavy mechanical stresses due to expansion, and the material tends to shed. Shedding can be restricted by i) reducing the utilisation coefficient of the active mass by increasing the thickness of the plates ii) wrapping the positive plate in a glass wool sheath to reinforce the positive active mass.

Mechanical strength

Batteries for non-stationary applications must not only have good electrical properties, but also be resistant to mechanical and vibrational stresses likely during normal operation. These effects occur where the plates are fixed to the strap of the semi-block, at the fixing points of the semi-block to the container.

Plates usually stand on rests on the bottom of the container, and are asymmetrically fixed to the strap. To eliminate vibration of the individual plates, the semi-blocks are bonded by a layer of epoxy resin. Only one end of the semi-block is fixed to the container through the inter-cell connection. In "heavy duty" batteries, the free end of the strap is attached to the nearest partition by a plastic arrestor.

b) Maintenance-free batteries.

The conventional SLI battery has certain drawbacks

- shelf life at open circuit is relatively short due to self discharge
- water consumption during charging and open circuit is relatively high, necessitating regular water addition.

The effects are mainly due to the presence of antimony in the metal grid. Antimony contributes higher mechanical strength but decreases both the hydrogen and oxygen overvoltages, (the gassing voltage), and enhances the electrolysis of water (see Section 3.7.2). The development of low-antimony (1-3% Sb) alloys which retain the favourable mechanical properties has given rise to low-maintenance (LM) batteries. These batteries may, however, need periodic topping up during the second half of their life. Antimony-free batteries generally utilise calcium grid alloys, and are referred to as maintenance-free (MF).

The relationship between gassing current and voltage is shown for the various types of SLI battery. The MF batteries require the highest voltage to begin the electrolysis process. Gassing is negligible below 14.1V for LM and MF types. As the batteries age, the gassing current of the 5%Sb and the LM increases considerably, while that of the MF does not change.

Further, the gassing current of the 5%Sb and LM is strongly affected by temperature, while the MF is not (Pavlov,1984:213).

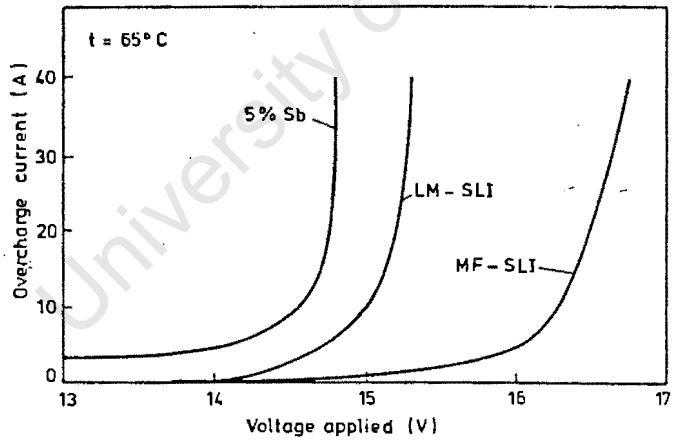

Figure 3.18 Gassing current vs voltage for various types of 12V, 77Ah SLI batteries. (Source: Pavlov,1984:fig.64)

The shelf life of MF batteries is considerably longer than for the other types.

The main shortcoming of the MF battery is its lack of performance under deep-cycle conditions. This is mainly due to the formation of a "non-conducting barrier corrosion layer" of $PbSO_4$ which forms between the positive active mass and grid,

and impedes current flow. The insoluble $PbSO_4$ reflects the lack of antimony, rather than the presence of calcium (see Section 3.6).

Shedding of the active mass is generally negligible in MF batteries. The active blocks can therefore stand directly on the base of the container. MF batteries are often provided with a state of discharge indicator to help prevent deep-discharge.

3.5.2 Electric Vehicle (EV) Batteries

Electric vehicle batteries must provide high energy and power under deep-discharge conditions. Modern EV batteries typically provide 1500-1800 cycles at 80% DOD. Requirements are high specific energy, long life, easy and inexpensive manufacturing, easy and cheap maintenance, and low initial investment. The lead-acid battery is up to now the only battery suitable in terms of price, materials and technology.

The life of the battery is determined by the irreversible processes taking place: corrosion of the grids, processes in the corrosion layer, sulphation of the negative plates, shorting, shedding of the positive mass (see Section 3.6.2).

EV battery design has resulted in an increase in specific power at the expense of battery life. Methods include increasing utilisation of the active mass, higher active mass/grid ratios and increasing the normal depth of discharge during cycling. Antimony grid alloys are favoured in the cycling environment.

Tubular and flat plate designs are used. The disadvantage of tubular plates is the cost, and at high current drains the increased current density may cause local heating and cracking of the corrosion layer. Tube diameters of 8-8.4mm are common, with an active mass thickness of 2-2.2mm.

Flat plate EV batteries have plates 4-6mm thick. The active mass has a lower utilisation coefficient and higher density than SLI batteries.

Flat plate batteries display higher power density than tubular designs at the expense of cycle life. Tubular plates typically achieve 2000 cycles, while flat plates can achieve 800 cycles before corrosion sets in.

3.5.3 Stationary Batteries

There are two main categories of stationary batteries,

- stand-by batteries: kept in a full state of charge to be used immediately a power failure should occur.
- load levelling and cyclic energy storage: often used to decrease system costs by allowing optimal utilisation of off-grid energy generators like electrical generator sets and PV systems, though also offering promise for direct load levelling within the utility network.

a) Stand-by batteries

Requirements are maximum reliability, long life under float charge conditions and low maintenance.

Special designs include

- Planté cells with positive plates made from pure lead
- tubular plates with low antimony spines
- pasted positive plates with calcium grids

Dilute H_2SO_4 is used (1.2-1.25 SG) as electrolyte, which reduces grid corrosion under the well controlled operating conditions.

The battery is kept topped up under float charge conditions (2.2-2.25V per cell). Gassing is minimised. Charge/discharge cycles are usually infrequent (less than five per annum).

The choice of grid alloy most affects cell operation under float charge. High antimony grids require low float charge voltages, and are most sensitive to temperature (see Section 3.5.1(b)). The antimony content is also directly related to the corrosion rate during float charge operation (Figure 3.19). During overcharge, gassing causes antimony positive grids to corrode. Excess gassing results in dissolution and transport of antimony to the negative plate (see Section 3.6.3(e)), where it decreases the negative plate voltage (see Section 3.7.2). The gassing must increase to keep the charge voltage constant (Figure 3.19). The corrosion rate will be enhanced (see Section 3.6.3). There is a possibility of runaway. The rate of water consumption will increase.

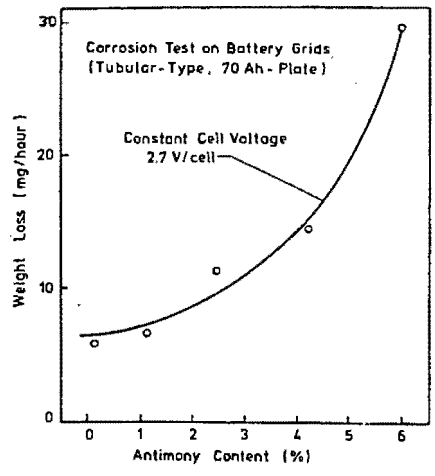

Figure 3.19 Dependence of the corrosion rate at constant cell voltage on the Sb content of the grid alloy. (Source: Pavlov,1984:fig.70)

Calcium grids under float charge gas less readily, normally consume less water, corrode less and are not as temperature sensitive as antimony grids. In the case of electrolyte contamination, the high gassing voltages will drop and more current will be involved in water electrolysis. If the calcium grid cell is deep-discharged or remains in a partially discharged state for a long period, insoluble $PbSO_4$ crystals will be formed in the corrosion layer and decrease the electrical conductivity considerably.

Correct grid choice is a therefore the major factor in stand-by battery selection.

b] Cycling batteries

In grid utility or diesel-electrical generator (genset) load levelling applications the main requirements of the battery are high charge acceptance rate, moderate energy efficiency and good deep cycle life.

Charging requirements are similar to EV batteries, essentially as fast as possible. Discharge requirements vary from mild low current discharges over several days to complete discharge over a few hours. High efficiency is desirable, but is not often attainable because of the high charge currents and reduced charging efficiencies. Much work has been done to eliminate cell internal resistances at the high currents. Low maintenance is low priority as personnel are usually on hand to tend to the electrical machinery.

These batteries are well catered for by the conventional designs. Antimony positive grid alloys provide ensure good grid life, while tubular positive plates provide robust housing for the active material and shield the grid from oxidation during the frequent gassing and overcharge cycles. Copper negative grids minimise cell internal resistance. In many cases EV batteries offer the best value.

c) Renewable energy cycling batteries

While batteries for renewable and solar PV applications fall into the stationary cycling battery class, their typical operating regimes are considerably different to the regimes experienced in the more conventional applications discussed till now.

Operating regimes are determined primarily by the availability of the solar resource, the profile of the load demand, and the match and configuration of the solar charger and the battery. Some important points applying to PV systems are:

- Different PV array and battery configurations can provide energy for the application.

- Battery DOD, cycling and overcharge depends on the battery/array configuration, and can vary substantially depending on the configuration.

- In some installations the battery may be required to operate in a partial state-of-charge for several months before it can be fully recharged.

- Charging currents are relatively low, varying from 1% to 5% of C_{10}, though they can be regularly lower than this.

- Constant charging currents are virtually impossible to attain due to variations in irradiance and load currents.

- Battery temperature variations may be high due harsh and variable climates where PV systems are typically installed.

- Regular maintenance may be difficult due to the often remote and inaccessible sites, or local maintenance personnel may not be on site so that the installation is maintained only once problems have occurred.

In the past specialist PV batteries have not been available, and battery choice has depended on selecting from the conventional types the battery most suited to one or other of these conditions. In some cases priorities have had to established, or else the PV system has had to be designed to suite the available battery designs, often at increased cost.

Additional theoretical knowledge is required before discussing specialist PV battery designs, in Section 3.13. This theory is discussed in Sections 3.6 to 3.9.

Sections 3.6, 3.7, 3.8 and 3.9 are theoretical discussions detailing the most important requirements for understanding competing chemical processes, benefits of particular designs, battery models and experimental procedures. These selected sections are extracted from abundant electrochemical literature of the lead-acid battery, and are considered the most relevant.

3.6 MICRO-PROCESSES DURING BATTERY OPERATION

This section discusses processes that occur during normal operation, as well as others that predominate during open circuit conditions.

3.6.1 Basic Lead-Acid Electrodes

The positive and negative electrodes are not the only electrodes active in the lead-acid battery. Operation is determined both by electrolyte behaviour and the interactions with further electrode systems operating on the positive and negative electrode surfaces.

a] Two stage electrolyte dissociation

The H_2SO_4 two stage dissociation is a rate determining step (Pavlov,1984:eqn.24):

$$H_2SO_4 \rightleftharpoons H^+ + HSO_4^- \rightleftharpoons SO_4^{2-} + 2H^+$$

where $\log({}^aSO_4^{2-}/{}^aHSO_4^-) = -1.92 + pH$

At pH<1, HSO_4^- is the predominant species
at pH>1, SO_4^{2-} is the predominant species.

At the negative electrode there is an equilibrium between Pb and $PbSO_4$. The reduction reaction occurs either as:

$$PbSO_4 + 2e^- \rightleftharpoons Pb + SO_4^{2-}$$
$$E_h = -0.356 - 0.029 \log {}^aSO_4^{2-}$$
or
$$PbSO_4 + H^+ + 2e^- \rightleftharpoons Pb + HSO_4^-$$
$$E_h = -0.302 - 0.029 \log pH - 0.029 {}^aHSO_4^-$$

depending on which electrolyte ions are dominant (Pavlov,1984:eqns. 8, 9), and E_h is the equilibrium potential of the electrode.

Similarly, at the positive electrode the reduction reaction occurs either as

$$PbO_2 + SO_4^{2-} + 4H^+ + 2e^- \rightleftharpoons PbSO_4 + 2H_2O$$
$$E_h = 1.685 - 0.118pH + 0.029 \log {}^aSO_4^{2-}$$
or
$$PbO_2 + HSO_4^- + 3H^+ + 2e^- \rightleftharpoons PbSO_4 + 2H_2O$$
$$E_h = 1.628 - 0.088pH + 0.029 \log {}^aHSO_4^-$$

depending on which electrolyte ions are dominant (Pavlov,1984:eqns 13, 14).

The steady-state reduction potential of the lead-acid cell is

$$E_{r,cell} = E_{r,right} - E_{r,left}$$

and using IUPAC[1] conventions,

E_{right} =1.685V
E_{left} =-0.356V
E_{cell} = 2.041V (Pavlov,1984)

These are the voltages under no-current situation. Several theoretical equations exist which attempt to determine the potential at non-standard states or when current flows. The Nernst equation determines the cell emf under open circuit conditions as affected by temperature and reactant activities (Pavlov,1984:eqn.78). The Butler-Volmer equation accounts for kinetic losses that occur during non-

1 IUPAC is the International Union of Pure and Applied Chemistry

steady-state conditions (McNicol and Rand,1984:eqn.29). The limitation of these equations is that they are only valid on the micro-scale, and are best left for detailed modelling of the chemical processes themselves.

b) Complex electrode systems - Pourbaix diagram

The conventional method of illustrating complex electrode systems is the Pourbaix diagram. Figure 3.20 shows that at a low pH typical of H_2SO_4 solutions there are several equilibria that are continuously competing, some of which have been previously mentioned.

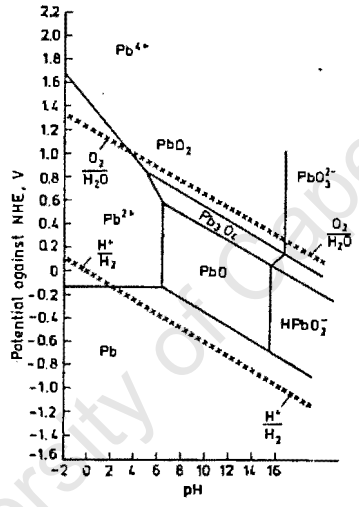

Figure 3.20 Simplified potential/pH diagram of the Pb/H_2O system. according to Pourbaix, at 25°C, for unity hydrogen ion activity.
(Source: Pavlov,1984:fig.1)

The main equilibria to be considered here are the

Pb/Pb^{2+} equilibrium and PbO_2/Pb^{2+} equilibrium

which form the main redox couple. The electrode potential is heavily dependent on the pH due to participation of HSO_4^- ions in the process. The effect of pH on electrode potential (as described in Section 3.6.1(a)) can be seen graphically in the Figure.

Two other electrodes are central to the understanding of battery behaviour:

- At low pH there is a potential exchange between the Pb/Pb^{2+} and the H_2/H^+ electrodes, which could liberate H_2 and oxidise Pb to $PbSO_4$. A mixed potential is established between the two electrodes on the Pb electrode surface.

- At low pH a similar equilibrium exists between the PbO_2/Pb^{2+} and the O_2/H_2O electrodes, which could result in O_2 evolution and reduction of PbO_2 to $PbSO_3$. A second mixed potential is established on the PbO_2 electrode surface.

The Pourbaix diagram also shows that the corrosion of lead by oxidation passes through a region of non-stoichiometric crystals (PbO_x), and the final corrosion mixture will consist of PbO_2 and PbO_x.

All of these processes are discussed in more detail in relation to the processes in the active mass and grid.

3.6.2 Processes in the Active Mass

The fundamental electrochemical process in the active mass in the presence of H_2SO_4 can be described by

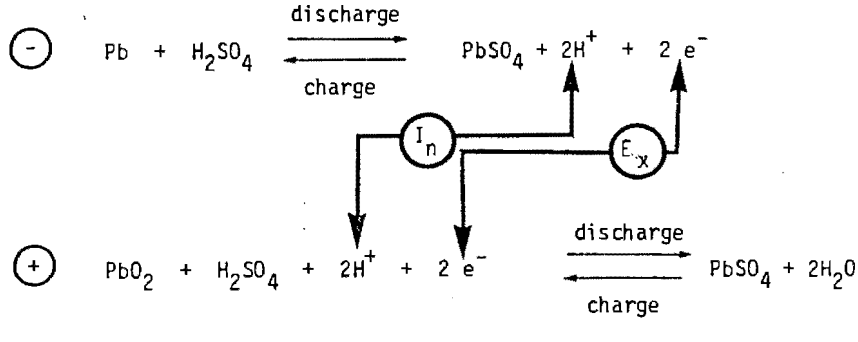

where I_n is the current flowing through the electrolyte, and E_x is the current through the external circuit.

H_2SO_4 plays a double role. Firstly, it reacts with the Pb^{2+} ions and forms an insoluble salt $PbSO_4$ when Pb^{2+} ions are formed on the either electrode surface. The lead of each electrode is not transported in the ion exchange process, and the electrode maintains its mass. Secondly, the charge of the Pb^{2+} ions formed are replaced by the H^+ ions from the H_2SO_4. Current is carried by H^+ and SO_4^{2-} ions (not Pb^{2+} ions). The high mobility of the H^+ ions is the reason for the low internal resistance of the lead-acid cell.

a) Active mass as a porous electrode system.

Cells are designed with high electrode surface area to promote good power performance. This is accomplished by using highly porous active masses. However, the move from smooth to porous electrodes imposes two new limitations.

Electrolyte concentration gradient

The transport properties of the electro-active species (H^+, SO_4^{2-} and H_2O) in the pores of the electrodes are related to the radii of the species. Diffusion limitations alter the composition of the electrolyte in the pores of the plates. Subsequent differences in the solution pH between the pores and the bulk solution may give rise to concentration gradients and polarisation (Section 3.7). During open circuit conditions the concentration gradient between the electrolyte in the pores and the bulk solution will eventually be removed by diffusion. (The SG should be measured after standing in open circuit for 24 hours.) Within a single cycle the phenomenon is considered reversible.

Electrical continuity

As the transfer of electrons between the grid and each site of the active mass is necessary to ensure good utilisation of the active mass, the Pb grid and the PbO_2 active masses are made of separate crystals, and must maintain good electrical contact to facilitate current flow during both charge and discharge. Part of the active mass is required to act as an extension to the grid and may not take part in the electrochemical process, while the remainder takes part and represents the energy providing structure. Replacement of both grids by lighter less expensive and H_2SO_4 resistant material is an ongoing area of research. The material should

be a good conductor, be immune to oxidation or reduction, and should not reduce the hydrogen and oxygen equilibria on the electrode surfaces.

b) Structural problems of the macro-system

In order to ensure high capacity and cycle-life, the energy providing and skeletal structures should be in an optimum ratio. The factors in play are the maintenance of electrical contact between the crystals during charge/discharge cycling, and maximisation of mass and material utilisation.

The reactions occurring during discharge at each of the plates are well known. At the negative plate Pb is converted to Pb^{2+}, the ions diffuse into the solution in the pores, $PbSO_4$ is formed in the pores, and H^+ and SO_4^{2-} diffuse between the pores and the bulk solution. On the positive plate the same electrolyte diffusion reactions occur, as well as solid-phase reactions in the PbO_2 crystals. The processes are reversed during charge.

The rates of reactions at each point in the active mass may be different due to the participation of diffusion and ion migration fluxes. The plates can be considered as several micro-systems, each associated with specific ion and electron fluxes and definite crystals in the active mass. Depending on the charge/discharge conditions and the design of the plates and active block, a distribution of the processes is observed. The distribution of reaction rates is according to the separate micro-systems along the cross-section, height and width of the plate. The distribution occurs during both charge and discharge.

In a given micro-system the elementary processes are not completely reproduced in terms of rate and location during a charge/discharge cycle. Irreversible processes may be considered to occur, eg. the morphology and size of separate crystals is altered during each charge discharge cycle. The micro-irreversible processes may not affect the macro-structure. On a macro-scale the skeletal/energy providing structure should remain unchanged, and the macro-structure is considered to be in a reversible state in terms of capacity, electrical and mechanical parameters.

If unidirectional changes in the micro-system occur during battery cycling then the macro-system as a whole may become damaged to such an extent that the

capacity is affected. Macro-irreversible processes include shedding of the active mass, bulging and hardening of the negative active mass. Causes are natural, but electrolyte stratification especially enhances these effects.

Regular equalisation charging (as described in Section 3.4.5) is the most efficient way to reduce these irreversible effects.

3.6.3 Grid Processes, (decay and life limiting processes)

During cell discharge only those parts of the negative grid exposed to the electrolyte solution are oxidised to $PbSO_4$. The oxidation process occurs until a passivating barrier layer of $PbSO_4$ crystal covers the grid. During charging the process is almost completely reversible on the micro and macro scales. This remains true for the service life of the battery, except if the negative electrode is left in a discharged state for a long period, in which case the $PbSO_4$ crystals become hard and insoluble.

Many patents have appeared which replace the negative grid with a more electro-conductive material. In all cases the replacement adversely effects the reliability, long term performance and increases cost.

Positive grid behaviour is central to the life span and capacity of the deep-cycle battery. Irreversible anodic corrosion occurs here, and changes the structure of the positive plate during cycling. A corrosion layer is formed between the grid and the active mass. It complicates the path of electrons between the active mass and the grid, while the porous part of the layer determines the ionic properties there. The structural, electrical and physical properties of this layer are altered during service life and adversely affect battery performance.

a) Formation of the barrier corrosion layer on the positive grid

The irreversible corrosion of the positive grid affects the battery in two ways:

- It reduces the grid cross section, decreasing the mechanical strength and increasing the electrical resistance.
- It forms a barrier corrosion layer to both electrical conductivity and chemical reaction.

These processes can be combatted by:

- selecting positive plate designs which ensure the least corrosion rate (tubular plates are better)
- use of alloying materials which decrease the corrosion rate
- controlling charging conditions to ensure shortest period of active oxygen evolution (during gassing).

The corrosion layer becomes a component of the positive plate structure. As the active mass is porous the electrolyte penetrates all the way to the grid. This allows processes to take place simultaneously at the corrosion layer and the active mass, both during charge and discharge. Competition may result in formation of $PbSO_4$ crystals in the corrosion layer, which if not oxidised during charging will form a barrier to current flow. The irreversible process begins during initial service life of the battery. The barrier layer exerts a more deleterious effect on battery cycle life than the corrosion process. It has been experimentally shown that lack of antimony enhances the formation of the barrier layer. Figure 3.21 shows the distribution of $PbSO_4$ crystals in Pb-Ca and Pb-Sb grid using electron micrographs. In the Pb-Ca grid the $PbSO_4$ crystals are heavily concentrated on the corrosion layer. The presence of $PbSO_4$ in the corrosion layer is signalled by bent positive plates, causes by mechanical expansion and stress.

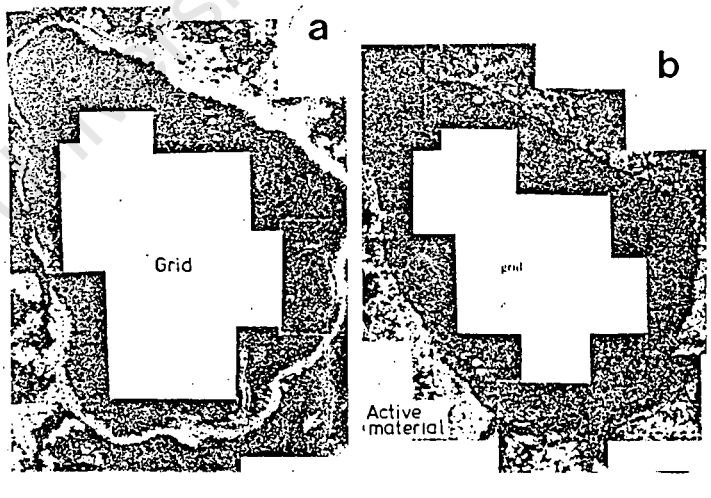

Figure 3.21 Cross-section of grid/corrosion-layer/active mass of plates with Pb-0.09% Ca, and Pb-4% Sb-0.2%. White dots show the distribution of $PbSO_4$. (Source: Pavlov,1984:fig.261)

Experimental evidence shows that the corrosion rate is reduced when the grid is effectively covered by the active mass in both pure lead and antimony alloy spines. There is evidence that the amount of antimony adversely affects the corrosion rate, but covering the grid with active mass eliminated this problem, during the float charge state (Pavlov,1984:476).

Further work by Pavlov shows that the corrosion rate is dependant on the type of polarisation (ie. float or cyclic service). The corrosion rate of pure lead in charge/discharge cycling is three times higher than during float charge. The antimony alloy displayed a reverse effect: the corrosion rate is reduced during cycling. The results provide a basis for selecting positive grid alloy of tubular plates.

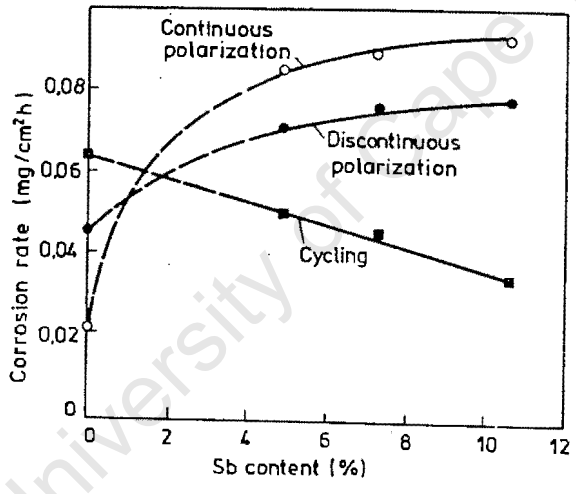

Figure 3.22 Corrosion rate vs antimony content of spines, polarised under three test conditions. (Source: Pavlov,1984:fig.249)

Flat plates behave differently under similar conditions. For 2.5% Sb grids the corrosion rate was 1.4 times higher under cycling than continuous polarisation.

The thickness of the active mass in tubular plates has also been shown to affect the corrosion rate. There is a critical thickness above below which grid corrosion is enhanced. Figure 3.23 equates cycle life to tube diameter.

b) Effect of cycling on corrosion layer structure

Rand et al (1980) have determined that the corrosion layer is initially located along the antimony rich eutectic[2] zones between the solid solution dendrites[3]. Due to changes in the molar volume, internal stresses result in cracking, and the corrosion layer is peeled from the grid. The cracking of the corrosion layer adjacent to the grid changes the transport mode of the electrolyte and the conduction paths through the corrosion layer.

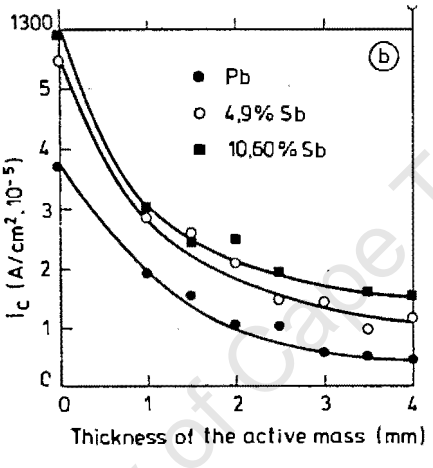

Figure 3.23 Spine corrosion rate as a function of the thickness of the active mass. (Source: Pavlov,1984:fig.250)

c) Corrosion and passivation during positive plate cycle life

The key to failure of the positive plate is the O_2 flux through the corrosion layer resulting from gassing. For small flows, few molecules will reach the grid and the corrosion rate will be low. The grid will last longer and the cycle life will be good. The low fluxes will slowly oxidise PbO formed at the grid to form non-stoichiometric oxides with high ohmic resistances. The resultant voltage drop will decrease the output power and capacity of the battery.

2 Arrangements of the constituents in the alloy arising from their simultaneous crystallisation from the melt.

3 Treelike crystal formations.

For high O^- fluxes the oxides formed will have high stoichiometric coefficients and good conductivity, and no passivating barrier layer is formed, but grid corrosion will be enhanced.

The corrosion and passivation are opposed. Pavlov (1984:485) recommends adding additives to the alloy that decrease the corrosion rate, yet act as impurities in the semi-conductive oxide and increase the conductivity of the layer. The additives could also accelerate the oxidation process of PbO and maintain the high stoichiometric coefficients and conductivity. Antimony is such an additive.

d) Stress-corrosion of the positive grid

Stress corrosion cracking occurs along the entire cross-section of the grid, usually following the grain boundaries of the positive grids. Often fissures are formed and the electrical conductivity is compromised. The cracking originates firstly in the formation of micropores in the cooling of the grid casting. The micropores provide a path for oxygen and subsequent corrosion.

The second cause is the mechanical loads to which the grid is subjected by the growth of the corrosion layer. The positive grid grows during cycling. The strains initiated between the grid and the corrosion layer lead to cracking of the grid and the corrosion layer itself.

During charge/discharge cycling the weight of the plate is increased and decreased. If the plate is not securely fixed, the changes in weight as well as vibrations are transmitted to the grid, and stress-corrosion is enhanced.

e) Loss of antimony

During the life of the battery the grids of the positive plate are corroded, the antimony from the grids moves into the corrosion layer, is dissolved into the electrolyte solution and is deposited onto the negative plate. The hydrogen overpotential (gassing voltage) of the negative plate is reduced. During overcharge, gaseous stibine (SbH_3) is formed and leaves the cell. Antimony on the negative plate can be oxidised by dissolved oxygen in the electrolyte, and be transported back to the positive plate via ionic migration.

3.7 POLARISATION AND OVERPOTENTIAL

In this section the concepts of polarisation and overpotential are introduced. Emphasis thereafter is on the highly polarised hydrogen and oxygen electrodes on the plate surfaces.

3.7.1 Types of Polarisation

Analysis of the discharge reaction can provide a great deal of information into the operation of the lead-acid battery. The battery electrolyte is an aqueous solution of sulphuric acid. Sulphate ions are consumed at both electrodes during discharge, while hydrogen ions are consumed only at the positive. Water is a by-product of the reaction at the positive electrode.

The depletion of the reactants at the electrodes and the production of water contribute to a phenomenon called polarisation. Polarisation reduces the capacity of the battery to do useful work, and is manifested as a voltage drop. Polarisation is an indication of the cell's inability to do reversible work under dynamic conditions. Polarisation is caused by overpotential.

There are three types of overpotential:

a) activation overpotential, resulting from limitations to the charge transfer process. ie. a rate determining step involving an energy barrier.

b) concentration overpotential, caused by the slow movement of the electro-active species, and the subsequent departure of the interfacial concentrations (in the porous mass) from the bulk values. This has been further divided into diffusion overpotential and reaction overpotential. Diffusion overpotential is caused by the depletion of reactants at the electrode surface. Reaction overpotential results from the existence of a rate determining step.

c) resistance overpotential arising from hinderance by the products of the reaction ie. formation of surface films of high resistance, such as the barrier corrosion layer.

During battery discharge the voltage is less than the rated cell voltage or open circuit voltage. Initially there is a voltage loss due to activation overpotential, (a loss typical of all lead-acid batteries) and a small loss due to internal resistance of the cell. As the discharge continues the voltage decreases. The decrease in voltage is due to the increase in diffusion polarisation effects, since to provide current, the electrolyte must penetrate the active mass.

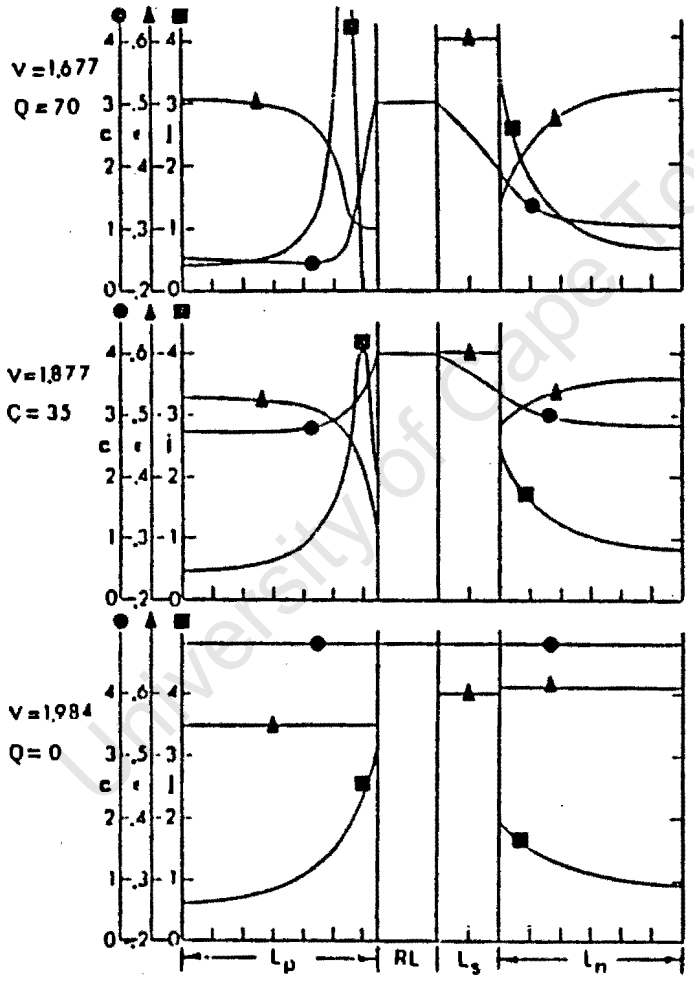

Figure 3.24 Transient behaviour of transfer current (j), electrode porosity (ε) and electrolyte concentration (c) within the cell during constant current discharge. (Source: Tiedemann and Newman,1978:fig.5)

During battery charging the voltage is greater than the rated cell voltage. The losses are initially due to increased resistance of cell electrolyte. As the cell

becomes charged, the conductivity of the electrolyte increases, but the ability of the cell to completely utilise the charging current is limited by diffusion effects. The charging current must be tapered (limited) to allow for limitations in the ion transfer process. If the current is not tapered the excess current, which cannot be usefully utilised for charging, is used to electrolytically dissociate water, as this is the reaction with the next lowest activation overpotential. The voltage increases sharply when the gassing phase.

The effect of polarisation on battery discharging and charging is shown in Figure 3.25. The lead-acid battery is regarded as weakly polarised, ie. the processes can proceed more or less reversibly until blocked by physical processes. The "internal resistance" of the battery consists of both real resistance and polarisation effects.

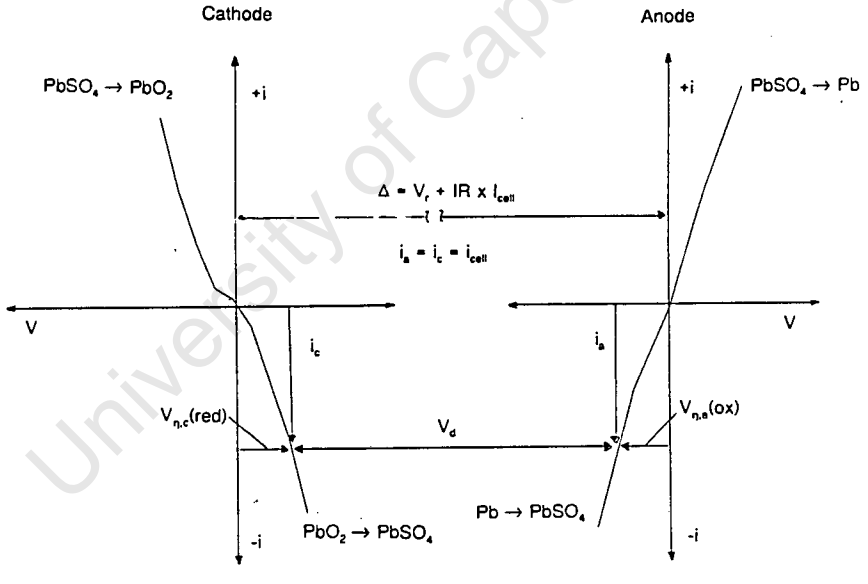

Figure 3.25 Variation of cell potential during discharge. Subscript r denotes equilibrium conditions, subscript i denotes operating conditions, while subscripts a and c denote anodic and cathodic processes. Subscript η denotes polarisation. (Source: McNicol and Rand,1984:fig.10)

The cell operating voltage is:

$$V_{i,cell} = V_{r,cell} + IRxI_{cell} + V_{\eta,c}(reduction) - V_{\eta,a}(oxidation)$$

$$I_{cell} = I_a = I_c < 0 \text{ for discharge}$$

As described above, V_η varies with SOC, and internal resistance, *IR*, varies with electrolyte concentration. Both are temperature dependant.

The Pourbaix diagram (Figure 3.20) showed that hydrogen and oxygen electrodes are established on the lead surface. These electrodes are very interesting because they are highly polarised, and their reactions proceed unidirectionally. Hydrogen and oxygen overpotential are discussed below.

3.7.2 Hydrogen Overpotential

In addition to the $Pb/PbSO_4$ equilibrium on the negative electrode surface, there is a hydrogen equilibrium reaction.

$$2H^+ + 2e^- \rightleftharpoons H_2$$

At steady-state a potential of close to 0.3V exists between the $Pb/PbSO_4$ and H_2/H^+ electrodes. At non-steady state conditions both electrodes become polarised. The relationship between the current and potential of the electrodes is shown in Figure 3.26.

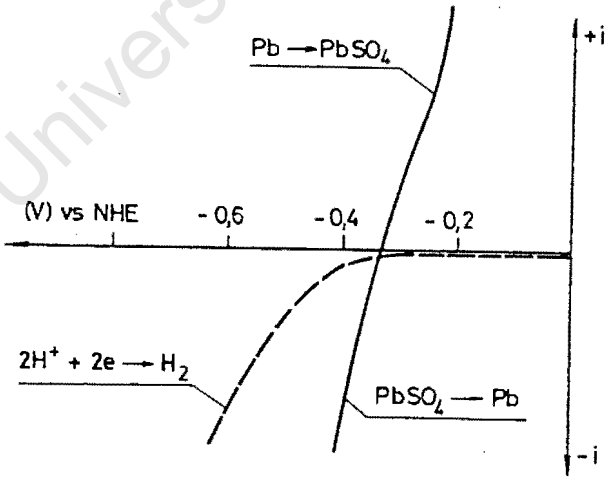

Figure 3.26 Current/potential curves for polarisation of $Pb/PbSO_4$ and H_2/H^+ electrodes in H_2SO_4 solution. (Source: Pavlov,1984:fig.6)

Polarisation of the $Pb/PbSO_4$ electrode is slight, so that the oxidation of Pb and the reduction of $PbSO_4$ proceed almost reversibly. The H_2/H^+ electrode is very highly polarised and is almost completely irreversible - the evolution potential of

H_2 has more negative values than the PbSO4 reduction. The highly polarised nature of this electrode has enabled its use in the lead-acid battery.

If the electrodes are stored in open circuit conditions a net reaction occurs between the H_2/H^+ and $Pb/PbSO_4$ electrodes. At the steady-state potential of -0.3V a very small steady-state exchange current is present. The current is so small that the equilibrium potential may be assumed to be equal to the steady-state potentials. Clearly, as shown in the diagram, the electron exchange will cause oxidation of Pb to $PbSO_4$ and reduction of H^+ to H_2. This reaction on the negative electrode is the "self-discharge of the electrode".

During discharge conditions the H_2/H^+ electrode is too highly polarised to take part in the reactions.

During charging conditions the ability of the Pb and $PbSO_4$ phases to exchange electrons ions will determine the period during which the $Pb/PbSO_4$ electrode will accept current. The rate at which current can be accepted may be limited by physical phenomena, such as blocking of ion exchange paths. If the potential required to reduce H^+ to H_2 is less than the potential to overcome the physical phenomena (diffusion overpotential), gassing in the form of H_2 will be seen to occur. The observed electrode potential on the $Pb/PbSO_4$ surface will be more negative.

The effect of grid additives on hydrogen overpotential can now be fully appreciated. Antimony and silver additives tend to decrease the hydrogen overpotential. Expanders tend to increase the overvoltage. The charge and the self-discharge of the negative plate is therefore directly affected by the use of additives. The higher the H_2/H^+ electrode overvoltage, the more efficient the charge and the lower the self-discharge.

3.7.3 Oxygen Overpotential

An oxygen equilibrium reaction co-exists with the $PbO_2/PbSO_4$ equilibrium on the positive plate in the same way as the hydrogen equilibrium co-exists on the negative electrode. The equilibrium potential difference between the $PbO_2/PbSO_4$ and H_2O/O_2 electrodes is about 0.5V. The relationship between the current and

potential of the electrodes is shown in Figure 3.27. The $PbO_2/PbSO_4$ electrode is considerably more polarised than the $Pb/PbSO_4$ electrode. The H_2O/O_2 electrode is very highly polarised and is completely irreversible; behaviour which has enabled its use as one of the electrodes in the cell.

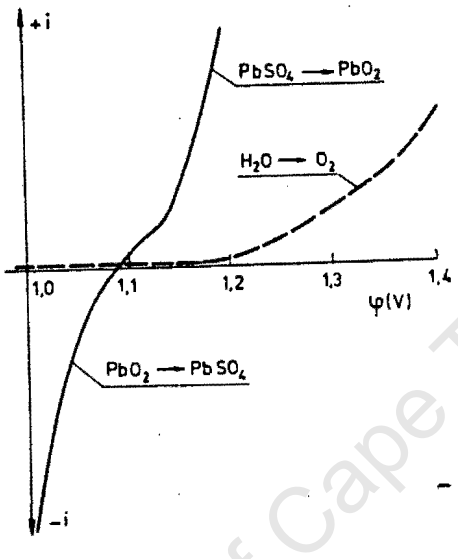

Figure 3.27 Current/potential curves for polarisation of $Pb/PbSO_4$ and O_2/O^* electrodes in H_2SO_4 solution. (Source: Pavlov,1984:fig.38)

During open circuit conditions the exchange current between the electrodes is equal. The steady state current exchange between the electrodes is small, but is sufficient to cause self-discharge of the negative plate over a prolonged period, with simultaneous oxygen evolution.

During discharge conditions the H_2O/O_2 electrode is too highly polarised to take part in the reactions.

During charging conditions the $PbO_2/PbSO_4$ electrode will normally donate electrons, as the potential required is lower than for the H_2O/O_2 oxidation. As the battery becomes more fully charged the $PbO_2/PbSO_4$ electrode becomes more polarised (due to diffusion overpotential or some other rate limiting steps) and cannot donate electrons at the required rate. The oxygen evolution reaction will begin. The positive plate potential will be increasingly better represented by the oxygen electrode potential as more of the charging current is consumed in oxygen evolution.

3.7.4 Overpotential and Polarisation During Charge

The change in "internal resistance" by polarisation during battery discharge has been discussed. The change in polarisation during battery charging is affected by the electrode polarisations, by changes in electrolyte conductivity, and also the interactions of the hydrogen and oxygen electrodes on the negative and positive cell electrodes respectively.

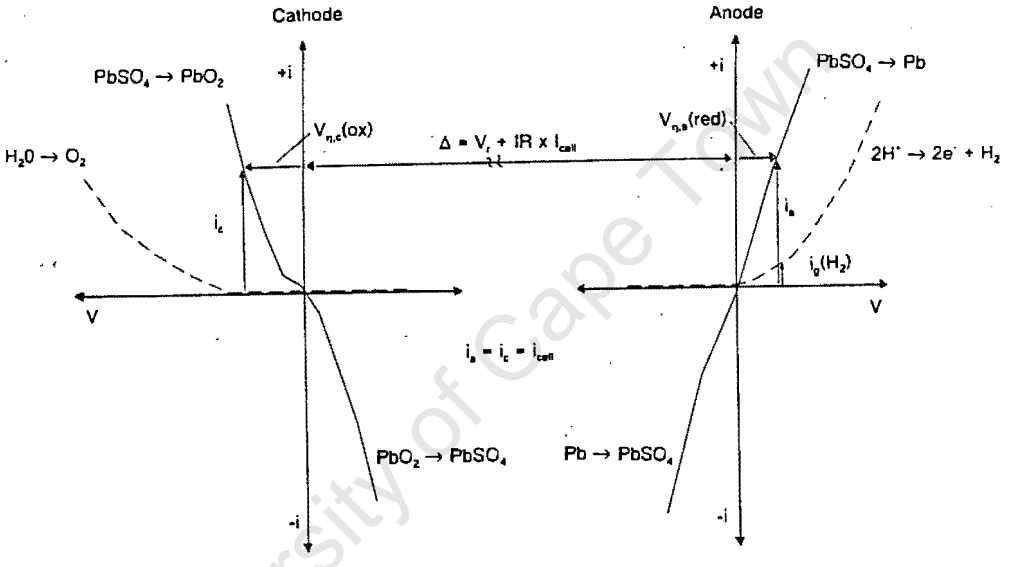

Figure 3.28 Variation of cell potential during charging. Subscript r denotes equilibrium conditions, subscript i denotes operating conditions, while subscripts a and c denote anodic and cathodic processes. Subscript η denotes polarisation, and subscript g gassing. The H_2/H^+ and H_20/O_2 electrodes are superimposed.

Cell voltage during charging:

$$V_{i,cell} = V_{r,cell} + IRxI_{cell} + V_{\eta,c}(oxidation) - V_{\eta,a}(reduction)$$

$$I_{cell} = I_a = I_c > 0 \text{ for charge}$$

$$I_{g,c} = I_g(O_2) = f(V_c) \text{ and } I_{g,a} = I_g(H_2) = f(V_a)$$

Under normal charging conditions, the charging efficiency at the cathode and anode are

$$\eta_c = (I_c - I_{g,c})/I_c, \text{ and } \eta_a = (I_a - I_{g,a})/I_a$$

As before, polarisation V_η varies with SOC, and internal resistance IR varies with electrolyte concentration. Both are temperature dependent.

When the cell is fully charged, $V\eta,c$ increases to correspond with the H_2O/O_2 polarisation curve, so that $Ig,c=Ic$ and all the charge current is consumed by gassing at the cathode. A similar phenomenum occurs at the anode.

3.8 MACRO-PROCESSES DURING OPERATION

3.8.1 Electrolyte Stratification and Recovery

Electrolyte stratification is often observed in flooded electrolyte batteries.

The concentration of the electrolyte in the upper reservoir of the cell decreases during discharge and increases during charge. During cycling processes concentration gradients are formed.

Experimental evidence shows that stratification is enhanced during deep cycling, and that concentration differences accumulate (Figure 3.29). It has also been shown that concentration gradients between the bottom and middle of the cell are less pronounced than the differences between the top and middle, implying that the top half of the cell participates more actively in the discharge process. The process can be visualised by considering the resistance paths and current flow.

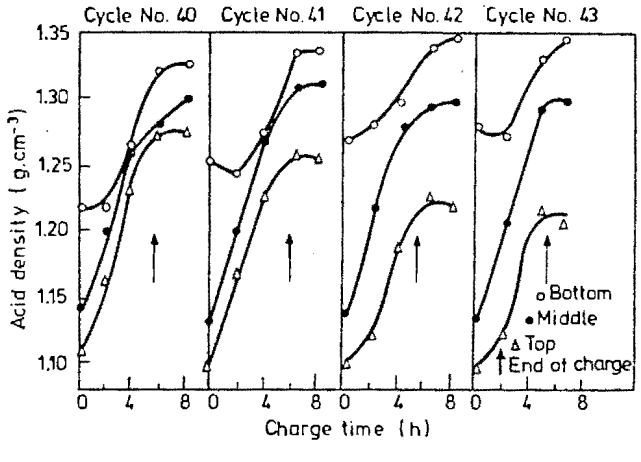

Figure 3.29 Stratification of electrolyte measured during charging to 2% overcharge and 100% DOD. (Source: Pavlov,1984:fig.223)

Because the electrolyte is an active material, stratification affects cell capacity. The capacity losses are due to the concentration differences, and are termed diffusion capacity losses. Diffusion losses are generally reversible: when the concentration gradients are removed, the capacity is restored. Gas evolution during overcharge causes efficient mixing by gas-lift stirring of the electrolyte, but it is has also been shown that excess gassing results in scrubbing of the active material, and leads to an increase in the rate of active material shedding (Rand et al,1980).

Stratification losses may not be reversible in the long term. On the macro-scale, the cell is worked unevenly. As a result corrosion and slow $PbSO_4$ formation will attack the grid unevenly and are likely to cause premature failure of the cell.

3.8.2 Gassing and Related Phenomena

Gassing in the lead-acid battery is central to the operation of the battery. The voltage at which gassing occurs (determined by the O_2 and H_2 overpotentials) determines the self discharge of the battery. Gassing directly affects the charging efficiency of the battery and is the only practical way to eliminate electrolyte stratification in flooded electrolyte cells. However, excess gassing may decrease the life of the cell by increasing the rate of active material shedding. Gassing also increases the flux of O^- radicals and enhances the corrosion of the positive grid. Gassing consumes water and determines the frequency of maintenance of the cell.

Further, the gassing voltage is negatively dependent on temperature, and is dependant on grid alloys and additives. The H_2/O_2 mixture is explosive, and in antimony grid cells the gas may contain traces of toxic gas.

a) Self-discharge

The discussion of hydrogen and oxygen overvoltage shows that the self-discharge produces H_2 and O_2 gas, and that self-discharge of the positive and negative plates need not proceed at the same rates. It is clear that the amount of gas evolved during self-discharge is small. Typical self-discharge rates are 1%-3% per month for a low antimony grid cell and water loss is approximately 0.4ml/Ah of self-discharge. Self discharge is increased by increased antimony content, and also by temperature. (See Figure 3.11.)

b) Charging Efficiency

The charging efficiency of the battery is, by definition, the amount of charge stored relative to the amount being input by the charging system. For input current I, and gassing current I_g, the charge efficiency is

$$\eta_{ch}=(I-I_g)/I.$$

As the battery becomes fully charged the charge efficiency progressively falls. The charge efficiency is related to the suppression of the H_2 and O_2 evolution and enhancement of Pb and PbO_2 formation rates. Further it is interesting to note that charge acceptance of the positive plate does not reach zero (Figure 3.30). This is because the reactions occur entirely within the potential region for O_2 generation (Lakeman,1989). The charge acceptance of the negative plate is almost 100% at 25°C (Bode in Pavlov,1984:422).

If the gas mixture is assumed stoichiometric (in H_2 and O_2) and the gas flow is measured, then the instantaneous charging efficiency can be estimated. Lakeman (1989) has monitored the separate plates and found the error due to this approximation is small. He finds that the gassing current can be easily estimated from the individual plate potentials.

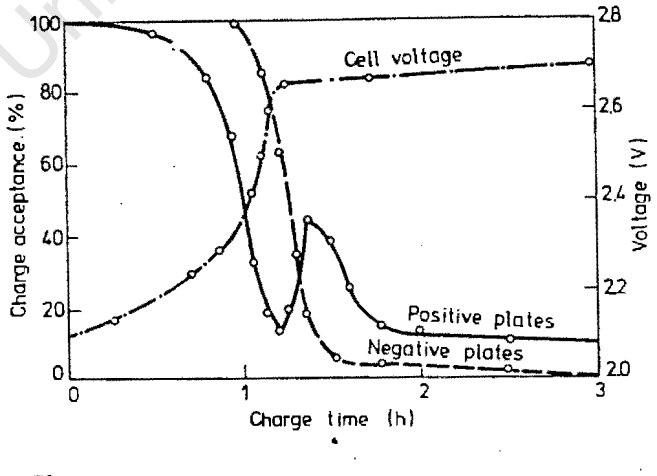

Figure 3.30 Charge acceptance of positive and negative plates at 40°C vs time. (Source: Pavlov,1984:fig.210)

c) Gas Composition

The ratio of H_2:O_2 is stoichiometric (2:1 ratio) when the cell voltage is high and when gassing rates are high. At slight gassing rates the ratio will be closer to 1.1:1, as is not uncommon for one plate to begin gassing before the other (Vinal, 1955:262). In most cases the mixture will approximate stoichiometric.

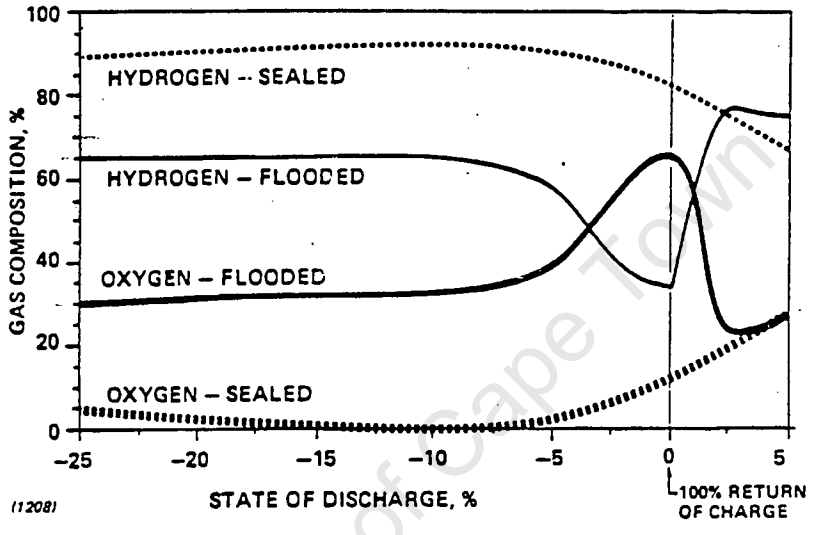

Figure 3.31 H_2/O_2 ratio during charge acceptance.
(Source: Lakeman,1989; Szymborski,1982:fig.18)

The transfer of antimony and arsenic to the negative plates during corrosion of the positive grid can result in release of stibine (SbH_3) and Arsine (AsH_3) during the gassing stage on the negative plate. Both these gases are extremely toxic. Varma et al (1989) have shown that after 10 charge/discharge cycles the rate of evolution of these toxic gases is reduced, and that by charging below 2.4V per cell the evolution is suppressed. The movement of antimony in the cell has already been discussed in Section 3.6.3(e).

d) Gassing and Grid Corrosion

Evolution of O_2 at the positive plate enhances corrosion of the grid, but high flux of O^- radicals will tend not to favour the formation of a low stoichiometric ratio and lead-oxide barrier layer of PbO_n with poor electrical characteristics. These competing reactions are discussed in Section 3.6.3.

e) Calculation of Gassing Current and Energy

Gassing is primarily the result of the decomposition of water. For every mole of water decomposed, 1 mole of H_2 and 2 moles of O_2 are evolved according to the equations

$$O_2 + 4H^+ + 4e^- \rightharpoonup H_2O$$
$$4H^+ + 4e^- \rightharpoonup 2H2$$

For each 4 moles of electrons provided, 3 moles of gas are evolved.

If the measured flow of gas is Xmls^{-1} per cell at standard temperature and pressure (STP)[4], then the overcharge current can be derived:

$$\frac{X \times 10^{-3} l}{s} \times \frac{1\,mole}{22.4l} \times \frac{1\,mole\,O_2}{3\,mole\,gas} \times \frac{4\,mole\,e^-}{1\,mole\,O_2} \times \frac{1.602 \times 10^{-19} C}{e^-} \times \frac{6 \times 10^{23} e^-}{mole}$$

$$= X \times 5.74A$$

This equates to a loss of 0.336ml H_2O per Ah of overcharge per cell.

3.9 METHODS OF REDUCING WATER LOSS

3.9.1 Water Loss

The primary maintenance requirement of the lead-acid battery is the replacement of water. The second requirement is regular equalising charge. (See 3.6.2(b) Structural Problems of the Macro-system.)

Water is lost from lead-acid batteries by three main routes
- electrolysis of water during overcharge (gassing)
- electrolysis of water during self-discharge
- evaporation, in hot climates or while the battery is heavily worked.

4 STP is defined as 0°C and 760mm of mercury.

Maintenance of cells is time-consuming, yet neglect of the cells could result in exposure of the plates to atmospheric O_2 with subsequent oxidation corrosion. Maintenance free characteristics may be desirable in remote power supply applications.

In the most basic case, a simple vent plug vents the gases to atmosphere. Water loss by gassing is not significantly reduced, typically only 5% reduction in conventional cells, but the reduction in spillage loss through sputtering and evaporation is noticeable in a well designed plug. The methods of reducing water loss that are appropriate for PV applications, and becoming widely used in specialised PV batteries, are:

- catalytic recombination of the gases
- auxiliary electrodes for closed H_2 and O_2 cycles
- increasing the O_2 and H_2 overvoltages by using antimony free alloys.

All of the methods affect the cell performance.

3.9.2 Catalytic Recombination of H_2 and O_2

The recombination of H_2 and O_2 tackles two problems simultaneously. Water loss is reduced so water addition is not required, and the need for a gas vent is eliminated. A catalytic plug is instead included. These plugs can easily be retro-fitted to most batteries.

H_2 and O_2 are recombined to gaseous water vapour over a platinum catalyst. The water vapour is then condensed to liquid The recombination efficiency of the plug is approximately 65%.

The gasses are required to be in a stoichiometric ratio for complete reaction, which is not necessarily the case (see 3.8.2(c)). Substantial heat is evolved during the recombination, and the temperature in the plug may reach 400°C (Pavlov,1984:376) when gas flow rates are high. This temperature is near the explosive point of the mixture. The heating at the plug may cause heating in the battery, which will decrease the O_2 and H_2 overvoltages and cause higher gas flows. The resultant heating provides a path for a thermal run-away situation. The conversion coefficient of the plug depends on the gas flow rate and temperature, the rate of

product removal. The catalyst may become poisoned by impurities through use. Grid alloys which produce poisonous vapours during gassing are therefore not viable options, yet it is precisely these grids that most require water recombination, as additives usually decrease the O_2 and H_2 overvoltages. Finally, the cost of platinum-group metals for catalyst is prohibitive.

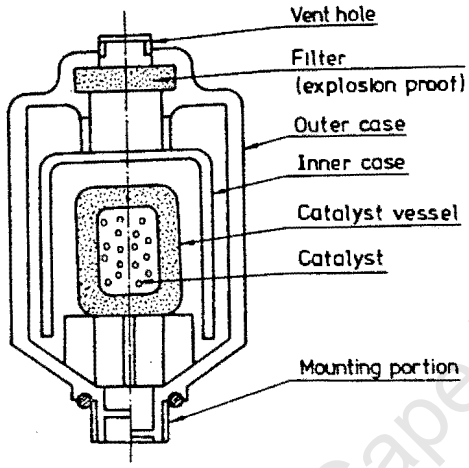

Figure 3.32 Cross section of a catalytic plug.
(Source: Pavlov,1984:fig.180)

3.9.3 Closed O_2 and H_2 cycles

When the gases are not evolved in stoichiometric amounts the full benefit of the catalytic plug cannot be obtained. The excess O_2 and H_2 can be fixed by introducing auxiliary electrodes into the cell.

a) Oxygen cycle with auxiliary electrode

The auxiliary electrode is a porous, hydrophobic, gas-diffusion, conductive, carbon electrode immersed in the electrolyte. The electrode contains a catalyst for oxygen reduction, and is maintained within a set voltage range by an external electronic circuit (Figure 3.33). Cobalt and iron will catalyse the reaction in the presence of acid.

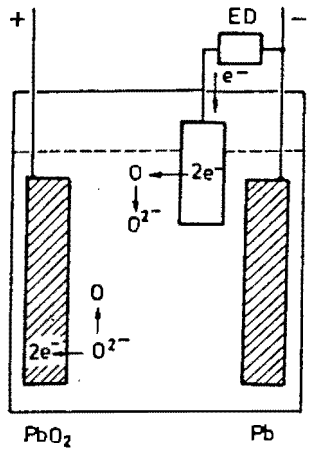

Figure 3.33 Schematic of a cell with an auxiliary electrode.
(Source: Pavlov,1984:fig.181)

The oxygen evolved at the positive plate is reduced at the auxiliary electrode, in the presence of hydrogen ions and the electrode current, to form hydrogen peroxide. One oxygen molecule can be temporarily stored by only one hydrogen molecule equivalent. When the negative electrode eventually begins gassing and sufficient H_2 is evolved, the peroxide is reduced to water by the second reduction reaction. The second reduction is linked to oxidation of H_2 at the negative plate. The reactions are

PbO_2 electrode: $2H_2O \rightleftharpoons 4H^+ + 4e^- + O_2$ (oxidation)

Auxiliary electrode: $O_2 + 2H^+ + 2e^- \rightleftharpoons H_2O_2$ (reduction)
$H_2O_2 + 2H^+ + 2e^- \rightleftharpoons 2H_2O$

The process shows that the excess oxygen is fixed till it can be recombined with hydrogen.

b) Simple oxygen cycle

A similar process proceeds without an auxiliary electrode. The oxygen evolved at the positive plate is reduced at the negative plate by the self-discharge reaction:

$$O_2 + 2Pb + 2H_2SO_4 \rightarrow 2PbSO_4 + 2H_2O$$

This reaction may be used to remove oxygen in a sealed cell, but is limited in a flooded electrolyte system by the rate of oxygen solubility and diffusion through the electrolyte to the plate. The rate limiting factors can be overcome by providing a direct pathway for gaseous oxygen. The oxygen is then consumed by the negative electrode, which remains in a partial SOC and prevents hydrogen evolution.

The oxygen recombination has a depolarising effect on the negative plate, (Mahato et al,1987; Maja and Penazzi,1989),and this is shown in Figure 3.34 (Tuphorn,1987). It is necessary to reduce the charging voltage once gassing has occurred, usually to 2.35V/cell.

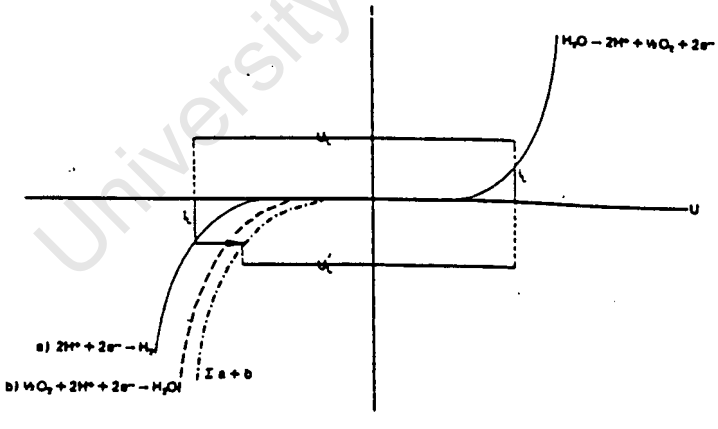

Figure 3.34 Influence of O_2 recombination on the polarisation of the H_2/H^+ electrode. (Source: Tuphorn,1987)

Areas of negative plates of both O_2 recombination types have been known to sulphate, mainly due to the diffusion of the peroxide with subsequent oxidising of the lead, which keeps the plate in a partial state-of-charge. During partial state-of-charge operation large grain sulphate crystals may form. If the cell is not air tight then the atmospheric O_2 is reduced to peroxide, and increases the rate of

negative plate self-discharge. The cells are usually sealed, operate at a slightly positive pressure and are equipped with an emergency pressure release valve.

For the cell pressure to stay within limits the rate of gas recombination should be greater than the rate of gassing. Ideally the rate of recombination should be expressed as a current, and the finishing charge current should be less than this current. A theoretical derivation for the current rate of O_2 recombination (I_{O2}) follows.

During recombination:

$$O_2 + 2H^+ + 2e^- \rightharpoonup H_2O_2$$
$$H_2O_2 + 2H^+ + 2e^- \rightharpoonup 2H_2O$$

The reactions show that 4 moles of electrons are required per mole of O_2 recombined.

As O_2 is gas in excess, the rate of change of O_2 is related to the pressure by the ideal gas laws:

$$\frac{dO_2}{dt} = \frac{V}{RT}\frac{dP_{O_2}}{dt}$$

The recombination current can be related to the rate of O_2 recombination by Faraday's laws:

$$I_{O_2} = \frac{dO_2}{dt}\frac{4e^-}{mole\,O_2}F = \frac{4FV}{RT}\frac{dP_{O_2}}{dt}$$

But pressure is exponential as the reaction is pseudo first order in O_2, so

$$\frac{d\ln P_{O_2}}{dt} = k$$

Integrating:

$$\ln P_{O_2} = kt + c$$

Rearranging:

$$P_{O_2} = e^{kt}e^{c}$$

Now differentiating yields:

$$\frac{dP_{O_2}}{dt} = ke^{c}e^{kt} = \frac{d\ln P_{O_2}}{dt}P_{O_2}$$

This result can be substituted back to yield:

$$I_{O_2} = \frac{4FV}{RT}\left[\frac{d\ln P_{O_2}}{dt}\right]_{T,V} P_{O_2}$$

b) Hydrogen cycle

The design of the closed hydrogen cycle is similar to the oxygen cycle, but is currently restricted by the cost of platinum-group catalysts. Further, it is normally O_2, not H_2, that is required to be stored as it is the first product of gassing.

3.9.4 Antimony-free Alloys

The manner in which positive grid antimony alloys enhance battery cycle life, yet increase self-discharge by decreasing gassing overvoltages have already been discussed in detail.

Non-antimonial grid alloys that do not lower the O_2 and H_2 overvoltages will decrease water loss considerably.

However, antimony-free cells are not suitable for cycling applications (due to the formation of a passivating $PbSO_4$ in the corrosion layer during deep discharge). Optimal performance is achieved in non-cycling applications, where the need for gassing is minimal as the accumulation of electrolyte stratification is slight. Gassing in antimony free cells is limited by maintaining the cells in a float charged condition, nominally 2.3V per cell.

3.10 ELECTRICAL CHARACTERISATION MODELS

3.10.1 Introduction

There are two broad categories of battery models:

i) physical/chemical
ii) phenomenological.

The first category is generally complex, focusing on the physical and chemical dynamics, and is useful for understanding the processes in the battery itself. It is a truly specialist approach, probably beyond the scope of the non-chemist or engineer. (For an illustrative example see Tiedemann and Newman (1978) in Figure 3.24).

The phenomenological model is more of a black-box approach. Some measurable parameters are input to the model, and some other measurable parameters are output. Little attempt is made to explain the dynamics, but emphasis is on linking the interdependencies of the measurable parameters, eg. to provide current and voltage in both charge and discharge operation, at various states of charge, different temperatures, etc. A phenomenological model, as applied to batteries, is simply a predictor model. It cannot be deterministic, as only the observed degrees of freedom (voltage, current, SOC, vs temperature) are mathematically modelled. Factors such as degradation, which depend on internal dynamics and cumulative effects, cannot be easily computed.

This review is concerned only with the phenomenological models of lead-acid batteries. The following topics are discussed: electrical characterisation, capacity, charging efficiency and self-discharge. Cycle life modelling is discussed in Section 3.12.

3.10.2 Electrical Characterisation of the Battery

This section reviews models that could be used to describe the current, voltage, SOC relationship in an operating battery. The models are considered for numerical simulation of PV systems.

a) Linear and non-linear circuit element analysis.

Some of the phenomenological models have used both linear and non-linear circuit analogues to describe the electrical characteristics of the batteries (Klingeret al,1980 and Waaben et al,1985). Linear analysis cannot simulate many non-linear characteristics, such as transients, recovery from deep-discharge and gassing effects. While non-linear analysis can be effective, integrated circuit simulation computer programs are required to solve these complex problems. Modelling of the battery in dynamic simulation environments is therefore too complex for normal use.

b) Numerical modelling

Most numerical models draw heavily on previous work by Shepherd (1965) and Lindstrom (1970), whose models are based on the variation of apparent "internal resistance" of the battery with SOC and current. Lindstrom observed that voltage during a constant-current discharge closely follows the relation:

$$V = E\ (\ q/q_{max}(I)\ ) - IR$$

where V is the voltage, E is the cell emf, q is the ampere hours discharged, $q_{max}(I)$ is the ampere-capacity at current I, and R is a constant resistance term.

Hyman (1977) developed a Lindstrom/Shepherd model variation that is optimised for large scale load-levelling discharge simulation. While accurate for high current work, this model is inappropriate for low current PV simulation.

Facinelli (1983) proposes a PV battery model founded on modified Shepherd (1965) discharge model, incorporating the temperature effect on voltage. A charge model of similar form is proposed:

$$V = V_c + IR_c\,(1 + M_cQ/(QC'-Q)\ ),\quad I>0$$
$$V = V_d + IR_d\,(1 + M_d(QD-Q)/(QD'+Q)\ ),\quad I<0$$

where open circuit voltages are

$$V_c = a_1+b_1T$$
$$V_d = a_2+b_2T$$

and internal resistances

$$R_c = a_3 + b_3/QC$$
$$R_d = a_4 + b_4/QD$$
$$QC' = a_5\, QC$$
$$QD' = a_6\, QD$$

Charging efficiency is simply a function of state-of-charge. (see charging efficiency modelling, Section 3.10.4.)

The Facinelli model is elegant, and contains sufficient variables to represent most batteries, but appears to have been verified using only high discharge currents and high charge currents (of about I_8). This belief is supported by the fact that discharge capacities are modelled using the Peukert equation (see capacity modelling, Section 3.10.3), which is widely recognised as being inadequate for low currents. The constants used in the Facinelli model are especially difficult to regress successfully when low currents typical of PV systems are considered. It remains, nevertheless, the most versatile model considered.

The Mobil-Tyco model was developed by Wood and Crutchen (1980), also for PV battery modelling. Voltage and current are calculated from experimentally derived expressions for cell internal resistance and open circuit voltage. The internal resistance is dependant on SOC and whether the battery is charging or discharging, but not the rate of charge (or discharge). Gassing is a function of SOC rather than of charging voltage, and occurs at 64% SOC (see charging efficiency model, Section 3.10.4). The model shows good correlations with discharge profiles, but correlation with charging profiles is accurate only in the 40% to 70% SOC range, with poor correlation elsewhere (BDM,1983).

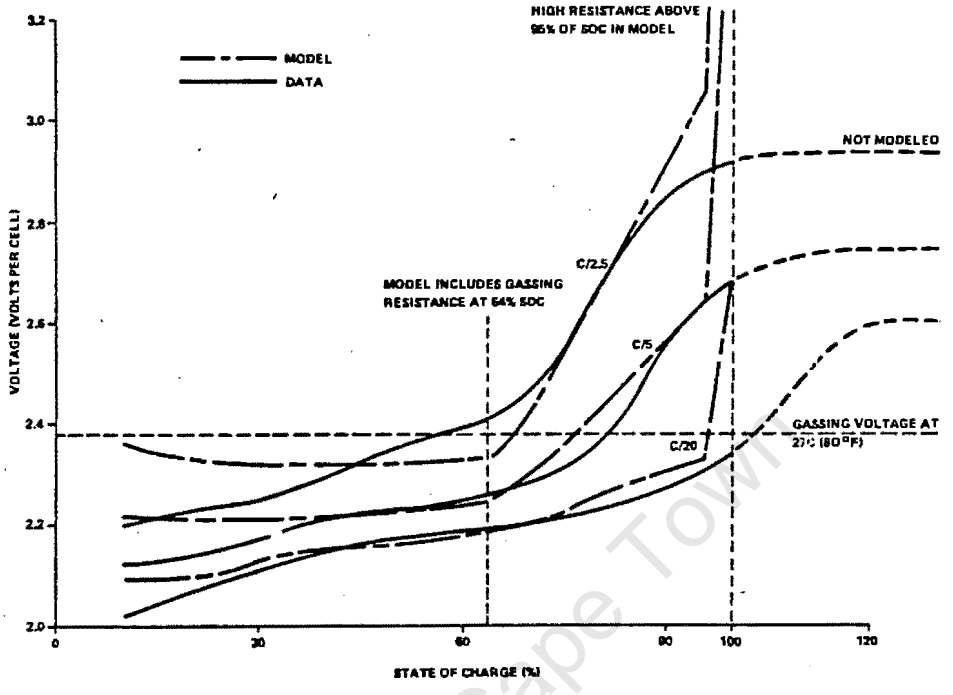

Figure 3.35 Comparison of Mobil-Tyco Model with measured data for charging. (Source: BDM,1983)

The BDM (1983) lead acid battery model was contracted by Sandia National Laboratories after the shortcomings of the Mobil-Tyco PV battery model were recognised. The model is formulated solely on the basis of the apparent resistance (RA), dependant on current and SOC. $RA_{SOC's}$ are calculated for constant-current charging and discharging. The RA ratio, ($RA_{SOC}/RA_{SOC=100}$), is independent of current, but dependant on whether the battery is charging or discharging. The model requires fitting of a third order polynomial to the ordered RA ratio:SOC data. This numerical approach can provide a far more satisfactory fit to measured data than the Mobil-Tyco model, but contributes little to understanding battery behaviour further than polynomial behaviour. Battery characteristics cannot be easily or meaningfully altered by changing simple model parameters, so the model becomes clumsy in that respect.

For precision modelling using real data, Liesgang et al (1988) propose a database method designed for Ni-Cd and Ni-H_2 cells. The database comprises families of constant-current curves describing the voltage versus state-of-charge as

determined in the laboratory and supplemented by interpolated curves. Battery modelling is accurate with minimal preprocessing requirements. This approach has been adapted to lead-acid batteries by Geerdts (1990), for accurate PV system simulation to obtain improved understanding of PV system sizing and dynamics.

3.10.3 Capacity

The standard model presenting capacity (C_d) as a function of discharge current (I_d) is the Peukert (1897) correlation.

$$C_d = \frac{K}{I_d^{(n-1)}}$$

where K is a constant dependant on the temperature, electrolyte concentration and design of the active block, and n is a constant approximately equal to 1.4, and is the slope of the log-log plot of discharge time versus discharge current.

The Peukert equation has been adapted for temperature by Baikie (1972).The term K is modified for temperature:

$$K_t = K_0(1-\alpha t)$$

where K_o is the Peukert constant at 0°C, and α is the temperature coefficient of capacity.

The Peukert equation is not valid at low discharge currents, since when I_d tends to zero, the capacity tends to infinite values. In this case the Liebenov (1897) equation provides a better fit.

$$C_d = \frac{A}{B+I_d}$$

where A and B are constants.

For all the capacity models, the constants can be determined by suitable regression of measured data.

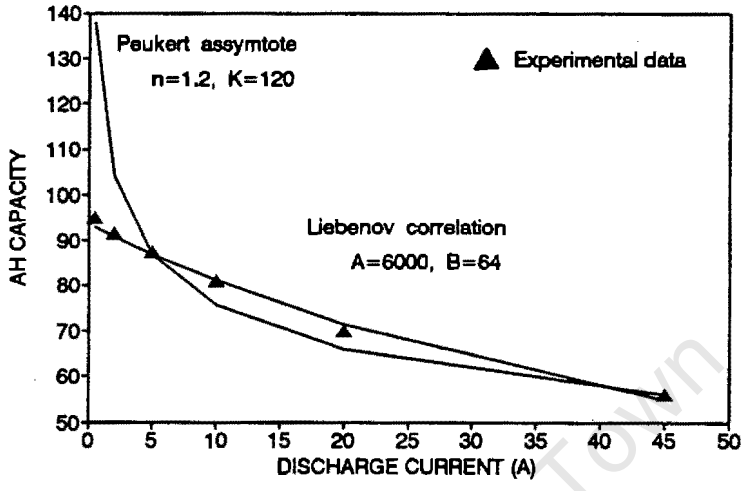

Figure 3.36 Comparison of Peukert and Liebnenov correlations with real data.

For temperatures in a narrow band, the change in capacity is given by IEC (1967).

$$C_d = C_d^{30^\circ}(1-0.008(t-30^\circ))$$

3.10.4 Ah Charging Efficiency

Many charging efficiency models are SOC based, with a fall-off in charging efficiency from about 85 percent SOC. Wood and Crutchen (1980) propose a model expressing the maximum rate of charge acceptance as a linear function of state of charge. Efficiency begins to fall from 64% SOC onwards, reaching zero at 100% SOC. This approach is theoretically incorrect, but can provide acceptable results.

Theoretically, the inefficiencies are determined primarily by the individual electrode voltages. A possible representation would present the gassing current (non-accepted charge) as a function of voltage, and be independent of SOC. This relationship is exponential, and is described in Section 3.7. The voltage-gassing current model requires scaling for different battery sizes and types.

3.10.5 Self-Discharge

Self discharge is usually quoted as the monthly loss of a percent of existing capacity. Self discharge in modern batteries is generally low, but can vary from 10% per month for 5% Sb cells to less than 0.5% per month for antimony-free grids. Lasnier et al (1988) have proposed an exponential self-discharge model which is most applicable to the non-linear self-discharge of calcium grid cells.

$$SOC = SOC_0 \times e^{(-kt)}$$
$$\text{and } k = 300 \times e^{(-4400/T)}$$

where SOC_0 is the initial SOC, T in Kelvin, t in hours and k in hours^{-1}, k=0.0001 at room temperature for calcium grid cells.

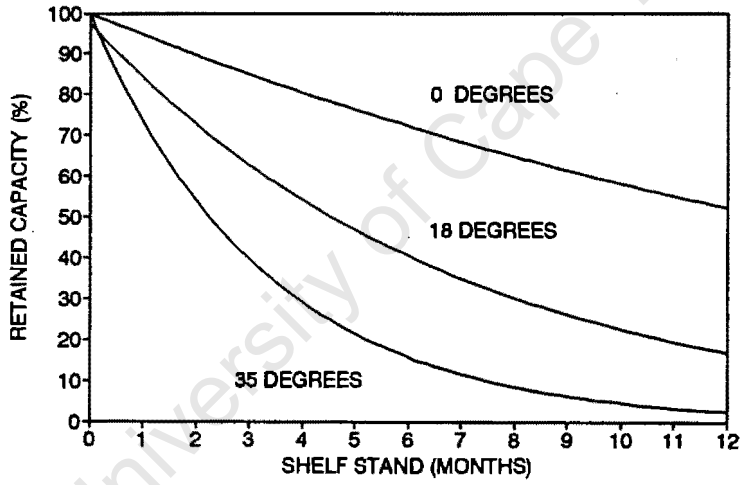

Figure 3.37 Self-discharge of SLI batteries under open-circuit conditions using the Lasnier model.

The concave shape of the Lasnier model is questionable. Some literature (Pavlov,1984) presents self-discharge as a straight line (see Figure 3.11), while a battery manufacturer shows the same graph as convex (see Figure 3.38) for antimony grid and calcium grid alloys. It is debatable which model is correct.

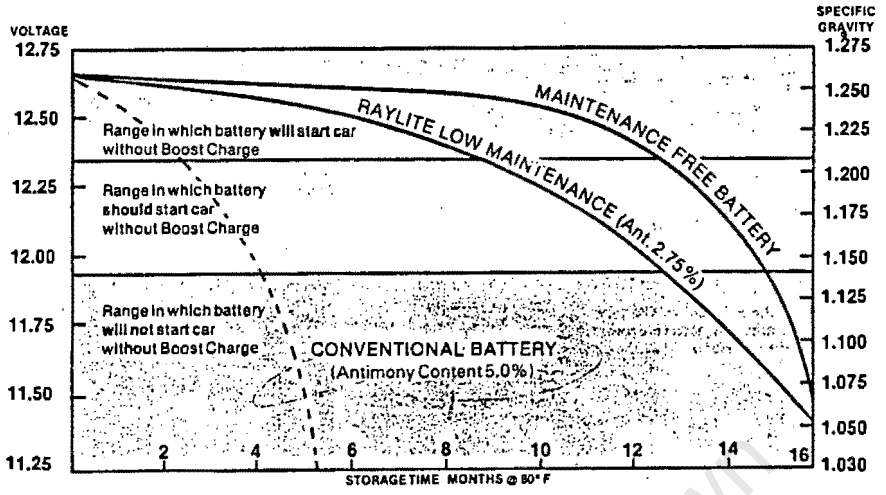

Figure 3.38 Self-discharge of SLI batteries under open-circuit conditions. (Source: Raylite SLI battery literature).

3.10.6 Conclusions

The first battery performance models originated from load levelling applications. Subsequent advances in PV battery models draw heavily on this work. In general, the models are optimised for high charge and discharge currents, and are complex, and great care is required in applying these models to low current PV simulations. In some cases the empirical database approach to characterisation may be more satisfactory.

Capacity models are generally best represented by the Liebenov correlation, with a temperature correction factor.

Charging efficiency is primarily voltage based, but unless real data is available SOC based models are more easily implemented.

Self-discharge may be inconsequential, but is easily modelled as a simple monthly capacity loss during open circuit conditions.

3.11 FAILURE AND WEAR

The lead-acid battery can fail in many ways, depending on the environment and duty cycle of the service. Some battery designs are more suited to specific applications than others. This section summarises the modes of failure that have been discussed in detail in other sections.

The positive plate generally limits cycle life because of shedding of the active material and corrosion of the grid.

Deep discharge of batteries having calcium alloy grids can lead to formation of insoluble calcium sulphate in the corrosion layer, between the grid and the active material. Proprietary processes[5] during manufacture can prevent this corrosion, but are costly. MF SLI batteries are not treated in this way, and may not be deep-discharged. PV batteries with treated calcium alloy grids are more costly, but can reach 1800 cycles at 8% DOD (Sieger,1981).

Tubular plate batteries are designed for deep-discharge service. The positive tubular plate usually fails by stress cracking near the top of the lead spine. Pasted plate designs usually fail by shedding.

The mechanical stresses during cycling are due to volumetric and mass changes in the active groups. Volumetric changes give rise to cracking of the corrosion layer and loss of electrical contact. Thickening of the grid occurs during prolonged deep-discharge when sulphation occurs. Irrecoverable sulphation may result if the batteries are not recharged.

The negative electrode can become sulphated during prolonged cycling. The large sulphate crystals cause loss of contact with the grid.

Repeated cycling can cause stratification of the electrolyte, which can contribute to uneven active material use and degradation in the long term.

Excess gassing can cause rapid corrosion of the grid in antimony alloy batteries. Gassing also causes water loss, which may expose the plates to the atmosphere.

5 Usually some form of heat treating of the negative grid.

The negative plates can self-discharge with the atmospheric O_2. Sulphation will occur.

Excess gassing can scrub some of the active material from the positive plate. Active material or sulphate that is lost from the plates by shedding or scrubbing will collect at the bottom of the battery as sediment. If the sediment reaches the bottom of the plates it will cause shorting.

The sediment can be redeposited by electrolyte stirring during gassing on both the positive negative plates. It is non-cohesive on the positive plates, and can easily be scrubbed off again. Material deposited on the negative plate is cohesive, and can accumulate to cause shorting around the separators. This is known as mossing. Some of the colloidal lead-sulphate may be reduced to lead, which may promote short circuiting. The negative mass may grow considerably, leading to stress of the grid.

Separators can degrade and cause shorting across the electrodes.

Operation of batteries at higher temperature promotes grid corrosion and reduces cycle life. High acid concentration affects the cycle life of the negative electrode by favouring corrosion processes.

3.12 CYCLE-LIFE MODELS

3.12.1 Cycle Life vs DOD

An important consideration in the design of a PV system with battery storage is the durability of the batteries. Though the failure modes of the lead-acid battery are well understood, real cycle life data can only be generated by controlled testing. Cycle life tests require considerable investment, and most results are heavily reliant on interpolation of available data using cycle life models. In the case of lead-acid batteries the models are generally based on small data samples only (Sieger,1981).

Battery life is usually represented as straight lines of cycles available versus DOD on semi-logarithmic paper.

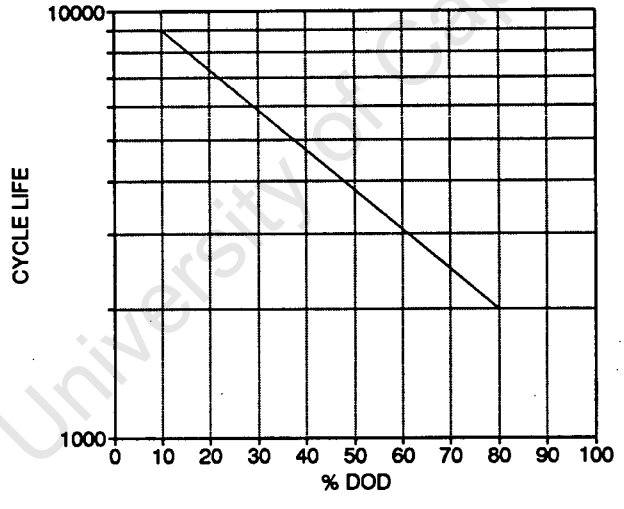

Figure 3.39 Typical representation of cycle life vs depth of discharge.

Delco (1979), however, portray a log-log plot of cycle life vs DOD that is a straight line for calcium grid cells. Sonnenschein literature for the A200 cell also fits the log-log model, and the literature is apparently an extrapolation of it.

Bode (1977) and Kordesch (1977) contest that a linear relationship exists between DOD and the logarithm of the number of cycles. Bode and Kordesch propose models of the form

$$Log\,L = a - b\,(DOD)$$

Sieger (1981) provides an interesting derivation for the semi-log model, by assuming that the molar volume effects of active material during cycling are the main cause of failure. He expects that the differential change in cycle life is proportional to cycle life and DOD of the cell. This takes into account the main mode of failure in the DOD range 20% to 80%. Presumably, alternative models could be derived for the different dominant failure modes under various operating conditions, an area of possible future research. The model yields:

$$L = L_0 \exp\left(a\,(1 - DOD)\right)$$

where L_0 is the cycle life associated with 100% DOD, and a, the slope indicates the failure mode. The derivation is shown in Appendix C. This model is not only based on lead-acid battery data, but on data for batteries of all chemistries using about four data points per battery. The lead-acid batteries tested include traction (a=1.3), SLI MF (a=4.14) and PV types (a=3.47).

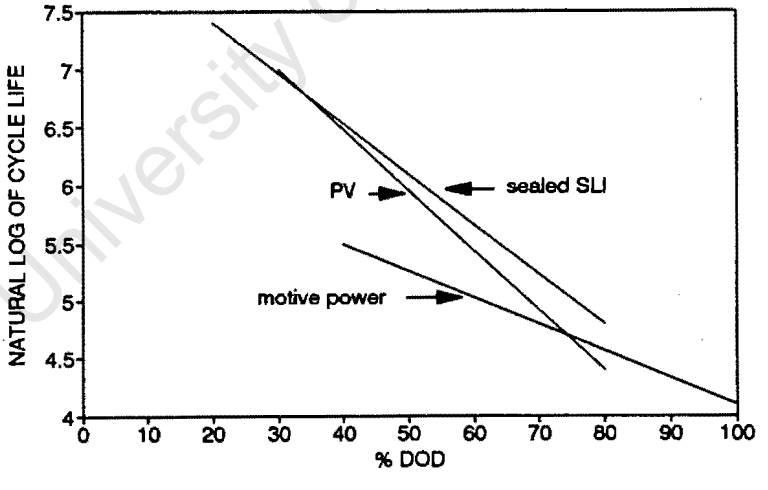

Figure 3.40 Life cycle correlations for traction, SLI, and PV type lead-acid batteries. (SLI = Eagle-Picher Carefree Sealed; EV = C&D; PV = C&D lead-calcium alloy grid) (Source: Sieger,1981)

Sieger (1981) also finds a strong dependence of cycle life on frequency of cycling. The cycle life is longer in batteries that are cycled more frequently, although

actual life is less. He attributes this to self-discharge processes that occur to a greater degree in less frequently cycled cells. Although insufficient data is available to determine a functional relationship, on the data available Sieger finds that cycle life depends logarithmically on the frequency for the single battery make tested. This is based on frequencies of 2, 5, and 10 cycles per week.

3.12.2 Temperature Effects

Lasnier et al (1988) have proposed a model that incorporates the temperature effect on battery life. In most cases data is unavailable from the manufacturer, and the model can not easily be applied. Sieger (1981) found only three data sources in the literature pertaining to temperature effects on cycle life. This data suggested that cycle life is greatly reduced at elevated temperatures, mainly due to higher rates of grid corrosion. At temperatures above 90°F (30°C) the semi-log relationship may no longer hold, indicating a different failure mechanism. This finding suggests that just as temperature affects the failure mode and the cycle life curve, so they could be affected by battery chemistry, and the Delco log-log life curve for calcium grid batteries is not necessarily defective.

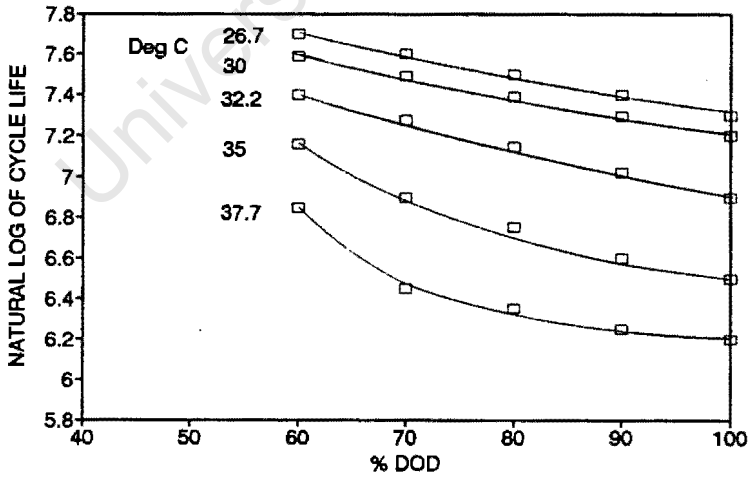

Figure 3.41 Cycle life vs DOD and temperature for a lead-acid motive power type battery. (Source: Sieger,1981)

3.12.3 Incremental Wear

Voss and Huster (1967) define an incremental wear due to each complete cycle from 100% SOC to a defined DOD and back again to 100% SOC. The battery is assumed to fail when the total incremental wear is unity.

$$\Delta W = 1/L_{dod}$$

where ΔW is the incremental wear, and L_{dod} is the expected cycles life at the cycle DOD. This model is widely accepted, but its accuracy is limited by the weaknesses of the original life cycle data.

The model is easily adapted for PV cycling to and from arbitrary DOD's, ie. partial cycles. The wear from partial cycling between DOD_1 and DOD_2 is calculated as:

$$\Delta W = (1/L_{dod2} + 1/L_{(dod2-dod1)})/2$$

This approach accounts for both cycling wear and a penalty for partial SOC operation, though it seems extremely arbitrary as the weighting attributed to partial cycling will certainly depend on the battery chemistry.

Lasnier et al (1988) treat the wear during partial cycling as if complete cycles were occurring. The justification is that prolonged partial SOC operation may be just as harmful in the long term as complete deep cycles with regular charging.

Partial SOC operation raises questions as to what constitutes a cycle. None of the authors are clear, but it seems reasonable that as the manufacturers' data is based on full cycles of 0-10% DOD and 0-80% DOD typically, that a cycle should comprise at least a few percent change in DOD. In PV applications this is complicated by the superimposition of smaller background cycles (noise caused by clouds) on the main cycle pattern. In cases where the battery cycle has a period of one year with prolonged partial SOC operation over a whole season, it is unclear whether the period used for life cycle calculations is daily cycling or annual cycling with some noise superimposed.

The manufacturers' cycle life curves are constructed from cyclic operations within strictly defined operating regimes, and prolonged partial SOC operation is not usually considered a subset of those regimes. The validity and significance of all the cycle life calculations and results based on these curves should be considered in that context.

3.12.4 Battery Strings

Thaller (1983) develops an interesting method for evaluating the cycle life versus DOD in single cells and cell strings using a statistical approach. This method is unfortunately not easily applicable to PV cycling without some adaption, as it draws heavily on the statistical data of expected cycle life of single cells.

3.12.5 Conclusions

Battery life modelling is complex and prone to errors as limited data is available and the models are not wholly satisfactory. Either the semi-log or log-log representations of cycle-life vs DOD should be considered. Compensation for temperature and frequency of cycling is based on even less data.

The incremental wear approach for complete charge-discharge cycles is easily implemented. Wear for partial SOC cycling is not as simple, but the various calculation techniques yield fairly similar results in typical PV operating regimes. Special consideration of peculiar operating conditions is warranted, and sensitivity to errors in the predicted life should be carefully considered.

Different models could fit different types of battery to a greater or lesser extent.

The cycle life models refer to regular modes of failure; in practice one can also expect irregular failures due to deviations from controlled regimes and for variations in cell construction. These are not modelled.

3.13 PHOTOVOLTAIC BATTERIES

3.13.1 Requirements of PV Batteries

The main requirements of a PV battery are listed below. They are in some order, but the priority depends on the site specific conditions, load demand profile and the system sizing method used:

i) complete and detailed battery data
ii) long and predictable cycle life
iii) high reliability

iv) deep discharge capability for cost effective sizing and robust power handling
v) low initial cost / Ah of storage
vi) low maintenance requirements for remote sites
vii) low cost / kWh of storage over battery life

viii) ability to withstand overcharge
ix) overcharge current, capacity and Wh output insensitive to temperature changes
x) ability to withstand prolonged states of discharge
xi) low self-discharge rate

xii) replaceable in modular format

3.13.2 Trends in the Design of PV Batteries

Field experience has raised several problem areas linked with conventional batteries installed in PV systems. Primarily, the duty cycle of PV batteries is quite unlike that of any of the batteries previously discussed.

While PV systems can be designed to accommodate any of the common battery types, the system design may require considerable overcompensation and electronic control to ensure suitable operating regimes for the battery. (Heavy duty EV type batteries typically require 6A charging current/100Ah, regular boost

charge). This can be both expensive in capital and inefficient in energy usage. Batteries designed specifically for PV load-levelling applications may, in time, offer the best solutions.

Specialist PV batteries are being developed now that the PV technology is maturing. There are distinct trends in design towards realizing this goal. A summary of the discussion is tabulated in Tables 3.2, 3.3, 3.4 and 3.5 at the end of the section.

3.13.3 Electrolyte

a) Conventional or flooded electrolyte

The dilute sulphuric electrolyte in conventional cells is subject to stratification during deep cycling. Excess gassing current is required to reverse this effect, which is cumulative and can have long term deleterious effects. Excess gassing itself causes deterioration of the positive plate (Mahato et al,1987), and results in lower cycle efficiencies.

If there is no mechanism for recombination, gassing leads to water loss, and electrolyte must be topped up manually. An advantage of flooded cells in transparent casing is that the behaviour can be monitored visually, but the maintenance requirements are still a disadvantage in many PV applications. MF versions of conventional batteries are discussed in section 3.5.2.

The low charging currents typical in PV batteries (2A-3A/100Ah) are unlikely to generate sufficient gassing to eliminate stratification, particularly in tall cells. Large and costly PV chargers are required to generate finishing currents of 6A/100Ah.

Immobilized electrolytes have been developed to eliminate stratification.

b) Gelled electrolyte

A gelled electrolyte is essentially H_2SO_4 immobilized by suspension in a silicon gel. Excess electrolyte can be designed into the battery to achieve good reserve

capacity. Mossing, shorting and dendrite growth is limited by the inability of lead to be absorbed into the electrolyte "solution".

It is important that gassing is limited. The gel develops fissures during gassing as gases escape through it (Tuphorn,1987), and the gel shrinks as water is lost. The fissures allow oxygen penetration to the plates where corrosion can occur, and also reduce contact of the gel with the plates. This can lead to non-uniform current distribution and unequal electrode utilization, and could result in significantly shortened cycle life, and make cycle life difficult to estimate because of inconsistencies in the battery itself.

A further limitation in gelled electrolytes is their inherently high internal impedance which limits high current performance. The insulating properties of silica gel, combined with gel shrinkage contribute to high internal impedance which is aggravated at deep discharges. Electrolyte conductivity after deep discharge is often sustained by the presence of some phosphoric acid in the electrolyte. The phosphoric acid does not react and is evenly distributed.

The useful life of the gel is also strongly dependent on temperature.

c) Absorbed electrolyte

Absorbed electrolytes are immobilized in a micro-porous absorbent matrix, usually the separator. The specialised separators are usually made from boro-silicate glass fibres of 2.0 microns. The felt-like porous matrix is not totally saturated with electrolyte, and the free volume allows unimpeded flow of gas, but not shorting of active material. Oxygen is often in direct contact with the positive plates by the uniform distribution of gas paths.

Efficient charging is possible in both gelled and absorbed electrolyte cells, as stratification is virtually eliminated and little gassing is required (Mahato,1987). Figures 3.42 and 3.43 compare gelled and immobilised electrolyte performance with flooded cells. Figure 3.44 compares the life of gelled and absorbed electrolyte systems under (unnaturally) prolonged overcharge conditions.

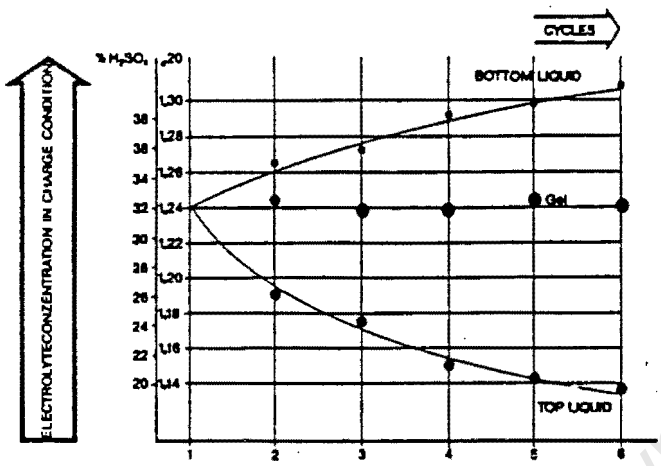

Figure 3.42 Electrolyte stratification of a 200Ah tubular cell in comparison to an A600 gelled cell. (Source: Tuphorn,1987:fig.4)

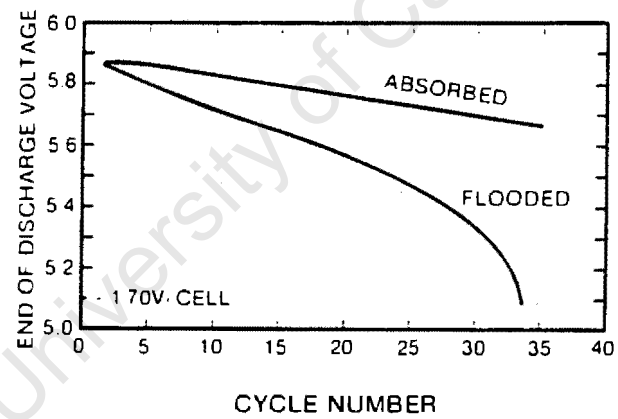

Figure 3.43 End of discharge voltage of a sealed 100Ah battery and comparable flooded electrolyte battery subjected to the deep cycle partial state-of-charge test (see Section 6.2.7)
(Source: GNB Technical Information:fig.8)

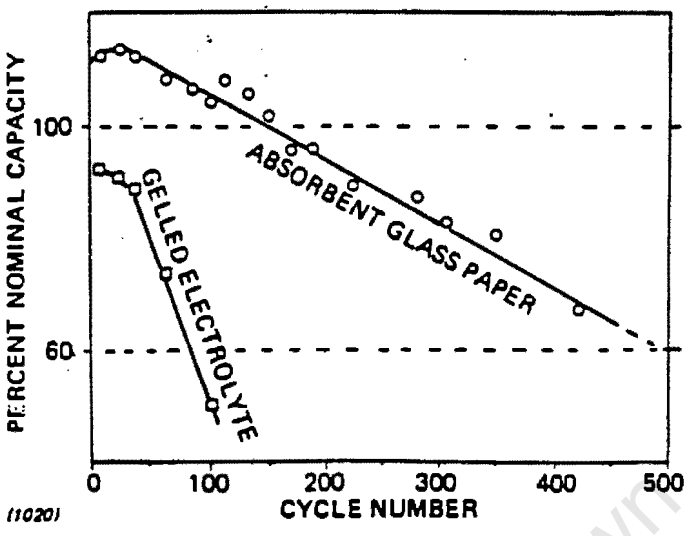

Figure 3.44 Effect of electrolyte immobilization on cycle life. C/4 discharge to 60%, recharge at C/10 with 50% overcharge.
(Source: Szymborski,1982:fig.2)

Both gelled and absorbed electrolyte systems are highly dependent on gas recombination cycles to prevent water loss, which would dry out the cell.

3.13.4 Gassing and Gas Recombination Techniques

Low antimony deep cycle flooded electrolyte solar batteries tend to have large electrolyte reservoirs above the active block to reduce the frequency of watering.

The more exotic batteries using immobilised electrolytes require gas recombination to prevent water loss as water cannot be added after manufacture. Techniques are catalytic recombination and O_2 or H_2 closed cycles. Closed cycles require sealed cells to prevent gas leakage. These methods have been discussed in detail in Section 3.9.

The finishing charge voltage is strongly affected by the method of water recombination and may be temperature dependent. Oxygen cycles have a depolarising effect on the negative plate, and require lower finishing voltages than for conventional cells of the same design (Mahato et al,1987). The voltage should be decreased further as the temperature and depolarisation increase due to

gassing. It is possible to develop a thermal run-away situation, which highlights the desirability of temperature compensated voltage regulation in general.

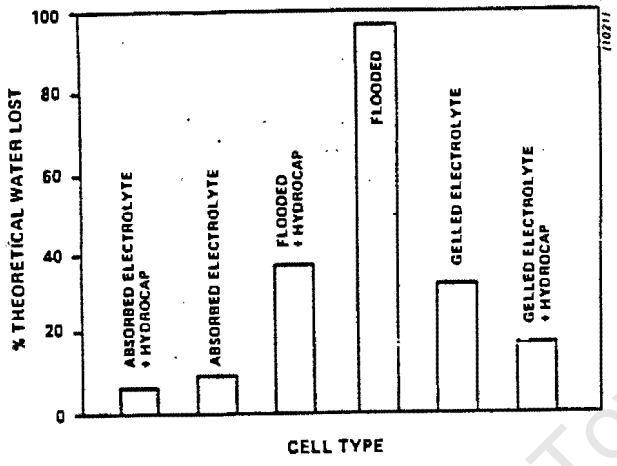

Figure 3.45 Gas recombination efficiencies of different cell designs using catalytic recombination devices. (Source: Szymborski,1982:fig.3)

3.13.5 Grid Composition

The grid composition has the largest single effect on battery characteristics. Grid alloy is selected on the basis of its resistance to corrosion by sulphuric acid, its overpotential characteristics and to facilitate manufacturing. Increasing antimony content of the grid decreases the hydrogen overvoltage, decreasing the gassing voltage and increasing its temperature coefficient, self-discharge rate and water consumption. Deep cycling ability in conventional cells is dependent on the presence of antimony for bonding of the active material to the grid (BP Solar Technical Specifications). Antimony also facilitates the manufacturing process. 1.4%-1.6% Sb is considered optimum for contributing to mechanical strength while minimising the adverse effects. Antimony is a poison to some gelled electrolytes.

In an effort to reduce maintenance requirements and many of the side effects of using antimony, researchers have endeavoured to develop alloys that perform satisfactorily during deep discharge, but otherwise exhibit similar characteristics to calcium grid cells, namely high gassing voltage and temperature independence and low self discharge rate. It is well known that conventional calcium grid (MF)

cells normally perform very poorly during cycling due to softening of the positive active material, grid corrosion, grid growth and mossing (Enochs et al,1984).

Grid growth has been reduced by using Pb-Ca-Sn (ternary) alloys instead of the usual Pb-Ca (binary) calcium alloy (Enochs et al,1984). Arsenic, selenium, cadmium, silver and other elements are alloyed to lead to add strength, improve creep resistance, improve corrosion resistance, modify grain structure and alter electrochemical characteristics.

Addition of phosphoric acid to the electrolyte increases the cycling capability considerably by reducing the grid growth rate by up to 75%, and eliminating grid growth as a life limiting factor (Enochs et al,1984). The addition of phosphoric acid is not without side effects, as it may increase the tendency towards mossing as it increases lead solubility. The working capacity of the cell is typically reduced by 10-15%.

Grid corrosion is a common mode of failure. Calcium grid corrosion can be reduced by increasing grid thickness. A 10% increase in thickness reduces corrosion by 30% (Enochs et al,1984). Grid thickness may be from 1,19mm for SLI type cells to 6.35mm for industrial types.

3.13.6 Positive Plate Design

The choice between tubular or flat plate positive designs has never been clear. In most applications there are serious trade-offs. The favourable characteristics of the flat plate are low cost, excellent high current capability and good utilisation coefficients. Cycling ability is fair. The tubular plate design has excellent deep discharge and cycling ability and long cycle life since shedding of the active material is prevented by binding of the fibre sheath. The low utilisation coefficient of the plate provides protection of the grid against corrosion, but at the same time decreases the energy density and the stored energy cost (Eggers,1984).

PV batteries designed with antimony free grids should ideally incorporate the tubular cell, as it protects the grid from corrosion, and contains the positive active material that goes soft and most likely to shed. Mossing can be further limited by the tubular sheath (Sonnenschein A600 Technical Specifications). The

corresponding decrease in energy density is unlikely to affect stationary applications.

The flat plate design may be more cost effective where grid corrosion is not as serious (1.6% Sb), or where high currents are required. Deep cycling is possible, but cycle life performance is shorter than for the tubular design.

3.13.7 Some State-of-the-art PV Batteries

The main features of three specialist PV batteries are described to illustrate how some of the design options are engineered together. The present generation of lead-acid PV batteries yields improved performance over conventional batteries, but at a higher initial cost. No figures are available for comparative costs over system lifetime, but if the batteries achieve their advertised cycle life, then they will provide better value in the long term.

a) BP Solar P-series

- Pasted positive plate, low antimonial grid for excellent cycle life (1200 cycles at 80% DOD). High current capability of flat plates not required.
- Flooded electrolyte enables regular and easy maintenance. Tubular cell can withstand gassing, gassing overcomes many problems associated with flooded electrolyte cells. Electrolyte SG can be selected to suit particular climatic conditions.
- Extremely large electrolyte reservoir, to cater for water consumption problems associated with antimonial grid cells. Topping up required only every 2-4 years under normal operation.
- Catalytic recombination can be retrofitted to reduce maintenance in extremely remote sites.
- Clear casing for ease of maintenance and monitoring.

but

- The batteries require substantial overcharge and high gassing currents to avoid electrolyte stratification.

b) Sonnenschein A600 Solar

- Tubular positive plate, pasted negative plate for good cycle life (10 year life expectancy under undefined conditions).
- Gelled electrolyte reduces maintenance and stratification problems of flooded systems. SG is optimised for high ambient temperature operation. Possibility of freezing at low temperatures is eliminated. Cell exterior is clean and acid free during operation.
- Antimony-free grid reduces water consumption and helps prevent drying of gel. Pb-Ca-Sn ternary grid improves cycle service.
- Efficient closed O_2 cycle for water recombination ensures minimal water loss, and protects electrolyte from drying. Self-discharge rate is very low.
- Rigid charging specifications supplied in battery data, to protect electrolyte against overcharge induced temperature increases.

but

- Well controlled charge regulation is required, particularly in warm climates.

c) GNB Mini-Absolyte 12V-5000

- Flat plate construction for moderate cycle life at low cost.
- Immobilized electrolyte reduces maintenance and stratification problems of flooded cells. The temperature sensitivity familiar to gelled cells is also avoided. Clean and acid free exterior during operation.
- Low antimony positive grid and heat treated lead-calcium negative reduce water consumption and self-discharge.
- Efficient closed O_2 cycle reduces rate of H_20 loss.

but

- Excess gas recombination may result in premature grid corrosion.

TABLE 3.2 Summary of electrolyte designs

Electrolyte design	Advantages	Disadvantages
flooded	i) level can be maintained and topped up	i) requires overcharge to prevent stratification ii) overcharge promotes active mass shedding ii) overcharge and shedding result in dendrite growth
gelled	i) no stratification ii) battery not required to be upright iii) dendrite growth physically prevented iv) can withstand partial SOC operation	i) temperature dependent operation ii) thermal runaway possible during charging iii) cycle life is temperature dependent iv) drying or fissuring of gel during gassing v) recombination required
absorbed	i) no stratification ii) battery not required to be upright iii) less temperature dependent than gel iv) can withstand partial SOC operation	i) less excess electrolyte than other choices ii) recombination required iii) continuous contact of O2 with grid results in corrosion iv) dendrite growth possible

TABLE 3.3 Summary of grid alloys

Pos. Grid Alloys	Advantages	Disadvantages
Antimony (1.6% Sb)	i) can withstand regular deep discharge	i) gases at low voltage, decreasing with age and temperature ii) high self-discharge rate ii) high water loss and maintenance ii) transfer of Sb to negative plate, corrosion, may poison electrolyte
pure lead	i) no impurities introduced	i) difficult to manufacture, expensive ii) cannot withstand deep discharge
lead-calcium (binary)	i) high gassing voltage, higher efficiencies ii) resulting in low self-discharge	i) poor deep cycle life
lead-calcium-Sn (ternary)	i) as above ii) better deep cycle life	i) higher cost

TABLE 3.4 Summary of plate designs

Plate Design	Advantages	Disadvantages
flat plate	i) low cost ii) high current density iii) moderate cycle life in thick plates	i) active material shedding during overcharge ii) low protection of calcium grid by shielding
tubular plate	i) no shedding of positive material due to binding ii) excellent deep cycle life iii) good protection of grid against corrosion by shielding	i) higher cost ii) capacity very dependent on discharge current

TABLE 3.5 Summary of water loss prevention designs

Water Saving Device	Advantages	Disadvantages
none	i) cheap	i) loss of h20
extra-electrolyte reservoir	i) cheap ii) less maintenance required	i) decrease in energy density
catalytic recombination	i) low maintenance ii) can be retrofitted in vent cap	i) high temperature 450oC ii) cause gassing voltage drop, possibility of thermal runaway iii) possibility of explosion iv) Pt catalyst cost v) requires stoichiometric H2 and O2 ratio
closed cycles	i) recombines h2 and o2 even when not in stoichiometric ratio ii) completely sealed cell iii) low temperature	i) Pt catalyst cost ii) extra-electrode required iii) sulphation of negative plate during recombination iv) gassing voltage drops during recombination, possibility of runaway

3.14 VOLTAGE REGULATION

The role of the voltage regulator in a PV system is to protect the battery, as batteries operate most reliably and efficiently in well controlled environments. The regulator restricts the range of battery state-of-charge (SOC) operation, and provides protection against both overcharge and overdischarge. Most PV systems require some form of voltage regulation.

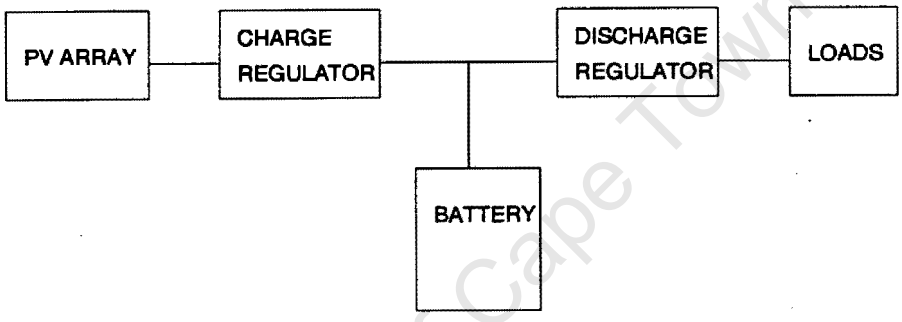

Figure 3.46 Voltage regulator in a stand-alone PV system.

The overcharge current and the accumulated Ah of overcharge in the battery must be limited. Excessively deep discharges of the battery should be avoided. Normally the battery is maintained within a specified SOC regime, and most regulators use battery voltage as an SOC indicator. In more sophisticated regulators Ah integrators and voltage sensors together give a more reliable SOC indication.

3.14.1 Charge Regulators

PV system costs can be reduced by efficient operation, that is by converting as much available PV power as possible to stored battery energy at maximum charge efficiency. The optimal method of charging a battery is by taper charging or reducing the charge current as the battery SOC increases. Before gassing starts any PV supply current available is approximately equally efficient in terms of charge efficiency, and the efficiency of the process is determined by the match

between array I-V curves and battery acceptance I-V curves. Figure 3.47 shows inefficient matching at 60% and 80% SOC. The currents in the non-gassing range are effectively set by the irradiance.

Since the array is basically a current generator, tapered current charging is intrinsically inefficient, but at this stage there is a surplus of PV power. The charging currents can only be tapered by discarding surplus PV energy, usually by charge regulation.

Figure 3.47 also shows a typical situation where a PV array without a regulator produces more end-of-charge power than is ideal for the battery, a situation which would occur if the array and panel were poorly matched. This mismatch also results in lower process efficiencies at lower SOC's. When a regulator is provided, voltage under dynamic conditions is used to determine SOC, and under conditions of constant battery temperature, the current can be tapered and gassing current can be limited (to about 0.5A/100Ah) by controlling the regulator output voltage. Regulation is a necessity in most PV systems with battery storage.

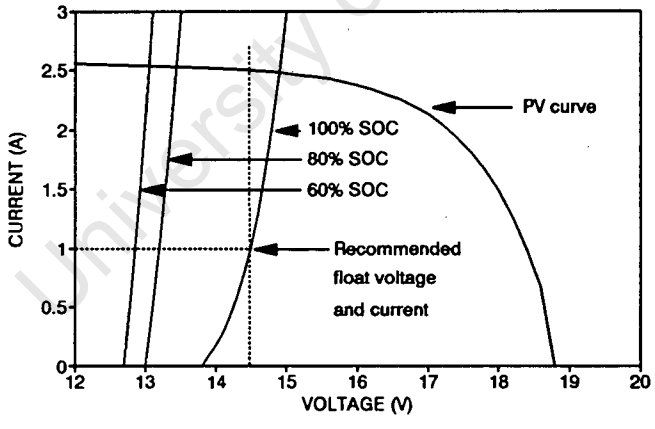

Figure 3.47 Typical situation for a PV installation, I-V curves for 33 cell 45W_p array, 100Ah lead-antimony battery[6]. T_{array}=47°C, I=1000W/m^2, T_{bat}=20°C.

6 In practice the effective PV array voltage may be lower, due to the voltage drop on array output of blocking diodes, regulator voltage drop and line losses.

There is, of course, the possibility of using PV panels that are well matched to the charging curves of the battery to eliminate the need for a regulator and to increase the overall process efficiency.

Matching is theoretically possible if the recommended battery float voltage and current are located below the knee of the PV I-V curve, so the battery charge rate naturally tapers as the SOC increases. The PV open circuit voltage decreases as a function of cell temperature (Figure 2.3), corresponding to the decrease in battery float voltage with temperature (Figure 3.48). The temperature coefficients of the array open circuit voltage and battery float voltage depend on the type of PV module and the type of battery.

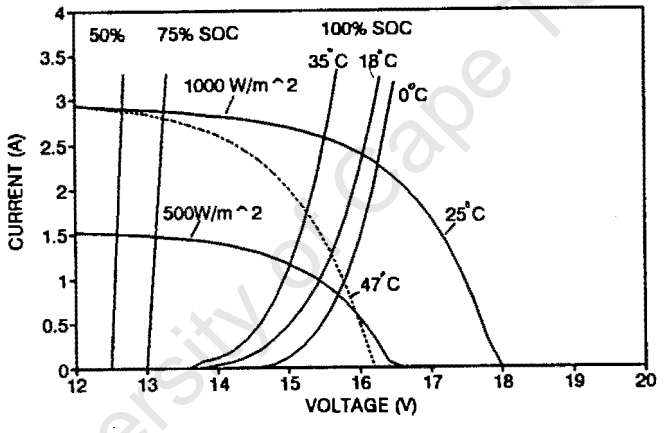

Figure 3.48 Self-regulation of a 100Ah lead-calcium sealed battery at 50%, 75% and 100% SOC (T_{bat}=20°C), with a 30 cell poly-crystalline 42W_p PV panel at the specified irradiance and panel temperatures.

Practically, matching the array with the battery requires reliable battery, array, irradiance and load profile data. Batteries with charge acceptance curves relatively unaffected by temperature will simplify the matching considerably, (here lead-calcium grid cells are preferable). Self-regulation requires careful consideration of battery characteristics, I-V characteristics of the different types of PV modules and estimates of PV module operating temperatures. Most panel manufacturers offer panels of 30 or 33 series cells that are optimised for direct connection to the battery. On a cautionary note, the designer should ensure that the panel voltage is sufficient for battery charging even at elevated panel temperatures, and some provision may be required for loss of panel voltage due

to shading of single PV cells. Normally series diodes are integral to self-regulating panels.

Self-regulating systems should be used regularly, as the charging current from the self-regulating panel to a fully charged battery may overcharge the battery if the system is not used for an extended time. The overcharge may result in high electrolyte consumption.

If these conditions can not be met then it may be preferable to use some form of charge regulation.

a) Charge regulator operation

Most charge regulators can operate in one of two modes:

Boost mode: charging current is unrestricted till the boost voltage is reached (±2.4V/cell for deep cycle lead-antimony cells), whereupon the voltage is clamped, and the charge current tapers to maintain the clamp voltage. Boost mode is usually used for deep discharge applications, or for periodic equalising charge (every month). (See Figure 3.49(a).)

Float mode: current is unrestricted till the float voltage is reached (2.3V/cell for shallow cycle lead-antimony cells). The voltage is then clamped as in the boost mode. After prolonged charge regulation in float mode the current may be decreased to zero. Once the battery voltage settles to a low voltage (about 2.17V/cell) the float charging resumes at the initial float voltage (2.3V/cell). The high/low voltage hysteresis window is most common in regulators where continuous voltage regulation is not possible (Relay type devices). (see Figure 3.49(b).)

Some regulators feature an auto boost mode. The charging current is unlimited till the boost voltage is reached. At this time regulation at the float voltage becomes predominant. Batteries charged in this mode will be boosted for a short time during each cycle, but not as vigorously as for a complete boost charge. (See Figure 3.49(c).)

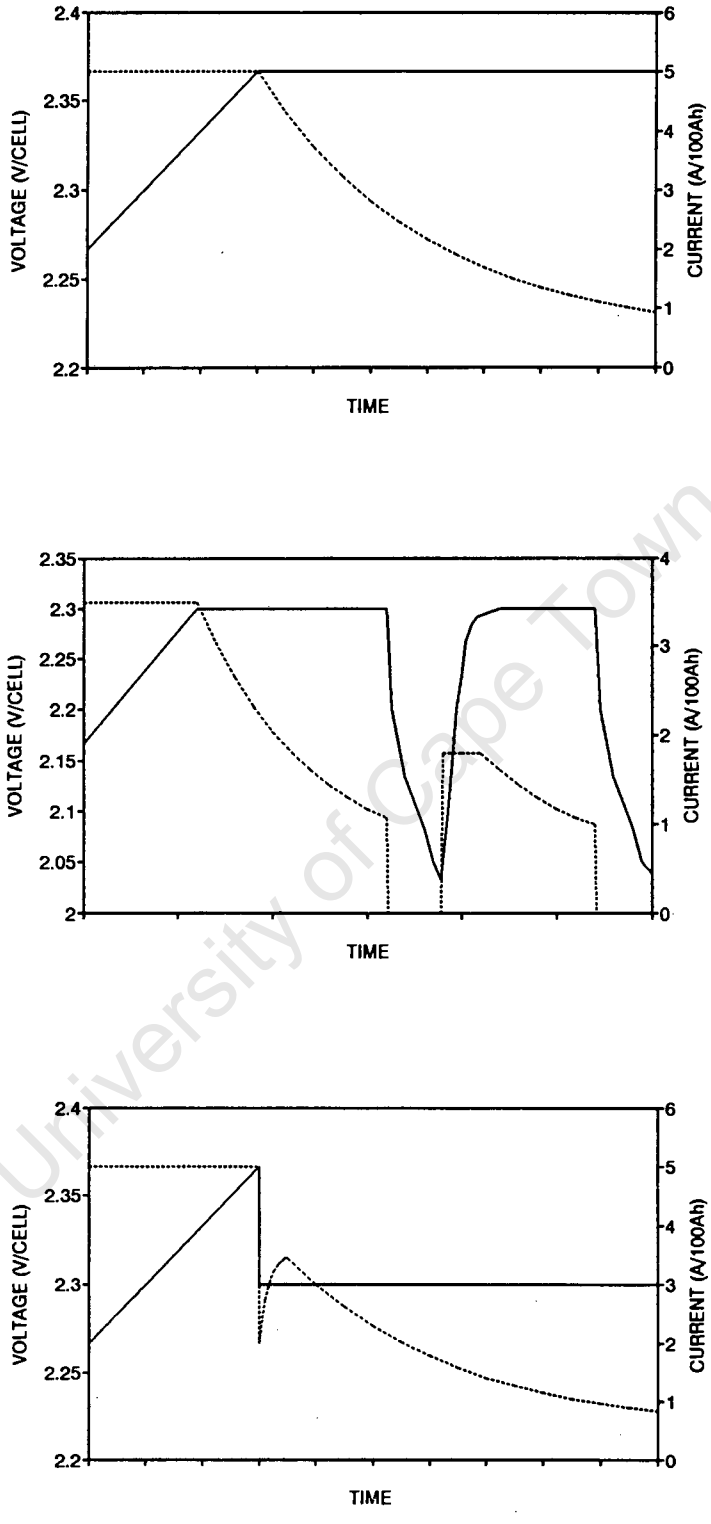

Figure 3.49 a) boost charge mode, b) float charge with current control, c) auto boost mode. The solid line represents voltage, the dashed line represents current.

b) Temperature compensation

Temperature strongly affects the maximum recommended charging voltage of most batteries. The overcharge current of antimony grid batteries is particulary temperature sensitive, and the life of such batteries is dependant on overcharge control. Temperature compensation of the boost and float voltages is a very desirable feature for applications where the battery temperature variations range more than 10°C. This may be directly caused by climatic conditions, or indirectly by internal battery heating.

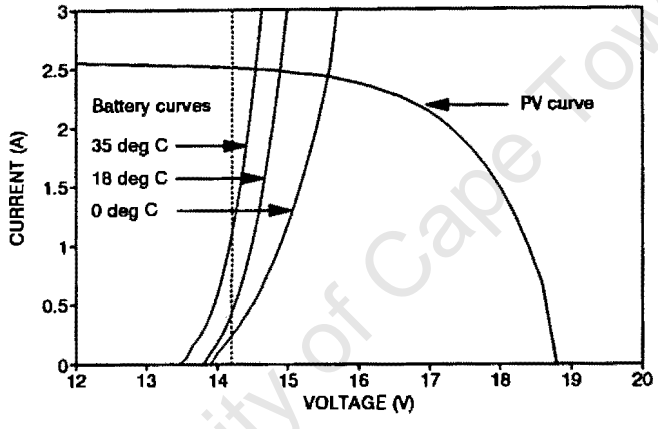

Figure 3.50 Effect of battery temperature on operating point for typical PV installation. I-V curves for a 33 cell 45W_p array, 100Ah lead-antimony battery. T_{array}=47°C, I=1000W/m^2, T_{bat}=20°C, SOC=100%.

3.14.2 Overdischarge Protection

Overdischarge protection is required to protect the battery from deep discharge in the short and long term. Where DOD is indicated by the battery voltage, protection against overdischarge is usually accomplished by disconnecting the loads that are the prime cause of the low voltage. All the loads, or some of the loads may be shed on a priority basis. Load shed is activated once the battery voltage falls below a selected drop-out voltage on the battery discharge curve.

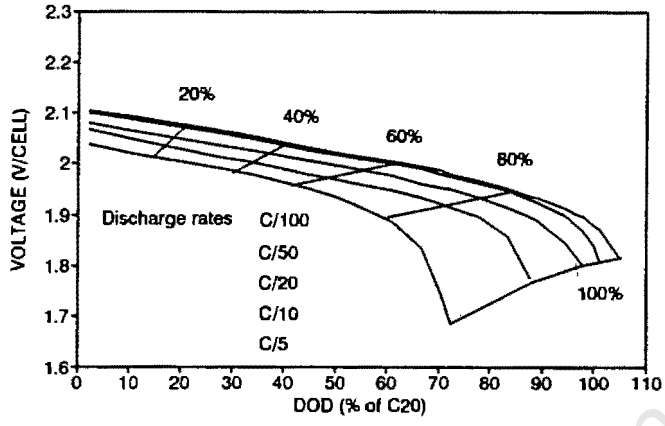

Figure 3.51 Standard battery discharge curves

As shown by Figure 3.51, the approximate discharge current must be known if load shedding is to occur anywhere above 50% DOD, since the drop-out voltage is a strong function of discharge current. For load shedding at deeper discharges the current is not as critical.

The implications for shallow cycle batteries are that in cases of variable loads, voltage control load shed regulators will load shed over a wide range of DOD's. Restriction of shallow cycle batteries to say 20% DOD becomes very difficult. Improved protection can be provided if the load shed voltage is compensated for load currents (decreasing the voltage setting with load current), or if Ah integration is used for DOD determination.

In PV systems the typical drop-out voltage is 1.9V/cell, as many regulators are preset to this value. Once the load has been shed the voltage rises slowly according to the relevant battery time constant. The load is typically reconnected once a voltage of 2V/cell is reached. The actual time for the voltage to rise also depends on the net charging current. When large discharge currents are load shed and a net charge follows, it is possible that rapid oscillation between the high and low voltages may result. The load shed voltage window should be set to prevent load shed relay oscillation. Bower et al (1990) have observed oscillation particularly with DC motors due to the high current drawn during startup.

Figure 3.52 shows measured rise times for a 100Ah flat plate Pb-Sb battery, under 0.5A/100Ah charging currents, after load shedding at 1.9V/cell at the specified currents.

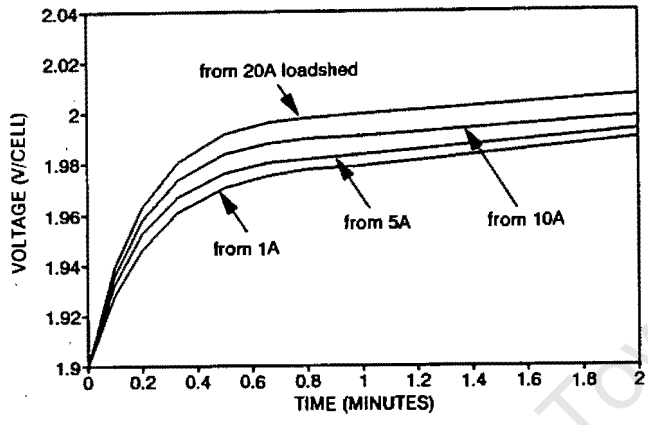

Figure 3.52 Battery rise times at 0.5A/100Ah charging current following various discharge currents, after load shedding at 1.9V/cell.

The battery drop-out voltage during discharge is relatively insensitive to temperature during shallow cycling. Beyond 50% DOD voltage is more strongly affected, as indicated by the broadening range of drop-out voltages in Figure 3.53, and for regular deep-cycling some temperature compensation on the load shed should be provided.

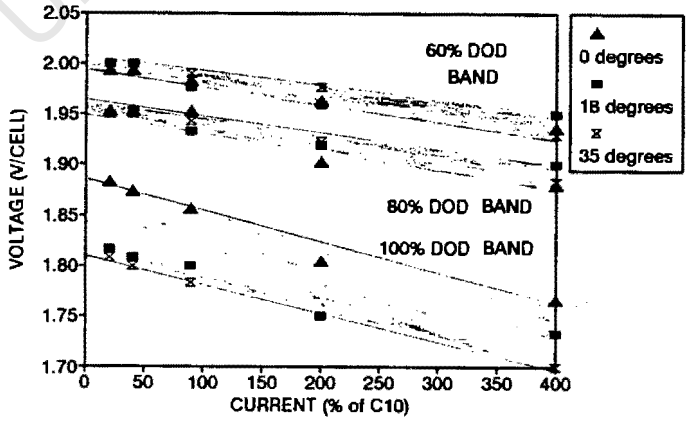

Figure 3.53 Battery drop-out voltage vs temperature and discharge current.

3.14.3 Regulator Adjustment

It is possible that any one of a variety of generic battery types could be chosen for the PV system. One type may even be substituted for one another in the same system. As different batteries require different conditions for optimal operation, it is crucial to be able to adjust the regulator accordingly. The table below relates the various battery types and operating conditions to the most suitable regulator settings, as recommended by the battery manufacturers.

Table 3.6 Approximate regulator settings for generic battery types

	Float mode (V/cell) (20°C)	Boost mode (V/cell) (20°C)	Temperature dependence (V/°C)	
			Float	Boost
5% Sb flat plate	2.3V	2.37V	-0.0020	-0.0033
5% Sb tubular plate	2.3V	2.47V (80% DOD)	-0.0038	-0.0052
LM 1% Sb	2.3V	2.5V	-0.004	-0.007
MF Sb free	2.3V	2.53V	-0.006	-0.006
Gelled electrolyte Sb free	2.3V	2.3V	-0.006	-0.006
Absorbed electrolyte Sb free	2.25V	2.45V	-0.0055	-0.0055

It is impractical and inefficient, not to mention costly in the long term, if the regulator settings cannot be easily adjusted to suit specific applications. This applies not only to the boost, float and load shed settings, but also the temperature compensation and voltage windows. Some of the regulators locally available are not adjustable, or are delivered without literature on how to adjust the settings (Langley,1990). The static, non-programmable nature of analogue regulators makes them relatively inflexible. Essentially, analogue regulators employ algorithms that are voltage driven and not easily compensated for various effects. Temperature compensation is difficult as the electronics has thermal drifts of its own, before the battery temperature coefficients are even considered. Regulators with digital control algorithms may still be voltage driven and accurately compensated, or they may rely on Ah integrators to determine DOD

and the appropriate action. Interfacing digital circuitry with micro-processors opens the door for software programmable regulation.

3.14.4 Microprocessor-controlled Regulators

There is abundant coverage of microprocessor-based PV regulators in the open literature. Most work on digital regulation evolved in the course of the US space programmes, but the falling cost of digital systems is making them a viable and versatile alternative for other applications.

A typical system can accurately perform the following functions:

- Battery charge control
- Battery discharge control
- Array control or power maximisation
- Control panel display
- Status and self test
- Data logging via RS232C port

SOC accounting is by Ah integrator and voltage sensing. Gassing current is estimated on the basis of SOC and voltage. Overcharge and overdischarge protection are provided in a similar way to the conventional regulators, but with additional capability to limit the Ah of overcharge.

Temperature compensation can be software controlled.

Equalisation charge is activated based on the number of partial charge/discharge cycles. The degree of overcharge required is calculated based on the number and depth of cycles and can be limited to avoid excessive gassing.

Cells are individually monitored. An energy balance around the battery, together with efficiencies, is logged and can be retrieved by digital computer via the RS232C port.

For optimum operation the system requires substantial battery data at various temperatures, charge and discharge rates.

The microprocessor-controlled regulators are in an advanced state of development internationally, and in developed countries can be purchased in various configurations. Higher reliability is expected than for analogue devices, as fewer components are coupled with protection provided by intelligent software. Costs of similar analogue and microprocessor-controlled regulators could be comparable, but the extra display and interface features on the microprocessor devices increase costs to twice or three times the analogue price. This price difference limits their general applicability to larger systems in developing areas.

3.14.5 Regulator Efficiency

The efficiency of the regulator is dependant on the control algorithm, the power electronics design and the choice of components. Control algorithms have been briefly discussed. There are two main power electronics configurations for charge regulators: series or shunt (see Figure 3.54); and two main component choices: relay or solid state. These are described in depth in Lasnier et al (1988).

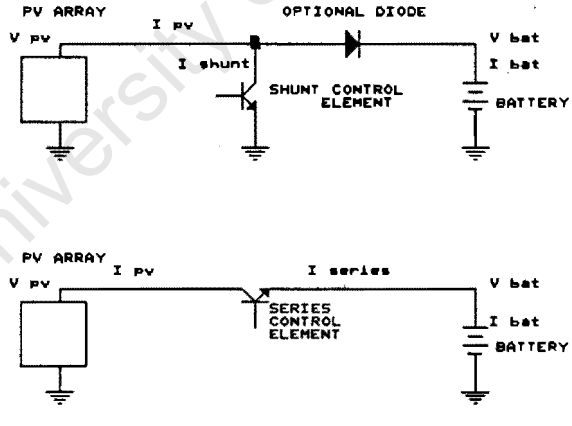

Figure 3.54 a) Shunt and b) series configurations

Regulators should normally be very efficient whether they employ relay or solid state technology. Most often the greatest inefficiency is attributable to the 0.6V blocking diode drop. The diode is used to prevent discharge of the battery into the panel during times of no insolation. In 12V systems the diode can limit the maximum charging efficiency to 95%, whereas in higher voltage systems the effect is less noticeable.

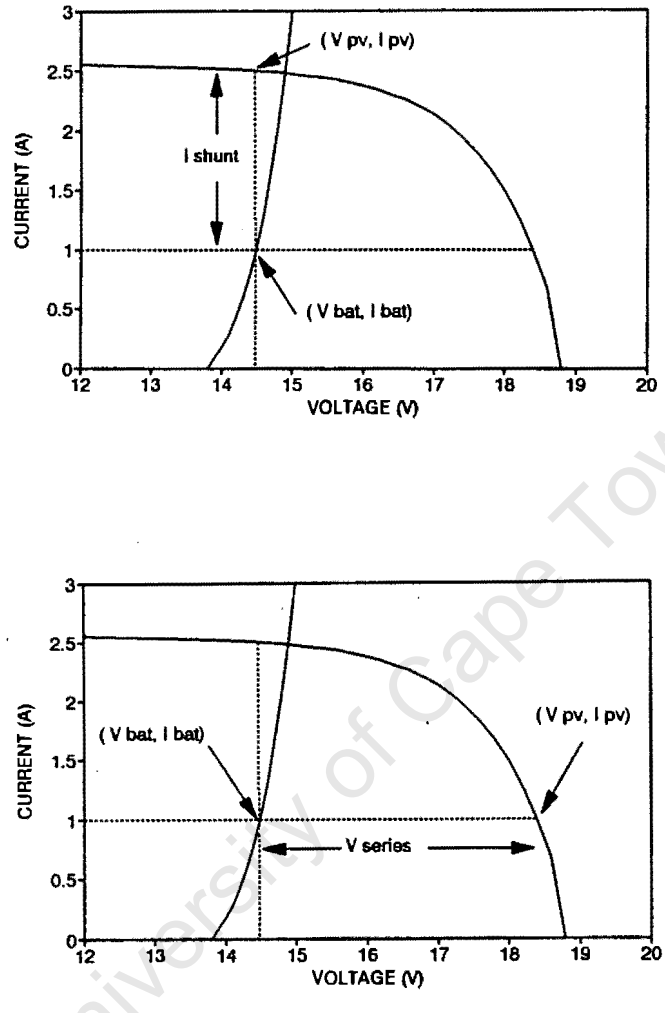

Figure 3.55 a) Shunt and b) series configurations, showing the PV operating points during regulation.

In the shunt regulator, $I_{pv}=I_{shunt}+I_{bat}$, $V_{pv}=V_{bat}=V_{shunt}$
In the series regulator, $I_{pv}=I_{bat}=I_{series}$, $V_{series}=V_{pv}-V_{bat}$

The relay in a series configured relay charge regulator can be opened in times of no insolation to prevent battery discharge, and the blocking diode can be omitted. In normal operation the efficiency may therefore be higher than for a series solid state regulator.

Solid state charge regulators operate by controlling charge at constant voltage, and can be designed to consume very little power.

Load shed regulators are generally the relay type, which consume a few μA during relay excitation. Standby power consumption of the load shed unit is only slightly affected by whether the relay is normally open or normally closed.

The efficiency of the regulator during regulation further depends on matching the type of regulator to the PV array. This is because the series and shunt configurations result in different PV array operating points. The series regulator and the array have the same current, but operate at different voltages, whereas the shunt regulator and panel operate at the same voltage but at different currents. The different operating points are shown in Figure 3.55.

3.14.6 Reliability

The questions of reliability and efficiency, and the debates regarding which of series, shunt, relay or solid state devices is best, are ongoing. Most international regulator manufacturers can supply both shunt and series devices. Some regulators incorporate simultaneous shunt and series regulation and improve efficiency, but at the expense of simplicity. There is application for each type in particular situations.

Generally, if a shunt regulator fails the PV system will still be operational, but in the long term the battery may become overcharged. A failed series regulator may cut out the PV charger, protecting the battery against overcharge; but the load must simultaneously be disabled to prevent overdischarge of the battery. The load will not be disabled if the load shed relay is of the normally closed type, and will be disabled if it is of the normally open type. It follows that a series regulator should preferably be used in conjunction with a normally open load shed relay unit, and the shunt design used with a normally closed unit. The application, degree of protection and approximate battery DOD profile will determine which is most appropriate.

Constructional aspects of regulator design are an important consideration. Basically, reliability decreases exponentially as a function of the multiplicity of

components. The exact relationship depends on the components used and their individual reliabilities. Some components are necessary to provide protection and have slight effect on operational reliability. Component reliability is usually described by stress analysis. For example, a 10W resistor run at 10W will not be as reliable as a 10W resistor run at 5W, and a relay rated at 10A DC will last much longer if it switches at only amperes. Specification sheets are available for higher quality components. Further than that, no generalisations can be made out of context of specific designs and components.

In SA, as in USA (Maycock, 1990) there is general consensus that the regulator is the weakest link in the PV system, followed closely by the battery. Battery lifetime depends critically on optimal regulation. In turn, optimal regulator design requires detailed knowledge of battery characteristics in a PV environment, and these related factors have been a primary motive for the present research.

The relative importance of the reliability of the regulator, or the battery, can be altered by the careful adjustment of system sizing. This is briefly discussed in a sizing example in Chapter 8.

3.14.7 Conclusions

Most PV systems require voltage regulation, both for charge and discharge protection. Temperature compensation of the charging voltage is a desirable feature. Overdischarge protection at shallow DOD's is not easily accomplished.

Regulator efficiency is important for optimising the overall system efficiency, but regulator reliability is far more important in the long term, as battery life may be in question. There are several regulator designs and configurations that can be chosen depending on the particular application. In all cases good battery data is required.

EDRC has undertaken to perform a major research project investigating in depth many of the above mentioned questions and aspects of battery regulation in PV systems.

CHAPTER 4

LABORATORY TESTS OF PHOTOVOLTAIC BATTERIES

4.1 INTRODUCTION

One of the main factors inhibiting the optimisation of PV system designs over the life of the system, and limiting the thorough assessment of particular designs, has been the lack of battery test data appropriate to PV applications. This situation is slowly changing where specialist PV batteries are concerned, but in most cases test data is unavailable that meets the needs of the PV system designer. The objectives of this chapter are to discuss (i) types of battery tests needed, (ii) battery test data presently available and (iii) test equipment and facilities required.

The material presented is discussed from the point of the PV designer, and not from the electrochemist or battery designer. The procedures are phenomenological in character, and references to electrochemistry are kept to a minimum.

4.2 BATTERY CHARACTERISATION TESTS

4.2.1 Discharge Capacity.

The first test likely to be performed on a new battery is a determination of its discharge capacity, which can be given in terms of Ah (ampere-hours) or Wh (watt-hours). The tests would be done using a constant-current discharge. For PV batteries the capacity is usually given in terms of Ah at the 100-h (C/100) rate, with a specified cut-off voltage. The capacity can depend significantly on both discharge rate and choice of cut-off voltage. This is especially true of lead-acid batteries discharged at high currents, less so at low PV currents.

a) Constant current discharge

To characterise a battery for use in a PV system, a series of discharge tests at various constant-currents should be performed with discharge times ranging from 100 h to 3 h. In constant-current tests it is important to maintain constant current during the entire test, even when the voltage begins to drop steeply near the end of the test (Figure 4.1). It is important to maintain a constant temperature for all the discharge tests, normally by providing a constant-temperature bath. Cell temperatures should be measured during discharge tests. Battery tests are normally performed at 20°C or 25°C for SLI batteries, and at 25°C for standby or EV cells. Constant-current discharge capacity tests are often presented in terms of a Peukert curve, which is a log-log plot of discharge current vs discharge time. A Peukert curve is presented in Figure 4.2, demonstrating the effect of cut-off voltage. For PV applications, the plot of capacity vs discharge current demonstrates more readily the limiting capacity available at low discharge rates.

PV battery discharge is not often in constant current mode, but may have an intermittent component. For this reason it may be worthwhile determining the effect of intermittent discharge on battery capacity using a simulated PV duty cycle.

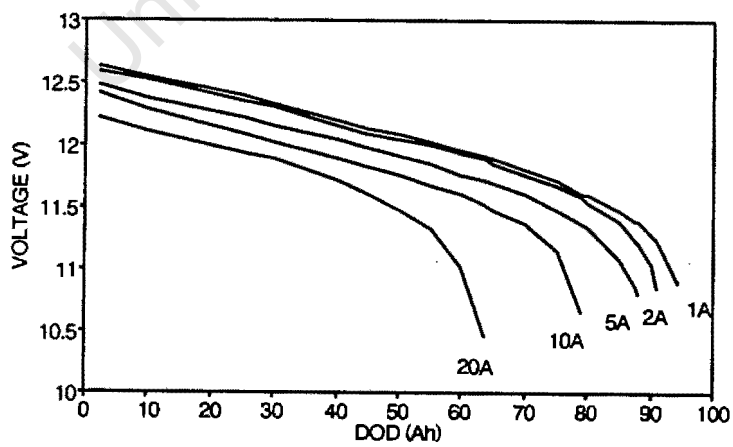

Figure 4.1 Constant current discharge curves for a lead-acid battery. (Source: experimental data)

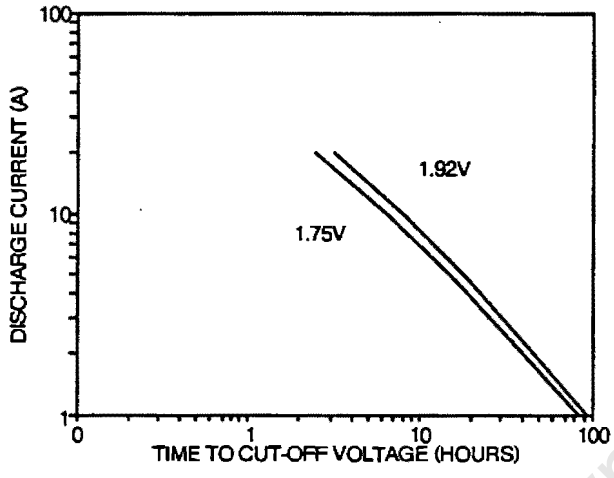

Figure 4.2 Peukert curve for a lead-acid battery, showing time to cut-off voltages. (Source: experimental data)

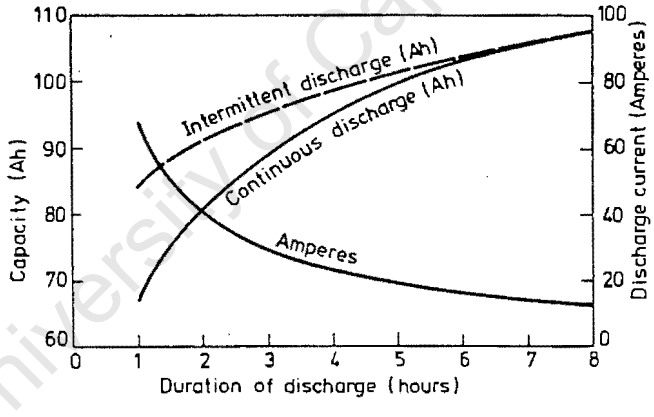

Figure 4.3 Change in capacity and discharge current vs duration of discharge under continuous and intermittent regimes.
(Source: Pavlov,1984:fig 235)

b) Constant power and constant resistance discharge

The effect of constant-power discharge may be important in PV battery testing. The main constant-power applications are DC-choppers for motor or pumping optimisation, and when driving AC loads through an inverter. Constant-power discharge results in rapid change in both battery voltage and current near the end

of discharge. This results in the capacity being smaller for constant-power than for constant-current discharge.

Constant-resistance discharging will affect the capacity, as well as the end of discharge current conversely to the constant-power discharge. Most static loads are constant resistance.

The effect of the different discharge modes on the power output of the battery is not easily derived from the energy output curves.

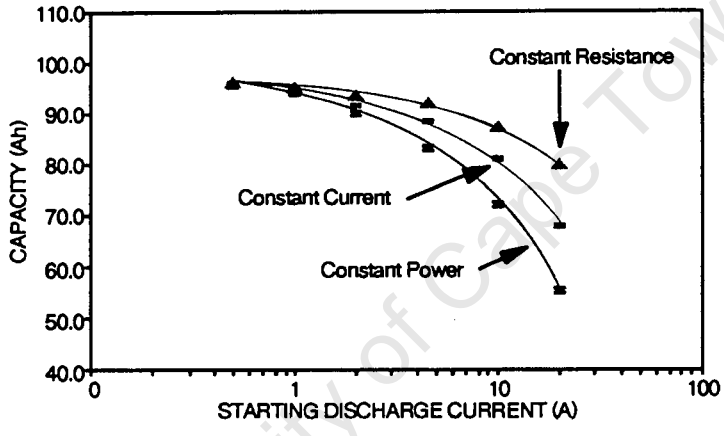

Figure 4.4 Effect of constant-current, constant-resistance and constant-power discharges on Ah capacity.

c) Pulsed discharge

Batteries subjected to constant-power discharge generally experience a pulsed controlled discharge, in which the peak current can be many times the average discharge current. In motor applications, pulsing is most often by PWM (pulse-width modulation) at high frequency (2000Hz). In inverter applications the frequency may be high if PWM is used, or at much lower mains frequency (50-60Hz) in non-PWM designs. Some inverter designs may actually pulse charge-discharge the battery, using is as a stabilising capacitance.

The effects of pulsing current have been studied in considerable detail (Cataldo,1978). If one properly accounts for changes in battery temperature,

utilises a mean battery voltage as cut-off, and compares the results with the constant-current method, the effect on capacity is less than 10%. The battery responds to the average current as far as capacity and mean voltage are concerned, and the instantaneous peak current to determine the transient voltage. Battery heating (I^2R) is considerably higher for pulsed discharging, and the temperature effects should be taken into account when estimating capacity.

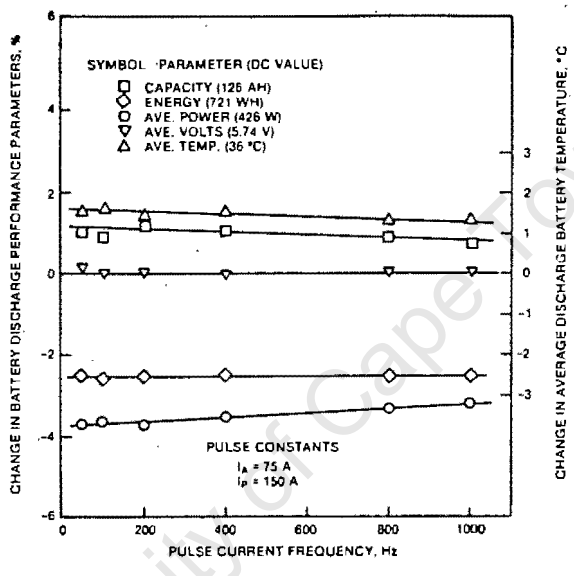

Figure 4.5 Effect of pulse current frequency on discharge performance of lead-acid battery. (Source: Cataldo,1978)

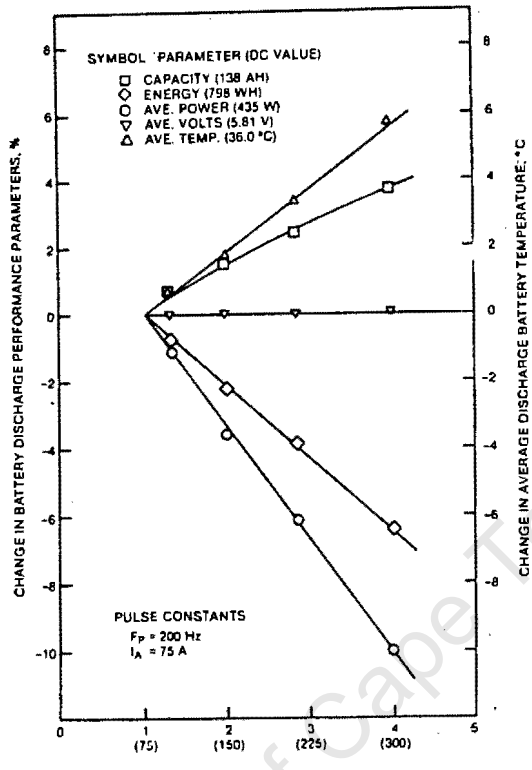

Figure 4.6 Effect of pulse to average current ratio on discharge performance of lead-acid battery. (Source: Cataldo,1978)

d) Load shed settings (discharge termination)

Battery life in PV applications is optimal if the end-of-discharge SOC is limited, usually to around 50% for deep cycle batteries. Voltage is often used as an dynamic indicator of SOC in PV applications, but is not very reliable unless several other parameters are also defined. The voltage/current/depth-of-discharge profile provides a means of estimating the regulator load-shed settings for a given current and maximum DOD (Figure 4.7). It is, however, difficult to provide reliable load shedding at less than 80% DOD, particularly when the load current may vary over a large current range.

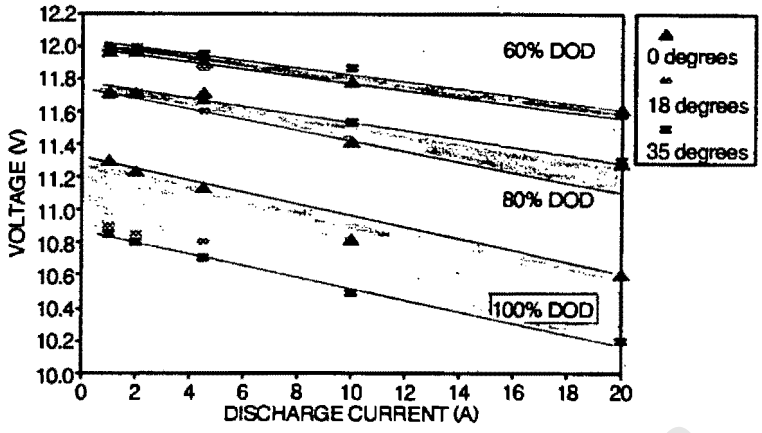

Figure 4.7 Load-shed settings as affected by current, SOC and temperature. (Source: experimental data)

4.2.2 Battery Charging Characteristics

Battery charging data pertinent to PV charging are needed by the system designer. The charging currents are generally low (<5A peak per 100Ah) and the charging times long (2-12h or as long as the solar charge current exceeds the load current). (Refer to Chapter 2).

Tests to determine charging characteristics require a controllable power source. The most important quantity to measure is voltage, which is greater than the open circuit voltage in the case of charging. The voltage during charging should be limited to some specified increment above V_{oc} at 100% SOC to avoid damage to the battery plates due to excessive gassing. Limiting voltage is strongly temperature dependent.

The proper design of a PV energy system and charge controller requires knowledge of the particular battery's charging characteristics, which can only be determined by testing. Characteristics include:

- voltage vs current profiles during charging
- charge termination criteria
- the effect of DOD on charging requirements
- the effect of battery temperature on charging requirements.

Charging characteristics vary significantly from battery type to battery type, and further for different designs within battery types. Determining the proper charging regimes and following them as closely as possible is critical to achieving long battery life.

a) Current-voltage profiles

There is general agreement that the optimum way to charge lead/acid batteries of all designs is to set and maintain a constant current until a specified maximum charging voltage is reached, and then maintain the voltage by tapering the current (controlled current-voltage current method). Charging is complete when some charge termination criterion is met. It is important that the maximum charging voltage is corrected for battery temperature, otherwise excessive gassing can occur, and the battery can be damaged. It is important that the battery is charged under the profiles recommended by the manufacturer, in order to attain a long battery life.

It is clear that PV batteries cannot be maintained in a fully charged state, and except in very specific cases cannot be charged according to the recommended charging regime. The exception is when the PV panels have been most uneconomically oversized. Otherwise, PV batteries may in fact operate mostly in partial state-of-charge, with slow state-of-charge changes during the day (see Chapter 2). Recovery from deep discharge may require several days. It is essential to appreciate the conditions that a battery typically experiences under a PV duty cycle.

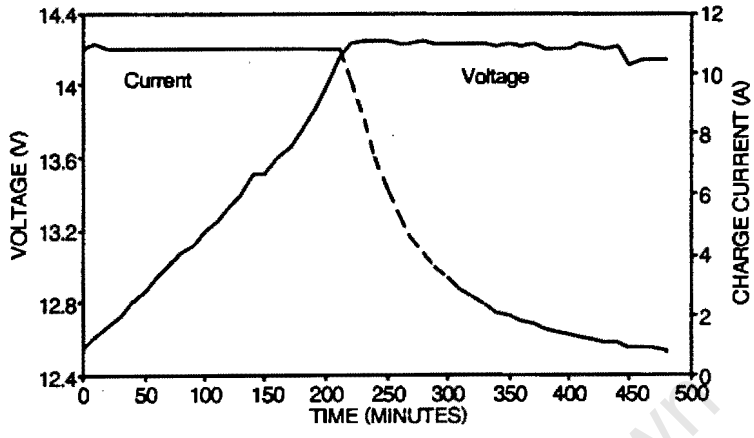

Figure 4.8 Lead-acid battery charging curves, using constant current, constant voltage method.

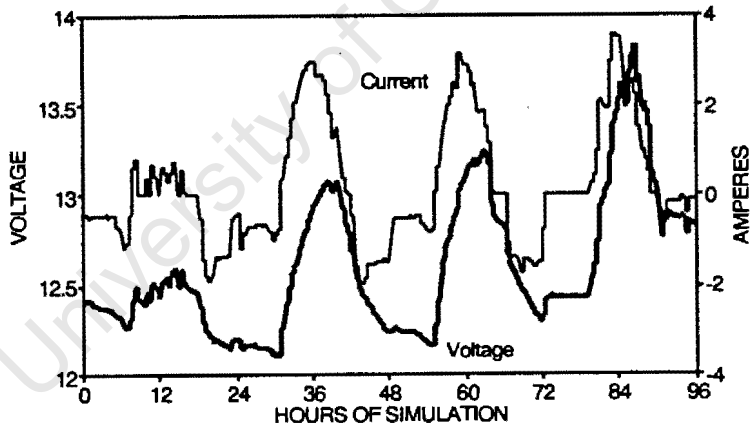

Figure 4.9 Lead-acid charge discharge cycling during PV operation. (Source: experimental data)

b) Charge termination criteria

Termination of charging without overcharging is a notable factor in achieving long battery life, in managing water loss and limiting plate exposure. Usually a manufacturer will specify the percent overcharge that is required and should not be exceeded. There are a number of criteria that can be used to terminate charging, namely: time after a specified event in the charging process, Ah

returned to the battery vs Ah removed, finishing current at a specified clamp voltage, voltage gradient (dV/dT) at a specified finishing current. Applicable charge termination criteria are required for both daily and equalising charging, and for a wide range of DOD. Charge termination criteria should also compensate for changes in battery temperature. The battery test data needed to adopt charge termination criteria for specific applications is seldom available.

The simplest method is to set a number of Ah to be returned to the battery, and to end charging when this is reached. This method requires measurement of Ah during discharge and charge. It is self adapting for aging and for temperature, but requires sophisticated regulation.

An easier method to implement is to terminate charge at a specified time after an identifiable event, eg attainment of a clamp voltage. This method makes it difficult to overcharge by a specific percentage, as the corresponding overcharge time varies widely with the initial Ah removed. Conditions appropriate for charging from a deep discharge (80%) would significantly overcharge the battery when it is charged from a shallow DOD (20%). This would damage the battery, and shorten its life, as well as reduce the charge/discharge efficiency, hence increasing the life cycle cost (LCC) of the PV system operation.

Most PV voltage regulators clamp at the finishing voltage, and do not ever actually terminate the charging process. The correct degree of overcharge can only regularly achieved on systems with controlled, predictable or regular loads (remote repeater stations), they are unlikely to be satisfied otherwise. The literature suggests that insufficient data exists on the profiles and variability of typical household loads to be able to predict overcharge variation.

Some other methods use current or voltage gradient, which are unfortunately sensitive to battery temperature and overcharge required.

The most straight forward method of charge termination is the approach in which a target Ah in is set based on the previous discharge, and charge is terminated when that Ah target is reached. This method requires the least extensive testing of the battery, and is most adaptable to batteries of different designs when complete cycles are the order of the day. The partial cyclic operation in PV applications makes determination of the target Ah more complex than for

complete cycles. It is difficult to predict whether the target Ah would be a function of the DOD alone, or whether the number of cycles at partial SOC (induced electrolyte stratification) should be part of the calculation. Only experimentation will indicate the percent overcharge required for various conditions.

4.2.3 Thermal Effects

The characteristics of a battery depend on temperature. In testing, the environment should be known and controlled. Most often a constant temperature water-bath is used.

The temperature effect on capacity of a lead-acid battery is typically about 0.75% per degree Celsius. The cut-off voltage for discharging is also temperature dependent.

The charging clamp voltage to limit gassing current is particularly sensitive to temperature. The available data is limited, and testing is needed to evaluate batteries for PV systems.

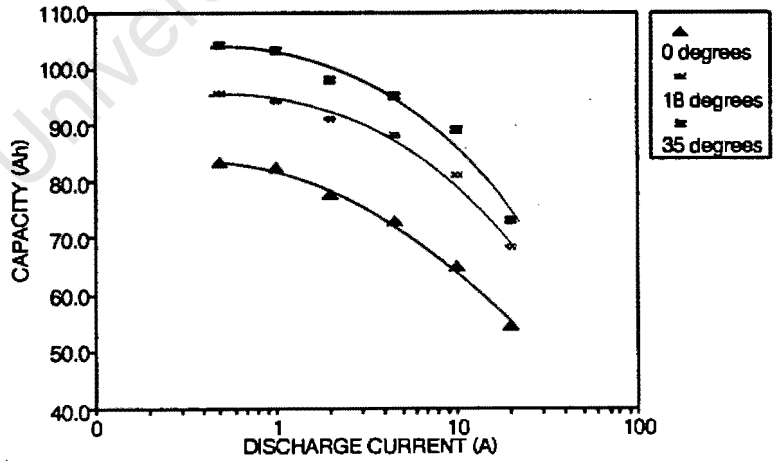

Figure 4.10 Temperature effect on capacity for a 100Ah flat plate flooded electrolyte cell. (Source: Experimental data)

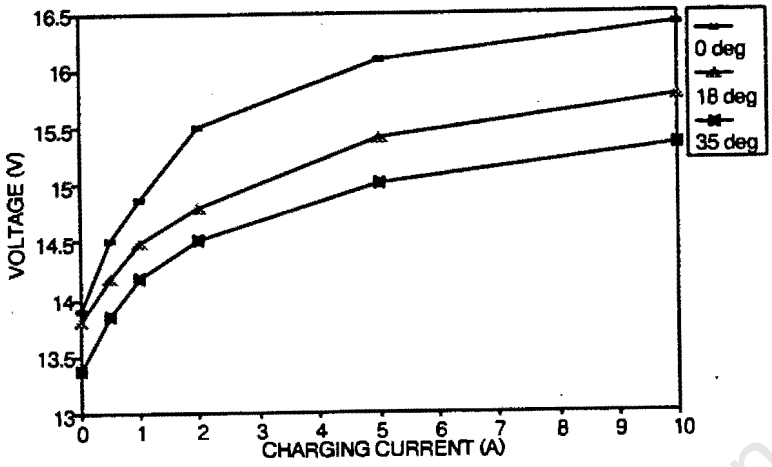

Figure 4.11 Finishing current vs temperature during battery charging for a 100Ah flat plate flooded electrolyte cell. (Source: Experimental data)

4.2.4 Cycling Tests

PV cycling of a shallow discharge battery usually results in the battery oscillating between the 75% SOC and the 90% SOC zones, with a period of one to three days. Typically the battery may bottom at 40% SOC. A deep discharge battery will commonly move between 90% and 50% SOC, and load-shed at 80% DOD. (See Chapter 2).

An effect of partial SOC operation is a temporary capacity loss due to electrolyte stratification in flooded electrolyte batteries. This may be aggravated by unequal utilisation of individual cells. Longer term life-limiting damage cannot be ruled out. The stratification capacity loss is a function of the DOD and the number of cycles before full charge is attained. The temporary capacity loss must be engineered in to the system design if the system is to perform as expected. If temporary, the loss may be recovered by a prolonged equalising or boost charging.

A second life-limiting effect resulting from low frequency cycling is the slow formation of large grain insoluble sulphate crystals by the self-discharge process. The capacity is likely to be affected in the long term.

Verado (1981) of Sandia National Laboratories has developed a test method to rank batteries according to the above mentioned failure modes. There are four variations of essentially the same test. The tests are named:

- standard shallow discharge cycle test
- partial SOC shallow discharge cycle test
- deep discharge cycle test
- partial SOC deep discharge cycle test

The partial state of charge deep discharge cycle test is described here, while the other tests are described in Chapter 6.

> The battery under test is discharged to 80% DOD, and sufficient Ah are added to return to 20% DOD, all at constant current (C5 rate). The battery is repeatedly cycled by discharging to 80% DOD and recharging to 20% SOC. The test terminates when the battery can no longer deliver 60% of capacity before the cut-off voltage is reached. The data of interest includes the end of charge and discharge voltages, and loss of capacity as the test progresses.

4.2.5 Self Discharge

In many applications battery self discharge is sufficiently slow as to be disregarded. In some PV systems partial SOC operation occurs for several months of the year. In those systems (large battery, small panel), the self-discharge rate may be of the same order of magnitude as the panel current. Self-discharge is significant for a system with a battery that can completely self discharge in 5 months. Self-discharge is responsible for the formation of hard large grain sulphate crystals which are difficult to reconvert to active material. Battery self discharge tests, or shelf life tests are usually open circuit tests, where the battery stands idle and the decrease in capacity is indicated by measurement of open circuit voltage and specific gravity. The limitations in open circuit tests should be recognised.

4.2.6 Life Cycle Tests

The life of lead-acid batteries is the main concern of most PV system suppliers and researchers. It has been emphasised throughout this chapter that PV battery cycling poses a tremendous stress on battery, particularly when it is deep cycled. The prolonged periods in partial state-of-charge not only enhance sulphate build-up, but also subject the battery to severe mechanical stresses due to physical expansion of the active masses, which could be damaging.

Life cycle testing cannot be done quickly, (compared with a few weeks for performance testing), and is therefore very expensive and time consuming.

Testing of flooded electrolyte batteries can be accelerated to a degree by operating at elevated temperatures. Matsumo (1984) has considered the applicability of accelerated testing, and concludes that the statistical distribution of the failure modes must be the same for both the standard and accelerated tests. The industry standard for accelerated testing is documented by Clifford (1982). The acceleration factor, F, is given by

$$ln\ F = k\ (T\text{-}25°C)$$

where F is the ratio of cycle life at 25°C to the cycle life at test temperature, T (Miller,1988). The coefficient k is generally assumed to have value 0.02 for small antimony grid cells.

Accelerated testing of batteries under development must be carefully controlled. Enochs (1984) shows a wide range of cycle life and failure modes for non-antimonial batteries under accelerated testing. It is uncertain whether the elevated temperatures will produce the same failure modes suitable for PV life cycle testing.

Lifetime is strongly affected by use-pattern and how the battery is charged (incomplete cycles, excessive overcharging). Battery lifetime is usually expressed in terms of number of regular and controlled cycles to a specified DOD. For example, lifetime stated as 500 cycles at 50% DOD, means that the battery could be discharged to 50% DOD and fully charged 500 times before the capacity falls

to 80% of the original usable value. Battery operation and failure is statistical in nature, and should therefore be performed on a large sample.

The limitations of life cycle data when applied to PV systems are particularly severe, and the repeated undercharging of the battery will certainly decrease the battery life compared with the manufacturers life cycle data.

As far as this author is aware, no battery life cycle data is yet available using PV simulated cycles. The Florida Solar Energy Center is working on this. Zmood (1988) has also done work determining user energy demand profiles for this purpose. Alternatively, the cycling tests developed by Verado (1981) of Sandia National Laboratories can be continued till battery failure and used as a approximation of PV conditions.

4.2.7 Scaling of Battery Test Results

Scaling of battery test results is possible if the batteries being considered have essentially the same active block design. The basis of the scaling is the thickness and construction of the plates, although the size and number of plates may be different. The Canadian Standards Association (1989) regard this data as extrapolated data of Grade C quality (see Section 4.3.2)

The Ah capacity and charge/discharge characteristics can be scaled with a reasonable degree of confidence. Ah/cell is a measure of plate area per cell, and indicates current density (Ah/cm^2) in the cell. Batteries of similar construction, operating at the same current density, will have the same voltage drop and internal resistance, regardless of cell size.

If one has current/voltage data for a cell of a particular capacity Ah_1/cell, the voltage/current characteristics for a cell of capacity Ah_2/cell can be inferred by scaling the current as

$$I_2 = \left(\frac{Ah_2/cell}{Ah_1/cell}\right) I_1$$

at the same relative depth-of-discharge. The internal resistance of small cells will be higher than for large cells, but is of small importance in low current applications. The resistance per cell is scaled as

$$r_2 = \left(\frac{Ah_1/cell}{Ah_2/cell}\right) r_1$$

The capacity as a function of discharge rate can be scaled by referencing the discharge current and capacity to a fixed condition such as the C_{10} rate. The smaller the discharge current, the better the correlation.

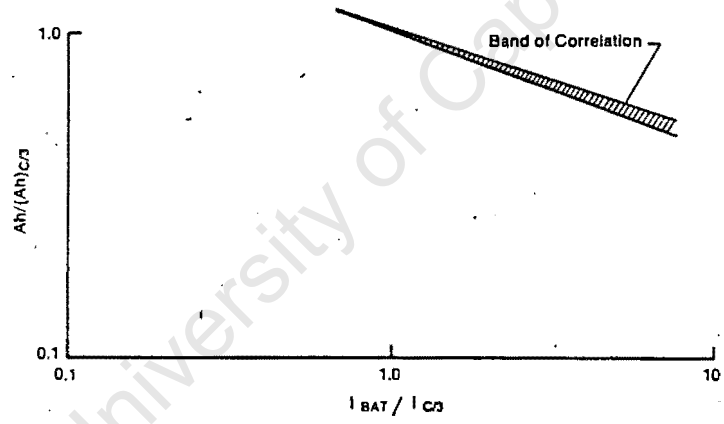

Figure 4.12 Correlation of normalised Ah capacity with normalised charge rate. (Source: Burke,1984:fig 39)

All the characteristics of a battery of a given type can be scaled. The rules apply to single cells, and to some extent complete batteries. Batteries connected in strings may be an exception to the rules, due to the statistical nature of their behaviour. Life cycle data and capacities of strings may be suited to scaling.

4.3 BATTERY TEST DATA

4.3.1 Introduction

There is limited lead-acid battery test data available in the open literature (Sieger,1981; Burke,1984), and data available is often in a form not particularly useful to the PV system designer. For a variety of reasons, test data may not be applicable in the field, or does not relate directly to field experience.

In general, imported batteries are better supported by laboratory data than locally manufactured competitors. In the case of specialist PV batteries, the foreign manufacturers have a bigger market and can afford the extra expense of extensive testing. Additionally, more primary research and development into batteries is done internationally than locally. Unique data is obtainable as a result of battery assessment subcontracts being an integral part of their development.

But data provided is rarely complete. In many cases the data supplied by the manufacturers is vague, unstandardised or of questionable accuracy. Much data is derived or approximated from tests on similar batteries. In many cases the data may be inappropriate to PV applications. Unfortunately, basic testing is often seen as secondary and supplemental.

4.3.2 Data Quality

The Canadian Standards Association (1989) classifies PV battery data supplied by the manufacturer into five categories according to quality:

Grade A1 - data is supplied by an independent test laboratory, obtained from tests on the specific battery model. Grade A1 is applicable only to the conditions under which the battery was tested.

Grade A2 - as for Grade A1 but testing is performed by the manufacturer in-house.

Grade B - data is obtained by extrapolation of Grade A1 or A2, but not verified by testing.

Grade C - scaled data. Derived on the basis of Grade A or B data, but from batteries of different size or capacity.

Grade D - data other than defined for the above categories. It should be evaluated for its validity and applicability for the given application.

This method of grading data is practical and concise, and is adopted for this report. Most battery data finally used by PV modellers and designers is Grade B or worse, as it must be extrapolated because of the difficulty in approximating PV conditions.

4.3.3 Data Available from Manufacturers

Data most often found in the open literature is listed below. The order of listing indicates the prospect of the data being available, and the data grading is shown in parenthesis:

- nominal capacity at 25°C or 20°C (A1,A2)
- capacity as a function of discharge rate (A1,A2)
- capacity adjusted for temperature (A,B)
- discharge voltage profiles at one temperature (A)
- discharge cut-off voltages (A)
- self discharge rate (C)
- self discharge rate vs temperature (C, B)
- cycle life vs DOD (B,C)[1]
- charge voltage (A,B)
- float charge voltage range (A,B)
- starting current for charging (C)
- finishing current for charging (C)
- charge voltage vs temperature (B)
- cycle life vs temperature (A,B,C)

[1] Cycle life is usually presented versus DOD. Two test data points are usually available, and further points are extrapolated using models. Results depend strongly on which model is selected.

Data that is practically never offered is listed below. Its availability is usually the result of specific requests.

- charging curves (A)
- charging efficiencies vs Temperature, Voltage (A)
- rate of water loss (where appropriate) (A)
- rate of acid stratification (A)
- overcharge requirements vs DOD (A,B)

4.3.4 Standards and Standardisation

Battery testing conducted by local manufacturers is mainly for quality control. Typical tests conducted for either SLI or EV batteries[2] are:

- High rate discharge: 3 second discharge @ 500A, mainly applicable to quality control of SLI type.
- Low temperature (-18°C) cranking test for SLI type.
- Capacity test @ various discharge rates.
- Overcharge test till failure: mainly applicable to SLI type. Of some relevance to PV, but not directly transferable.
- Shelf life extremes 1,2,3 etc months at controlled temperatures.
- Life cycle (not directly transferable to the field).
- Other specific tests where requested.

The focus of the tests is conformation to manufacturing standards (SAE for the UK, DIN for Europe and SABS for South Africa). SABS standards for PV batteries are non-existent, but standards are available for SLI and EV quality control. European and American standards exist only for PV installation and maintenance.

2 Discussion with Raylite Batteries

Battery characterisation standards exist (Canadian Standards Association,1989), but the mandatory testing is limited and perhaps of questionable application in the field[3].

The introduction of standards has a further role over and above quality control, which is to assist the manufacturers in offering data which conforms to

- specified formats,
- according to specified and relevant test procedures,
- and which allows transfer of the laboratory test data to real applications outside the laboratory environment.

Characterisation standards provide a means of ranking the batteries according to their suitability for the application.

4.4 BATTERY TEST EQUIPMENT

4.4.1 Broad Equipment Requirements

It is most often necessary to characterise a battery to aid component selection for PV systems development, or to generate characteristic data for computer simulation. The battery data required may not be available from the battery manufacturer, and the researcher may have to perform independent tests in the laboratory.

The equipment needed to perform the typical battery characterisation tests (See Section 4.2) in a small scale laboratory environment is described below.

If only a few cells are to be tested at once, the power requirements are modest and the equipment is commercially available. If complicated test programme s or high power tests are to be carried out, equipment is not always available or is expensive. The Battery Evaluation Laboratory at Sandia National Laboratories is

3 Canadian Standards specify a dynamic cycling test which is based on the cycling tests developed by Sandia Laboratories (see "cycle testing", Section 4.2.4). These test are not mandatory, and the focus of the Standards is on capacity, and average cycle efficiency during charge and discharge.

an example of a sophisticated system, with twenty test stations under computer control and elaborate software for instantaneous performance readout (Verado,1981). This system is beyond the means of most research budgets. Kuiper (1989) has developed a versatile, small scale and lower cost battery test rig suitable for battery characterisation and cycling.

a) Discharge testing

Voltage varies with SOC during battery discharging at constant-current. A variable load is required to maintain constant-current or constant-power during the discharge. If a resistive load is used, the resistance varies proportionally to the voltage, and for constant power resistance varies as the square of the voltage. For ease of testing it is desirable that the load be programmable so the discharge current profiles can be easily maintained or changed.

Programmable solid-state or semi-conductor loads are commercially available in the power ranges required. Most loads can be interfaced with a micro-computer so discharge testing can be done under computer control. This is particularly helpful for discharge testing under simulated load profiles, or for low current discharge tests of long duration.

For constant current or constant power testing, the instantaneous load would be programmed by a feedback signal derived from the measured battery current and/or voltage.

b) Charge testing

Equipment for charging batteries is commercially available for a wide range of power requirements and resolutions. Equipment should be capable of constant current and constant voltage operation. Both the current and voltage should be adjustable. Interfacing the charging equipment with a micro-computer enables PV charger simulation by feedback of the battery voltage and current. The programmable charging capability can also be used for automatic correction of the charging voltage for battery temperature, if a temperature sensor is interfaced to the computer.

c] Temperature

Battery temperature is usually controlled during capacity determination, but in overcharge testing is often an observed variable. A constant temperature water bath is most often used in conjunction with a laboratory temperature controller. Basic controllers are widely available commercially; more sophisticated controllers with a control and measurement interface to the computer can be purchased.

d] Specific gravity

The SG of the electrolyte is important in lead acid battery testing. SG is normally measured manually and intermittently using a hydrometer. Matsui (1987) of Yuasa Battery Co. has developed an optical hydrometer with digital output. With only a little adaption this device could be used for automatic SG data capture on a computer or data-logger.

e] Software

Selection of suitable software for computer control is dependent on the type of tests to be performed. In most cases the software can be quickly developed for small scale systems. The software should include graphical outputs of selected variables, automatic termination of cycles and easy programmability. The frequency of data-logging (once every minute) does not necessitate especially high speed or complex software.

4.4.2 System Power-handling and Test Equipment Sizing

a] Programmable load

The programmable load should be capable of simulating typical PV load profiles, as well as performing standard constant current/resistance/power discharges as described above.

The nominal system voltage of stand-alone PV systems is usually in the range 12-48V. Steady state load currents are typically in the range 0-10A per 100Ah of installed battery capacity for DC loads. Intermittent high discharge currents of 20-45A are possible when an inverter is used, or due to surge currents during DC motor start-up. High inverter currents are typical of low voltage systems.

In some battery ranges (tubular cells) the smallest cell available for testing may be 200Ah capacity. The programmable load current requirements for such a battery are doubled, though, of course, scaling should be used where possible. Scaling is of limited potential when strings of batteries are under consideration, where it is advantageous to test the string as a whole. This is more economical than conducting separate tests on each cell, and enables effective collection of statistical data.

A programmable load capable of sinking 45A at 12V (the low voltage case), and approximately 30A at 48V (60V nominal) should cater for most cases.

b) Power supply

The programmable battery charger should operate under constant current or voltage control; and be capable of simulating PV array charging. The charger should complement the programmable load: it should be capable of simultaneous connection to the battery under test without danger of short-circuit or malfunction.

The charging voltage of small stand-alone PV systems typically ranges between 15-60V for 12-48V systems. Operating currents are normally kept below 15A by increasing the system operating voltage. For testing batteries of nominal capacity 100Ah, the charger should be capable of sourcing 0-10A. For larger batteries, the required current is scaled proportionally, eg. 10A/100Ah. The charger should be capable of charging entire strings of batteries (12-48V) to complement the programmable load. 2V cells of 200Ah capacity are capable of sinking 15A even under float charge mode. Three 2V cells are likely to be tested in series connection to provide sufficient voltage for programmable load operation. Under equalisation charge mode (parallel connection), these three cells will together sink at least 45A.

The charger should be capable of sourcing 45A at 3V (2V nominal) and 15A at 60V (48V nominal). If two supplies are available, then one precision supply in the 10A/60V range, and a lower precision supply in the 50A/36V range would suffice.

c) Accuracy and precision

The desired programmable accuracy of the test equipment is generally specified as better than one percent over the entire range. The precision should be of the same magnitude. The current measurement resolution required is the lesser of one percent or 20mA for both charge and discharge. The voltage resolution is particularly crucial, as it is voltage change that is important. Voltage resolution should be within one percent or ±15mV.

d) Temperature

Temperature effects are not particularly important over small ranges (1-2°C). Temperature control of the battery within ±1°C of the set value, and measurement of the electrolyte within ±0.5°C is sufficient.

CHAPTER 5

EQUIPMENT DESIGN

5.1 INTRODUCTION AND OVERVIEW OF REQUIREMENTS

Equipment requirements for small scale laboratory testing and battery characterisation are discussed in detail in Section 4.4. The overall system requirements have been specified as:

1) A micro-computer controlled battery test unit, with variable charge and load cycling and automatic data capture. Software controls power electronics to simulate PV system charge and discharge regimes.

2) A programmable DC power supply capable of sourcing 50A at 60V, for a maximum power of 3000W. A matching programmable load capable of sinking 50A at 12V, 30A at 60V for maximum power of 1800W.

3) Resolution for control and readback of battery voltage, supply current and load current is to be better than 0.5%, with programmable accuracy and precision to be better than 1%.

4) A water bath to allow battery temperature control, and sensors to read back the water temperature to the computer.

The overall system layout is shown in Figure 5.1. The equipment design is discussed sequentially, beginning with the electronics of the programmable load and power supply, then the computer interface, control software, and temperature control.

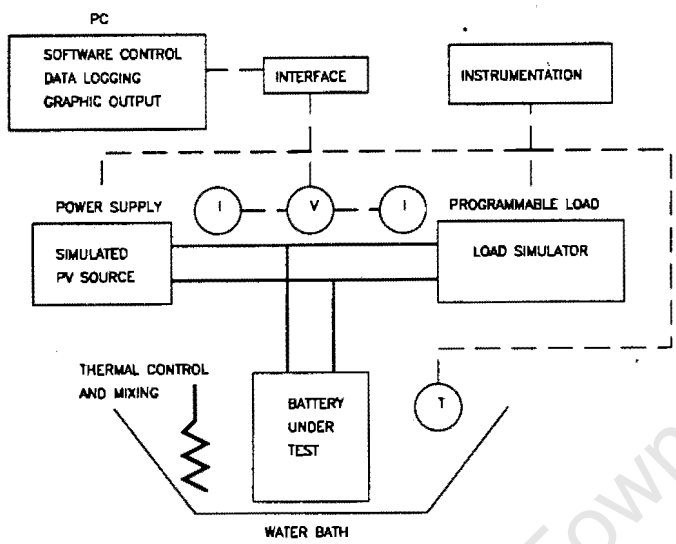

Figure 5.1 Block layout of the programmable battery test unit. Dashed lines indicate communication linkages. I=current, V=voltage, T=temperature.

The remainder of this chapter is concerned with test equipment design as follows:

5.1 Overview and selection of appropriate electronic design
5.2 Electronic design and component selection
5.3 Software requirements and design
5.4 Thermal control and measurement

5.1.1 Overview of DC Power Supplies and Loads

Many laboratory electronics equipment suppliers can provide excellent DC power supplies and loads (Burke,1984:954). However, this apparatus is typically over-specified for battery testing, and is generally very costly. Suitable equipment can be built in-house at lower cost, although there may be a significant equipment set-up time.

A broad range of basic electronic designs is available for DC power supplies and programmable loads. These are tabulated, listing the advantages and disadvantages of each particular power electronics design.

Table 5.1 Overview of electronic load designs.

DESIGN	DISADVANTAGES	ADVANTAGES
Transistorised Load	semi-conductor prevents full current operation at low voltages	low power requirement if FET driven
	bulky due to transistors to dissipate heat	simple to design
		low cost
Digitally Switched Resistive Load	bulky - large number of resistors	operates at low voltages if required
	high cost: precision resistors and contactors	extremely rugged
SCR Mains Regenerative	cost: requires professional to construct	low heat dissipation: power regenerated to mains
	cannot operate at very low voltages	rugged SCR components
	some research still required	elegant solution

Table 5.2 Overview of DC power supply designs.

DESIGN	DISADVANTAGES	ADVANTAGES
SCR and Filter	large filter required to eliminate mains frequency voltage ripple	uncomplicated to assemble
	battery is an active component in filter, causing battery heating	moderate response
Series Linear Regulator	high power dissipation over series transistor, low efficiency	high precision
	bulky, large number of transistors to overcome heating	easy to design and construct
		very fast response
Switch Mode Regulator	cannot operate at zero output current (swinging choke saturates)	high precision in designed operating region
	tricky to design, build and protect	small and compact, high efficiency (80%)
	output noisy, contains spikes	fast response to load and line changes
Series Linear Regulator with SCR Tracking Pre-regulator	bulky, essentially two supplies in series; both SCR and low dissipation, high current, linear regulator	lower power dissipation over transistors, higher efficiency than linear regulator
	more difficult to design, two control loops to consider	fast response
	linear response slowed by pre-regulator	high precision industry standard design

5.1.2 Design Choice

a) Programmable load

The selected design is a transistorised electronic load operating as a current sink, with a grounded high current supply, which is actually the battery under test. The load is controlled by a 0-10V analog signal, with analog current readback of 0-10V for both current and voltage. The voltage programmable load is calibrated to sink 50A for a 10V input. Load current can be read from the control panel.

The transistorised load is preferred to the other options on the grounds of simplicity and cost. The cost is estimated at R1000. The resistive load design is estimated to cost R5000, mostly due to precision resistor windings and DC contactors required for switching. The SCR mains regenerative device requires further substantial development. The transistorised load is an industry standard design which has superseded the more bulky resistive set-up (Hewlett-Packard,1989).

The design of the programable load is covered in Section 5.2.1.

b) Power supply

The preferred design is a linear power supply with SCR tracking pre-regulator using the grounded load configuration, with return line current sensing. The power supply operates as a constant current source, and is calibrated to source 0-50A for a 0-10V analog input signal. Output current is read back by a 0-10V analog output signal. Simultaneous output to instrumentation is required.

This particular design is the only reasonable choice under the required range of operating conditions for the following reasons:

- the power dissipation requirements are simply too high for a linear series pass regulator,
- all advice recommended strongly against attempting to build a switch mode supply (Horowitz et al,1980:211).
- The SCR rectifier, even with a filter, could generate sufficient mains frequency ripple current to cause heating to the battery under test,

- thereby casting doubt over the suitability of the similar SCR mains regenerative device as well.
- Although the regulator with pre-regulator is bulky, the efficiency is moderate and the output quiet, with low noise and ripple. The supply reacts quickly to line and load changes.

The SCR tracking pre-regulator with linear regulator design is an industry standard for precision power supplies that are required to operate over a broad range of voltage and current conditions (Hewlett-Packard,1989; Fry,1973).

As the power supply consists of several discrete subsections, the power supply design is covered linearly, beginning with the output stage in Sections:

5.2.2 Output stage, the linear regulator
5.2.3 LC filter
5.2.4 Tracking SCR pre-regulator
5.2.5 Isolation transformer

Safety considerations for the electronic load and power supply are discussed in Section 5.2.6.

Figure 5.2 is an overview diagram of the load and power supply, and shows the layout and main design sections.

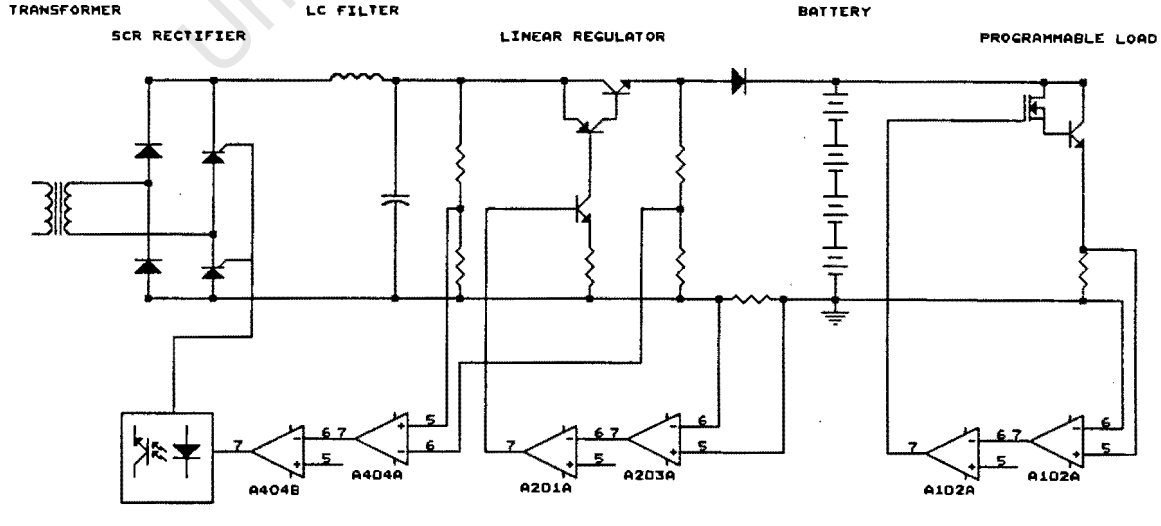

Figure 5.2 Electronic design components of the battery test unit.

c) Electronics / computer interface

The programmable power electronics cannot be designed without discussion of the computer interface. The Eagle PC-30 A/D-DAC Interface was selected for this purpose. This versatile and simple, off-the-shelf card plugs into one expansion slot of the IBM PC/XT/AT compatible computer, is favoured over a one-off design, or to interfacing to the power electronics via a parallel port interface and analog/digital converters mainly because of its quick set-up time. The parallel port interface option would only provide 8 bit resolution if a PC were used. A 16 or 32 bit machine is not justified for a single test rig, though for multi-tasking the speed is required and the resolution is a valuable spin-off.

The PC-30 provides sufficient features and digital resolution for the control and readback signals. These are:

- programmable load control; 50A, 12 bit D/A
- programmable load current readback; 50A, 12 bit A/D
- programmable load voltage readback; 60V, 12 bit A/D
- power supply current control; 50A, 12 bit D/A
- power supply current readback; 50A, 12 bit A/D
- temperature readback, 2 off; 12 bit A/D

Section 5.2.7 covers computer interfacing and control.

5.2 ELECTRONIC DESIGN

The electronic design is divided into six major sections. These are discussed as follows:

5.2.1 programmable load design
5.2.2 power supply, output linear series regulator
5.2.3 power supply, LC filter
5.2.4 power supply, SCR pre-regulator
5.2.5 power supply, power transformer
5.2.6 safety circuits and switches

5.2.1 Programmable Load Design

a) Transistorised load - general description of operation

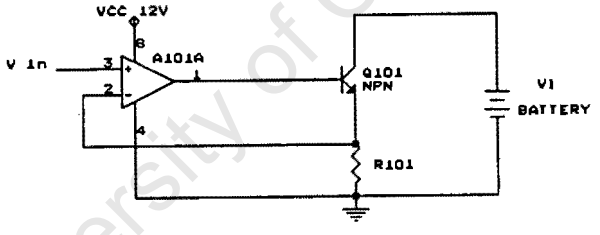

Figure 5.3 Transistorised load operation

The battery provides the load voltage, V_L, to the collector of transistor Q101. The control voltage, V_{in} (0-10V), is at the positive input of op-amp A101A. The op-amp provides base current to Q101, such that the voltage drop across resistor R101 is equal to V_{in}, by negative feedback. The current from the load is therefore under linear control. The main limitation is the heat dissipation over Q101, which is in reality an array of transistors.

b) Power transistors

The low cost 2N3442 NPN power transistors were chosen for the current sink (specifications in Appendix E). The low cost 2N3442 has moderate current gain,

and can dissipate up to 115W at DC. There is no danger of second breakdown at the maximum load voltage of 60V.

Heat dissipation of the array

The maximum electronic load current is 50A, and the maximum power handling capability is 1.6kW over the transistor bank.

Calculations based on specified thermal resistances suggest that each 2N3442 can dissipate 97W when derated for case temperature of 55°C.

The real heat dissipation was determined experimentally for six transistors mounted on a 50cm length of heavy duty heatsink cooled by forced convection. Under these conditions the maximum power dissipation per transistor is only 55W. The actual case temperature under these conditions is 104°C at ambient temperature of 40°C. The discrepancy in power dissipation is due to limitations in the heatsink heat transfer convection coefficients. The transistors are certain of safely dissipating a conservative 45W of heat even at ambient temperatures of 40°C. (See Appendix E for details of experiment and calculations).

Assuming 45W dissipation, the maximum power dissipation for six transistors is 270W per 50cm heatsink. Therefore six 50cm heatsinks, or 36 transistors, are needed to dissipate 1600W of heat. At the maximum load current of 50A, the current per individual transistor is 1.39A, well within the SOAR (see Appendix E).

This conservative estimate of transistor power dissipation pays dividends in terms of current gain and base drive requirements.

Current gain

The DC current gain (H_{fe}) is both temperature and collector current dependant, and is conservatively assumed to be 30 at the maximum current of 1.39A per transistor. The 36 individual transistors are connected in parallel to form the load array, which is assumed to have the same current gain. It follows that the base drive current for the transistor array is 1.66A at rated current.

The base current to the load array is elegantly provided by MOS technology, the power FET MTM15N45 is an N-channel enhancement mode device. The voltage driven FET has the advantage of exerting no load on the op-amp. The FET easily dissipates 3A at 60V at case temperatures approaching 60°C, but for safety the FET is not mounted on the same heatsinks as the load array. The FET has suitable on-region characteristics right down to V_{DS} of 2V. (See specifications in Appendix E).

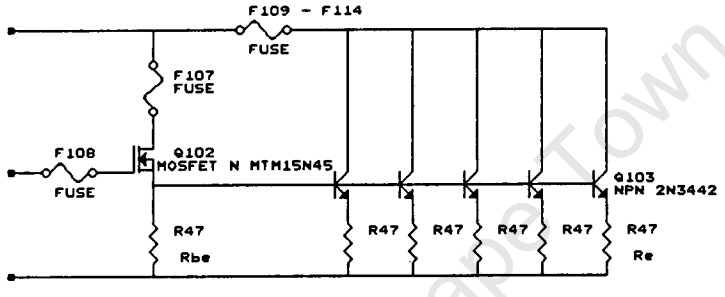

Figure 5.4 Load transistor array with FET driver

Figure 5.4 shows the complete load array. This design is formally called a "bipolar transistor booster". The emitter resistors (R_e) are added to ensure that each transistor carries the same current and heat load. The resistor (R_{be}) from base to emitter of the 2N3442 array improves array response as well as preventing the FET leakage current from biasing the transistors into conduction.

The actual load array current gain at 50A was experimentally determined to be 40, and the graph of load array DC current gain is shown in Appendix E for comparison with the data sheet.

c) Current feedback measurement

The 0-50A load current operating range requires a special measurement circuit to ensure 1% accuracy over the entire range. This can be achieved either by using a low power current sensing resistor with expensive high gain instrumentation amplifiers, or a larger high power and temperature stable resistor with more basic

amplification. High gain amplifiers will degrade the feedback frequency response of the constant current source.

Power resistor

Alkrothal temperature-stable wire rated for 1% deviation at 300°C was wound into a high power resistor which provides 1V at 50A and dissipates 50W. Experimental evidence shows that a stable temperature of 120°C at 50A can be maintained with fan cooling.

Current feedback measurement circuit

A differential amplifier amplifies the voltage signal from the current sensing resistor, even though the current sensing resistor is earthed. The differential configuration improves precision, since at high currents the spurious voltage drops through the wiring between power resistor and earth become significant.

Figure 5.5 shows the basic current sensing amplifier. Note the trimming circuit for trimming the input offset voltage so that the output of the amplifier can be zeroed. The versatile LM358 was chosen as it can be powered from a single supply, and the inputs can go all the way to ground, and even to 300mV below. The gain is set at ten, so that the 1V resistor signal is amplified to a 10V signal suitable for feedback.

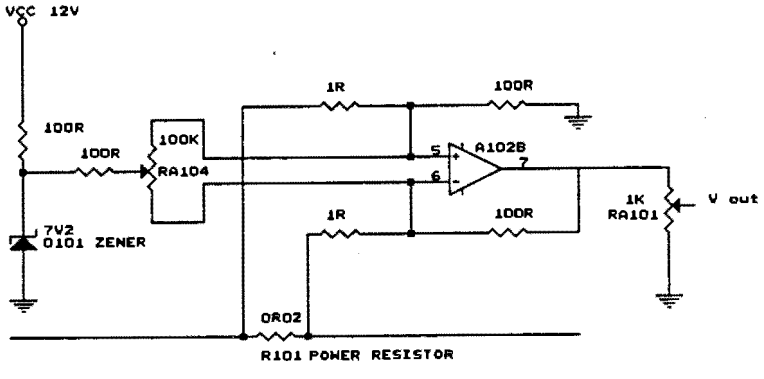

Figure 5.5 Load current sensing and feedback amplifier

d) Current control loop and stability

The high performance of the current sink control loop shown in Figure 5.3 depends on a high closed loop gain (CLG), in turn dependant on the gain of amplifier A101A. This amplifier must be in differential configuration and the gain is set nominally at 33. An LM358 single supply op-amp is used. Resistors are chosen to ensure input impedance matching at the main control amplifier. The control loop is shown in simplified block format in Figure 5.6.

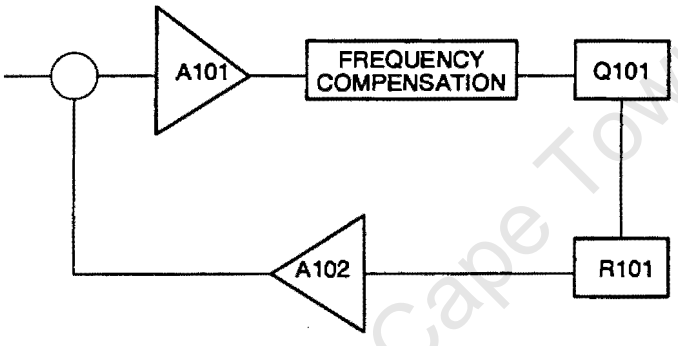

component	gain	break point
A101	A1=33	bp=30kHz
Q101	A2=50A/7V	bp>1MHz
R101	A3=1V/50A	no bp
A102	A4=10	bp=100kHz

Figure 5.6 Block diagram of load control loop

The gain of the load array was experimentally determined, and observed on a digital storage oscilloscope to have excellent frequency response characteristics beyond 1MHz.

The CLG is $A_1 \times A_2 \times A_3 \times A_4$

$$= 33 \times 50A/7V \times 1V/50A \times 10 = 47 = 33dB$$

with breakpoints at 30kHz and 100kHz.

The Bode plot for the current control loop shows instability at frequencies beyond 100kHz due to the CLG roll-off at -12dB per octave. Some feedback compensation is required.

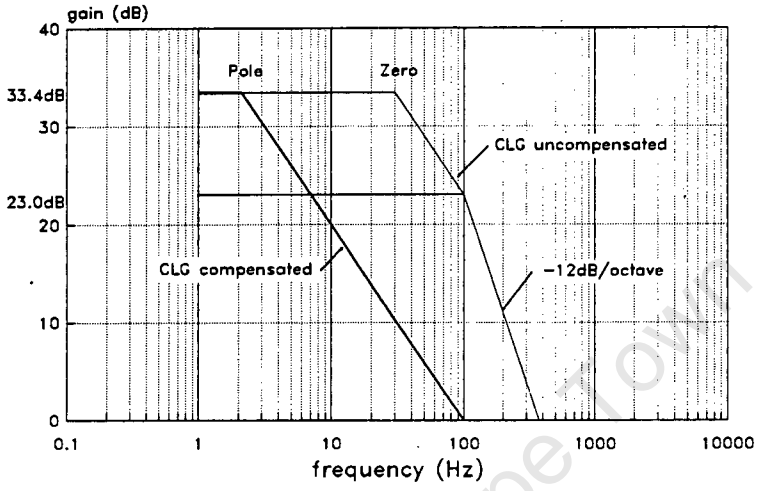

Figure 5.7 Bode plot of CLG before and after frequency compensation.

Lead-lag compensation is the most suitable in this case. The pole and zero are marked on the Bode plot, which has a compensated gain roll-off of only -6dB per octave. The frequency of the pole (f_p) is 2.24kHz, and the frequency of the zero (f_z) is 30kHz. The component values of the capacitor (C101) and resistors (R102, R103) of the lead-lag network are calculated in Appendix E. The circuit diagram of the complete control loop is displayed in Figure 5.8.

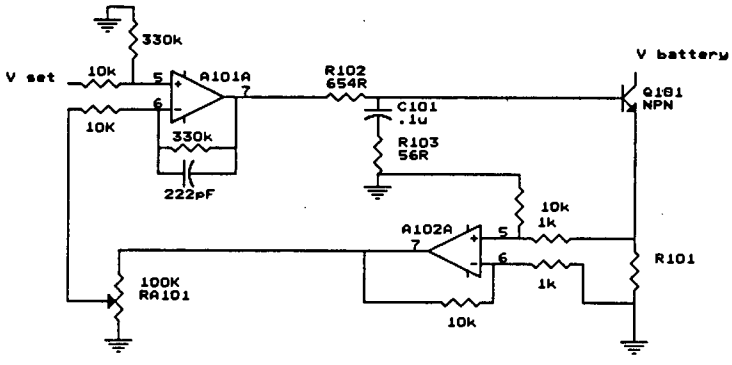

Figure 5.8 Electronic load control loop circuit.

e) Protection

Current limiting

Simple current limiting is all that is required, since when the input to the current sink is shorted to ground no current can flow. The current limit operates by using the signal directly from the current measurement resistor (R101), buffered by a unity gain op-amp. The op-amp output is adjusted by a trim-pot onto the base of a transistor, which pulls down the control voltage of the main control loop when current limiting is effected. The minimum current limit setting is about 30A.

Overcurrent protection

There is a further comparator circuit which normally provides base current to a transistor that supplies the coil of a reed switch which controls input power to the entire electronic load. When the load current resistor signal exceeds a set reference (equivalent to 60A) the base current is removed, consequently tripping out AC power to the entire system. The switches are shown in Section 5.2.6.

Finally, fuses are liberally placed to prevent runaway overcurrent. Most importantly they are located on the load array, positioned at the drain of the FET (2.5A) and one fuse (10A) for every five 2N3442 transistors. The layout is shown in Figure 5.4.

Power limiting

At voltages below 32V the current limit of 50A keeps power dissipation below 1600W. Additional current limiting is required at higher voltages. This is most easily accomplished by software, rather than auto-ranging hardware, where the product of measured voltage and current is kept within the power range by limiting the output current set value.

f] Measurement and instrumentation

Current readback measurement

The output signal from the current feedback amplifier (A102) cannot be used directly as input to an A/D converter or long instrumentation lines without affecting the feedback response, unless the signal is buffered. Further amplification and trimming circuits for measurement, instrumentation and accurate A/D conversion are required. These are shown in Figure 5.9.

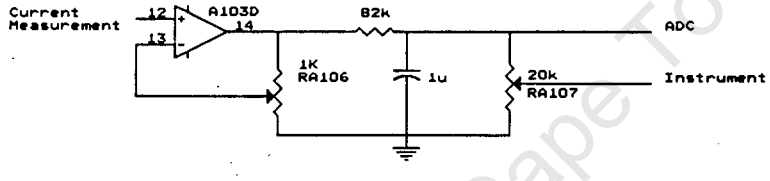

Figure 5.9 Buffered output current signal to A/D and instrumentation from electronic load.

The feedback signal is fed to a buffer amplifier (A103D). The gain is set to give a 10V signal at full current which is suitable for direct A/D conversion. The same 10V signal is divided down by pot R107 to give the 500mV at 50A signal required for the panel instrumentation (10mV=1A).

Voltage measurement

Voltages observed during battery testing typically do not vary by more than 20 percent on either side of the nominal. It is therefore important that small changes in voltage are accurately detected. In particular, experiments measuring the temperature effect on battery voltage are important. The use of a high quality temperature compensated amplifier is justified in this case.

The specified input voltage range is 0-60V. For a 12V battery, the variability of voltage is usually 10V-14V. Resolution and stability are of prime importance. The complete measurement circuit is shown in Figure 5.10, together with a zero

offset trimmer. This configuration requires a split supply, and the op-amp is powered from a +12V -5V supply.

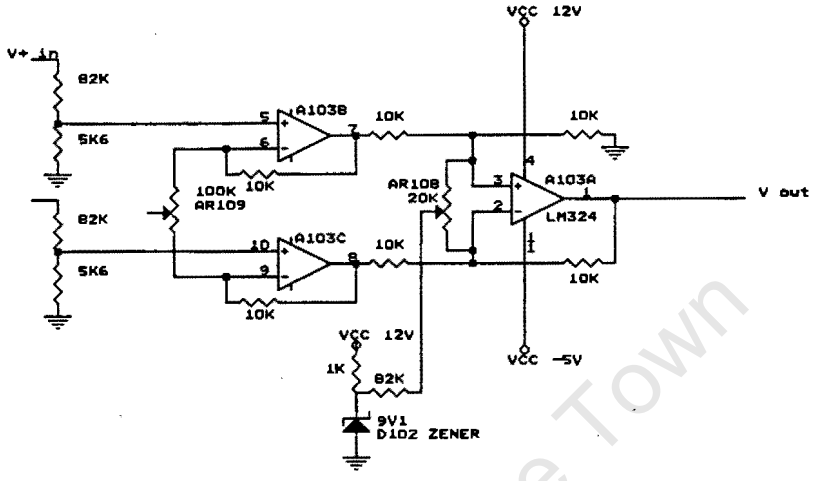

Figure 5.10 Voltage measurement circuit

5.2.2 Power Supply Design, The Output Stage

Series Pass Regulator

It is conventional to begin the design by starting with the output stage, ensuring that specifications are realised, then working back towards to the input stages, allowing for inefficiencies on the way (Fry,1973). The main electronic design components are shown in Figure 5.2 in Section 5.1.2.

a) Linear current regulator - overview of operation

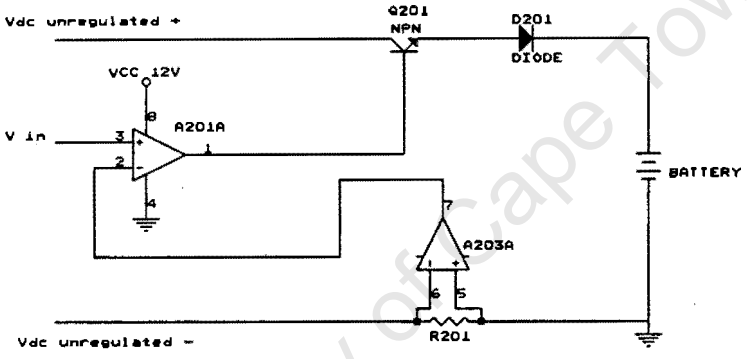

Figure 5.11 Linear regulator, principle of operation

The SCR pre-regulator provides the rectified but unregulated power to the collector of transistor Q201. The control voltage, V_{in} (0-10V), is at the positive input of op-amp A201A. The op-amp provides base current to Q201, such that the voltage drop across resistor R201, amplified by op-amp A203A, is equal to V_{in}. Op-amp A203A simply ground references the current signal, which would otherwise be negative.

The result is a voltage programmable DC current source. As with all linear regulators, the series transistors are most vulnerable to overheating.

b) Power transistors

2N3442 NPN power transistors were selected, as for the programmable load.

Heat dissipation in the transistors

The current rating for the regulator is 50A, and it is assumed that the pre-regulator maintains the voltage drop over the transistors at less than 10V. Then the maximum power dissipation over the transistor bank is 500W.

When six transistors are mounted per 50cm heatsink, each transistor can safely dissipate 45W of heat even at ambient temperatures of 40°C. Therefore two such heatsinks are required to dissipate 500W of heat. For safety, 3 heatsinks are used, giving a total of 18 transistors. At the maximum load current of 50A, the current per individual transistor is 2.77A, and this well within the SOAR (see Appendix E).

Current gain

Assuming a conservative transistor gain of 30 at the maximum individual transistor current of 2.77A, the base drive current for the transistor array is 1.66A at rated current.

The base current to the regulator array cannot be directly supplied from the op-amp because the transistor base voltage requirements will in most cases be higher than the power supply to the op-amp. The problem is easily resolved by driving the power supply array with a PNP transistor, which is driven by a ground referenced NPN transistor. (Figure 5.12).

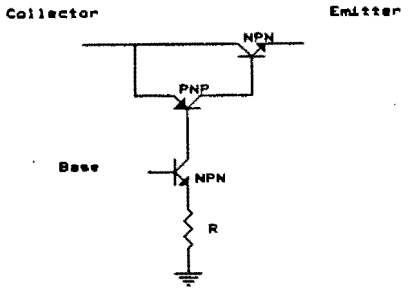

Figure 5.12 Linear regulator base drive arrangement

The PNP transistor selected is the MJ802 (Q203). The MJ802 easily dissipates 2A at 60V at case temperatures approaching 60°C, but for safety the PNP is not

mounted on the same heatsinks as the regulator array. The DC current gain is estimated to be 30. The base current to be removed from Q203 is a maximum of 55mA.

The PNP complementary transistor is driven by a TIP31C NPN power transistor (Q202), capable of dissipating 35W at case temperatures of 45°C. The DC current gain of the TIP31C at collector current of 55mA is close to 150, so the maximum current to be supplied by the op-amp (A201A) is less than 1mA. The collector current through the TIP31C is limited to a safe 0.5A by an emitter resistor of 22 ohms, which operates by pinching V_{be} to less than 0.6V.

FIGURE 5.13 shows the complete power supply array and base drivers. The design is formally named a "complementary Darlington".

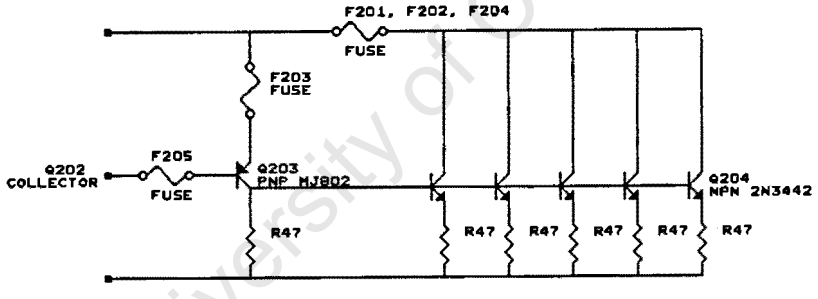

Figure 5.13 Linear regulator array.

The actual 2N3442 array current gain at rated current was experimentally determined to be 35, and the graph of regulator array DC current gain is shown in Appendix E for comparison with the data sheet.

c) Current feedback measurement

Similar problems apply to the power supply as to the programmable load, and the same solutions were adopted, namely a high power resistor with modest amplification.

Current feedback measurement circuit

The power resistor is positioned in the circuit for "return line current sensing". It is important to see that only the linear regulator current is sensed, and base drive current from Q202 is not included.

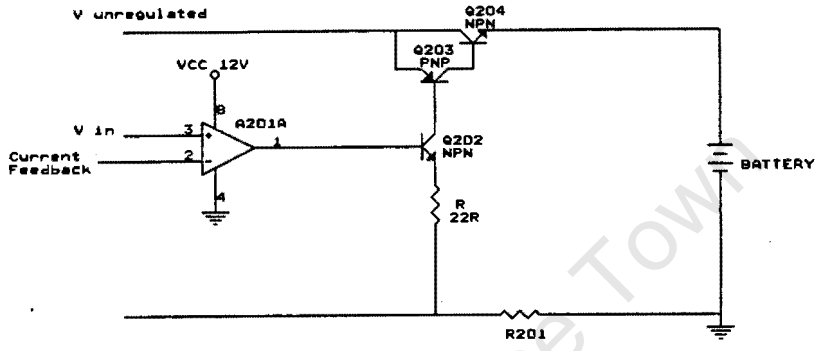

Figure 5.14 Return line current sensing

A unity gain differential amplifier (A305A) is used to amplify the voltage signal from the current sensing resistor. Figure 5.15 shows the basic current sensing amplifier which operates below ground, with a maximum negative input voltage of -1 volt. As the amplifier can handle only -300mV input from a positive supply, a split supply is required (+12V, -5V).

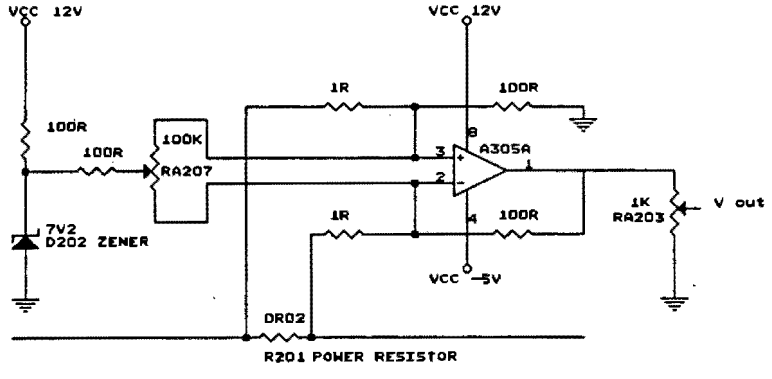

Figure 5.15 Current sensing amplifier

d) Current control loop and stability

The performance of the current source control loop depends on a high closed loop gain (CLG). The gain of differential amplifier A201A is set at 44.

The CLG (calculated as for the programmable before) is

$$= 44 \times 50A/5V \times 1V/50A = 8 = 19.8dB$$

with a breakpoint at 29kHz.

Figure 5.16 illustrates the Bode plot for the current control loop, which is inherently stable at frequencies below 264kHz.

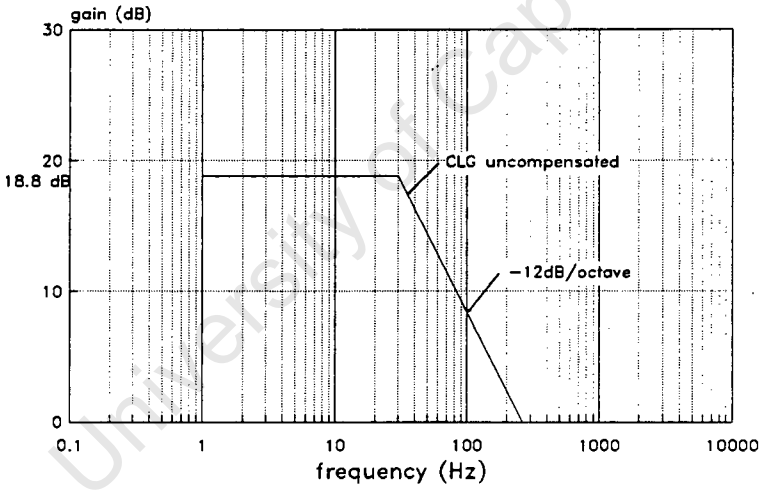

Figure 5.16 Bode plot for linear regulator

e) Protection

Current limiting

The current limit operates by using the signal directly from the current feedback amplifier. The signal is adjusted by a trim-pot AR202 onto the base of a transistor, which pulls down the control voltage of the main control loop when current limiting is effected. The minimum current limit setting is about 20A.

Overcurrent protection

Fuses are liberally placed to prevent runaway overcurrent. Most importantly they are located on the regulator array, positioned at the collector of the NPN (2.5A) and one fuse (10A) for every six 2N3442 transistors. The layout is shown in Figure 5.13.

f) Current measurement and instrumentation

A buffered signal from the current feedback amplifier is used directly by the A/D converter and instrumentation, as for the programmable load.

5.2.3 Power Supply Design - LC filter

The main overview sketch of the test unit (Figure 5.2) shows that the linear charge regulator is fed by a SCR pre-regulator. SCR rectifiers regulate voltage by adjusting the phase angle at which SCR firing occurs, usually causing sharp spikes in the output waveform. Not even a fast linear regulator would be able to smooth such sudden peaks, so it is necessary to remove the steep rise of the SCR output by filtering.

The LC filter is usually used for SCR output filtering, as it filters both current and voltage. The filtering of the LC filter is given by

$$\frac{V_o}{V_i} = \frac{1}{\omega^2 LC - 1}$$

For SCR rectification, the second harmonic is the dominant source of distortion at all firing delay angles (Figure 5.17), and this harmonic should be eliminated as far as possible. The frequency of the second harmonic is 100Hz.

If the filter is to provide unity gain at 10Hz, then we can solve for L given C. Details of the calculation are given in Appendix E.

The final component choice for the filter is C301 = 30000uF, and L301 = 8.4mH.

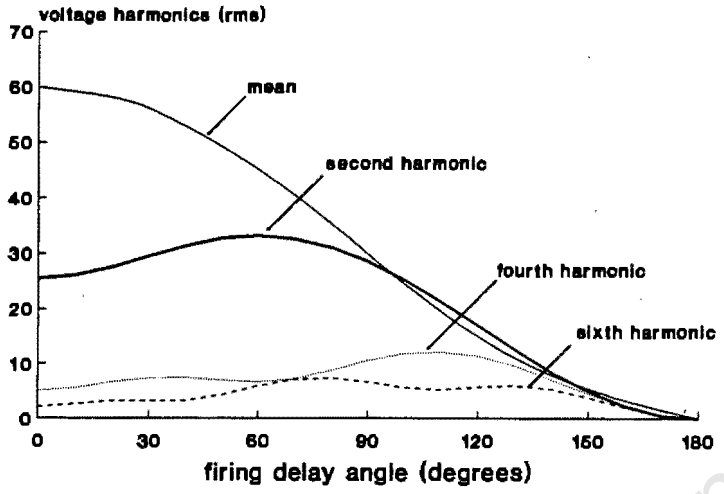

Figure 5.17 Harmonic content of SCR rectifier, $60V_{rms}$ input. (Source: Lander,1981:270)

5.2.4 Power Supply Design - SCR Tracking Pre-regulator

The SCR pre-regulator has the role of rectifying the AC input voltage, and maintaining the rectified voltage for a fixed voltage drop over the linear regulator, regardless of regulator output. It is necessary to keep the voltage drop to a minimum to prevent heating of the series pass transistors in the linear regulator.

a) SCR tracking pre-regulator - overview

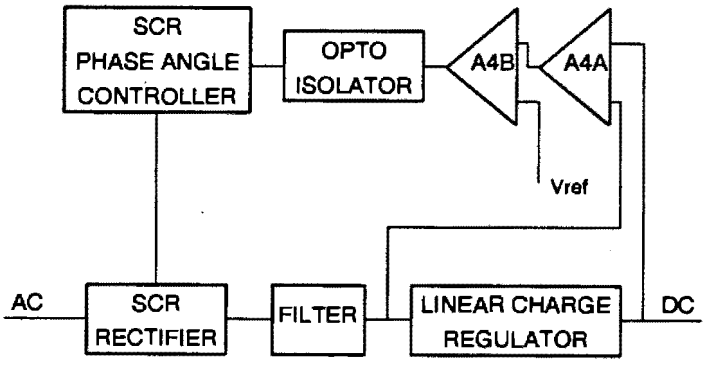

Figure 5.18 SCR pre-regulator, principle of operation

Differential amplifier A4A senses and amplifies the voltage drop over the linear charge regulator. The amplified voltage drop is compared with the reference voltage V_{ref} in A4B, and the A4B's output drives the SCR phase angle controller. For safety reasons the SCR phase angle controller is programmed through an optical-isolator. The phase angle controller provides gate pulses to the SCR bridge rectifier to pre-regulate the input voltage to the linear regulator as required.

b) Altronics AM024 SCR converter

The Altronics AM024 SCR converter is an off-the-shelf board used for gate control of SCR output. It has analog inputs and outputs, with digital logic circuits. It is more than a simple phase angle controller, in that it has the following extra features:

- linear operation (input-output voltage is linear, rather than output-phase angle being linear with input voltage).
- maximum and minimum SCR output voltages can be set
- maximum SCR current can be set
- maximum SCR output dV/dt can be set

The main disadvantage with this card is that the inputs are not isolated from the rest of the board, and an opto-isolator must be used in series between the controller and any other control circuitry to prevent ground earths or shorting.

c) Optical isolator

An optical isolator was supplied by Altronics. A grounded DC differential signal, is input, and the output is a floating differential signal that is isolated from the input by a transformer. There is some DC-AC-DC conversion on the way.

This isolator is versatile; it can accept inputs of 0-10V, and provides floating outputs of adjustable range, with an adjustable output minimum voltage as a percentage of the range.

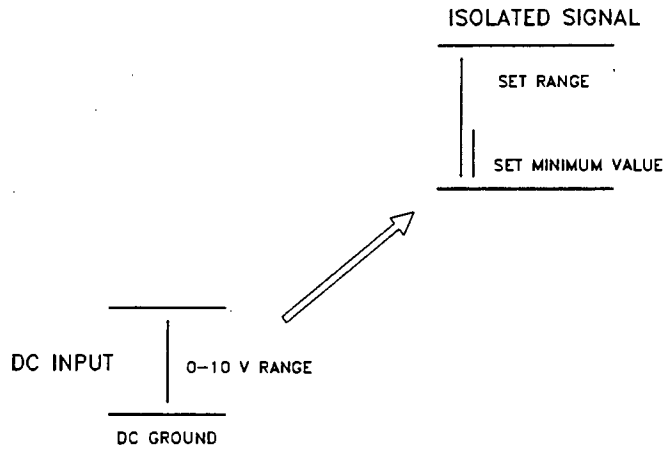

Figure 5.19 Altronics opto-isolator

d) SCR tracking circuit

The SCR tracking circuit overviewed in Figure 5.18 works on a feedback basis. Its closed loop response time is not very fast, nor is it easy to pinpoint. It is easy to see why the response time is slow without doing a thorough analysis:

- the LC filter begins to roll-off from DC at 10Hz
- the Altronics AM024 converter has maximum dV/dt of 30V/s
- the SCR can only respond every 50Hz (once per cycle)
- the SCR rectifier has inherent time delays

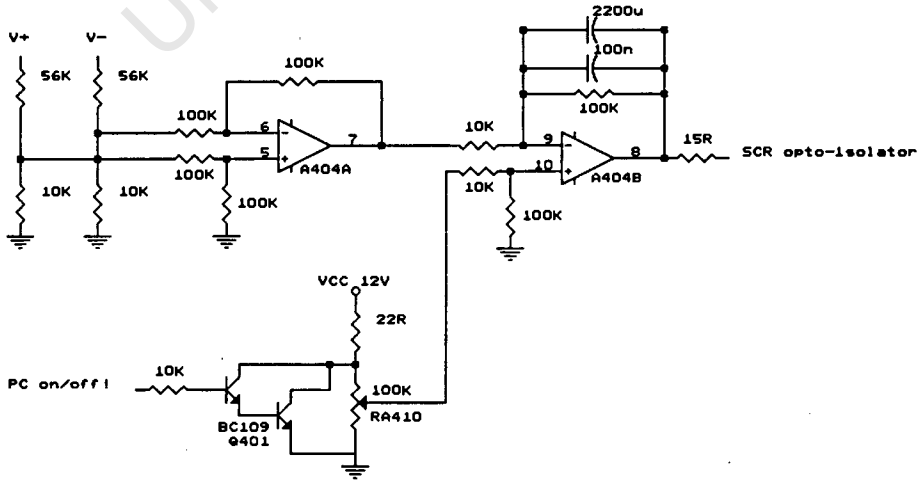

Figure 5.20 SCR tracking circuit

Unity gain differential op-amp A404A feeds op-amp A404B of gain 65. Op-amp A404B begins its frequency response fall-off at 0.34Hz. The CLG of the circuit is high, but the system is overdamped to prevent oscillation due to the discontinuities, time delays and very slow response times.

The positive input to A404B is pulled low at system startup by darlington Q401. This action prevents massive current surges through the SCR since the SCR controller will be full-on. Once startup is complete, the transistor is turned off, and the reference slowly returns to its setpoint. The SCR controller reaches its set value without surging.

e) SCR rectifier bridge

A half controlled bridge is preferred to a fully controlled bridge for the power rectifier, mainly because of the better current waveform. The various circuits are shown in Figure 5.21. The Altronics AM024 controller will trigger any of the circuits.

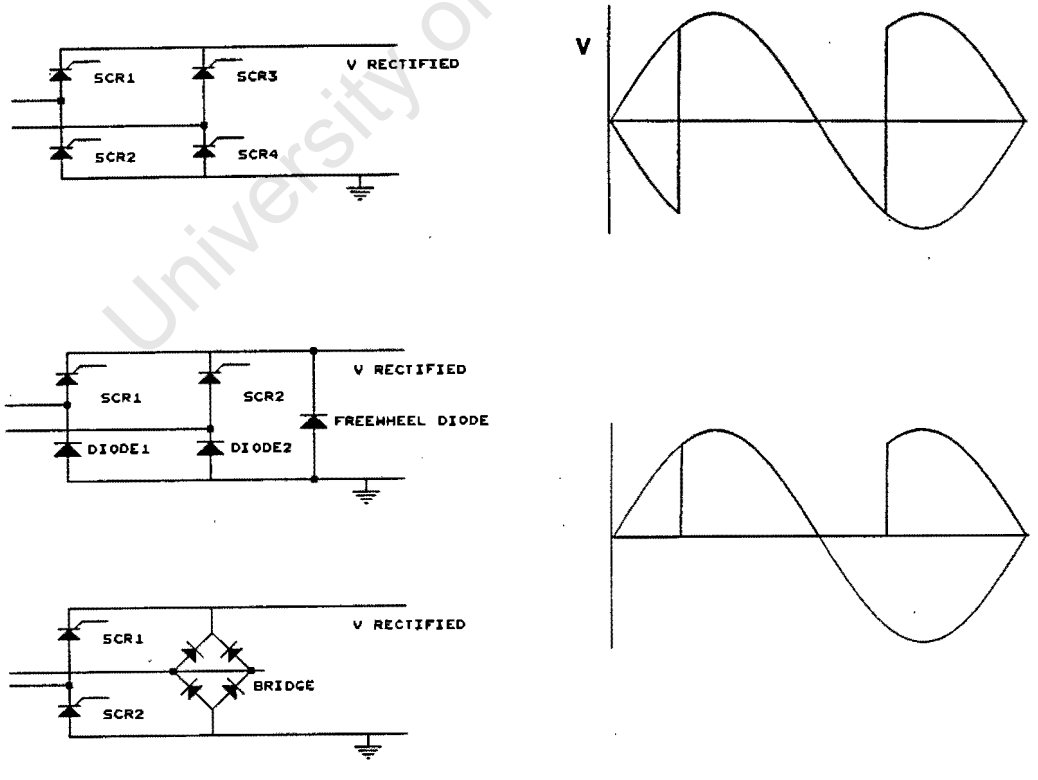

Figure 5.21 Bridge rectifier output waveforms. a) fully controlled bridge, b) and c) half controlled bridge. (Source: Lander,1981:41)

A half controlled bridge consists of two SCR's and a diode bridge, although the same control as for four SCR's is required (see Figure 5.21(b)). A free-wheel (commutating) diode is required to provide a reverse current path for the SCR's to regain their blocking states. In Figure 5.21(c) the bridge diodes double as commutating diodes. The load voltage is always positive due to the presence of the commutating diode. The half controlled bridge has a characteristically more distorted input current waveform, and requires a larger isolation transformer on the input.

The diode bridge selected is the AEG B2 250-30Si. This silicon bridge handles 250V and is rated at 30A continuous per diode. When connected as in Figure 5.21(c) the diode bridge has a continuous rating of 60A. The SCR block selected is the AEG TT45N 200 K power block, capable of 100A maximum and 51A continuous at 60°C. Maximum voltage is 200V, with gate turn-on typically at 1.4V and 120mA. (see Appendix E for specifications).

The entire bridge is mounted on a large natural convection heatsink.

f) SCR minimum load circuit

During testing of the SCR output it was observed that at very low currents the SCR's failed to trigger on every AC cycle, resulting in current pulses of irregular frequency. As the LC filter can only efficiently filter ripple of regular frequency it is not surprising that down-the-line effects on the output of the linear charge regulator are observed.

Further monitoring showed that a mean holding current of 7A is required to ensure that the SCR's are fired every cycle. This is mainly caused by the LC filter, which has a ripple current of $7A_{peak}$ (See LC filter in the Appendix E). To ensure even and regular current SCR current flow, the mean current through the filter must be greater than the ripple current.

A dummy load, consisting of two 2N3442 transistors driven by a TIP31C (Q402), draws current in parallel to the linear regulator. The circuit operates to ensure that at least 7A flows through the low power resistor R401. The current flowing through the dummy load does not affect current measurement for the linear regulator.

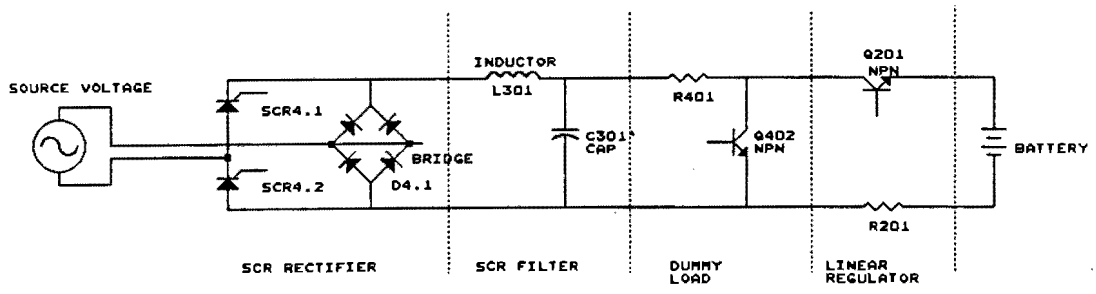

Figure 5.22 SCR minimum load circuit location

The circuit to maintain the minimum current is shown in Figure 5.23. Pot RA406 is used to adjust the minimum current.

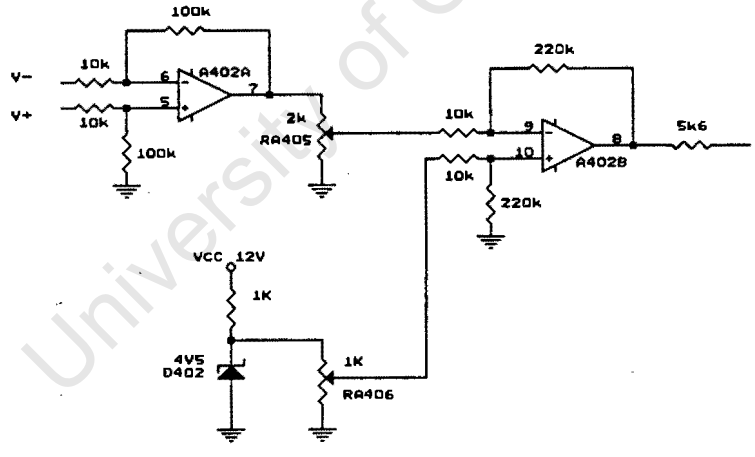

Figure 5.23 SCR minimum load control circuit

Although lower LC filter ripple current could have been achieved by using a more expensive filter. (see Appendix E, LC filter design), the need of the dummy load could not be totally eliminated as there is always some ripple.

5.2.5 Power Supply Design - Isolation Transformer

The whole DC power supply should be isolated from the AC mains supply for safety reasons. Additionally, the single phase mains supply can only normally provide 15A at 220V, so some form of step down, current boosting transformer is needed to achieve 50A DC output. The basic sizing for transformer T5 follows.

Power transformer sizing

Transformer Primary
$V_{rms,primary}$ = 220V
$I_{rms,primary}$ = 15A maximum

Transformer Secondary
For $I_{rms,secondary}$ = 50A
then
$V_{rms,secondary} \leq 66V_{rms}$
and
$V_{s,max} \leq 93.3V$
$V_{s,mean} \leq 59.4V$

If $V_{s,mean}$ is 59.4V, with losses over the regulator of 2.0V and similarly 2.0V over the SCR , then the maximum obtainable power supply output is 55.4V. This estimate of the output voltage does not allow for mains voltage fluctuations, which can be up to ±15% of the nominal. A constant voltage transformer was found to be extremely costly and therefore rejected.

Further, the transformer power rating should compensate for the distorted (non-sinusoidal) input current typical of half-controlled rectifiers. This factor is used to increase the core rating of the transformer. A factor of 20% is used.

The final sizing for transformer T5 is

primary winding	secondary winding
$Vp=220V_{rms}$	Vs=66Vrms
$Ip=15A_{rms}$	Is=50A

kVA rating is 220V×15A = 3.3kVA
compensated by 20% = 4.0kVA

5.2.6 Auxiliary Equipment, Safety and Layout

In this section the safety requirements of both the power supply and programmable load are considered.

a) Auxiliary power supplies

The control electronics of the load and power supply each require a 12V supply capable of 0.5A, and a low power -5V rail for the current sensing amplifiers. These are provided using 3-terminal regulators and standard circuits. The T8606 inverting regulator is interesting because it uses capacitive pumping to generate a negative rail from only a positive supply.

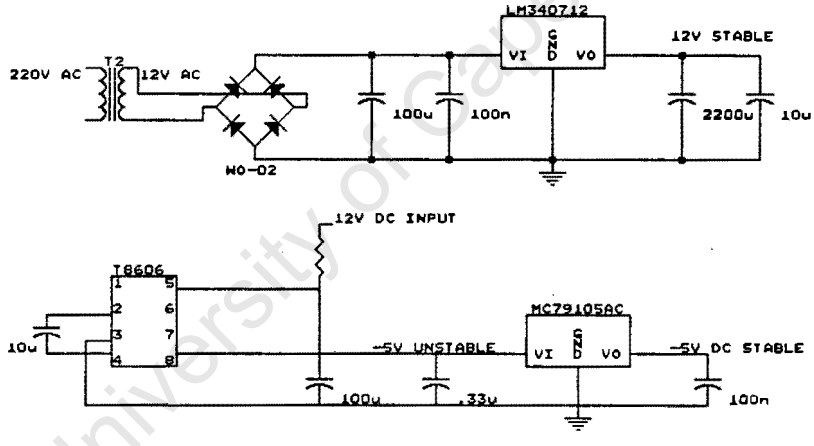

Figure 5.24 Auxiliary power supply for control electronics

The SCR-controller is equipped with its own power supply operating directly off the mains. As the rectifier is to run off a nominal $60V_{rms}$ secondary of T5, it is safer to take the 60V output and transform it back to 220V using T4, rather than connecting directly to the mains (see Figure 5.26). For one, this approach ensures that the SCR controller and the SCR's are always in phase.

b) Instrumentation and instrumentation power supply

An Eagle Electric digital volt meter (DVM) range 0-2V was selected for the panel instrumentation. A selector switch allows either programmable load current or

power supply current to be displayed. The DVM inputs are not isolated from its power supply inputs, so a dedicated and isolated 5V power supply is provided to enable the inputs to float above ground. Once again a 3-terminal regulator rated at 500mA and standard circuitry is used.

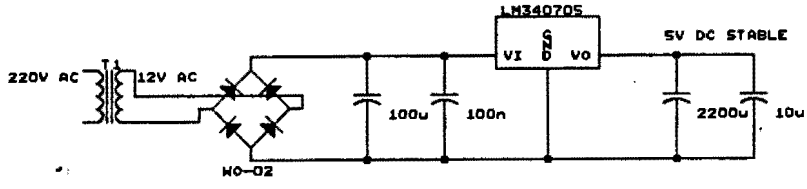

Figure 5.25 Instrumentation power supply

c] Fuses and safety

Fuses are liberally placed to prevent accidental burn-out of major equipment. These are shown in Figure 5.26. Additional fuses protect each heatsink of transistors used in arrays Q101 and Q201.

d] Isolation and common point earthing

Figure 5.26 shows how the entire system is isolated from the mains supply. All the power supply and load electronics is clearly common point earthed. The only connection between the power supply electronics and the SCR controller is via an opto-isolator.

The computer can be connected to the system via the same common point earth without fear of ground earths interfering with accuracy or worse.

As the computer is isolated from the mains via its own power supply, there can be no ground earths through the mains earth system. If the computer's power supply is not isolating, then the ground pin of the main power wall plug should be disconnected as a precaution.

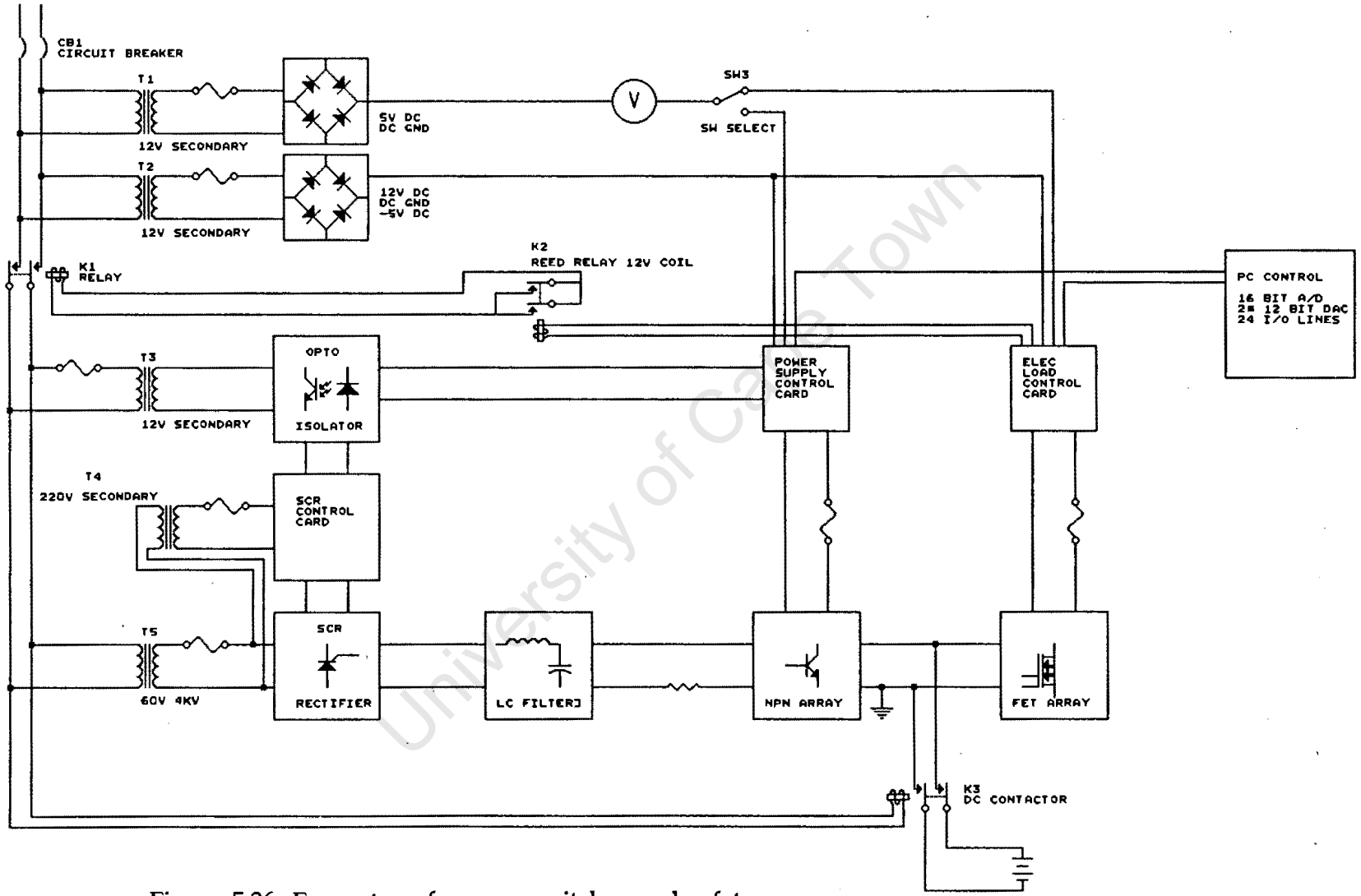

Figure 5.26 Fuses, transformers, switches and safety

e) Switches, relays, contactors

There are several switching devices in the system, both for safety and for control. These are shown in Figure 5.27.

On the control panel is the main trip switch (CB1), with current trip rating at 15A. This is the main on/off switch for the system.

A 3 contact relay (K1) with each contact rated at 10A AC is turned on by the (normally open) start button (SW1) on the control panel, provided that the computer gives the OK by activating the reed relay (K2). The (normally closed) emergency stop button (SW2) on the control panel de-activates the 3-contact relay. The reed relay coil is rated at 12V DC and is operated by the computer, while the main contacts are rated at 1A, which is sufficient to carry the coil current for the 3-contact relay. A DC contactor (K3) rated at 60A DC connects the battery under test to the power circuit.

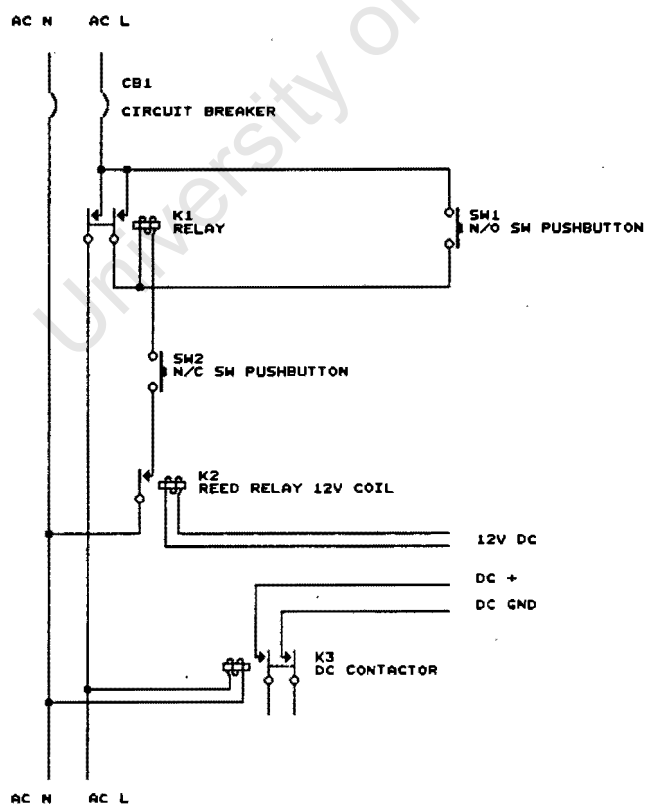

Figure 5.27 Panel wiring showing main switches

f) Physical layout

The power supply and programmable load are mounted together in a single fan cooled mounting.

The casing is divided into two compartments. The forced convection section, located in the rear, is cooled by five fans and houses high heat dissipation components such as transistor arrays and power resistors. The natural convection section for low heat components contains the transformer, LC filter, SCR pre-regulator and control electronics. The lid of the casing is slightly raised to allow heat to escape. Switches and instrumentation are mounted on the front of the panel on the doors of the natural convection section. The layout is shown in Figure 5.28.

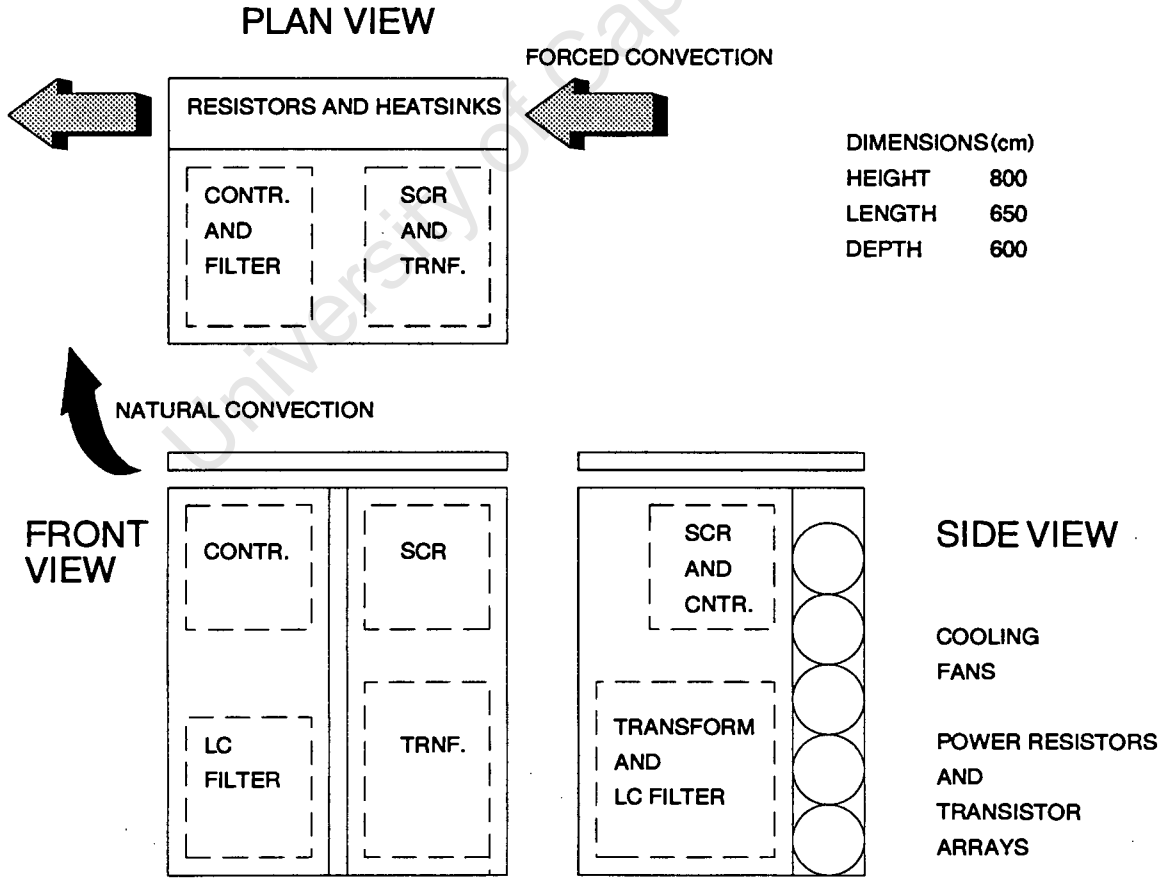

Figure 5.28 Layout and cooling of the battery test unit

5.2.7 Digital Interface and Computer Control

The interface between the digital computer and the analog electronics is the Eagle Electric PC-30 analog multi-function board. The PC-30 is a plug-in board with the following features:

- 12 bit A/D converter with 25μS conversion time (0V to 10V, -5 to +5V, or -10V to +10V inputs)
- 16 channel A/D multiplexer
- two 12 bit D/A converters with 1μS conversion time (-10V to 10V, or 0V to 10V outputs)
- two 8 bit D/A converters with 1μS conversion time (outputs as above)
- 24 digital I/O lines (8255A programmable peripheral interface, PPI)

The A/D and D/A conversion utilities are required for:

- programmable load control; 12 bit D/A
- programmable load current readback; 12 bit A/D
- programmable load voltage readback; 12 bit A/D
- power supply current control; 12 bit D/A
- power supply current readback; 12 bit A/D
- temperature readback, 2 channels; 12 bit A/D

All ranges are set to 0V to 10V for both input and output.

The Intel 8255A PPI is required for setting switches either on or off.

a) A/D & D/A conversion channels

The base address of the PC-30 card is set to 1792 (700 Hex).

A/D conversion for data input: The data is read by specifying the channel number (in the range 0 to 16), which is then accessed by the multiplexer and the 12 bit word is read into the computer. The 12 bit word (value 0 to 4095) is converted to the relevant units using calibrated curves.

The A/D channels are used for measuring battery voltage, current to the battery, current from the battery, and battery temperature as described below. (Temperature control is in Section 5.4).

Channel	Measurement
7	battery voltage
8	power supply current
9	load current
12	temperature sensor 1[1]
14	temperature sensor 2

D/A conversion for control: Data is transmitted by specifying the PC-30 base address, together with the specific D/A address and the required digital output.

Both the load and power supply operate under current control by fixed gain control circuits. In both cases, 10V input to the control circuit results in 50A output. 4095 digital input is equivalent to 10V D/A output, and the voltage is linearly proportionally to the digital value. The electronics can therefore be accurately calibrated digitally, so that a fixed digital input gives a fixed current output.

b) Intel 8255A Programmable peripheral interface

The 24 digital I/O of this interface lines are used for switch control. They can be programmed in 3 groups of eight lines (A,B,C), either as inputs or outputs. Port B is programmed as output, and the ports A and C as inputs.

Each digital output line can source 1mA, which is sufficient to provide base drive to a darlington transistor. The low power digital output can control heavy duty switches. Two lines of port B are used.

[1] See Section 5.4 for more details on temperature measurement.

- Port B7 activates a darlington which excites the reed relay (Section 5.2.5(e)). The reed relay (and the entire power system) can therefore be switched on or off digitally.
- Port B6 activates a darlington (Q401) which switches the SCR tracker on or off (Section 5.2.4(d)).

The input lines are used for status checking of power supply rails, relays, etc.

- Port A4 provides status of the reed relay.
- Port A0 provides status of 12V power supply rail on the power supply control card.
- Port A6 provides status of 12V power supply rail on the load control card.

The I/O lines are used by the computer to check system integrity, overriding the manual start button until the main systems are properly connected and functional.

c) Startup procedure

A startup procedure has been designed which performs some simple system checks before the power supply and load an be connected to the battery. the checks are performed by software, in conjunction with the PPI. The startup procedure is outlined in flow diagram format in Figure 5.29. The flowchart shows the system checks that are performed, and which must be successful before the start button on the instrument panel becomes functional.

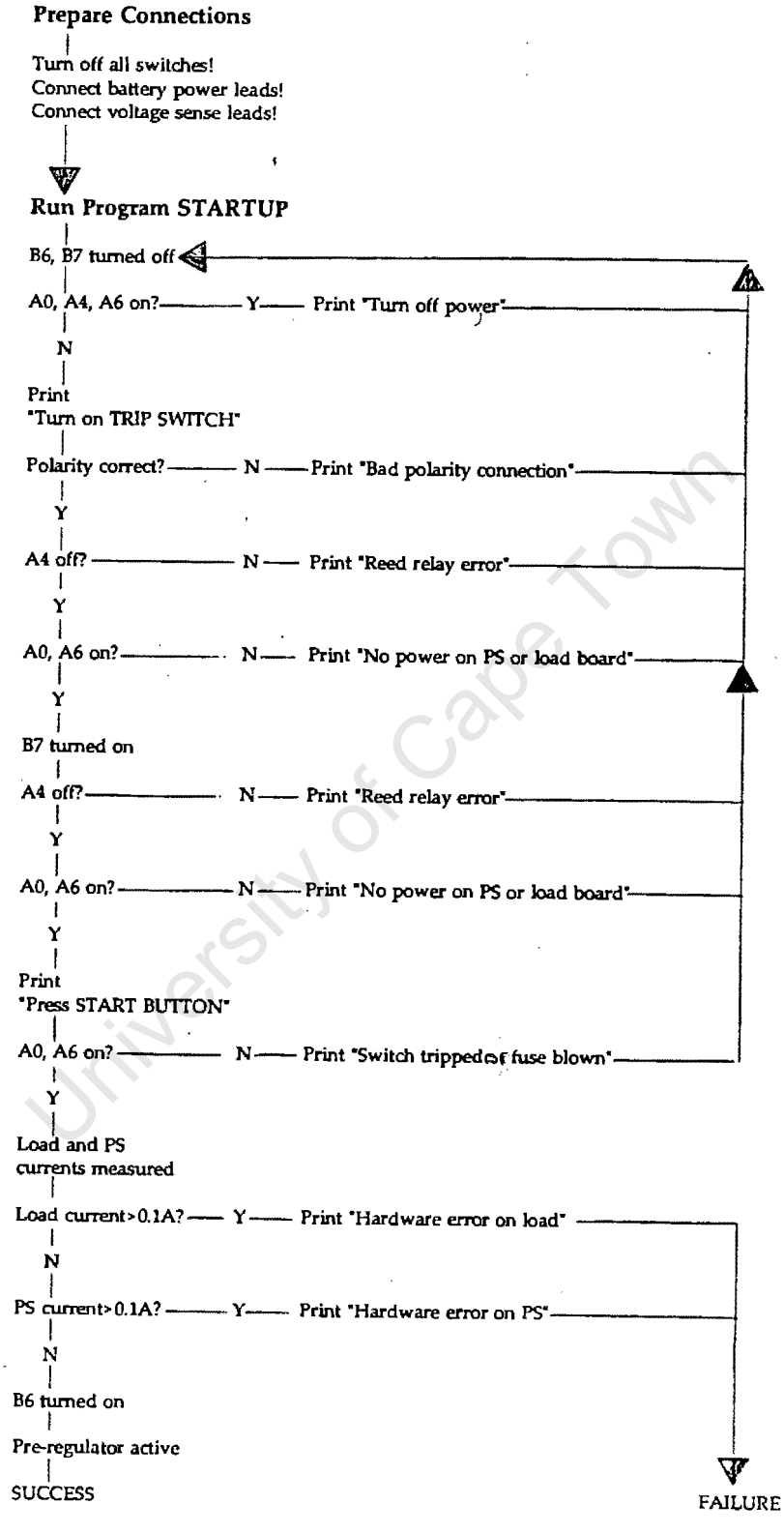

Figure 5.29 Startup procedure flowchart

5.3 CONTROL SOFTWARE

5.3.1 General Requirements of the Control Software

The requirements are listed, with expansion where appropriate.

- Remote data capture of about five main variables at regular intervals, and storage of the five variables and permutations of them at selected intervals.

  Battery tests normally take 50-100 hours to complete. It essential to be able to capture data automatically.

- Remote capture of various status/switch settings

  Regular monitoring of the status settings of the electronic hardware ensures early warning of system failure, and enables the control computer to terminate the test.

- Remote control of the load in constant current mode and in pseudo-constant voltage mode by constant control of the current.

  The load electronics are designed for constant current operation. Constant resistance operation can be simulated by using the computer as a digital feedback loop. This requires regular sampling of the battery current and voltage, and adjustment of the current till the required voltage:current ratio (resistance) is obtained.

- Remote control of the power supply in constant current mode and in pseudo constant voltage mode and in pseudo PV simulation mode.

  The power supply electronics are designed for constant current operation. Constant voltage operation can be simulated by using the computer as a digital feedback loop. This requires regular sampling of the battery current and voltage, and adjustment of the current till the required voltage is obtained.

PV simulation can be achieved in much the same way. The current is adjusted till both current and voltage fall on the PV operating curve. This is best done by regular calculation of the battery resistance, and using adaptive feedback to solve for the expected operating point.

- Real time numeric display of relevant variables.

- Graphic display of any of selected variables vs any other.

  Because the tests typically take so long to complete, it is useful to have the facility to monitor the results from an early stage.

- Ability to queue various operations,
  to automatically terminate operations based on one or many termination criteria,and to automatically begin the following operation

  For some battery tests the computer executes charge discharge cycles consisting of a series of sequentially executed operating steps. For each cycle, control and limit values are used are used to establish the operating condition and termination condition.

- Limited operator control at any time

  In any process control environment it is preferable to have operator override in case of problems.

A Block diagram of the idealised process is shown in Figure 5.30.

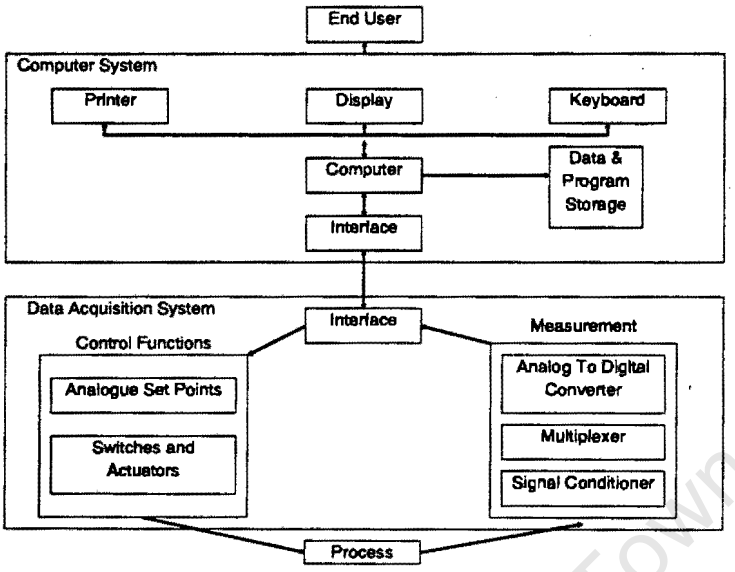

Figure 5.30 Process characterisation block diagram.
(Source: Hewlett-Packard)

5.3.2 Implementation

A single processor, standard IBM XT is used for control. The above processing requirements are formidable given the speed of the machine.

The power electronics that is controlled is simple, and it can be digitally calibrated, yet it is all constant current operated without self-contained microprocessors. The computer must perform all of the normal processing tasks, and then regulate the power supply and load when they are used in non-constant current modes, by using a slow digital feedback loop.

The ideal situation, short of an on board micro-processor on the power supply and load, would be some kind of priority scale run tasking by the computer.

5.3.3 Program

In order to keep the system reasonably low cost, some precision has to be sacrificed.

The power electronics control and data capture is executed every minute. This is satisfactory (Verado et al,1981) if it is assumed that no significant drift away from the set conditions will occur when in non-constant current modes.

While the PC is not controlling or capturing data it stands idle. During this time the operator can select changes to the screen output parameters, change to graphics mode, control the hardware etc. Thereafter control is transferred back to the PC for further data capture and control functions.

Data flow

The simplified program flow is described in Appendix E, with the subroutine names in parentheses.

5.3.4 Digital Feedback Loop Stability

Non-constant current modes of operation include constant voltage operation and PV simulation. These modes are emulated by periodically adjusting the current so that the required output voltages are obtained.

The concept of a digital feedback loop has been raised to overcome limitations in the electronic hardware, namely the presence of purely current control electronics. Like any control loop, the digital loop must be stable, must not exhibit conditions such as overshoot or ringing when subjected to a step change, but should not be overdamped so that performance is unacceptably sluggish. The schematic for the control loops is shown in Figure 5.31.

The battery is part of the loop, in the role of a current to voltage converter. The conversion ratio (equivalent to the internal resistance) has been found to be in the range 0.25 to 0.45 for a 100Ah 12V cell. The electrical pseudo time constant for a step change in current is shown in Figure 5.32. It is expected that most lead acid batteries will exhibit similar behaviour regardless of age.

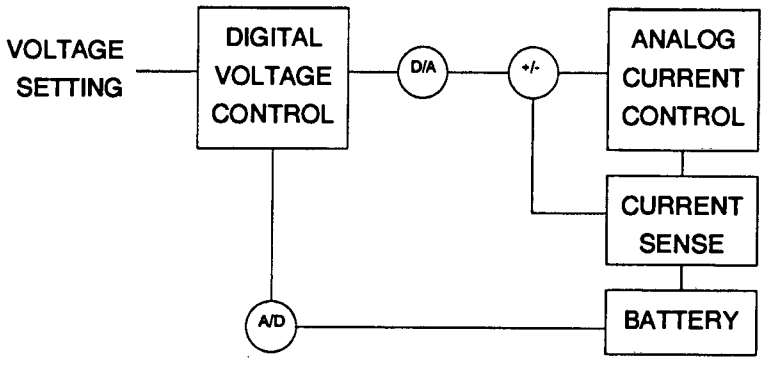

Figure 5.31 Digital control loop

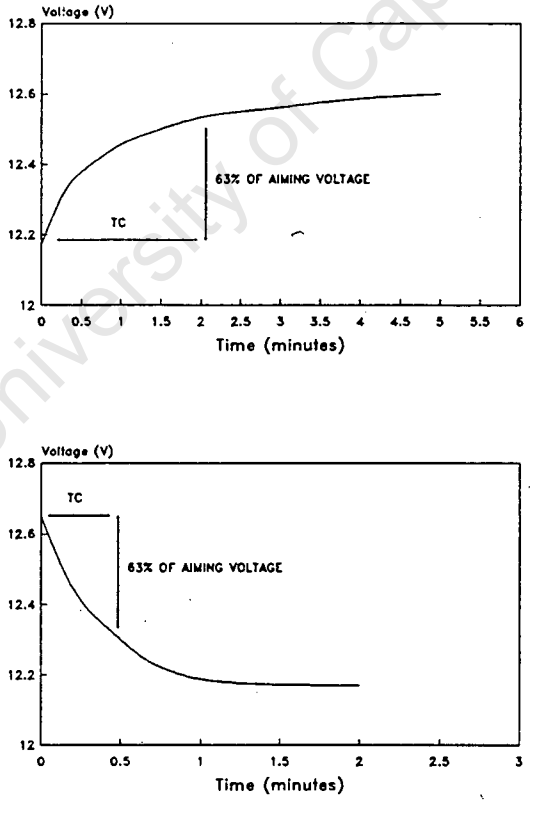

Figure 5.32 Battery pseudo time constants. 100Ah battery response to step change in current. Battery SOC = 90%, a) current change = 10A, b) current change = -10A.

If the digital feedback system used continuous feedback, its speed would be limited by the long battery time constant, and be inherently stable, as the software is at least an order of magnitude faster than the battery in response time. However, the software only samples for about 15 seconds of every minute, and this discontinuous feedback causes its response to be correspondingly degraded. The software must therefore become the slowest component for the loop to be stable. This is achieved by limiting the step change in current output by the digital feedback loop to 63% of the desired change. Satisfactory results have been obtained for a range of battery sizes.

5.3.5 PV Simulation

PV simulation is accomplished by software, with digital feedback and controlled interaction between power supply current and voltage.

a) PV model

A PV model that is simple and easy to implement is used (Rausenbach,1980:59). The model requires only four constants for complete definition of the base case, which is specified at 25°C and 1000Wm^{-2}:

V_{oc} the open circuit voltage
I_{sc} short circuit current
I_{mp} current at maximum power
V_{mp} voltage at maximum power

The four constants are shown on a typical PV curve in Figure 5.33.

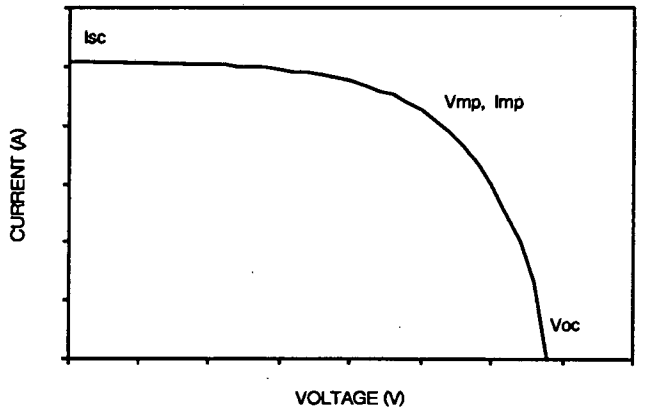

Figure 5.33 PV panel I-V curves showing constants for PV modelling.

The model is listed below for the base case.

$$I = I_{sc}(1 - C_1\{\exp[\frac{V}{C_2 V_{oc}}] - 1\})$$

where

$$C_1 = [1 - \frac{I_{mp}}{I_{sc}}]\{\exp[-\frac{V_{mp}}{C_2 V_{oc}}]\}$$

and

$$C_2 = [\frac{V_{mp}}{V_{oc}} - 1][\ln(1 - \frac{I_{mp}}{I_{sc}})]^{-1}$$

Transformations are applied to the base case constants to obtain the I-V curves at any insolation, *Insol*, and temperature,*T* (Lasnier et al,1988:365):

$$I = I + \alpha(T - 25) + (\frac{Insol}{1000} - 1)I_{sc}$$

$$V = V + \beta(T - 25)$$

where

$$\alpha = \frac{\delta I_{sc}}{\delta T} \qquad \beta = \frac{\delta V_{oc}}{\delta T}$$

b) Battery model

The battery is the only real component of the PV system under simulation in the laboratory. The battery is, however, described by a constant resistance superimposed on a constant fixed voltage for the purpose of solving for the operating point in PV simulation and in constant voltage operation. The slope (*B*) and intercept (*A*) of the line are weighted with real experimental data on a regular basis during program execution. The model is essentially a resistance model where *B* is the inverse of the battery resistance (Vinal,1955:323).

$$I_{bat} = A + B \times V_{bat}$$

c) Locating the PV operating point

The PV operating point lies on the intersection of the PV and battery operating lines.

The locus of the operating points (V,I) is given by
the equation:

$$f(V) = I_{sc} C_1 \exp\left(\frac{V}{C_2 V_{oc}}\right) + BV + \left(A - I_{sc} C_1 - I_{sc} \frac{Insol}{1000}\right)$$

The locus of the derivatives at the operating points is given by the equation:

$$\frac{\delta f(V)}{\delta V} = \left(\frac{I_{sc} C_1}{C_2 V_{oc}}\right) \exp\left(\frac{V}{C_2 V_{oc}}\right) + B$$

The operating point can therefore be located by iterating using the familiar algorithm of Newton-Raphson (Gerald,1978:15).

5.4 TEMPERATURE CONTROL

The temperature control system should be able to keep the battery temperature within ± 1°C of the control temperature. A temperature controlled water bath facilitates good thermal contact with the battery and ensures short thermal lag times. The water also has large thermal capacitance which prevents the battery from greatly affecting the water bath stability. The water bath temperature can be controlled by a standard process plant temperature controller.

a) Water bath size

The battery should be immersed to within 1-3 cm of the upper cell surface, and water should circulate freely under the cell. To test tall tubular cells of between 400-600mm a depth of about 700mm is required. For the tank to maintain its thermal inertia, at least as much water as is displaced by the cells should remain in the tank.

The water bath selected has dimensions:

length 800 mm x width 600 mm x height 700 mm

The normal operating volume is about 240 litres. An adjustable base tray able to support 70 kg is used to position batteries of various heights.

b) Heater size

The heater is used to keep the water bath temperature within ±1°C of the set point. In the worst allowable case the temperature oscillates between these conditions. The period of the oscillation should be much less than the thermal time constant of the battery, to ensure that the battery does not experience the temperature variations. The thermal pseudo-time-constant of a battery is typically 120 minutes.

The thermal heating rise time to heat the water from -1 to +1°C of the set point, depends on the element size. the heat input required, Q, for the two degree rise can be calculated from the water volume and water properties as:

$$Q = p \; x \; V \; x \; Cp \; x \; T$$

$$1kg/l \times 240l \times 2°C \times 4.17kJ/kg°C = 2003kJ$$

The rise time for a heater of power P is Q/P. Any heater over 1kW will have a rise time shorter than 33 minutes and be sufficient. The larger the heater the shorter the period of oscillation and rise time. The largest heater that can operate from single phase supply using domestic connections is 3 kW, which is the size selected.

c] Temperature controller

A Shimaden SR10 temperature controller with type K thermocouple was available. Specifications are shown in Appendix E. The operating range is 0-1500°C, so the accuracy in the 0-100°C range is limited. The minimum neutral zone in the control output is 1% of full scale or 1.5°C. This corresponds to the worst case of allowable temperature deviation.

d] Temperature measurement

Temperature measurement is by two LM35D semi-conductor temperature sensing devices. Two devices are used to obtain an average temperature reasonably independent of temperature gradients in the tank.

The LM35D output of 1 mV/°C is amplified using temperature compensated amplification circuits (see Appendix E) to give outputs of 10 V at 60°C. These outputs are captured on computer via the Eagle PC-30 Interface through D/A channels 12 and 14.

CHAPTER 6

METHOD OF INVESTIGATION AND TESTING

The technical evaluation of the selected batteries is based on a broad range of test procedures. This chapter first presents the batteries selected for testing, then describes each test procedure in detail, and ends with the outline for test result presentation.

6.1 BATTERY SELECTION

The aims of evaluating batteries are to provide generic test data suitable for photovoltaic system simulation, specific data on different batteries that are suitable for PV applications and in so doing to investigate evaluation methodologies suitable for the different battery types.

For this evaluation it is most important to select a range of batteries that includes the most appropriate lead-acid types. Due to the nature of the battery industry, and the similarities in short term performance between almost equivalent batteries from different manufacturers, it is not efficient to test "competing" batteries of a given type from the various manufacturers. Given that the time requirement for complete characterisation tests on a single battery is 42 days, it is clear that some rationalisation is needed. If cycle life tests are included then this is where the difference in quality will show, and competing batteries should be tested.

The batteries selected for testing were chosen mainly on the basis of their interesting physical characteristics. These are tabulated below.

Table 6.1 Batteries selected for laboratory testing

Battery	Design use	Grid Alloy	Plate Structure	Electrolyte	Method of reducing water loss
Delco 2000	Solar	Pb-Ca	Flat	Flooded	MF design, single vent
GNB Absolyte 12V-5000	Solar	Pb-Sb	Flat	Immobilised	Oxygen closed cycle
Raylite RMT108	Standby	Pb-Sb	Tubular	Flooded	none
Raylite Solar	Solar	- CSM	NA	NA	NA
Sonnenschein A200	Standby/aircraft	Sb-free, Ternary Pb-Ca	Flat	Gelled	Oxygen closed Cycle
Willard 774	Portable/leisure	Pb-Sb	Flat	Flooded	none
Willard LS90 Vantage	Standby/UPS	+ Pb-Sb - Pb-Ca	Flat	Flooded	LM design, single vent

LEGEND
CSM copper stretch metal (Raylite patent)

Of these, the Raylite Solar was not available at the time of testing.

The Sonnenschein A200 was selected for testing, but preliminary tests on two 'used' A200's made available showed that the condition of the batteries would have compromised the tests results. The poor conditions are not a reflection of the batteries themselves, but rather a reflection of the previous use patterns and (lack of) maintenance. The A200's were omitted as the Rand cost of this imported battery was excessive.

6.2 BATTERY TESTING METHOD

The main test procedures and related questions that arise are discussed in the sections below.

The areas of interest are:

- Ah capacity
- temperature effects
- discharge curves and Wh capacity
- charging curves
- charging efficiency and gassing
- specification of current and voltage ranges for charging
- cycling effects
- partial state of charge operation
- stratification effects

6.2.1 "On Delivery" Assessment

Perform a visual inspection, reviewing data available from the manufacturer and categorising data according to its quality. Categorise the battery according to main features and operating characteristics as it is advertised.

Collect additional data from the manufacturers on physical structure, and perform theoretical calculations regarding active mass utilisation coefficients.

If life cycle data is not available then estimate cycle life based on data for similar batteries. Use cycle life models where necessary. The semi-log plot of cycle life versus DOD requires only two data points. The cycle life data can be supported by testing in many cases. The optimum DOD for cycling can be determined from the cycle life data, corresponding to the optimum Ah delivered by the battery over its entire life. The Ah delivered over entire life is calculated as:

$$Ah_{life} = C_{20} \times DOD \times Cycles_{DOD}$$

Initial estimates of battery cost and battery value can made. Wh cost is the cost per Wh as purchased. kWh value relates to the total kWh delivered over the battery life, and is usually calculated at the optimum DOD.

$$Wh\ cost = Cost\ in\ Rands / (C_{20} \times nominal\ voltage)$$

$$kWh\ value = Cost\ in\ Rands / (Ah_{life} \times nominal\ voltage) \times 1000$$

Before embarking on any tests it is necessary to "size" the battery in relation to PV systems. In other words, establish the range of charge and discharge currents the battery could be exposed to if normal PV system sizing methods were used. A battery of several hundred ampere-hours would be expected to handle many amperes of charge and discharge current under normal operation, whereas a ninety Ah battery would typically handle currents of less than ten amperes. This sizing is done to ensure that tests are performed in the relevant current regimes. Sizing the battery may require some calculated estimates of battery life vs DOD, possibly based on data for similar batteries. Deep and shallow cycle batteries have different operating parameters and test requirements. Shallow cycle cells may be sensitive to certain conditions which need to be taken into account in "sizing" the battery.

All tests are performed using the programmable battery test-rig. Temperature control is by a water bath at the relevant temperature, or an ice bath at 0°C. The battery is allowed 16 hours to acclimatise each time it is to be tested at a new temperature. In each case the thermal time constant of the battery in water is recorded.

6.2.2 Initial Test and Forming Charge

a] Determine the "as received" condition

Measure specific gravities, voltages and determine the "as received" capacity at the C_{10} rate.

b] Forming charge

Most new lead-acid batteries require several cycles to convert residual lead from manufacturing to active material, and to allow homogeneous grain structure.

Recharge as recommended by the manufacturer, then discharge at the rated current and recharge as recommended, cycling five times. Shallow cycle batteries are discharged to only 50% DOD to avoid damage. Follow by an equalising charge after the last cycle. Establish a reference capacity.

6.2.3 Capacity Tests

The capacity test starts with a battery that has been equalise charged, and the battery temperature allowed to stabilise at the test temperature in the temperature controlled water bath for up to 16 hours. SG's are recorded where possible. The capacity tests are conducted at constant discharge current, and the battery voltage is recorded at regular intervals. The test is complete when the battery voltage drops to below the cut-off voltage recommended by the manufacturer. If no cut-off voltage is provided, then the knee of the (voltage vs natural logarithm of time) curve determines the end of discharge.

a) Determine C_{20} (@ 35°C, 18°C, 0°C)

Capacity is a function of rate of discharge and temperature. Nominal capacities are usually given at 20°C for the 20 hour rate (C_{20}) for SLI (starting, lighting, ignition) cells and C_{10} for EV (electric vehicle) cells. The three temperatures selected for testing cover the range of likely operating temperatures for batteries in PV systems. Determine the effect of temperature on capacity at the rated current (eg. I_{10} @20°C). All tests are followed by equalisation charge.

b) Determine C_{50} C_{20} C_{10} C_5 etc.

Determine the variation in capacity with discharge current. (For PV systems the relevant current is about the 20 or 30 hour rate). Temperature can be included as a further variable if required. Care should be taken not to deep-discharge the battery below the knee of the discharge curve as subsequent tests could be unreliable and inconsistent, particularly for lead-calcium grid cells. Shallow cycle batteries can alternatively be discharged to a cut-off of 1.9V/cell, and the capacity compared with the capacity to 1.9V/cell obtained from that recorded at C_{20} rate.

6.2.4 Discharge Tests

The capacity tests in Section 6.2.3 also yield discharge curves, of V_{cell} as a function of constant discharge current and ampere-hours removed. (DOD at any time is less valuable as a variable than ampere-hours removed, because the number of ampere-hours remaining in the cell depends on the subsequent discharge current.) The discharge curves can be integrated to show the watt-hour capacity at constant current. The discharge cut-off voltages as a function of current, DOD and temperature can be determined from the discharge curves.

a) Investigate variable current discharge curves

Most PV loads vary throughout the day, particularly domestic loads, which may draw on average less than ten amperes (per 100Ah battery), but could for short periods draw close to one hundred amperes (per 100Ah battery). Particular questions that arise are: How is capacity affected? What time is required for the voltage to stabilise after a step change in output current? (eg. the polarisation effect). Investigate this analytically in terms of the active block design; the number of plates (eg. current density), plate design and thickness, electrolyte SG, temperature. The actual range of currents selected for testing depends on how the battery is "sized" in a PV system.

6.2.5 Charging Curves

Charging of batteries can be by constant-current (CC), constant voltage (CV), CC with voltage limit, CC with step current change, CV with step voltage change, and many variations on these options. The charging curve in each case would require charging from a defined DOD, plotting V_{cell} vs Ah returned (or time), and noting the current or voltage where step changes have occurred.

The charging method in typical PV systems corresponds to none of these, in the same way as discharge current is not usually constant.

The best approximation is possibly a variable charging current with an upper voltage limit representing voltage regulation. A charging test has been developed which charges the battery at a constant typical PV current (2-3A/100Ah), with an

upper voltage limit of approximately 2.37V/cell. Charging is in this mode till a set number of Ah have been delivered to the battery (10Ah/100Ah battery). At this stage a current scan is activated. During the scan the current is set to 10A/100Ah and held till the voltage stabilises, when the voltage, Ah returned and charge current are recorded. Time to stabilise is usually less than 10 minutes. The scan current is consecutively set to 5A, 2A, 1A, 0.5A /100Ah and the relevant recordings are taken. After the last current has been scanned charging is resumed at the constant PV current and the same upper voltage limit. The current scan is repeated when a further set number of Ah have been delivered. The process is repeated till the battery is fully charged. The advantage of this method is that a range of charging data can be quickly generated in one test. Experimental charging results are shown in Figure 6.1 for a 100Ah battery recharged from 60% DOD.

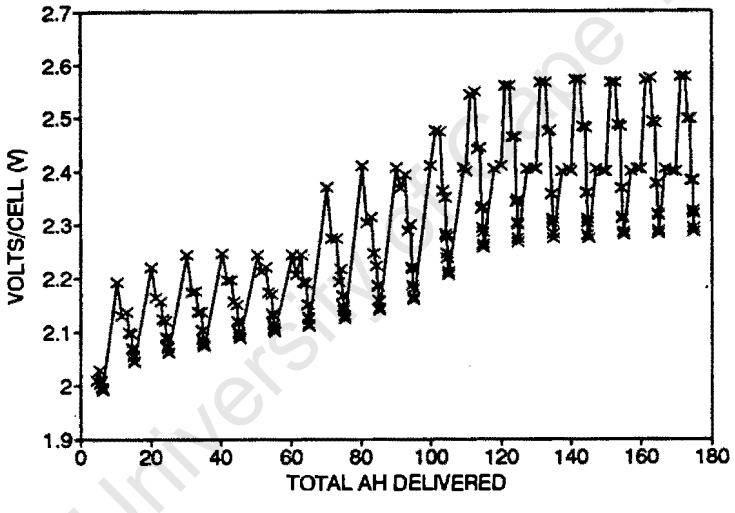

Figure 6.1 Experimental charging curves.

a) Determine experimental charging curves @ C_{50} C_{20} C_{10} C_5 (@ 35°C, 18°C, 0°C)

Determine charging curves using the scanning method, at constant temperatures, ensuring operation in the PV charging regime. These curves will give V_{cell} as a function of charging current and total Ah delivered.

b) Generate compensated charging curves

Coulombic charging efficiency is less than 100%, mainly due to losses by gassing at higher SOC's. A charging curve that plots charging current and voltage vs the Ah effectively delivered can be constructed by compensating the experimental charging data for gassing losses. The gassing losses are defined as current loss as a function of the battery voltage, as determined by the instantaneous charging efficiency (Section 6.2.6). The compensated charging curve is easily constructed by considering the Ah delivered at a particular voltage, and compensating this to effective Ah by multiplying by the instantaneous coulombic efficiency. The points of equal current can be joined to result in the compensated charging curve in Figure 6.2.

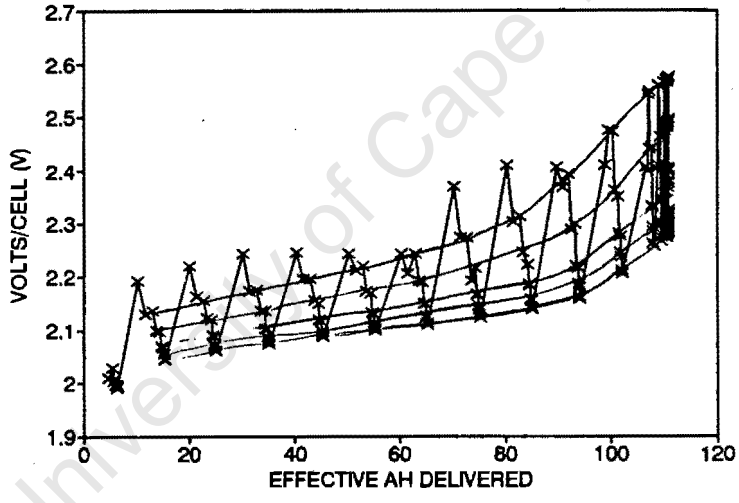

Figure 6.2 Compensated charging curves.

c) Construct quasi-constant current charging curve

Each compensated charging curve can be "uncompensated" to show the total Ah that would have to be delivered to fully charge the battery at constant current. This is done simply by dividing the compensated Ah at a particular voltage by the instantaneous coulombic efficiency at that voltage. The total Ah required can be easily accumulated. The higher charging rates are expected to require more Ah than the lower rates due to greater gassing rates and gassing durations encountered. Figure 6.3 shows a set of quasi-

constant current charging curve. These curves are not significantly different from real constant-current charging curves, are more representative of PV charging, and are comparatively quickly generated.

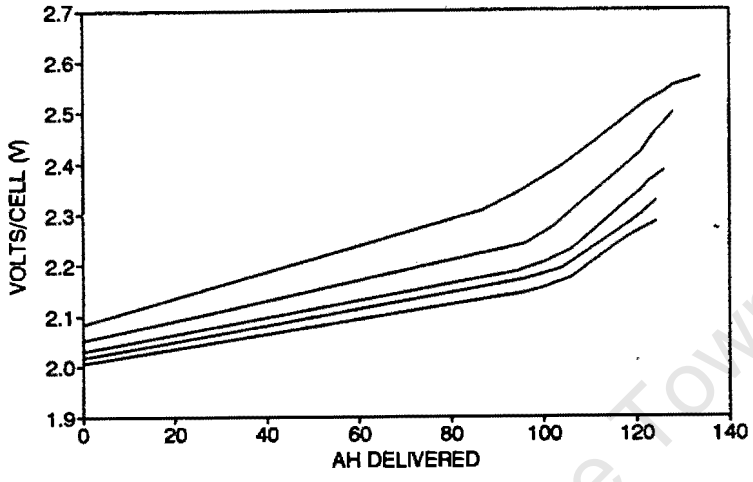

Figure 6.3 Quasi-constant current charging curves.

d) Investigate variable current charging in PV systems

Residual questions: How does charging under the PV regime compare with the charging curves generated? What are the effects of transients? What time is required for voltage to stabilise after a step change in charging current? These questions are most easily answered by simulating PV charging currents (using the PV simulator) and monitoring battery behaviour.

6.2.6 Charging Efficiency, Average and Instantaneous

The average coulombic charging efficiency in cells can be defined as the Ah effectively delivered to the cell divided by the total Ah delivered. The deficit is mostly caused by gassing. The average charging efficiency is useful for determining the overcharge required to fill a cell from a fixed DOD under fixed charging conditions. The average charge efficiency is DOD and charge current dependent, necessitating many repetitive and similar tests. Data collection is complicated as charging efficiency is decreased in old or unhealthy batteries as the gassing current increases.

Average charging efficiency can be estimated by:

i) measuring the difference between Ah delivered and Ah recoverable. The test requires repeatedly cycling between full charge and various DOD's to determine the effect of DOD on charging efficiency.

ii) comparing Ah returned to the cell with SG, a linear indicator of SOC.

iii) by attempting to measure inefficiencies causing cell temperature increases. The rate of battery temperature increase is related to the gassing rate. However, it is probable that external factors will make this method impractical. (Accurate determination of heat transfer coefficients will be difficult).

If the **instantaneous charging efficiency** can be determined it provides a much more useful method of analyzing battery performance. It can be used in conjunction with charging curves to determine overcharge requirements regardless of starting DOD. Instantaneous efficiency also provides information on the instantaneous gassing rates, although it is complicated by different rates of charge acceptance at the positive and negative plates (see Figure 3.30). Even though errors may be introduced, instantaneous charging efficiency provides greater insight into battery operation than average charging efficiency. The instantaneous efficiency can be measured by:

iv) estimating current losses due to gassing by measuring gas flow rate, a method widely used by battery researchers. The SOC, temperature, current, voltage are important parameters.

The instantaneous flow rate of gases evolved is measured by tapping gas flow from the cells through a soap bubbler, and recording the time to produce a volume of gas. If the gas is assumed to consist of only H_2 and O_2 in the ratio 2:1, then the current loss due to gassing is (see Section 3.8.2e for derivation):

$$I_g = X/N \times 5.74 \times P/1 \times 273/T$$

where
X = gas flow (cm^3/s)
N = number of cells tapped
P = gas pressure (atm)
T = gas temperature (kelvin)

If the gas composition can be determined (by mass spectrometer or Orsat analysis), then the gassing current at each electrode can be calculated and correction made for the individual electrode efficiencies. Because the positive and negative electrodes have different charge acceptance rates the instantaneous gas compositions may be non-stoichiometric in different SOC regions, but they approach stoichiometric at full charge (see Figure 3.31). Lakeman (1989) has calculated that the average ratio H_2:O_2 over the charge regime following deep discharge is very close to 2:1.

The gas flow method of charge efficiency determination will be accurate when the gas mixture is stoichiometric, so at 100% SOC should be reliable and accurate.

The gas measurement method is not recommended for sealed cells as substantial electrolyte is lost and cannot be replaced. Allowance may have to be made for some gas recombination in vented cells, typically 5%.

or

v) measuring the rate of recombination in sealed cells.

Sealed cells with oxygen closed cycle gas recombination operate under pressure (3 psi). As described in the theory (Section 3.9.3(b)), the rate of recombination is limited almost entirely by the rate at which oxygen can migrate to the negative electrode where hydrogen is generated.

The theory shows that for a pseudo-first order reaction in oxygen, the current equivalent (I_{O_2}) to the rate of oxygen recombination is:

$$I_{O_2} = \frac{4FV}{RT}\left[\frac{d\ln P_{O_2}}{dt}\right]_{F,V} P_{O_2}$$

where
V = volume of gas in the headspace (m^3),
F = Faraday constant (9.648×10^4 C mol^{-1})
R = gas constant (8.31441 J K^{-1} mol^{-1})
T = gas temperature (kelvin)
P_{O_2} = oxygen partial pressure (Pa)

If the cell is charged at constant potential the pressure in the cell quickly settles at an equilibrium. At the equilibrium it can be assumed that the rate of oxygen evolution at the positive electrode is equal to the rate of oxygen recombination at the negative electrode at the measured cell potential. If the charger is suddenly disconnected so that the battery is in open circuit, then the rate of pressure drop can be measured to determine the rate of O_2 recombination, hence the rate of O_2 production at the charging current, voltage, SOC and temperature. For every mole of O_2 produced, 2 moles of H_2 are assumed to be evolved. The total gassing current can be shown to be equal to the O_2 recombination current.

The main limitation with this method is the error caused by the difficulty in estimating the headspace volume, V, if the data is not readily available from the manufacturer. If a manometer is used for pressure measurement the free air in the manometer may be significant and should be accounted for.

Considerable flexibility is afforded if it is realised that the gassing currents (at each plate) are related primarily to the plate potentials, V_{pos} and V_{neg} (see Section 3.7.4). Although temperature dependence is significant, electrolyte concentration influences gassing to a far lesser degree. The instantaneous

charging efficiency at each plate can be inferred from the voltage at that plate (Lakeman,1989). By a further approximation, the instantaneous charging efficiency of the cell relates to the total cell voltage. Though there are disparities in charge efficiency behaviour between the positive and negative plates, the errors anticipated by this overall approximation are small considering the usefulness and simplicity of the method. Lakeman (1989) finds that theoretically determined gas flow rates, using plate potentials and using overall cell potential, are in good agreement with experimental determinations under controlled charge conditions. He points out that unacceptable errors could occur from using cell potential alone in uncontrolled charging regimes, with no voltage limit. However, PV charging regimes are inherently controlled; and if not limited by the array output characteristics, are limited by voltage regulation. The result is that the gassing current can be estimated from the cell voltage and temperature alone. This assumption can be extended to good effect to generalise for the instantaneous charging efficiency determined in the two above methods.

The last method of estimating efficiency, applicable to all cell types, is by:

vi) measuring the end of charge current at constant potential

The assumption that charging efficiency is a function only of voltage and temperature has further implications. If the rate of charge acceptance of a fully charged cell is zero (true for negative plate, almost true for positive, see Section 3.8.2(b)), then the overall charging efficiency is practically zero and the charging current into a fully charged cell at constant potential is the gassing current. All that has to be done to determine the gassing current vs voltage is to charge a fully charged cell with several constant voltages and measure the current. This provides a valuable cross-check for the other methods of calculating charging efficiency.

a) Determine the gassing currents at various states of charge (in the region of 70-95% SOC).

Determine the instantaneous charging efficiency using the method in 6.2.6vi, corroborated by as many other methods as possible. Investigate this in terms of the number of plates (ie. current density), plate design and

thickness, grid design, electrolyte SG, temperature. It is eventually hoped to show that this parameter is one of the most significant in PV battery selection. In addition this test may indicate suitable cut-off voltages for voltage regulator float, boost and equalisation charge settings. The test will provide valuable data for designing microprocessor type energy management systems. The gassing current data can be incorporated with charging curve data to generate charging curves corrected for gassing loss. (See instantaneous charging efficiency measurement in Section 6.2.6(iv))

b) Determine the average charging efficiency of the cell.

Determine the efficiency at the recommended starting and finishing charging currents and voltages from a suitable DOD. This will not necessarily be the upper limit for the charging efficiency. Method 6.2.6(i) may be most appropriate, alternatively the average efficiency can be calculated from the instantaneous charging efficiencies or from the quasi-constant-current charging curve.

c) Determine the charging efficiency in the PV current regime.

Actual finishing current will most likely be far under the recommended finishing current. The decreased gassing will probably yield a higher charging efficiency than for (b). The reduced gassing is associated with a degree of compromise between charging efficiency and cell life. A certain amount of gassing is required to promote electrolyte mixing, reduce stratification and prolong useful cell life. The quasi-constant-current charging curves may be useful, although cycling tests (Section 6.2.7) may also be required.

d) Estimate self-discharge rates.

Gassing and self-discharge of cells are together related to grid type. Cells that can gas at low current will tend to have high rates of self discharge. Estimate self discharge rates based on the charging efficiency curves.

6.2.7 Cycling Tests

Cycling tests provide early information on temporary or permanent, short or longer term performance degradation. Through cycling batteries in defined regimes, information on overcharge requirements, start and finishing currents and voltages can be determined. Capacity tests after cycling tests indicate any loss of capacity during the testing. In the industry, cycling tests are conducted for several months at a time. In this programme time limitations generally restrict cycle testing to only a few days.

Sandia National Laboratories (Verado,1981) have identified two modes of operation in describing battery requirements for PV applications. If a battery has been sized to provide long term energy storage for the time the PV array is unable to produce power then the battery will experience shallow cycling with complete cycling once or twice a year (see Chapter 2). If the array is almost always able to provide the daily power demand, and the battery is only required for load-levelling or peak-lopping, then the battery will probably experience deep cycling on a daily basis. In both cases, prolonged operation at partial state-of-charge is possible. The cycling tests described below were developed by Sandia National Laboratories (Verado,1981). Although charge and discharge currents, voltages, overcharge and times are specified, they are not intended to be rigid. Sandia recommends that they be modified to suit particular batteries depending on manufacturer's data and experience with particular batteries.

Analysis and interpretation of the tests provide useful comparative data on charge acceptance rates, charging efficiencies, susceptibility to stratification, energy efficiencies and changes in capacity. It may be preferable to perform the same tests on different batteries, so that the batteries are compared on the same basis, rather than attempting to customise each test to suite individual batteries for which sparse data is available.

Standard cycle tests

Fully charging cells from shallow or deep cycles results in reduced charging efficiencies, and longer charging time requirements due to gassing losses in the 80%-100% SOC range. Some overcharge is required to overcome charging inefficiencies, and some overcharge is required to prevent electrolyte stratification. Charging voltages may have to be limited to control gas formation rates. The standard cycling tests can be used in conjunction with charge and discharge curves to determine whether these criteria are being met. Cycling may be deep or shallow cycle depending on the battery.

i) Standard shallow discharge cycle test

A fully charged battery is discharged for two hours at the C_{20} rate, removing 10 percent of the rated capacity. It is then recharged for two hours using constant potential with the current limited to C_{10} and the overcharge limited to 10 percent of the Ah removed, theoretically sufficient to completely recharge the battery. This charge/discharge cycle is repeated for a predetermined number of cycles, (six cycles per day are possible) and is terminated with a battery capacity test. The form of the test is illustrated in Figure 6.4.

ii) Standard deep discharge cycle test

A fully charged battery is discharged for four hours at the C_5 rate, removing 80 percent of the rated capacity. It is then recharged following the manufacturer's specifications for eight hours using constant potential and the overcharge limited to 15 percent of the Ah removed. This charge/discharge cycle is repeated for a predetermined number of cycles, (see Figure 6.5) (two cycles per day are possible) and is terminated with a battery capacity test. The test can be restarted once the battery is fully charged.

For the standard cycle tests trends in the end-of-discharge voltage, end-of-charge-current and loss of capacity are particularly interesting.

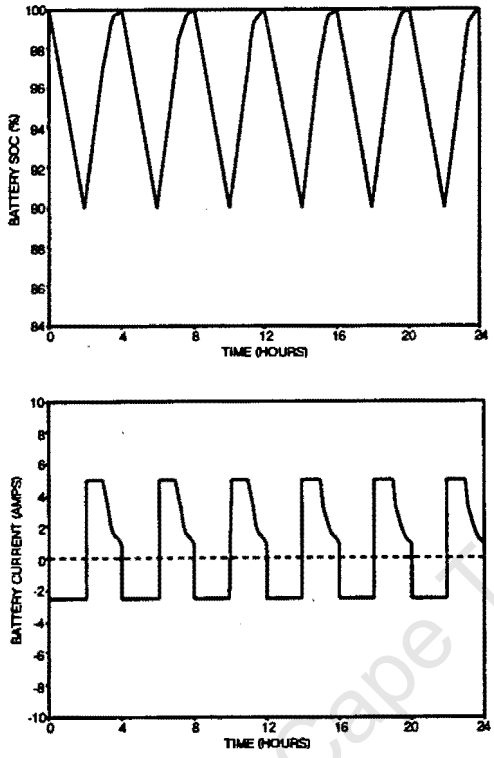

Figure 6.4 Standard shallow discharge cycle test for a 50Ah battery.

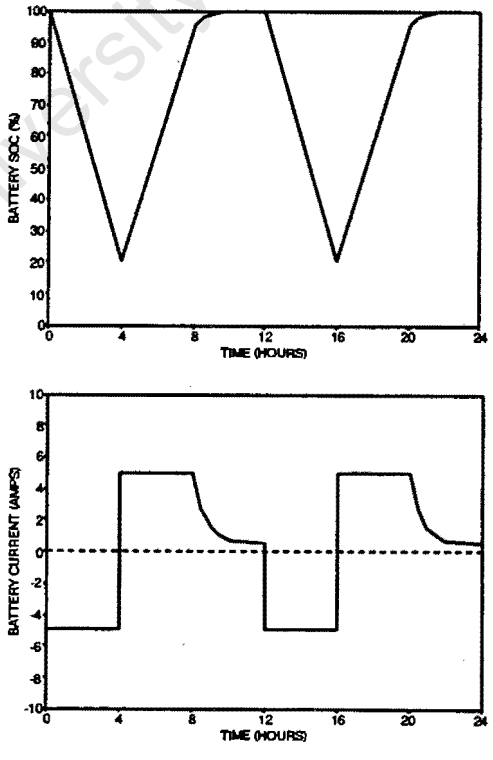

Figure 6.5 Standard deep discharge cycle test for a 25Ah battery.

Partial state of charge cycle tests

Deep discharge and subsequent slow recharging of batteries so that they remain in a partial state of charge enhances electrolyte stratification in flooded electrolyte cells, and promotes hard sulphate crystal formation on the negative electrodes of all cells, leading to temporary (or permanent) losses of capacity and energy efficiency. The aims of these tests are to investigate the effects of cycling without overcharging and gassing, and to determine the magnitude of the reversible and irreversible capacity and energy efficiency losses. As before, cycling may occur at a deep or shallow cycle.

iii) Partial state-of-charge shallow discharge cycle test

Figure 6.6 shows the test cycle for simulating partial SOC operation at shallow discharge. A fully charged battery is discharged for eight hours at the C_{20} rate, removing 60 percent of the rated capacity. A cycle consists of a two hour recharge at C_{20}, followed by a two hour discharge at C_{20}, theoretically removing and returning 10 percent of the capacity each cycle, cycling between sixty and fifty percent SOC. After the initial discharge, six cycles per day are possible. This charge/discharge cycle is repeated for a predetermined number of cycles, and is again terminated with a battery capacity test.

iv) Partial state-of-charge deep discharge cycle test

The test cycle is illustrated in Figure 6.7 is used for simulating partial SOC operation at deep discharge. A fully charged battery is discharged for four hours at the C_5 rate, removing 80 percent of the rated capacity. The battery is recharged at C_5 till sixty percent of the charge has been replaced, and then cycles continuously using a three hour discharge at C_5, followed by a three hour charge at C_5, theoretically cycling between 80 percent and 20 percent SOC. After the initial discharge, four cycles can be completed per day. As for the other tests this test is terminated with a battery capacity test.

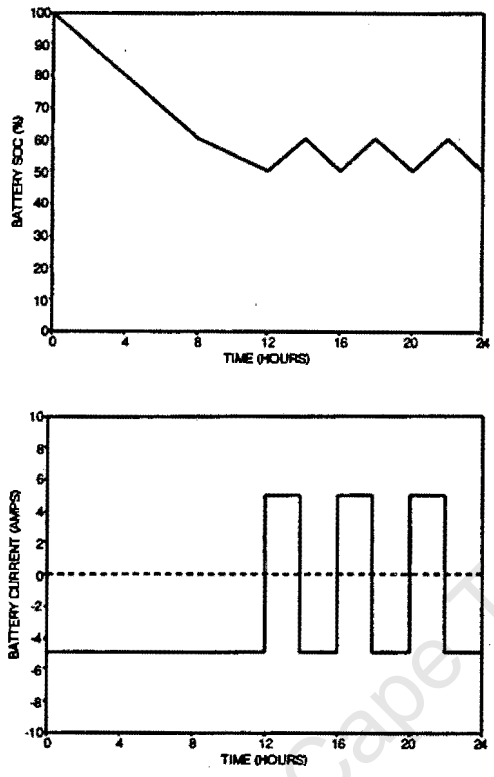

Figure 6.6 Partial SOC shallow cycle test for a 100Ah battery.

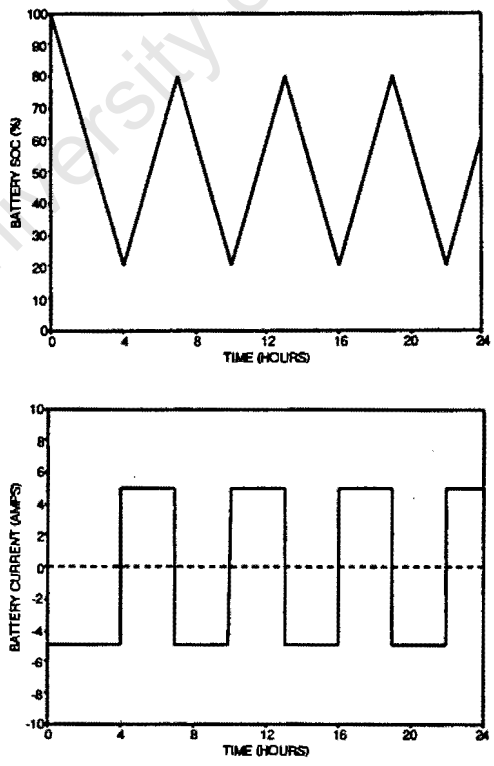

Figure 6.7 Partial SOC deep cycle test for a 25Ah battery.

a) Perform cycling tests

Conduct relevant cycling tests at suitable DOD, currents, voltages and time constraints. These parameters are considered and determined separately for each battery.

6.3 REPORT FORMAT

This section describes the presentation of the test results. The report numbering is consistent for all the batteries examined.

7.x BATTERY NAME

7.x.1 General Information

Data summary

The battery is categorised, and overview data presented.

Costing

The battery cost (R),

Wh cost (R/(C_{20} x voltage)),

kWh value (R/($Ah_{over\ life}$ x nominal voltage/1000)) at the optimum DOD over the operational life is estimated. Operating and maintenance costs and salvage value are excluded.

7.x.2 Physical

Physical construction

Relevant physical and chemical data is presented where available.

Active mass utilisation coefficients

Active mass utilisation shows which active materials are limiting in capacity and which may limit cycle life.

In addition, the excess electrolyte capacity and SG at deep discharge are calculated to determine the danger of electrolyte

freezing during operation.Low end-of-discharge SG's can also adversely affect battery internal resistance.

7.x.3 Basic Operating Data Available

Charging requirements and limits

Charging data provided or collected from similar batteries.

Discharge curves

Life cycle data

If cycle life curves are provided then they are presented, otherwise cycle life estimates are made using data available from similar batteries in conjunction with battery models.

Cycle life data is required for determining testing regimes as well as estimates of the optimum DOD and Ah over the battery life. The accuracies of these figures are verified by cycling tests where possible.

Extent of manufacturer's data

Extent of data is discussed and data graded according to quality. The gradings used are:
Grade A1 - data from independent laboratory
Grade A2 - data from the manufacturer's laboratory
Grade B - extrapolated from Grade A data
Grade C - extrapolated from Grade A or B from batteries of similar materials but different size
Grade D - other data
(See Section 4.3.2 for more details)

7.x.4 Test Results and Discussion

a) Capacity and discharge tests

Capacity, temperature effect on capacity, discharge curves and suitable voltage regulator load shed settings are considered.

b) Charging and efficiency tests

The quasi-constant current charging curve is presented together with the gassing current curve. The quasi-constant current curve is compensated by the gassing inefficiencies to yield the compensated charging curve. This sequence is used for ease of presentation. The practical sequence (Section 6.2) is to determine an experimental charging curve and gassing current curve, then calculate the compensated charging curve. The quasi-constant current charging curve is derived from the compensated curve and the gassing current curve.

c) Cycling tests

Test selection

Relevant cycling tests and parameters are selected.

Analysis of cycling:

Deep cycle full SOC test
Deep cycle partial SOC test
Shallow cycle full SOC test
Shallow cycle partial SOC test

Capacity at end of cycle tests

The change in capacity is used to verify the cycle life curve where possible.

H_2O consumption

H_2O loss rates are estimated and compared with experimental results.

Charging current and voltage requirements

Charging requirements during cyclic operation are considered.

7.x.5 Sizing and Selection: considerations in PV applications

Particular considerations are presented in order of priority.

CHAPTER 7

TEST RESULTS

This chapter presents and discusses the results of tests and experiments on selected batteries.

7.1 WILLARD 774 PORTABLE BATTERY

7.1.1 General Information

Data summary

Capacity:	C_{20} = 90Ah @ 20°C
Voltage:	12V
Application:	leisure/portable power
Group:	flat plate, antimony grid, flooded
Description:	Flat plate 12V power pack. Vented with flooded electrolyte. Essentially a modified SLI design, with thicker plates for better cycle life. Antimony and other grid additives are used in the positive and negative plates. Black plastic casing.

See Appendix D1 for manufacturer's data sheet.

Costing

Cost:	R294 per battery (@ 23/10/1990)
Wh cost:	R0.27/Wh
Wh value:	R1.81/kWh over battery life, assuming 300 cycles at 40% DOD, the optimum DOD. These figures should be regarded as approximate. (See Section 7.1.3.)

7.1.2 Physical

Physical construction

Dimensions:	height, width, length:	225 x 172 x 342mm
	height over terminal:	225mm
	mass:	25.6kg
Plates:	design:	15 flat plates/cell
		7 positives, 8 negatives
	pos. active material:	97g
	neg. active material:	94g
	active block mass:	2.768kg/cell
Grid:	positive:	1.6% Sb
	negative grid	pure lead
	grid mass:	1.107kg/cell
		(40% of active block mass assumed)
Dry mass:	17.7kg	
Electrolyte:	SG:	1.260 @ 20°C
	volume:	5.9l
	mass:	7.43kg
Wet mass:	25.6kg	
Gas venting:	automotive type vent caps	
Casing:	black plastic	
Terminals:	standard lead pillar	

Active mass utilisation coefficients:
(Calculated)

	Active mass	Electrolyte	SG @ end of test
capacity @ 100% utilisation	152Ah	121Ah	1.000
utilisation @ nominal capacity (90Ah)	59%	74%	1.055
utilisation @ 100 hr rate (98Ah)[1]	65%	80%	1.04
utilisation @ opt. DOD (39Ah @ 40% DOD)[2]	32.5%	40%	1.17

Under normal operation, the SG of the electrolyte will limit capacity, as well as resulting in higher internal resistances which reduce efficiencies.

7.1.3 Basic Operating Data Available

Charging requirements and limits

No charging data was provided. Data provided for charging a similar battery (Raylite RR2) following deep discharge is:
starting charge: 12.6A or 14.0% of C20
finishing charge: 6.3A or 7.0% of C20
equalising charge: 2.7A or 3.0% of C20

1 See discharge data in SECTION 7.1.5(a)

2 See life cycle data in SECTION 7.1.3

These are figures used by manufacturers for many batteries, and represent a rule of thumb. There are two limitations to charging current, both related to gassing. Gassing must be limited to reduce grid corrosion, and to prevent physical stripping of the active mass.

Discharge curves

Complete discharge curves at 20°C are available ranging from 10 minute to 50 hour rates.

Life cycle data

No life cycle data is available. The manufacturer suggested that 200 cycles @ 80% DOD and 400 cycles at 20% DOD was attainable under normal operating conditions. The low cycle life is a reflection of the high active mass utilisation coefficients. Similar batteries in SAPV's have achieved 700 cycles at 10% DOD, and models suggest that 200 cycles at 80% represents 750 cycles at 10% DOD for similar failure mechanisms (refer to Section 3.12 on Battery Models). Common failure modes include grid corrosion and active mass shedding. The optimum battery utilisation for the higher life estimate occurs in the range 40% to 60% DOD. (See Figure 7.1.) The optimum cycle life is relatively insensitive to DOD in this range.

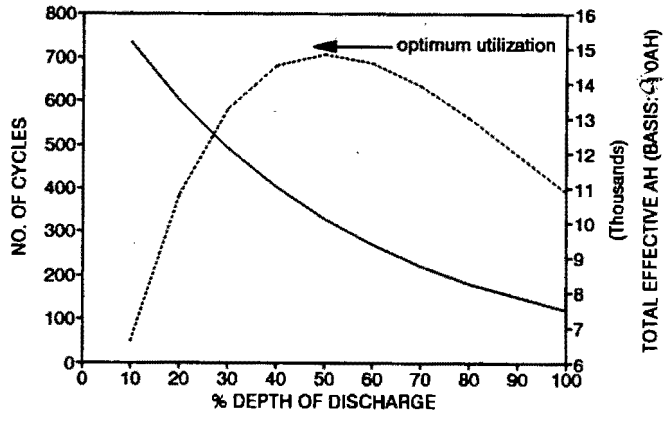

Figure 7.1 Estimated cycle life vs depth of discharge.

Extent of manufacturer's data

Data Quality:
The only data provided is the discharge and capacity data, which is Grade A2 (performed by the manufacturer in-house on the specific battery).

Data as purchased:

- No data was provided, except nominal capacity.

Additional data on request by personal communication:

- Standard discharge curves were provided: (Grade A2).
- Plate masses, (dry and wet), overall masses and dimensions,
- Life cycle data: estimated at 200 cycles @80% DOD: (Grade C).

See Appendix D1 for manufacturer's data sheet.

7.1.4 Test Results and Discussion

a) Capacity and discharge tests

Three complete sets of capacity tests were conducted, at 0°C, 18°C and 35°C. Discharge currents were 1A, 2A, 4.5A, 10A and 20A.

Before each test the battery was equalise charged, till the SG's were within specification, ie 1.260. The battery was discharged to the manufacturer's cut-off voltages (see manufacturer's data), and capacities achieved were within 5% of the manufacturer's specifications, although usually a few percent below.

The standard discharge curves at the three temperatures are shown in Figure 7.2. The variation in capacity with temperature is shown in Figure 7.3.
The available battery capacity (at 10A discharge current) decreased by less than 1% below the initial capacity after all the discharge tests (15 discharges down to 100% DOD).

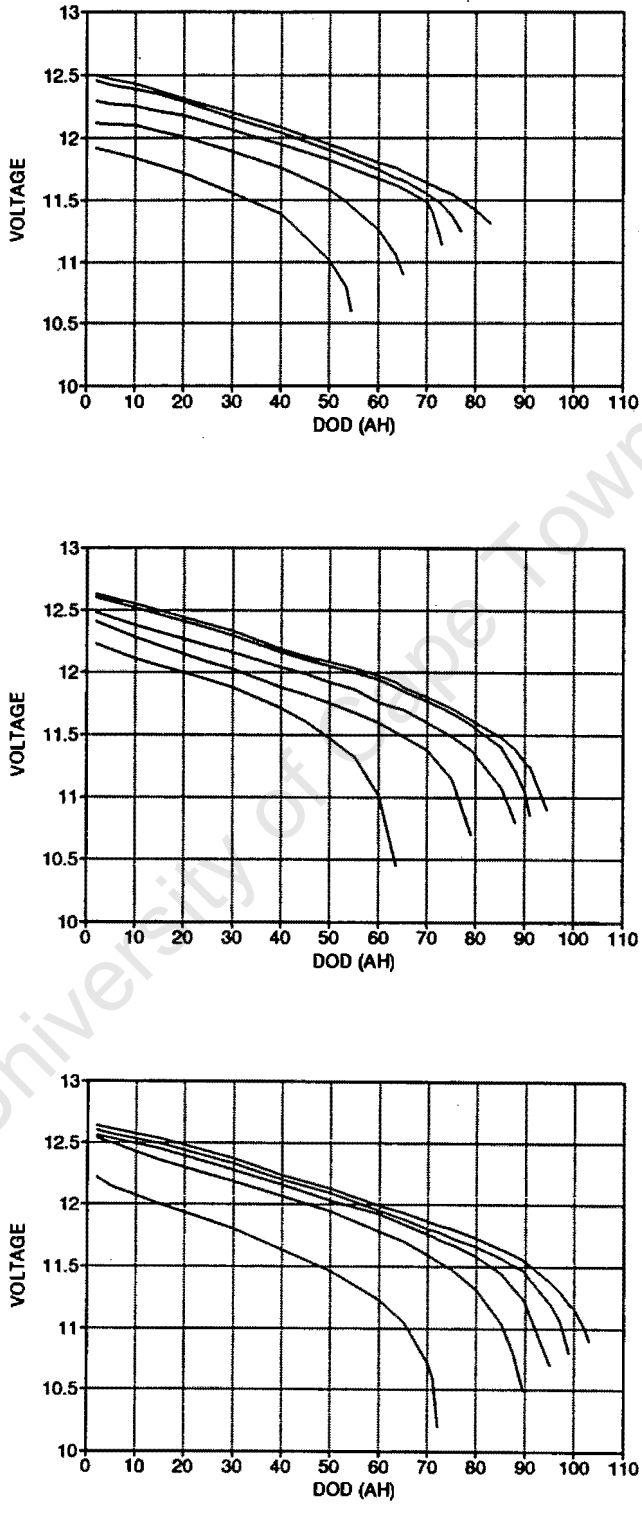

Figure 7.2 Discharge curves at a) 0°C, b) 18°C, c) 35°C. Discharge currents are 1A, 2A, 4.5A, 10A and 20A in each case.

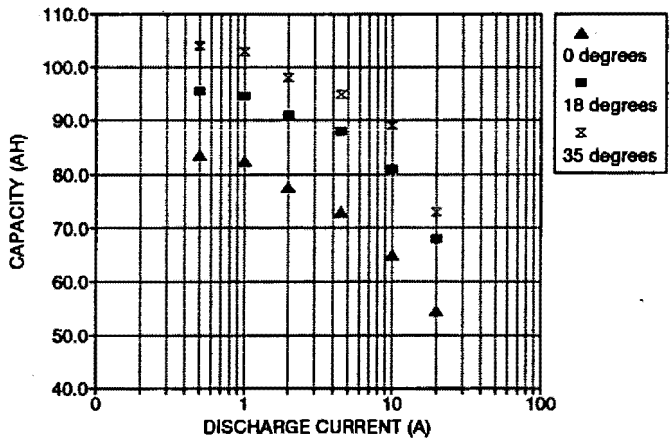

Figure 7.3 Discharge capacity vs temperature and discharge rate.

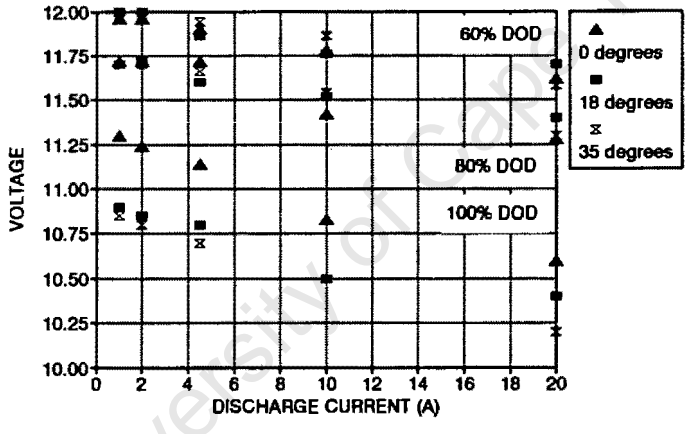

Figure 7.4 Cut-off voltages vs discharge rate, SOC and temperature.

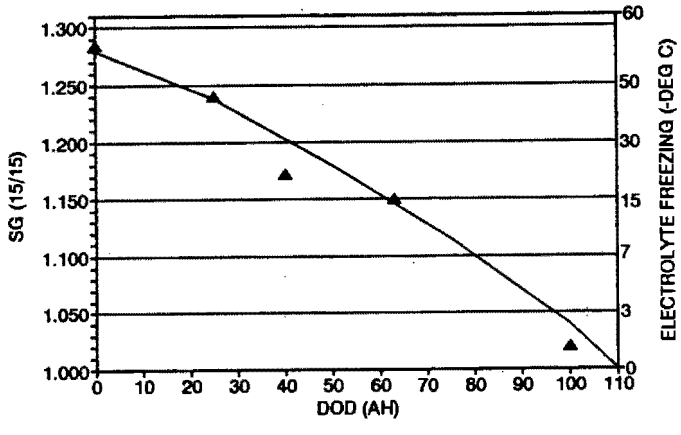

Figure 7.5 Electrolyte SG and freezing points vs DOD. Triangles represent measured data.

Figure 7.4 is derived from the discharge data and shows the cut-off voltages vs DOD, discharge current and temperature, that are suitable for voltage regulator load-shed settings. The graph shows clearly that load shed settings are current and SOC dependant. Settings should be selected after consideration of average and peak loads, desired load shed DOD and expected battery temperature. Temperature is not critical for load-shed settings when the DOD is less than 80% and battery currents are less than 10A.

Figure 7.5 shows electrolyte SG vs Ah removed. The curve is theoretically based, but experimental SG measurements are shown. The difference in SG's may be ascribed to concentration gradients between the bulk fluid and the pores of the active masses. The electrolyte freezing temperature vs SG is superimposed. Note how the cell is increasingly vulnerable to freezing at DOD greater 75%. The freezing point at 80% DOD vs C_{100} is -5°C.

b) Charging tests

Charging tests were conducted as described in Section 6.2.5. Charging rates used were 10A, 5A, 2A, 1A, and 0.5A. The temperature compensated charge voltage limits used were 14.8, 14.5 and 14.2 volts at 0°C, 18°C and 35°C respectively.

The quasi-constant current charging curve at 18°C is shown in Figure 7.6. The curve shows that a minimum of 4.4Ah of overcharge is required to reach full charge at 18°C and 14.4V, regardless of the initial DOD. At the recommended finishing current (6.9A), the voltage will be 15.5V, and the overcharge required is 15.0Ah.

Charging efficiency was determined by measuring the rate of gassing, assuming a gas composition based on literature, and calculating the current required to produce the gas flow rate (for method see Section 6.2.6(iv)). Gassing occurred at 13.6V regardless of the SOC. Figure 7.7 shows the gassing current at 100% SOC at 23°C and 33°C, and the good agreement for 80% SOC. Gassing seems dependant only on voltage and temperature, and independent of SOC, certainly in the voltage range likely to be encountered in PV applications.

A second method (Section 6.2.6(vi)) was used to corroborate the results of the first method. The end-of-charge current is assumed to be equal to the gassing current. This approach shows good agreement with the experimental method. The main difference is probably due to the non-stoichiometric gas ratio that occurs in reality. (See Figure 3.31.) The gassing curves are shown in Figure 7.8.

The charging curves after compensation for gassing and overcharge losses are shown in Figure 7.9.

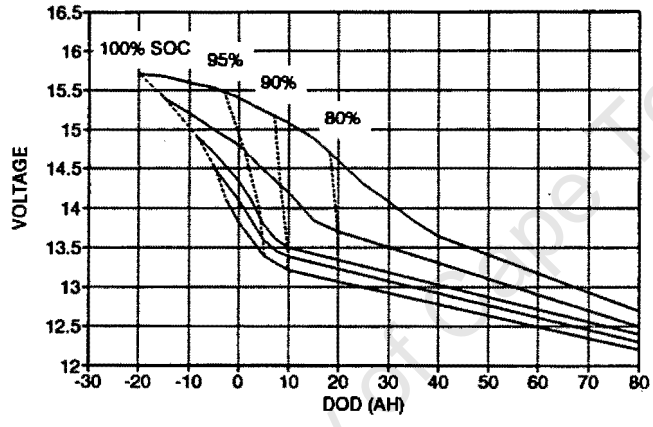

Figure 7.6 Quasi-constant current charging curve at 18°C.

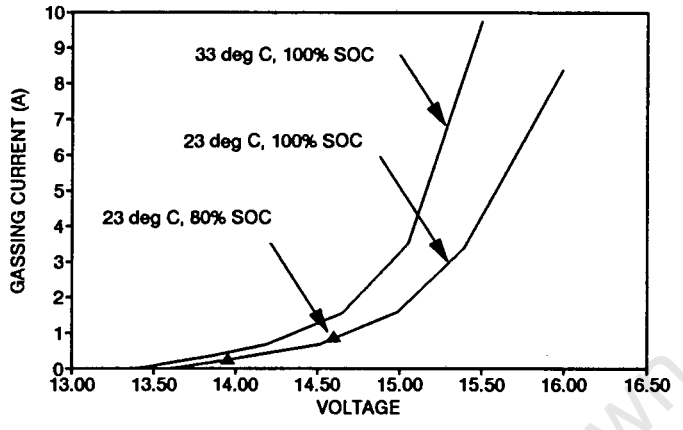

Figure 7.7 Gassing current determined by gas flow measurement, vs SOC and charge potential.

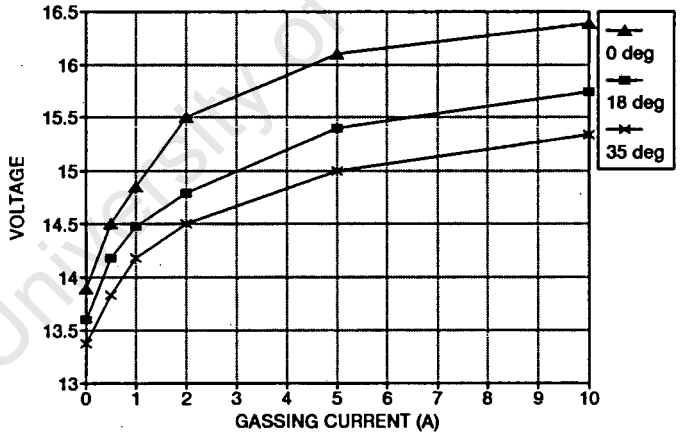

Figure 7.8 Gassing current as function of voltage and temperature.

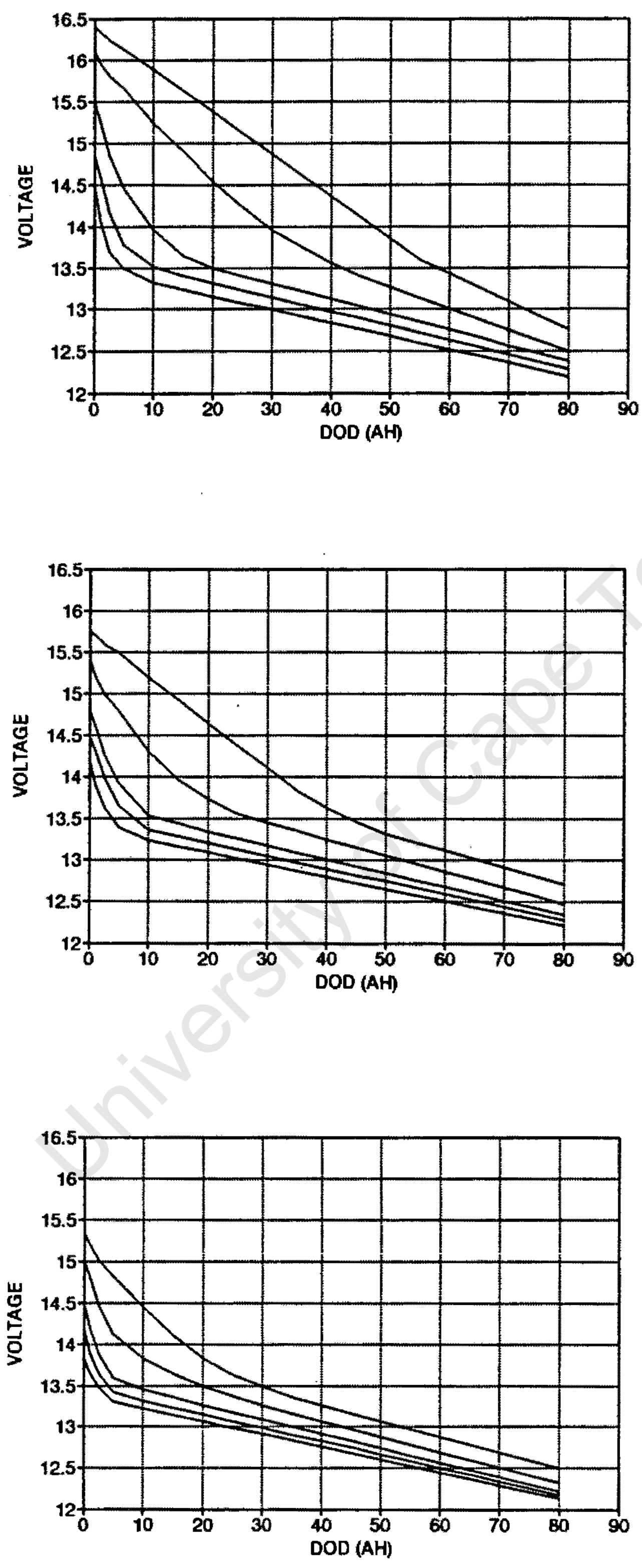

Figure 7.9 Compensated charging curves at a) 0°C, b) 18°C, c) 35°C. Charging currents are 0.5A, 1A, 2A, 5A and 10A in all cases.

c) Cycling tests

Cycling tests selection

The 774 battery is designed for portable power applications, where it can be expected to be regularly deep cycled. Cycle life curves show an optimum DOD of about 40-60% for regular cycling. In PV applications deep and shallow cycle tests are relevant. A deep cycle full SOC cycling test is required to determine the overcharge cycle to eliminate stratification, and to determine the effect on cycle efficiency of deep cycling. A shallow cycle full SOC test is useful for determining the minimum charge voltage during shallow cycling, particularly since unnecessary gassing is to be avoided. In many PV applications the system size (energy capacity) is increased by increasing battery size using low cost batteries while maintaining the same panel area. This may result in shallow cycling at partial SOC (see CHAPTER 2), so a partial SOC shallow cycle test is useful. The cycling tests are described in Section 6.2.7. All cycling tests were conducted at 20°C.

Deep cycle full SOC test

The test was set-up so the battery was repeatedly cycled between a fully charged state and 40% DOD. The discharge rate was C10 (9A). The battery was recharged at 2.35V/cell, with a current limit of C10, an overcharge limit of 10% (3.6Ah/cycle) and a maximum charge time of 5 hours. Any one of the charge limitations could prevent the fully charged state from being attained.

Figure 7.10(a) shows the increasing end-of-charge current and stable end-of-discharge voltage. The increase in the end-of-charge current signifies a decrease in the end-of-charging-cycle SOC from cycle to cycle. The SOC stabilises at 97% SOC (determined form the charging curves at 1.95A). Figure 7.10(b) shows that the time to recharge the battery decreases steadily as the end-of-cycle SOC decreases and then stabilises, indicating that the set overcharge is insufficient to recover full charge. The stable end-of-discharge voltage indicates that the 10% OC provides sufficient gassing to restrict stratification.

The watt-hour efficiency for cycling is stable at 82.5% and indicates a state of dynamic equilibrium. The Ah efficiency is 87%. (See Figure 7.10(c).)

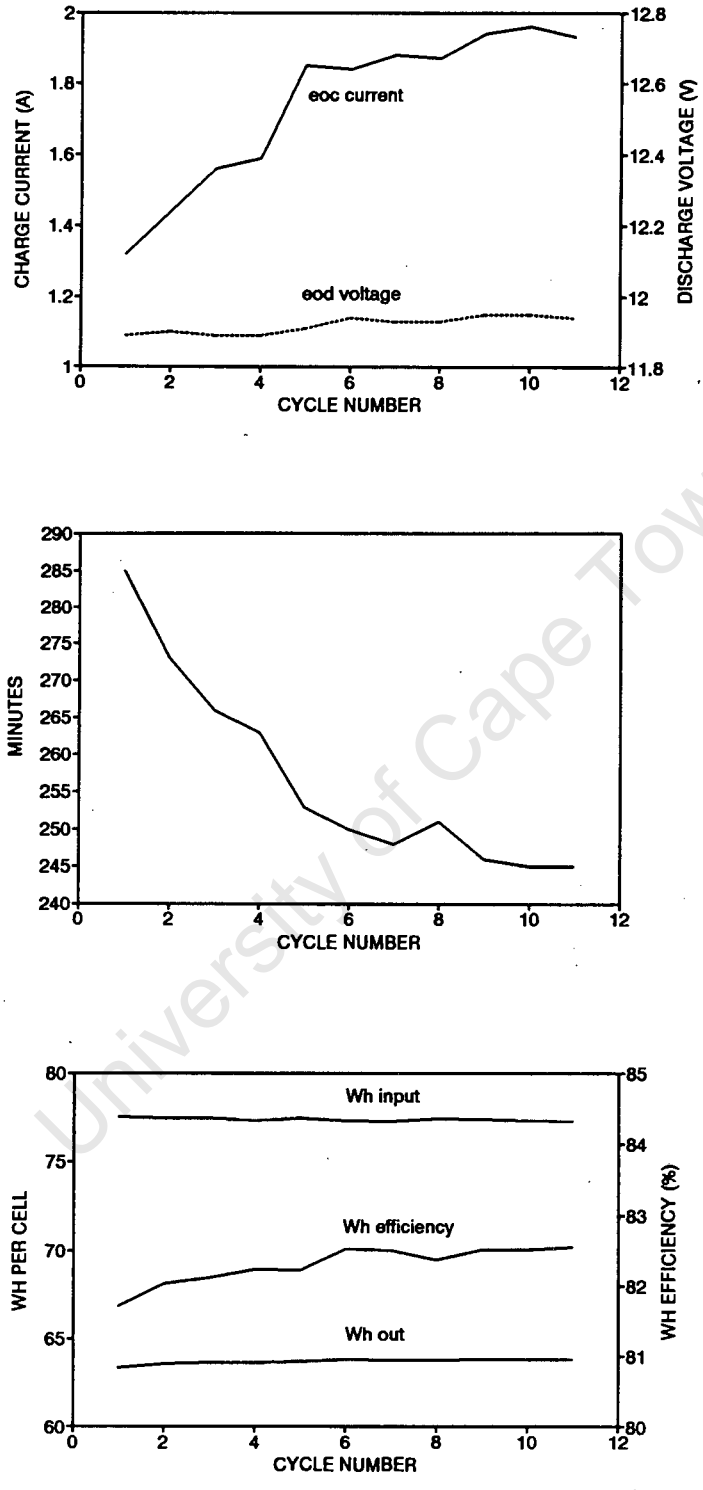

Figure 7.10 Deep cycle full SOC test. a) end-of-cycle conditions, b) charging time, c) Wh cycle efficiencies.

Shallow cycle full SOC test

The battery was cycled between a theoretical 100 and 90% SOC at discharge current of C10, and charge voltage of 2.35V/cell, with a limiting current of C10 (9A). Overcharge was limited to 10%, and the time for charging limited to two hours.

Figure 7.11(a) shows the end-of-charge current and end-of-discharge voltage. The high end-of-charge current (2.5A) suggests that the battery does not reach full charge, and instead reaches a top of cycle dynamic equilibrium around 96% SOC. Only 85 minutes of the allowed 120 minutes is required to charge the battery, indicating that 10% OC is insufficient to reach full charge. The maximum calculated gassing current is 0.5A. The end-of-discharge voltage is constant at 12.2V.

The watt-hour efficiency is stable at 82% at the chosen currents. The Wh input is high (27Wh/cell per cycle) compared with similar batteries. (Figure 7.11(c).)

Shallow cycle partial SOC test

The battery was repeatedly cycled between 10% and 20% DOD at charge and discharge rates of C10 (9A), which is below recommended starting charge rate.

Figure 7.12(a) shows the end-of-charge and end-of-discharge voltages as the test commenced. The slight decline in the end-of-discharge voltages during partial cycling indicates a decrease in available capacity, and together with the initial increase in end-of-charge voltage shows the onset of some physical phenomena, probably electrolyte stratification combined with sulphation of the negative and positive electrodes, and possibly, though unlikely, some charge inefficiency.

The short term effect of these physical phenomena on battery performance is shown in Figure 7.12(b) by the steady drop in the Wh cycle efficiency. This efficiency seems to have reached a lower limit probably around 92%. However, the continued decrease in Wh out per cycle indicates that no real equilibrium has been reached, and further stratification and sulphation is likely.

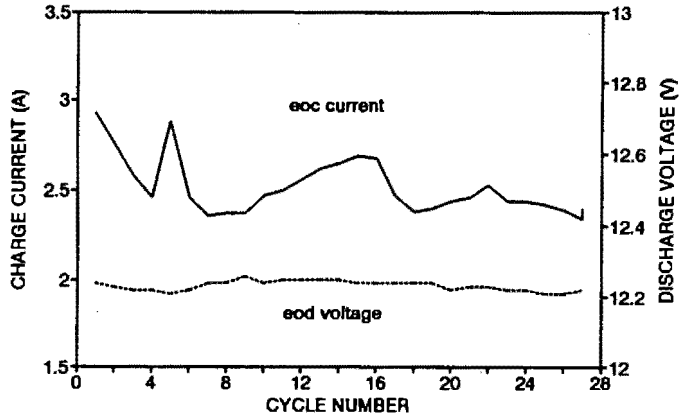

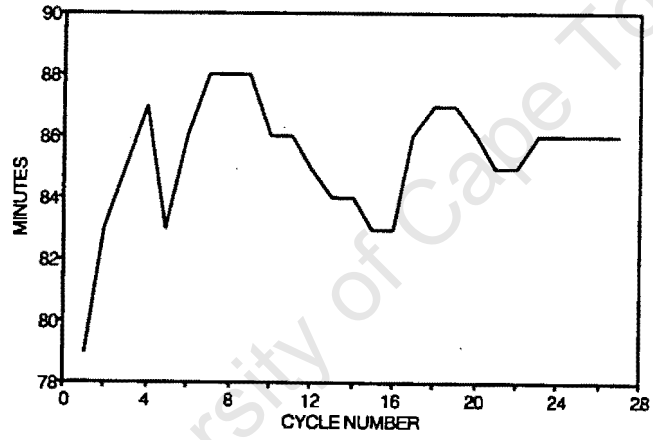

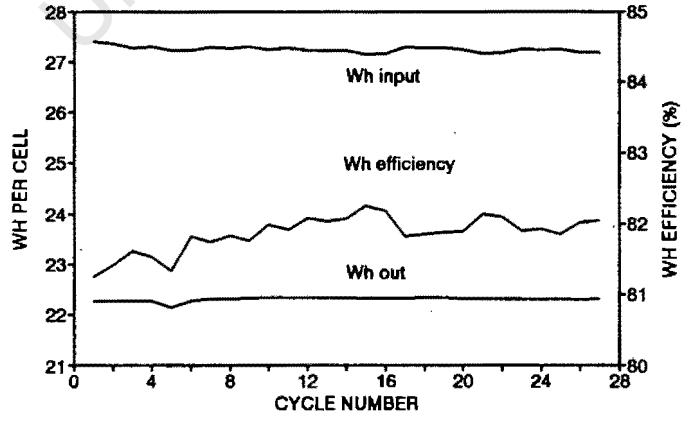

Figure 7.11 Shallow cycle full SOC test a) end-of-cycle conditions, b) charging time, c) Wh efficiencies.

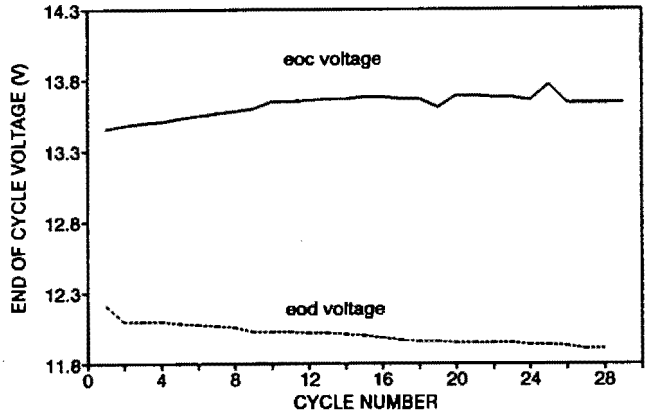

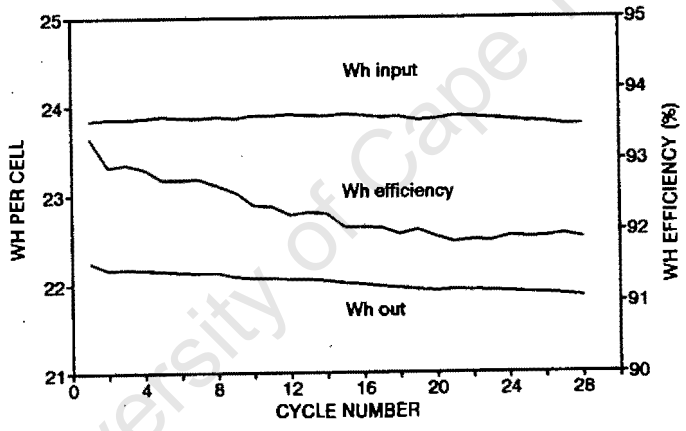

Figure 7.12 Shallow cycle partial SOC test a) end-of-cycle conditions, b) Wh efficiencies.

Capacity at end of cycle tests

The cell was equalised and the capacity determined at the C10 rate to be 81.5Ah, compared with 83Ah at the start. The drop in capacity of 1.5Ah represents 1.8%. If the useful battery life is assumed complete when the drop in capacity is 20%, then this cell has lost 9% of that 20%.

The percent of useful life used can be theoretically calculated using models (see Section 3.12). The incremental wear due to:

28 cycles @ 10% DOD (735 cycles expected over battery life)
28 cycles between 10% and 20% DOD (661 life cycles expected)
11 cycles @ 40% DOD (403 cycles expected)

is

28/735 + 28/661 + 11/403 = .108 or 10.8%

H20 consumption

During the cycling tests the accumulated overcharge was approximately 56Ah, which would account for a theoretical water loss of 20.5ml per cell (theoretically 0.366ml H_2O/Ah). Water consumption could not easily be measured because of the non-translucent casings. Practical experience suggests that 5% gas recombination efficiency by the vent plugs can be expected.

The vent plugs allowed considerable electrolyte seepage, particularly during charging. This leakage not only necessitates more frequent maintenance, but is dangerous and messy. The problem has since been rectified by the manufacturer.

Charging current and voltage requirements

The optimum charging requirements for the Willard 774 are difficult to determine as there are two conflicting criteria. Prevention of stratification is obviously a high priority, but at the same time gassing should be absolutely minimised. Gassing in SLI type batteries quickly corrodes away the thin positive grids, particularly in antimony cells. Additionally, gassing will expose the plates and reduce available capacity.

For deep cycling to about 40% DOD, 3.6Ah of overcharge is sufficient to prevent stratification, but just insufficient to fully recharge the battery at 9A and 2.35V/cell. Similarly, for shallow cycling to 10% DOD and charging at 9A and 2.3V/cell, 1Ah of overcharge prevents stratification but does not allow complete charging of the cell. The accumulation of undercharging during cycling results in the gradual establishment of a SOC limit. For shallow cycling at 2.3V the OC requirement due to gassing is about 1.5.Ah/cycle, for deep cycling it may be 4.0 at 2.35V.

Shallow cycling may be feasible if the amount of OC can be finely controlled to just prevent stratification and limit gassing to a minimum. If gassing cannot be easily restricted (due to temperature effects), then it will be better to cycle the battery to about 40% DOD and use the excess gas for electrolyte mixing. The shorter battery life (in years) will not be limited by grid corrosion, as may be the case in the shallow cycle situation, where uncontrolled gassing may occur for long periods. In either case, the charge regulator settings should be carefully considered, and temperature compensated if possible.

7.1.5 Sizing and Selection: considerations in PV applications

1) Optimise battery life by choosing suitable daily DOD. Low DOD is not necessarily optimal as overcharge may be excessive.
2) Avoid deep DOD for any period during very cold seasons, as electrolyte freezing may occur.
3) Avoid excessive gassing during normal operation, which could enhance corrosion of the thin SLI type grids. A charge regulator is almost certainly required. Carefully select the regulator charge voltage settings.
4) In extremely variable climates, watch for runaway gassing at higher temperatures due to the high temperature coefficient of gassing. Special care in regulator type selection may be required. Consider a temperature compensated voltage regulator.
5) Minimise electrolyte stratification. The battery can easily recover form short term stratification by gassing though this is best prevented, by allowing up to 4Ah overcharge per deep cycle under carefully controlled charge conditions. However, such control may be difficult to achieve in small PV systems.
6) Calculate the maintenance period based on projected H_2O consumption. Add a safety margin to allow for evaporative losses. Water loss may expose the plates and cause permanent damage.

7.2 RAYLITE RMT 108 STANDBY CELL

7.2.1 General Information

Data summary

Capacity: C_{10} = 108Ah @ 20°C
Voltage: 4V
Application: standby power
Group: tubular, antimony grid, flooded, tall
Description: Tubular, standby battery. Vented with flooded electrolyte, in transparent EVA casing. A broad size range is available from the RMT/RST family of batteries, from 15Ah single plate cells to 2500Ah 20 plate cells. All are designed on the same principles, are similar and test results are suitable for scaling across the size range.

Costing

Cost: R198 per cell (@ 23/10/1990)
Wh cost: R0.93/Wh as purchased (see Figure 7.13 for size/cost reduction for RMT range)
Wh value: R0.58/kWh over battery life, assuming 4000 cycles at 40% DOD, the optimum DOD. (See Section 7.2.3.)

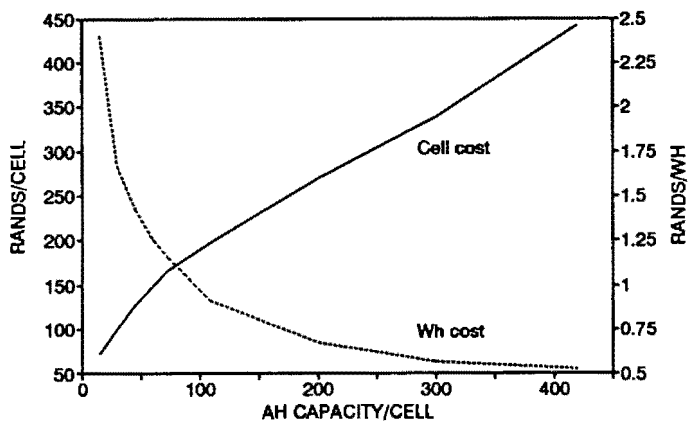

Figure 7.13 Size/cost reduction for Raylite RMT/RST batteries. (Rands/Wh cost assumes 4000 cycles at 40% DOD)

7.2.2 Physical

Physical construction

Dimensions:	height, width, length:	312 x 208 x 180mm
	height over terminal:	360mm
	mass:	23.2kg
Plates:	positive design:	3 × 36Ah tubular plates/cell
	spines per positive:	NA
	positive plate weight:	NA
	negative design:	flat pasted plate
	negative plate weight:	NA
	active block mass:	5.88kg/cell
		(80% of dry mass assumed)
Grid:	positive:	1.6% Sb
	negative grid	pure lead
	grid mass:	2.235kg/cell
		(40% of active block mass assumed)
Dry cell mass:	14.7kg	
Electrolyte:	SG:	1.250 @ 20oC
	volume:	6.8l
	mass:	8.5kg
Wet mass:	23.2kg	
Gas venting:	screw type vent caps, rubber seal, sintered glass membrane	
Casing:	transparent EVA	
Terminals:	bolt type, for which M6 316 stainless nuts, bolts, washer and inter-cell connectors are supplied.	

Active mass utilisation coefficients

(Calculated)

	Active mass	Electrolyte	SG @ end of test
capacity @ 100% utilisation	423Ah	385Ah	1.000
utilisation @ nominal capacity (108Ah)	25%	28%	1.190
utilisation @ 100hr rate (180Ah)[3]	43%	47%	1.150
utilisation @ opt.DOD (43Ah @ 40% DOD)[4]	10%	11%	1.230

Under normal operation, the SG will not fall below 1.19, but under extreme conditions may drop to 1.15. The cell is designed with large reserve electrolyte capacity.

7.2.3 Basic Operating Data Available

Charging requirements and limits

(As recommended by the manufacturer, following deep discharge. No specifications provided for shallow cycling or float charge operation)

starting charge: 15A or 13.8% of C10
finishing charge: 7.5A or 6.9% of C10
equalising charge: 3A or 3.0% of C10

3 See discharge tests in SECTION 7.2.4(a)

4 See SECTION 7.2.3

Discharge curves

Complete discharge curves are provided for discharge rates greater than the 10 hour rate.

Life cycle data

No life cycle data is provided, but the manufacturer suggested that 1200 cycles @ 80% DOD was possible, with a maximum life of 15 years under ideal conditions. This seems reasonable as active mass utilisation coefficients are low at rated capacity. On the basis of the utilisation coefficients and real test data for similar tubular cells (grade A2 data: Lucas P series[5]), the RMT108 data was modelled to produce a cycle life vs DOD curve. The similar shape curves indicate similar failure mechanisms. This curve was used to infer an optimum DOD for the most effective battery utilisation (Figure 7.14), which occurs in the range 30% to 60% DOD.

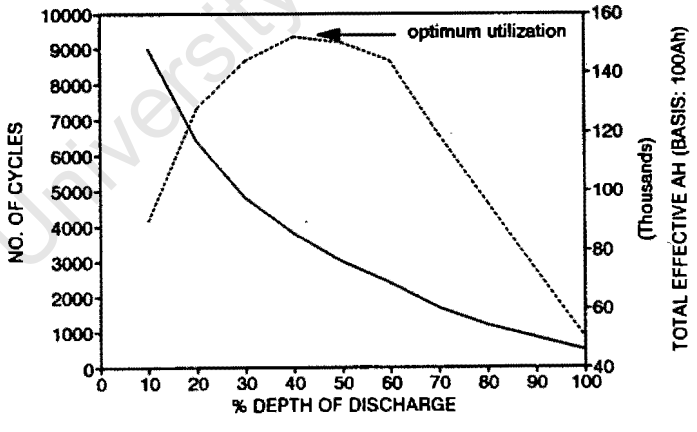

Figure 7.14 Estimated cycle life vs DOD for Raylite RMT108

5 The Lucas P series, and indeed most tubular cells have similar active mass utilization coefficients, grid alloys, etc. Lucas P series life cycle curve is from personal communication with BP Solar (SA)

Extent of data from Manufacturer

Data Quality:

All batteries in the RMT range are similar, and it seems unlikely that data has been generated for each and every battery. While some data is specific (Grade A2), most is probably scaled data of Grade C.

Data provided:

- Capacity and voltage vs discharge rate and discharge time. Format is graphical and tabular: (Grade A2 or Grade C)
- Recommended charge rates (starting DOD not specified): (Grade C)
- Masses, dimensions

See Appendix D2 for the manufacturer's data sheet.

Additional data on request by personal communication:

- Life cycle data: roughly estimated at 1200 cycles @80% DOD: (Grade C)
- Float voltage operating parameters

Many SA cells are based on designs developed by parent companies. Raylite tubular cells are based on the established Hagen design[6]. It is odd (and reprehensible) that lifecycle data are not readily available for these important and widely used barreries.

7.2.4 Test Results and Discussion

a) Capacity and discharge tests

Two sets of capacity tests were conducted at 18°C.

In the first set the cells were equalise charged, till the SG's were within specification, ie 1.250. The cells were then discharged at 25A, 16A, 8.8A, 3.2A and

6 Hagen Batterie AG, Germany

1.5A till the recommended cut-off voltages (see manufacturer's data). Capacities achieved were 20% higher than the manufacturers specifications. C_{100} is estimated at 180Ah. (See Figure 7.15).

In the second set of discharge tests the cells were recharged with 15% overcharge but not equalised. Average SG's after charging were 1.220. The cells were then discharged at the same rates as before. The capacities were 20% lower than previously, but approximately coincident with the manufacturers specifications at discharge rates greater than C3.

The variation in capacity between the equalised and partially stratified cells is shown in Figure 7.16. The watt-hour capacity for the first test is included.

Further capacity tests were conducted at 0°C and 35°C at the 16A and 8.8A rates, starting from the defined state. The average change in capacity as a function of temperature is shown in Figure 7.17.

Figure 7.18 shows the SG vs Ah removed, and the electrolyte freezing temperature. It is clear from the discharge data that a maximum of 200Ah can be removed at discharge rates higher than 1.5A, before the voltage falls dramatically, so the electrolyte SG will never be below 1.150. At low temperatures this capacity is further reduced. The electrolyte is therefore never in danger of freezing at temperatures above -10°C. Active mass utilisation for both electrolyte and active mass will normally be around 10% at 40% DOD cycling. The low utilisation is typical of tubular batteries; the tubular construction allows higher active mass utilisation while diffusion problems reduce the average effective performance at higher currents. This can result in overspecification of the battery if operation is in the low discharge current regime.

Figure 7.19, derived from the discharge data, shows the cut-off voltages vs DOD and discharge current, suitable for voltage regulator load-shed settings for unstratified cells.

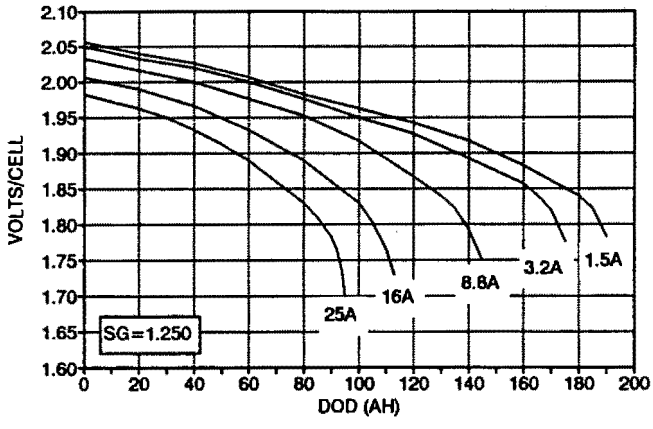

Figure 7.15 Standard discharge curves at 18°C.

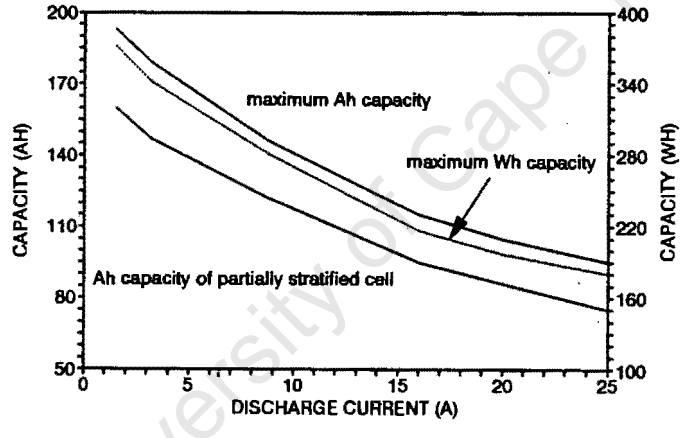

Figure 7.16 Ah and Wh capacities vs discharge current, showing the effect. of stratification

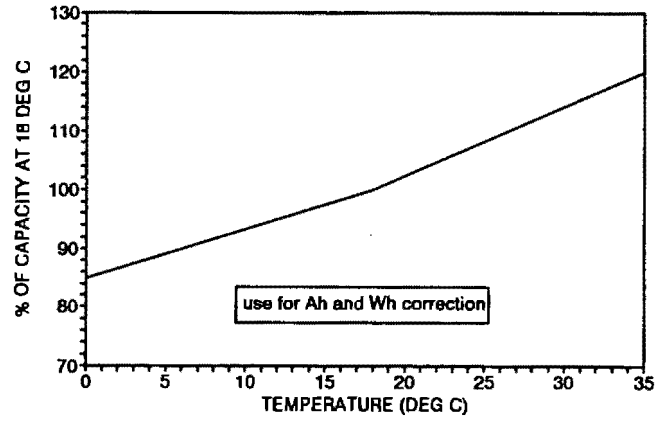

Figure 7.17 Capacity adjusted for temperature.

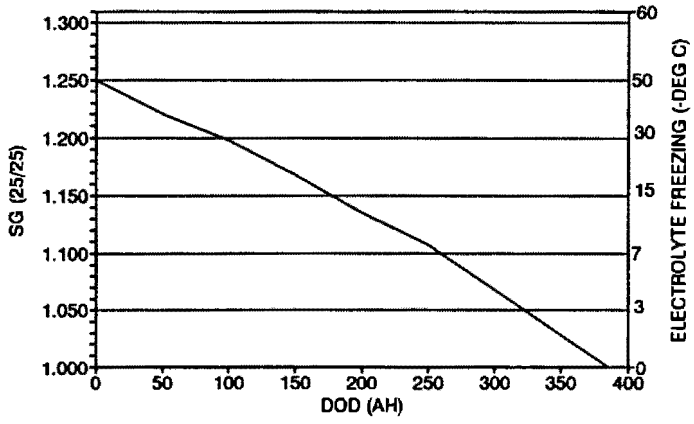

Figure 7.18 Electrolyte SG and freezing temperature vs Ah removed.

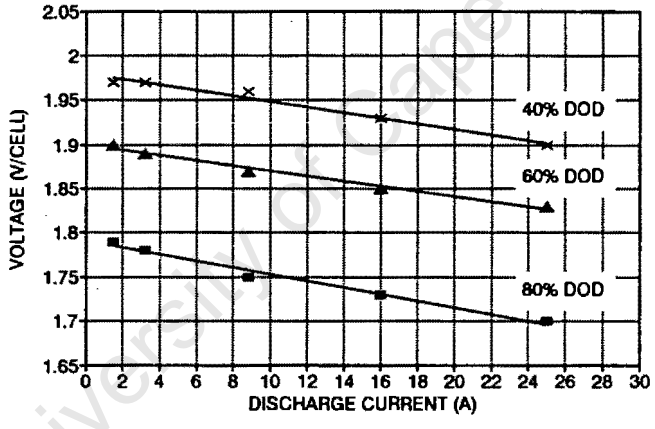

Figure 7.19 Cut-off voltages at 18°C, suitable for load shed settings.

b) Charging tests

Charging tests were conducted as described in Section 6.2.5 using variable charging current. Charging rates used were 16A, 8.8A, 3.2A, 1.5A, and 0.7A. The temperature compensated charge voltage limits used were 2.45, 2.35 and 2.28 volts per cell at 0°C, 18°C and 35°C respectively.

The charging curve at 18°C is shown in Figure 7.20. These curves show that a minimum of 5.5Ah of overcharge is required to reach full charge at 18°C and 2.366V/cell, regardless of initial DOD. At the recommended finishing current (7.5A), the voltage will be 2.45V/cell, and the overcharge required is 7.0Ah.

Instantaneous charging efficiency and gassing currents were determined by using the end-of-charge voltage method in Section 6.2.6 (vi). The derived gassing or overcharge current curves are shown in Figure 7.21.

The charging curves after compensation for gassing and overcharge losses are shown in Figure 7.22. The end of charge voltage can be read from these curves, as well as the sensitivity of end-of-charge current to the voltage setting. The gradual increase of the slope of the compensated charging curves near full charge indicates the early gassing, and relatively inefficient charging regime.

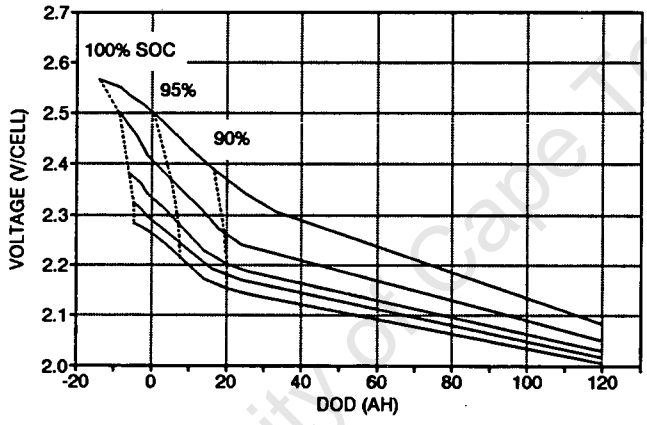

Figure 7.20 Quasi-constant current charging curve at 18°C. Charging rates used were 16A, 8.8A, 3.2A, 1.5A, and 0.7A.

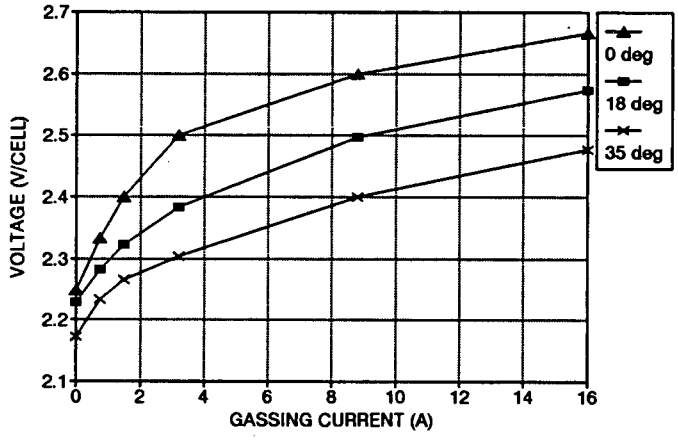

Figure 7.21 Gassing current as a function of voltage and temperature.

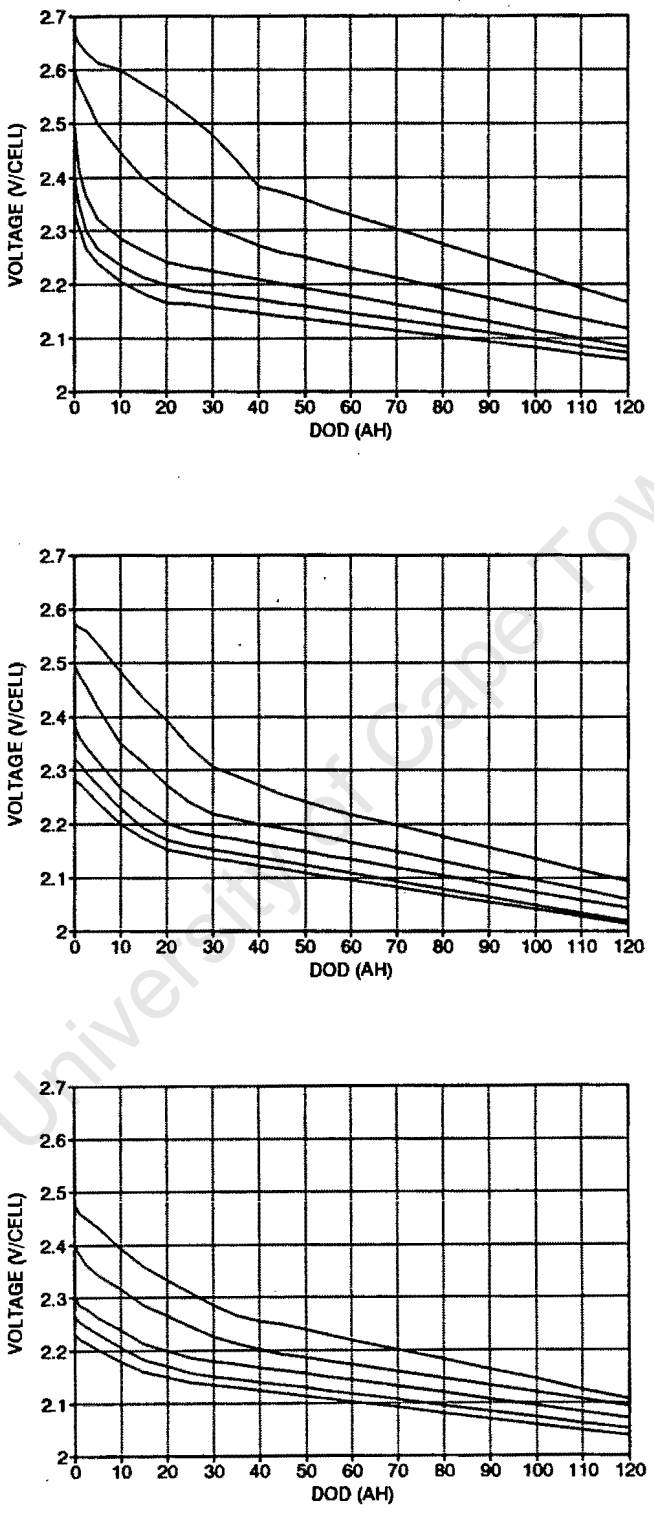

Figure 7.22 Compensated charging curves at a) 0°C, b) 18°C and c) 35°C; charging rates used were 16A, 8.8A, 3.2A, 1.5A, and 0.7A.

c) Cycling tests

Cycling tests selection

The RMT108 battery is designed for deep cycle applications. However, the tall flooded electrolyte cell it is particularly susceptible to electrolyte stratification. As stratification is enhanced during partial state-of-charge operation, a deep cycle partial SOC cycling test is relevant. A deep cycle full SOC cycling test is required to determine the overcharge cycle to eliminate stratification, and to determine the effect on cycle efficiency. A shallow cycle full SOC test is useful for determining the minimum charge voltage during shallow cycling, since unnecessary gassing is to be avoided in antimony grid cells. Details of the tests are described in Section 6.2.7.

Deep cycle partial SOC test

The battery was repeatedly cycled between 15% and 55% DOD at charge and discharge rates of C8 (15A), which is the recommended starting charge rate for the cell. No overcharge allowance was made for the partial SOC tests.

Figure 7.23(a) shows the end-of-charge and end-of-discharge voltages as the test proceded. The steady decline in the end-of-discharge voltages indicates a decrease in available cell capacity. This phenomena is due partially to gassing losses (±0.25Ah/cycle or 7.5Ah over the whole test). However, the drop in end-of-discharge voltage from 1.93V/cell to 1.8V/cell is equivalent to a gassing loss (accumulated undercharge) of 50Ah, which cannot be entirely explained by inefficiencies as the variation in charging curves from cycle to cycle are remarkably consistent. The steeper slope of the end-of-test discharge curve (Figure 7.23(b)) suggests that the only logical explanation is a change in dynamic operation brought about by electrolyte stratification and negative grid sulphation, which is particularly clearly illustrated.

The short term effect of these physical phenomena on battery performance is shown in Figure 7.23(c) by the steady drop in the Wh output and Wh cycle efficiency. This efficiency would reach an unspecified lower limit. The long term

effects of stratification would be seriously damaging. Gassing or equalisation charging is the best remedy for removing stratification. Prolonged equalisation may be required to reverse hard lead sulphate on the negative electrode. The gassing rate of about 0.25Ah per cycle is unquestionably insufficient in this partial SOC cycling regime.

The overcharge and equalisation charges to eliminate this stratification and sulphation were determined by measuring the Ah input during equalisation charge. At the maximum gassing current of 3A, 60Ah of overcharge is required. At a higher gassing current, say 7.5A (recommended after deep cycle), fewer Ah would be required as mixing would be more effective, though the high end-of-charge voltage would promote grid corrosion.

The total Wh efficiency of the cycle test, including the equalisation charge to return to the defined state, was 78%.

Deep cycle full SOC test

The battery was repeatedly cycled between full charge and 45% DOD. The discharge rate was C8 (15A). The battery was recharged at 2.4V/cell, with a current limit of 15A. A high overcharge limit of 15% (6.75Ah/cycle) was chosen to facilitate good electrolyte mixing.

Figure 7.24(a) shows the end-of-charge current and end-of-discharge voltages. The slight decline in the end-of-charge current is probably due to good electrolyte mixing and reduced resistance as the test proceded.

The watt-hour efficiency for cycling is stable at 75.7% and indicates a dynamic equilibrium; the gassing is at least sufficient to prevent stratification. If the cell was regularly overcharged then the OC could be reduced below 15% accordingly. The Ah efficiency is 87%. (See Figure 7.24(b).)

The Wh efficiency calculated from the charging curves is 74.2%. The end-of-charge current and voltage of 3.3A at 2.4V indicates that the battery is fully charged at the end of each cycle.

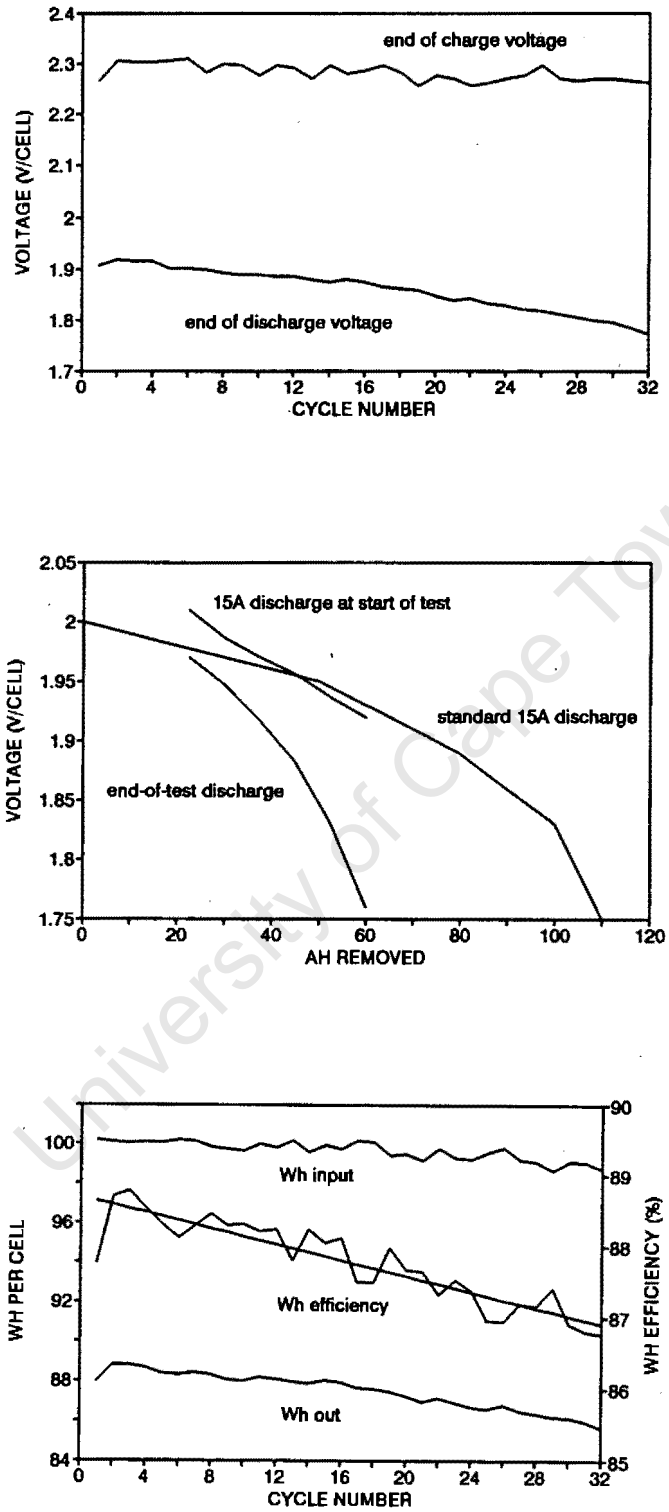

Figure 7.23 Deep cycle partial SOC test. a) end-of-cycle conditions, b) change of discharge profile with cycling, c) Wh efficiencies.

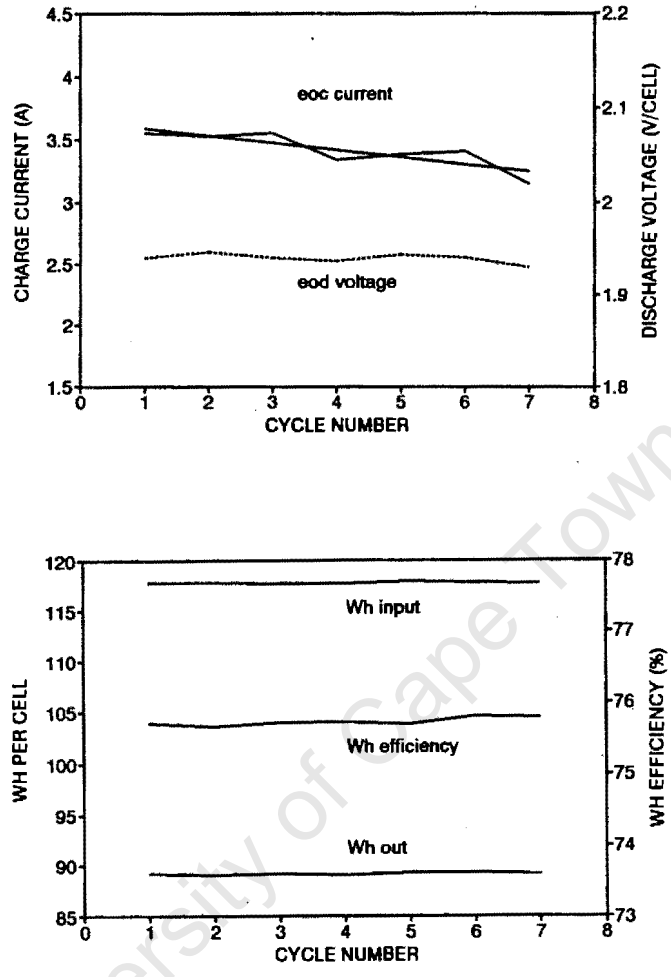

Figure 7.24 Deep cycle full SOC test. a) end-of-cycle conditions, b) Wh efficiencies.

Shallow cycle full SOC Test

The battery was cycled between 100 and 90% SOC at discharge current of C10, and charge voltage of 2.3V/cell, with a limiting current of C10 (10.8A). Overcharge was limited to 10%, and the time for charging limited to two hours.

The end-of-charge current and end-of-discharge voltage are shown in Figure 7.25(a). The maximum calculated gassing current is 1A at 2.3V.

The watt-hour efficiency is stable at 82.7% at the chosen currents (Figure 7.25(b)). The efficiency from charging curves is estimated at 81%. The overcharge of 1Ah per cycle is easily sufficient to prevent stratification during shallow cycling. The problem is that the battery is never fully charged, and reaches a maximum of about 96% SOC. The long term effects of this will be permanent loss of capacity in this uncharged 4% of the active material, followed by further capacity losses in a similar manner. During shallow cycling to full charge most cells operate at low efficiency, particularly the lead-antimony type. The Wh efficiency to completely recharge the cell at 2.3V each cycle will be about 65% (calculated from the charging curves).

Capacity at end of cycle tests

The cell was equalised and the capacity determined at the C10 rate to be 141Ah, indicating no significant capacity loss during the test. This showed that the stratification and sulphation losses were totally reversible. The theoretical capacity loss for the test cycles based on cycle life curves is also negligible.

H20 Consumption

During the cycling tests the accumulated overcharge was approximately 157Ah, which would account for a theoretical water loss of 52.7ml (theoretically 0.366ml H2O/Ah). Water consumption was measured over the duration of the cycling tests. On average 50ml/cell was lost by gassing and evaporation, indicating a 5% gas recombination efficiency. This is consistent with practical experience for vented cells. At no time did electrolyte splash or seep from these vent caps.

The volume of water contained between the maximum and minimum electrolyte levels is 304ml. If the daily overcharge is 10Ah (sufficient to prevent stratification, little enough not to promote corrosion), then the time between refilling is about 87 days. There is a further safety margin of 200ml before the plates are exposed. The time will be dependent on several external factors such as temperature and humidity.

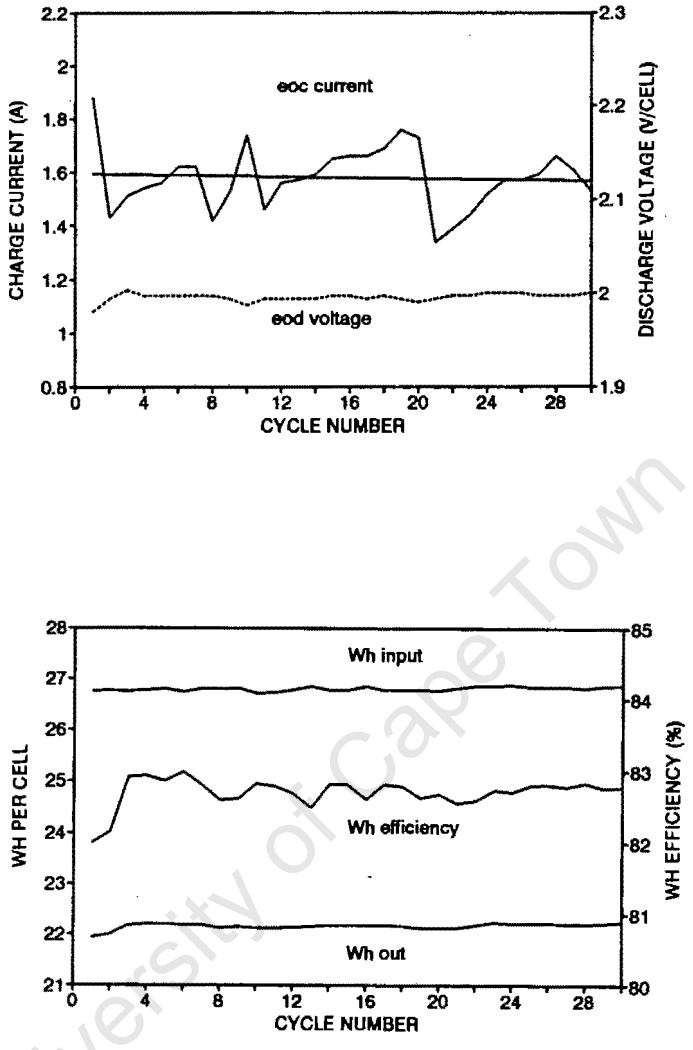

Figure 7.25 Shallow cycle full SOC test. a) end-of-cycle conditions, b) Wh efficiencies.

Charging current and voltage requirements

It is extremely difficult to determine exact overcharge requirements for the battery. OC depends on charge rate, as each charge rate has its own linked efficiency, as well as efficiency linked to starting DOD; OC to overcome stratification is a further complication. There may be some overlap. For the RMT108 there are two points on the curve that can be used with confidence (see Figure 7.26).

For full cycling to 45% DOD and charging at 15A and 2.4V, 6.75Ah of overcharge is sufficient to overcome both charging inefficiencies and stratification. For shallow cycling to 10% DOD and charging at 10A and 2.3V, 1Ah of overcharge is enough to prevent stratification but insufficient to overcome charging inefficiencies. Both criteria should be met if possible. Ignoring for a moment the stratification problem, if the battery in a PV application is to be cycled and recharged on a daily basis, then the average OC required for 10% DOD, 2.3V charge is 4Ah or 40% OC. For 45% DOD, 2.4V the OC is 6.5Ah or 14%, and for 80% DOD, 2.5V, the OC is 8.5Ah or 10%. The correct overcharge will meet both the overcharge inefficiency and stratification requirements.

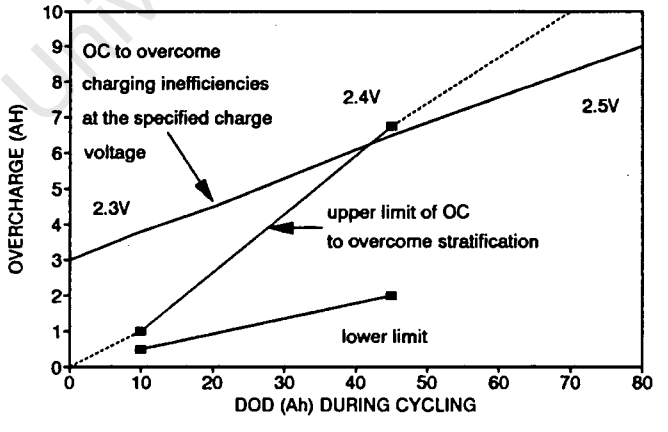

Figure 7.26 Overcharge requirements to overcome charging inefficiencies and to prevent stratification during cyclic operation.

7.2.5 Sizing and Selection:considerations in PV applications

1) Optimise battery life by choosing a suitable daily DOD.
2) Avoid or minimise electrolyte stratification by ensuring that both charging and stratification prevention criteria are met. Equalising charge is required approximately once a month, not more frequently, certainly no less.
3) Ensure suitable charging currents from the PV array. Low average currents will be insufficient to meet the charging needs.
4) Allow up to $C_{10}/10$ Ah overcharge per deep cycle, though this will make cycling less efficient.
5) The charge regulator setting is critical in controlling gassing. Excess gassing will be damaging, but less so than for SLI type cells.
6) Take special care in regulator type selection, and consider temperature compensation of voltage regulator in extreme climates.
7) Calculate the maintenance period based on projected gassing and H_2O consumption.

It is important to treat a long life battery moderately. If all these factors are taken into account, the battery could provide 4000 cycles at 40% DOD, or last 10 years.

7.3 WILLARD VANTAGE LS90 UPS BATTERY

7.3.1 General Information

Data Summary

Capacity:	C_{20} = 90Ah @ 20°C
Voltage:	12V
Application:	UPS/float charge applications
Group:	flat plate, antimony positive, calcium negative, flooded
Description:	Flat plate 12V power pack. Vented with flooded electrolyte, in black casing. Essentially a modified SLI design, with thicker plates. Antimony positive, lead-calcium negative.

See Appendix D3 for manufacturer's data sheet.

Costing

Cost:	R364 per battery (@ 23/10/1990)
Wh cost:	R0.34/Wh
Wh value:	R5.62/kWh over battery life, assuming 300 cycles at 20% DOD, the optimum DOD. (See Section 7.3.3.)

7.3.2 Physical

Physical construction

Dimensions:	height, width, length:	220 x 172 x 342mm
	height over terminal:	235mm
	mass:	25.6kg
Plates:	design:	15 flat plates/cell
		7 positives, 8 negatives
	positive plate weight:	97g
	negative plate weight:	94g
	active block mass:	2.768kg/cell
Grid:	positive:	1.6% Sb
	negative grid	lead-calcium
	grid mass:	1.107kg/cell
		(40% of active block mass assumed)
Dry mass:	17.7kg	
Electrolyte:	SG:	1.260 @ 20oC
	volume:	5.9l
	mass:	7.43kg
Wet mass:	25.6kg	
Gas venting:	No vent caps, but single sintered glass gas escape. As far as the user is concerned, the battery is MF.	
Casing:	black plastic	
Terminals:	M6 316 stainless stud type. Washers and nuts are provided.	

Active mass utilisation coefficients

(Calculated)

	Active mass	Electrolyte	SG @ end of test
capacity @ 100% utilisation	152Ah	121Ah	1.000
utilisation @ nominal capacity (90Ah)	59%	74%	1.055
utilisation @ 100 hr rate (98Ah)[7]	65%	80%	1.04
utilisation @ opt. DOD (18Ah @ 20% DOD)[8]	12%	15%	1.25

Under normal operation (shallow cycling), the SG of the electrolyte is not limiting.

7.3.3 Basic Operating Data Available

Charging requirements and limits

The LS90 battery is normally operated in a very mild float charge mode. The recommended voltage is 13.6V (2.226V/cell) at 20°C. Because antimony and calcium grids are used, it is optimal to minimise overcharge to prevent contamination of the negative by antimony transfer through gassing.

7 See discharge data in SECTION 7.3.4(a).

8 See life cycle data in SECTION 7.1.3

Discharge curves

Complete discharge curves at 20°C are available ranging from 10 minute to 50 hour rates.

Life cycle data

No life cycle data is available. The manufacturer suggested that possibly 100 cycles @ 80% DOD and 200-300 cycles at 20% DOD would be attainable under normal operating conditions, but emphasised that the LS90 is not a cycling battery, and would be optimal under float charge polarisation. The low cycle life expectation is a reflection of the high active mass utilisation coefficients and presence of a conventional calcium grid negative electrode. The optimum battery utilisation for the estimated figures occurs in the DOD range greater than 40% (see Figure 7.27), which conflicts with the assertion that the battery is not a cycling battery. The tests confirm that the battery life during partial SOC cycling is lower than projected. (See Section 7.3.4(c).)

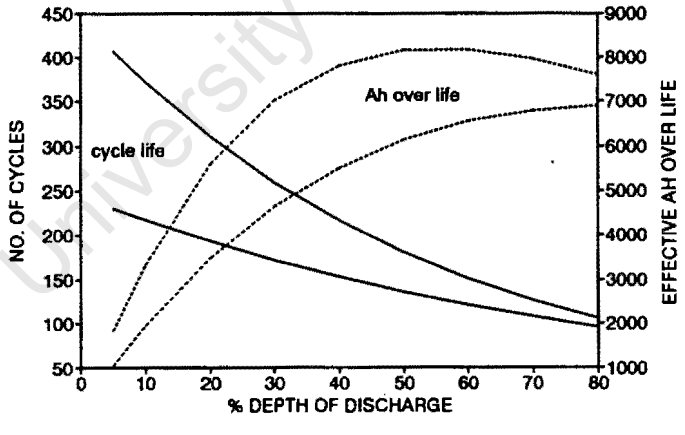

Figure 7.27 Estimated cycle life curve for Willard LS90.

Extent of data from manufacturer

Data Quality:
The only data provided is the discharge and capacity data, which is Grade A2 (performed by the manufacturer in-house on the specific battery).

Data as purchased:

- Nominal capacity and discharge curves printed on battery casing.

Additional data on request by personal communication:

- Plate masses, (dry and wet), overall masses and dimensions,
- Life cycle data: estimated at 100 cycles @80% DOD, 200-300 cycles @20% DOD: (Grade C).

See Appendix D3 for manufacturer's data sheet.

7.3.4 Test Results and Discussion

a) Capacity and discharge tests

Only one discharge test was performed because:

- the battery is expected to lose capacity rapidly when repeatedly deep discharged, invalidating the results of further tests,
- the capacity is expected to change rapidly with age,
- discharge curves for a new LS90 are available and can simply be verified,
- the design and structure of the active mass is similar to the WILLARD 774, which has been completely tested.
- the battery will normally operate in the shallow discharge zone only, and capacity limitations will not be encountered.

A new LS90 was equalised and stabilised at 18°C, then discharged to a cut-off of 10.8V at 10A. The discharge curve agreed exactly with manufacturers data. Further, the WILLARD LS90 manufacturer's discharge curves were found to be identical to WILLARD 774 discharge curves, which is not surprising as the active block design is almost identical. The curves were accepted as valid for a new battery. (See Figure 7.28.)

Two further LS90's were equalised and stabilised at 0°C and 35°C, and also discharged at 10A to a 10.8V cut-off to determine the effect of temperature on capacity. The measured capacities (62Ah and 85Ah respectively) represent a

change of ±0.66% per °C, and coincide approximately with the sensitivity projected from the WILLARD 774 data.

There is generally no need for cut-off voltage curves for shallow cycle batteries, but load shed settings at shallow DOD are strongly current dependent and load shedding is this region is unlikely to be accurate (see Section 3.13).

Figure 7.29 shows electrolyte SG vs Ah removed, and the electrolyte freezing temperature. Electrolyte freezing may occur if the cell is deep discharged. Freezing point at 20% DOD vs C100 is -5°C.

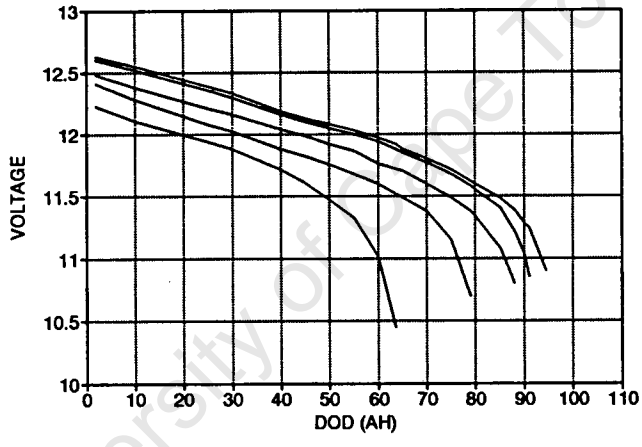

Figure 7.28 Discharge curves at 18°C at 1A, 2A, 5A, 10A and 20A.

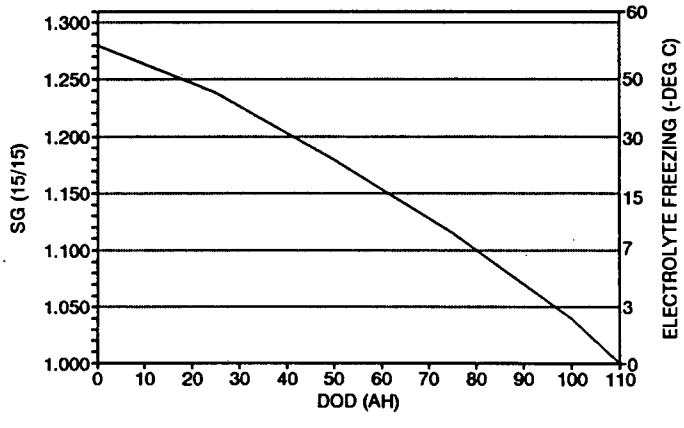

Figure 7.29 Electrolyte SG and freezing point vs DOD.

b) Charging tests

Charging tests were conducted as described in Section 6.2.5. Charging rates used were 10A, 5A, 2A, 1A, and 0.5A. The temperature compensated charge voltage limits used were 14.8, 14.5 and 14.2 volts at 0°C, 18°C and 35°C respectively. In each case charging was started from 50% DOD.

The quasi-constant current charging curve at 18°C is shown in Figure 7.30. The curve shows that a minimum of 1Ah of overcharge is required to reach full charge at 18°C and 14.4V, regardless of the initial DOD. At the recommended float voltage of 13.6V, the battery accepts virtually no charge.

Charging efficiency was determined by the method in Section 6.2.6(vi). The end-of-charge current is assumed to be equal to the gassing current.

The charging efficiency was verified by a second method based on measuring the rate of gassing, assuming a gas composition based on literature, and calculating the current required to produce the gas flow rate (for method see Section 6.2.6(iv)). This necessitated the removal of a plastic cover of the battery to expose the sintered glass vent plugs. No gassing occurred till 14.0V at 100% SOC. This approach shows good agreement with the first method. The main difference is probably due to the non-stoichiometric gas ratio that occurs in reality. The gassing curves are shown in Figure 7.31.

The charging curves after compensation for gassing and overcharge losses are shown in Figure 7.32.

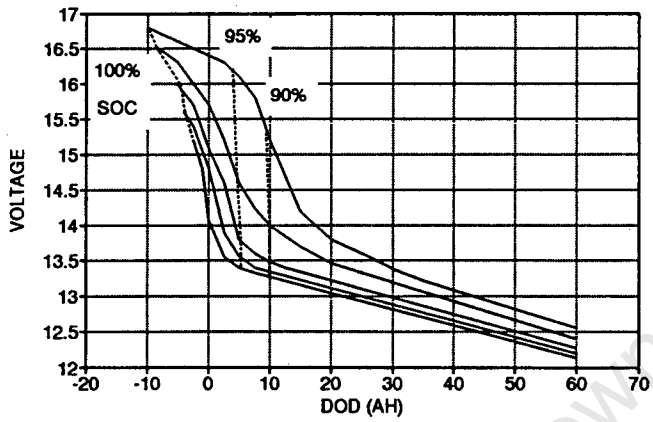

Figure 7.30 Quasi-constant current charging curve at 18°C. Charging rates used were 10A, 5A, 2A, 1A, and 0.5A.

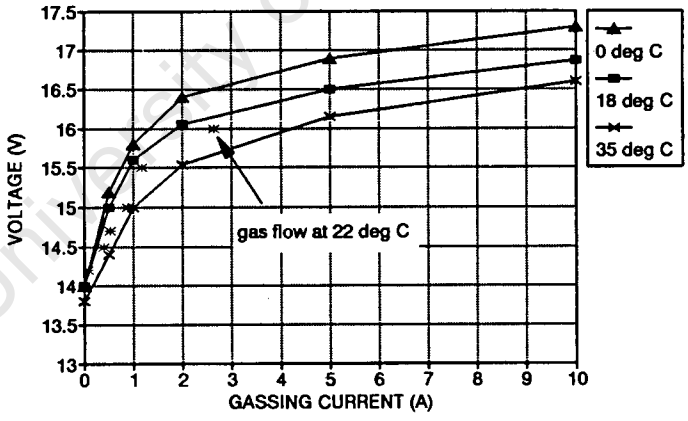

Figure 7.31 Gassing current as function of voltage and temperature. Gassing current determined by gas flow determination is shown superimposed.

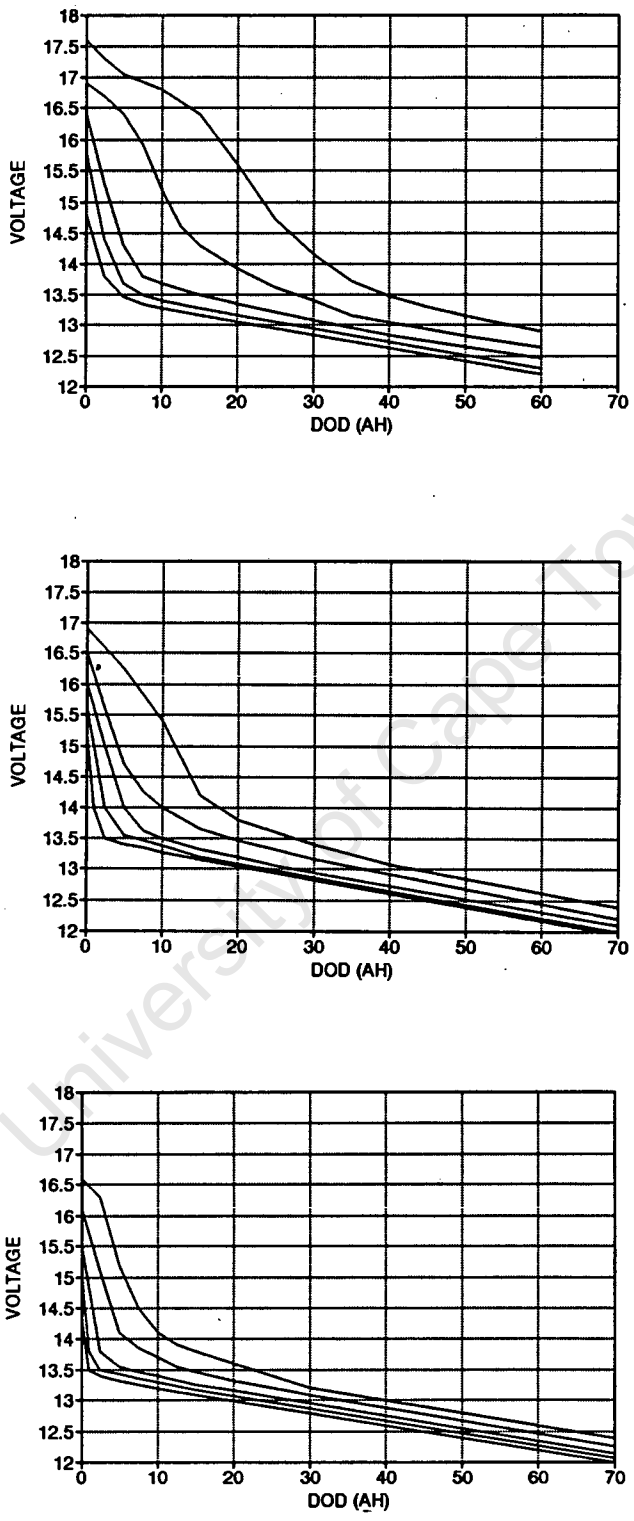

Figure 7.32 Compensated charging curves at a) 0°C, b) 18°C, c) 35°C. Charging rates used were 10A, 5A, 2A, 1A, and 0.5A.

c) Cycling tests

Cycling tests selection

The LS90 battery is designed primarily for un-interruptible power supply (UPS) applications, where it will normally be subjected to prolonged float charge polarisation. Deep cycling would be infrequent. This type of operating regime is unlikely in PV applications. It would be possible if the battery bank were sufficiently large to restrict cycling to shallow DOD. Either way, only shallow cycling is relevant. A shallow cycle full SOC test is useful for determining the minimum charge voltage during shallow cycling, particularly since unnecessary gassing is to be avoided. As mentioned, in many PV applications the system size (energy capacity) is adjusted by increasing the installed battery capacity using low cost batteries while maintaining the panel area. This may result in shallow cycling at partial SOC (see Chapter 2), so a partial SOC shallow cycle test is useful. The cycling tests are described in Section 6.2.7. All cycling tests were conducted at 20°C.

Shallow cycle full SOC test

The battery was repeatedly cycled between a fully charged state and 10% DOD. The discharge rate was C10 (9A). The battery was recharged at 2.30V/cell, with a current limit of C10, and an overcharge limit of 10% (1Ah/cycle) for a maximum of 2 hours per cycle.

Figure 7.33(a) shows the sharply decreasing end-of-charge current and end-of-discharge voltages. The decline in both current and voltage would normally signify the onset of electrolyte stratification. Figure 7.33(b) shows that the amount of charge that can be delivered at 2.3V in 2 hours is limited. Only after the battery has adjusted to an equilibrium SOC can sufficient charge be delivered. From this time continued stratification from undercharging is limited. The efficient self-regulating or current tapering by the battery during constant voltage charging is characteristic of the gassing curve, which is dependant on the high polarisation potential of the lead-calcium negative electrode. (Compare gassing curve with the WILLARD 774).

If the battery is operated in float charge mode, then stratification is minimal, and the regulating effect will limit gassing. If the battery is cycled, then the self-regulating effect may limit gassing and charging rates so that either the cell cannot be fully charged in the limited time available, or the lack of gassing results in extreme and prolonged stratification setting in. Raising the charging voltage will help in the short term, but in the long term the self-regulating effect will be removed (by antimony transfer to the negative through gassing and reduction in H_2 polarisation potential), and the benefits of self-regulation destroyed.

The watt-hour efficiency for this controlled cycling stablilised at 86% and indicated a state of dynamic equilibrium. (See Figure 7.33(c).) The Ah efficiency is 86%.

Shallow cycle partial SOC test

The battery was repeatedly cycled between 10% and 20% DOD at charge and discharge rates of C10 (9A).

Figure 7.34(a) shows the end-of-charge and end-of-discharge voltages as the test proceded. The slight decline in the end-of-discharge voltages indicates a decrease in cell capacity, and together with the marked increase in end-of-charge voltage shows the increase of cell internal resistance.

The change in charging curve cycle during the test is illustrated in Figure 7.34(b). The rapid increase in the end-of-charge voltage is probably due to a combination of electrolyte stratification and hard sulphation of the calcium alloy negative grid, leading to higher internal resistances. The theory has shown that calcium alloy grids perform poorly under cycling polarisation, while the antimony positive is unlikely to be seriously affected in the long term.

The short term effect of stratification on battery performance is shown in Figure 7.34(c) by the steady drop in the Wh cycle efficiency. This efficiency seems to have reached a lower limit around 89.5%. However, the continued increase in end-of-charge voltage indicates that no real equilibrium has been reached, and further stratification and sulphation is likely.

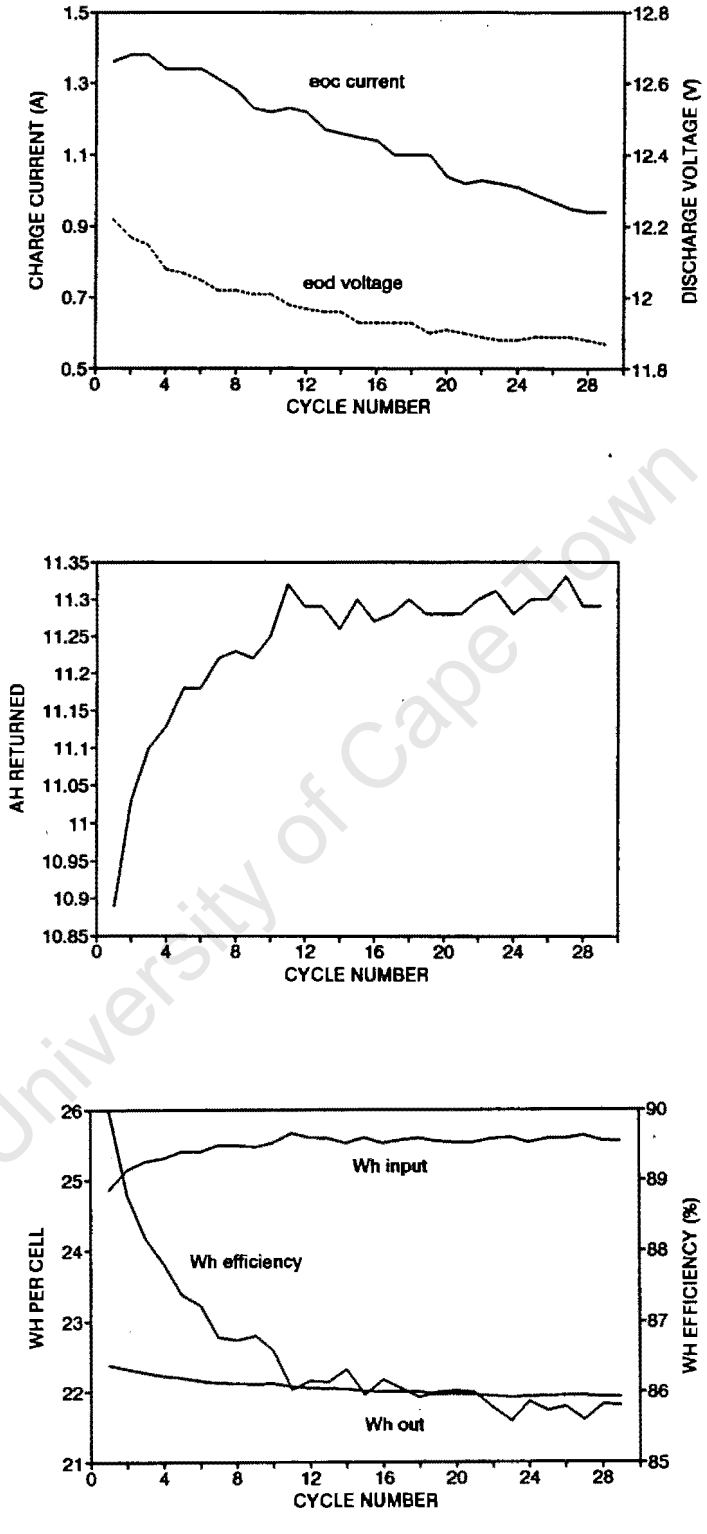

Figure 7.33 Shallow cycle full SOC test. a) end-of-cycle conditions, b) Ah returned, c) Wh cycle efficiencies.

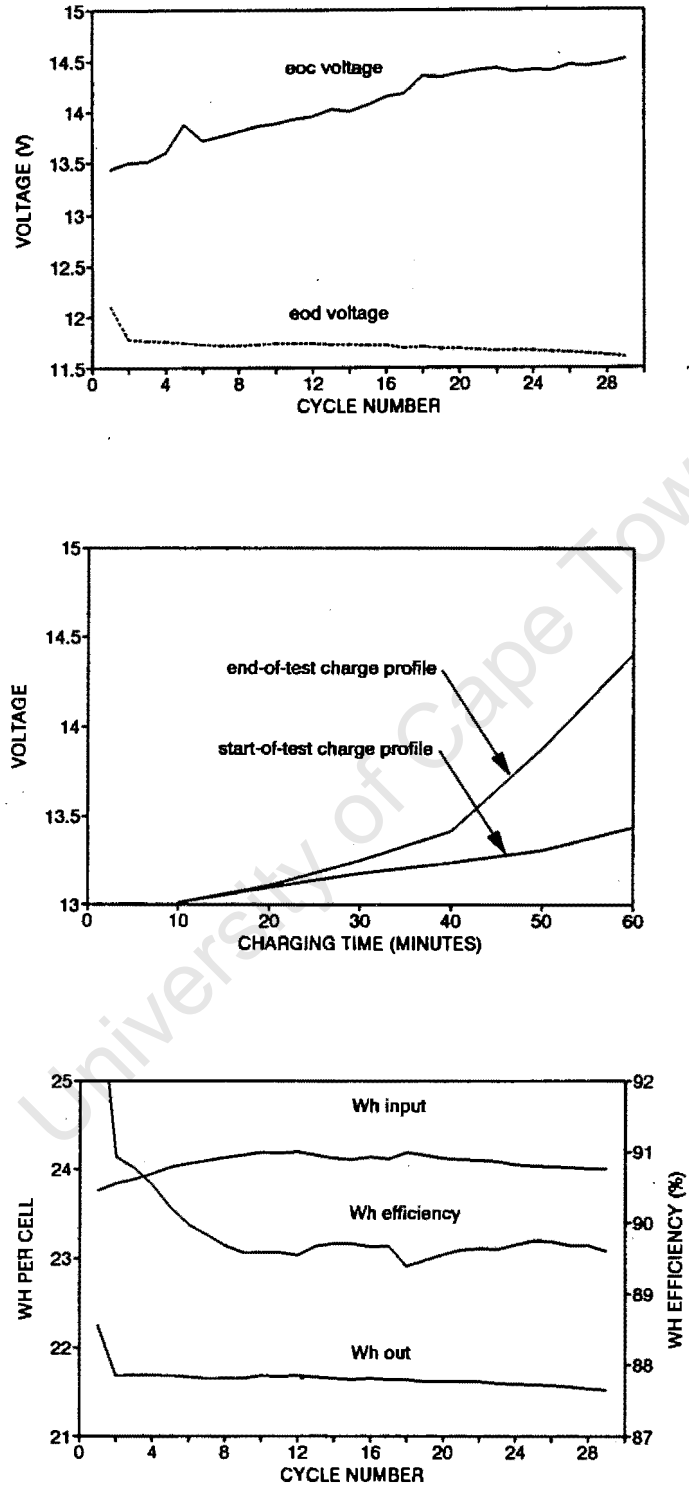

Figure 7.34 Shallow cycle partial SOC test a) end-of-cycle conditions, b) variation in charging profile, c) Wh efficiencies.

Capacity at end of cycle tests

The cell capacity at the end of the partial SOC test was 27Ah to 10.5V. After boost charging and equalisation at 14.2V (2.37V/cell) the capacity was determined at the C10 rate to be 38Ah, and after further boosting at 15.0V (2.5V/cell) the capacity was 50Ah. The temporary loss in capacity due to stratification and positive grid sulphation is therefore 23Ah during the partial SOC test.

The useful cell capacity after recovery was only 50Ah compared with 82Ah at the start. The permanent loss due to hard sulphation of the negative was 32Ah, representing a 39% loss. The cell seems to have passed its useful life after only 29 full shallow cycles and 29 partial cycles.

A new LS90 was equalised, tested and subjected to the same shallow cycle partial SOC test to determine the validity of the first test. The initial capacity was 81.48Ah (10A, 18°C). After 30 cycles and a boost charge at 2.5V/cell the available capacity was 70.47Ah, representing a permanent capacity loss of 17%.

The incremental wear according to battery models based on the manufacturer's lifecycle estimates (see Section 3.12) is:

for the first battery:

29 cycles @ 10% DOD (400 cycles expected over battery life)
29 cycles between 10% and 20% DOD (300 life cycles expected)

=

29/400 + 29/300 = .169 or 16.9%

and for the second battery:

29 cycles between 10% and 20% DOD (300 life cycles expected)

=

29/300 = .0.966 or 9.7%

Finally, a third new battery was tested under shallow cycle full SOC regime for 35 cycles, and the partial SOC regime was studiously avoided. The capacity at

the end of the test was 79Ah (10A, 18°C). As there was no capacity determination prior to cycling the drop in capacity cannot be accurately calculated. Based on the initial capacities of the first two batteries the cell seemed to have retained about 96% of its initial capacity.

These batteries have a negative electrode that is limiting to cycle life (see Section 3.6.3), and that life depends strongly on charging regimes and DOD. Partial SOC is particularly damaging, as the difference in retained capacity between batteries two and three shows. The cell was not tested in float mode, where it would possibly (and probably) have lasted longer than most deep cycle batteries. Therefore for float application this cell could possibly be considered.

H20 Consumption

The accumulated overcharge during the cycling tests was minimal. Water consumption could not easily be measured because of the sealed nature of the batteries. It can be deduced from the gassing curves that under continuous float charge (13.6-14.0V at 20°C) water consumption should be negligible, and the sealed battery should never suffer from plate exposure.

If strong gassing takes place the gassing current will increase in the long term, and water loss may be sufficient to cause problems.

Charging current and voltage requirements

Optimal operation for the Willard LS90 is clearly in a float charge regime. The charging voltage should provide sufficient gassing the prevent electrolyte stratification. The manufacturers recommends 13.6V (2.27V/cell) regardless of temperature, yet the gassing curves would suggest about 14.3V at 18°C, to provide 0.25A of gassing to prevent stratification. Electrolyte loss at 14.3V would be minimal.

7.3.5 Sizing and Selection: considerations in PV applications

1) Optimise battery life by choosing shallow cycle operation.
2) Avoid deep discharges, and any partial SOC operation at all. Partial SOC operation will result in rapid battery failure.
3) Use system sizing rather than relying on load-shed regulators to limit cycling to 20%. The regulator's ability to regulate accurately at this DOD on the shallow slope of discharge curves depends on a good knowledge of the average and peak load currents. Accurate load shedding in this region is doubtful.
4) Minimise sulphation of the negative electrode and electrolyte stratification by ensuring mild float charge operation for most of the charging cycle. The battery cannot easily recover form short term stratification by gassing as gassing is very low at the recommended charge voltage. Prolonged float charge gassing is a feasible alternative.
5) Stay within the recommended charge voltages, as excess gassing could, in the long term, cause a runaway situation by lowering the gassing voltages and result in the battery plate exposure. Although 13.6V is recommended by the manufacturer for UPS use, for PV applications 13.8V at 30°C and 14.2V at 15°C is recommended.
6) Consider self-regulation. The steep rise in the charging curve voltage at full charge has a current-limiting, self-regulating action. By the nature of these curves the LS90 may be suitable for a self-regulating PV system with matched panels and no charge regulator. However, caution is required to prevent excess gassing which would lead to plate exposure if the panels are not matched to the recommended charge voltage.

7.4 GNB 12V-5000 PHOTOVOLTAIC BATTERY

7.4.1 General Information

Data Summary

Capacity:	C_{24} = 93Ah, C_{100}=100Ah @ 20°C
Voltage:	12V
Application:	photovoltaic
Group:	flat plate, antimony alloy positive, treated calcium ternary negative, absorbed immobilised electrolyte, sealed
Description:	Flat plate 12V power pack. Sealed and pressurised operating on the closed O_2 recombination cycle. Absorbed electrolyte suspended in the separators, can operate in any orientation. Pressure relief by safety vent at 5PSI. Specialist PV design. Low antimony alloy positive, treated lead-calcium-tin negative. Maintenance free operation. In black polypropylene casing with orange cover.

See Appendix D4 for manufacturer's data sheet.

Costing

Cost:	R659 per battery (@ 23/10/1990)
Wh cost:	R0.59/Wh
Wh value:	R1.14/kWh over battery life, assuming 1300 cycles at 40% DOD, the optimum DOD. (See Section 7.4.3.) This can only be regarded as an estimate

7.4.2 Physical

Physical construction

Dimensions:	height, width, length:	216 x 173 x 324mm but can operate in any orientation.
	mass:	29kg
Plates:	design:	9 flat plates/cell 4 positives, 5 negatives
	positive plate weight:	NA
	negative plate weight:	NA
	active block mass:	NA
Grid:	positive:	low Sb alloy (unspecified %)
	negative grid	treated lead-calcium-tin
	grid mass:	not specified, but thickened grid used
Electrolyte:	NA, but estimated	SG = 1.260 @ 20oC volume = ±5.9l mass = ±7.43kg

absorbed in the pores of the active material, or in the fibreglass separator matrix (mean fibre diameter = 0.5 to 2.0 microns).

Gas venting: Six interconnected vent caps, for pressure control. Pressure relief at 5PSI, self resealing. Vent caps are not for user removal. Battery design is MF.

Casing: black plastic

Terminals: bolt type terminal, M6 316 stainless bolts and washers provided.

Active mass utilisation coefficients

(Calculated)

Accurate utilisation coefficients cannot be determined without figures for active masses. These figures are estimates, based on batteries of similar mass.

	Active mass	Electrolyte	SG @ end of test
capacity @ 100% utilisation	152Ah	NA	NA
utilisation @ nominal capacity (93Ah)	61%	NA	NA
utilisation @ 100 hr rate (100h)[9]	66%	NA	NA
utilisation @ opt. DOD (40Ah @ 40% DOD)[10]	26%	NA	NA

7.4.3 Basic Operating Data Available

Charging requirements and limits

Charging of sealed batteries is usually voltage limited, as this is the easiest way to control and prevent loss of water which cannot be replaced. Recommended charging voltages (specified at 25°C) are:

2.3V/cell for 0%-2% daily DOD
2.35V/cell for 0%-5% daily DOD
2.40V/cell for DOD above 5%.

Temperature compensation is -0.02V/cell per °C.

9 See discharge data in SECTION 7.4.4(a).

10 See life cycle data in SECTION 7.4.3.

Discharge curves

Complete discharge curves are not provided, however capacities to 1.75V/cell at 25°C are listed:

8hr	85Ah
24hr	93Ah
48hr	96Ah
100hr	100Ah

A temperature compensation curve is provided, showing 0.85% loss per °C below 25°C.

Life cycle data

A life cycle curve is provided, showing 500 cycles to 80% DOD and 1600 cycles to 30% DOD. Additional text claims at least 1200 cycles to 20% DOD. The optimum battery utilisation for the cycle life figures (based on the curve) occurs at 40% to 50% DOD. (See Figure 7.35.)

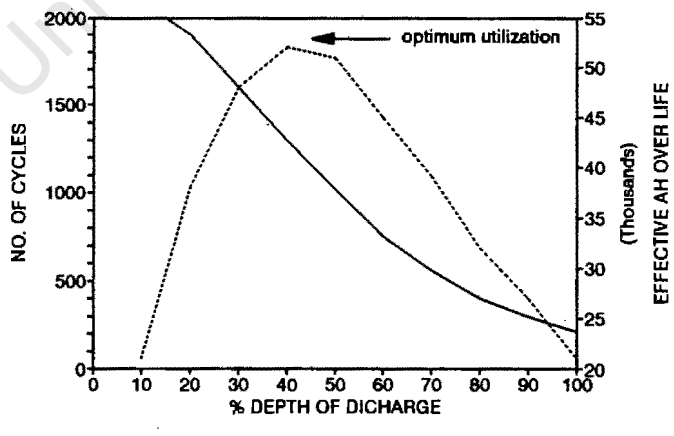

Figure 7.35 Manufacturer's life cycle curve for GNB 12V-5000.

Extent of manufacturer's data

Data Quality:
The data provided is probably Grade A2 (performed by the manufacturer in-house on the specific battery).

Data as purchased:

- Nominal capacity and capacities at various discharge rates.
- Temperature correction for capacity
- Recommended charging voltages
- Cycle life curve
- Self-discharge rate
- Safety valve relief pressure

Additional data on request by personal communication:

- Experimental and research papers from manufacturer's laboratory, though probably also available through open literature.

See Appendix E4 for manufacturer's data sheet.

7.4.4 Test Results and Discussion

a) Capacity and discharge tests

A new battery was equalised and stabilised at 18°C, then discharged at 10A to a cut-off of 10.6V to yield 74.8Ah. Conversion of this capacity to 25°C using the supplied capacity adjustment curve results in a capacity of 83.33Ah, or within 2% of the rated capacity which is 85.5Ah at 10A (to 10.5V). 10 Cycles of the battery using 40% DOD cycles and 2.40V/cell charging increased the capacity by a further 2% to within specification. The full capacity was considered available, and discharge tests performed at 18°C at 10A, 5A and 2A are shown in Figure 7.36.

The battery was again equalised and stabilised at 0°C, and discharged at 10A, 5A, 2A and 1A to a 10.8V cut-off to determine the effect of temperature on capacity. The discharge curves at 0°C are in Figure 7.37. The battery was also recharged

and discharged at 10A at 35°C. The measured capacity change averaged 1.67% per °C below 18°C and coincides with the expected sensitivity projected from the manufacturer's data. (See Figure 7.38.)

Figure 7.39 shows the relationship between capacity at 25°C and the discharge current, comparing manufacturer's data with temperature adjusted experimental data.

Figure 7.40 shows cut-off voltages suitable for load shed setting for deep discharge cycling.

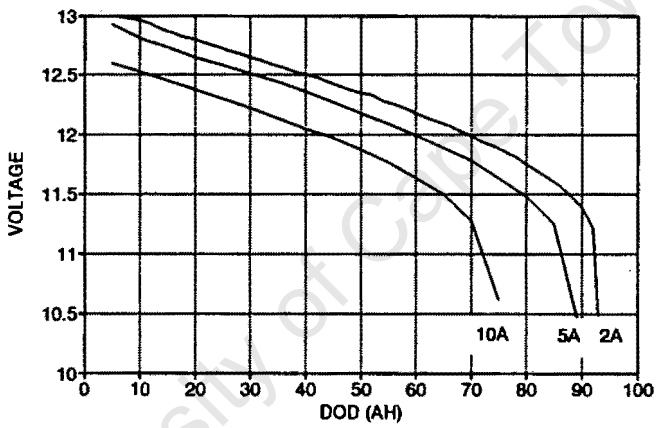

Figure 7.36 Discharge curves at 18°C.

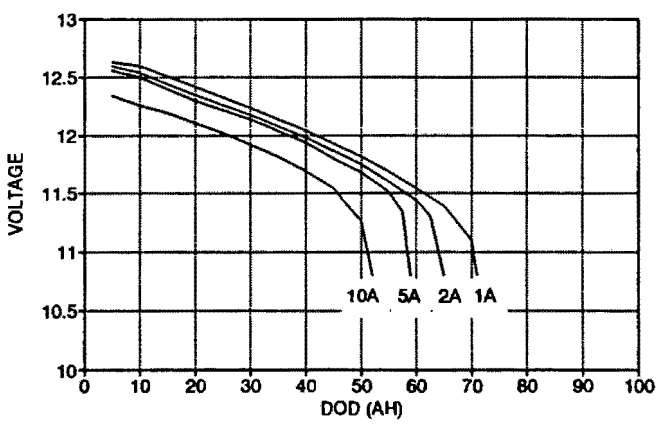

Figure 7.37 Discharge curves at 0°C.

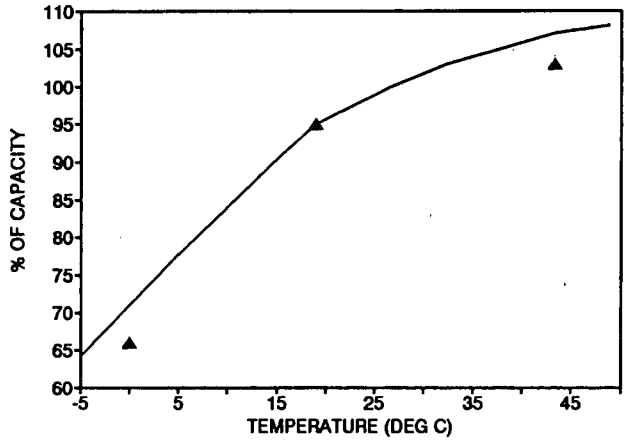

Figure 7.38 Retained capacity vs temperature. Triangles represent experimental data.

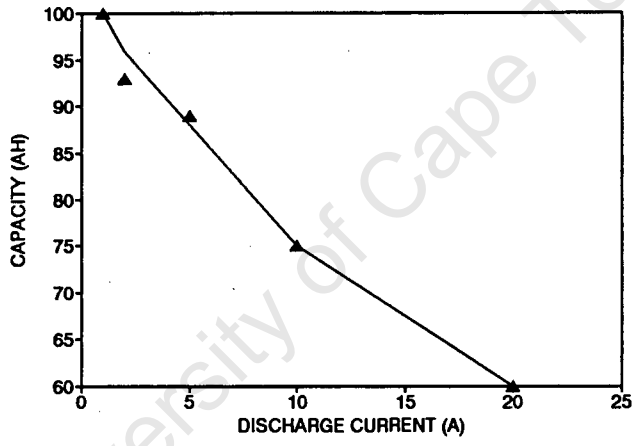

Figure 7.39 Capacity vs discharge current at 25°C. Triangles represent experimental data.

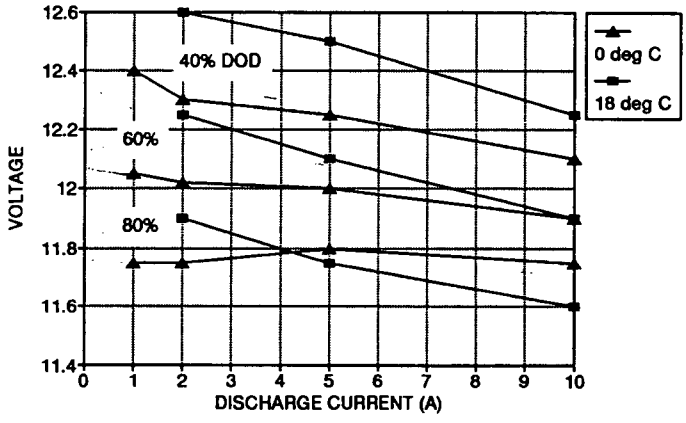

Figure 7.40 Cut-off voltages for regulator load shed settings.

b) Charging tests

Charging tests were conducted as described in Section 6.2.5. Charging rates used were 10A, 5A, 2A, 1A, and 0.5A. The temperature compensated charge voltage limits used were 15.0, 14.6 and 14.1 volts at 0°C, 18°C and 35°C respectively. In each case charging was started from 90% DOD.

The quasi-constant current charging curve at 18°C is shown in Figure 7.41. The curve shows that a maximum of 1Ah of overcharge is required to reach full charge at 18°C and 14.4V, regardless of the initial DOD. At the recommended float voltage of 13.6V, the battery accepts virtually no charge (self-regulation by current tapering).

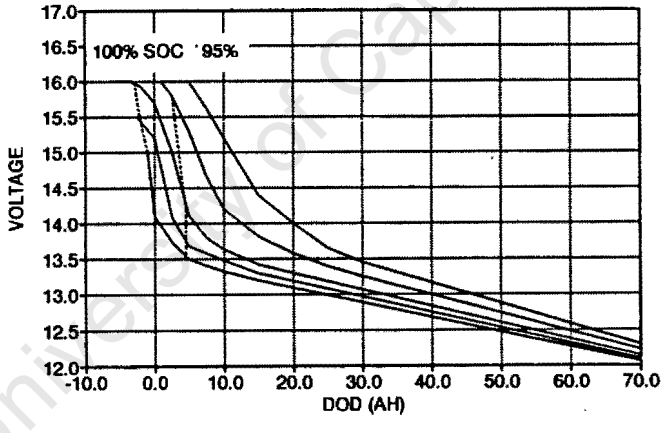

Figure 7.41 Quasi-constant current charging curve at 18°C. Charging rates used were 10A, 5A, 2A, 1A, and 0.5A.

Charging efficiency was determined by the method in Section 6.2.6(vi). The end-of-charge current is assumed to be equal to the gassing current. The curves are shown in Figure 7.42.

The charging efficiency was verified, and other useful data generated, by measuring the rate of gas recombination during and after gassing. The method is described in Section 6.2.6(v) and necessitated the installation of a pressure tapping in the casing. The volume of the headspace (0.00154m^3) was determined by compressing the gas in the headspace isothermally, measuring the volume

change and applying the ideal gas law. This volume is the headspace above all six cells. The fully charged cell was charged as described in the method at constant potentials 14.2V, 14.4V, 14.6V, 15.0V, 15.5V and 16.0V. The equilibrium cell pressures at these voltages are in Figure 7.43.

Some venting occurred at 3.8 PSI, at 16.0V (compared with specifications presenting a venting pressure of 5 PSI ±2PSI). Clearly this is the limiting voltage at 18°C.

The gassing curves determined by the two methods are in Figure 7.44, and there is good agreement. No gassing occurred till 14.0V at 100% SOC. Determination of the limiting charge voltage at different temperatures is difficult without experimentation, as the rate of O_2 recombination (which must be equal to the gassing rate at steady state) is temperature dependant in addition to temperature dependence of the rate of gas evolution. If the charging voltages are kept to the recommended values then there ought to be no gas venting.

The charging curves after compensation for gassing and overcharge losses are shown in Figure 7.45.

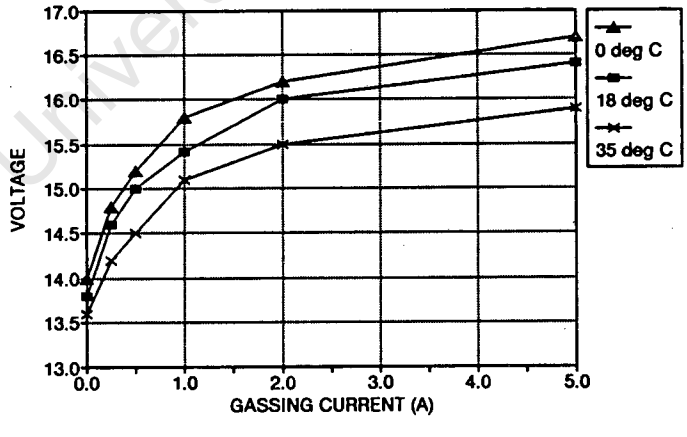

Figure 7.42 Gassing current as a function of cell voltage and temperature.

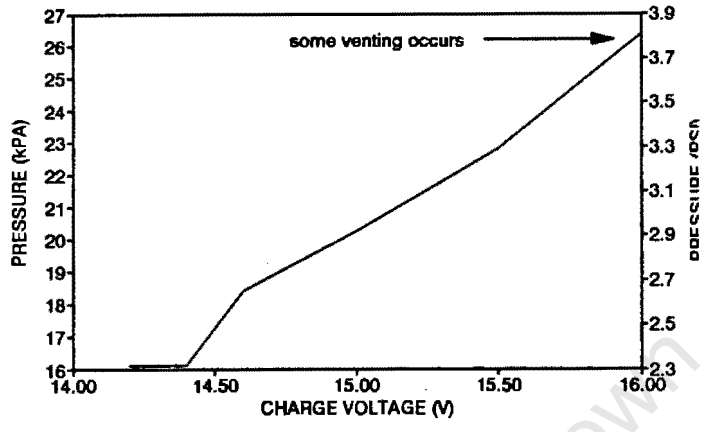

Figure 7.43 Steady-state cell pressure vs charging voltage.

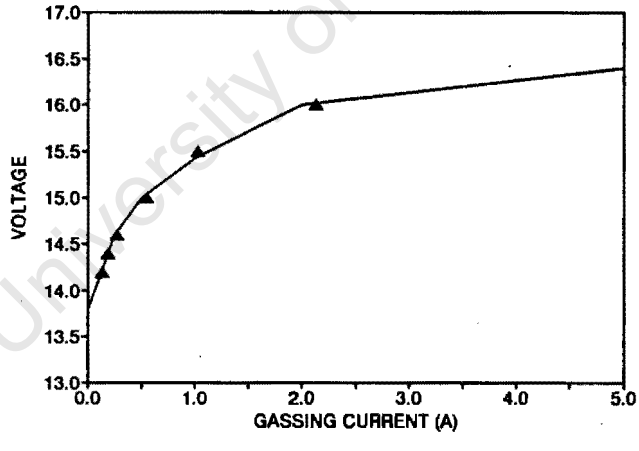

Figure 7.44 Gassing current as function of voltage and temperature. Triangles represent the gassing current determined by monitoring cell pressure change.

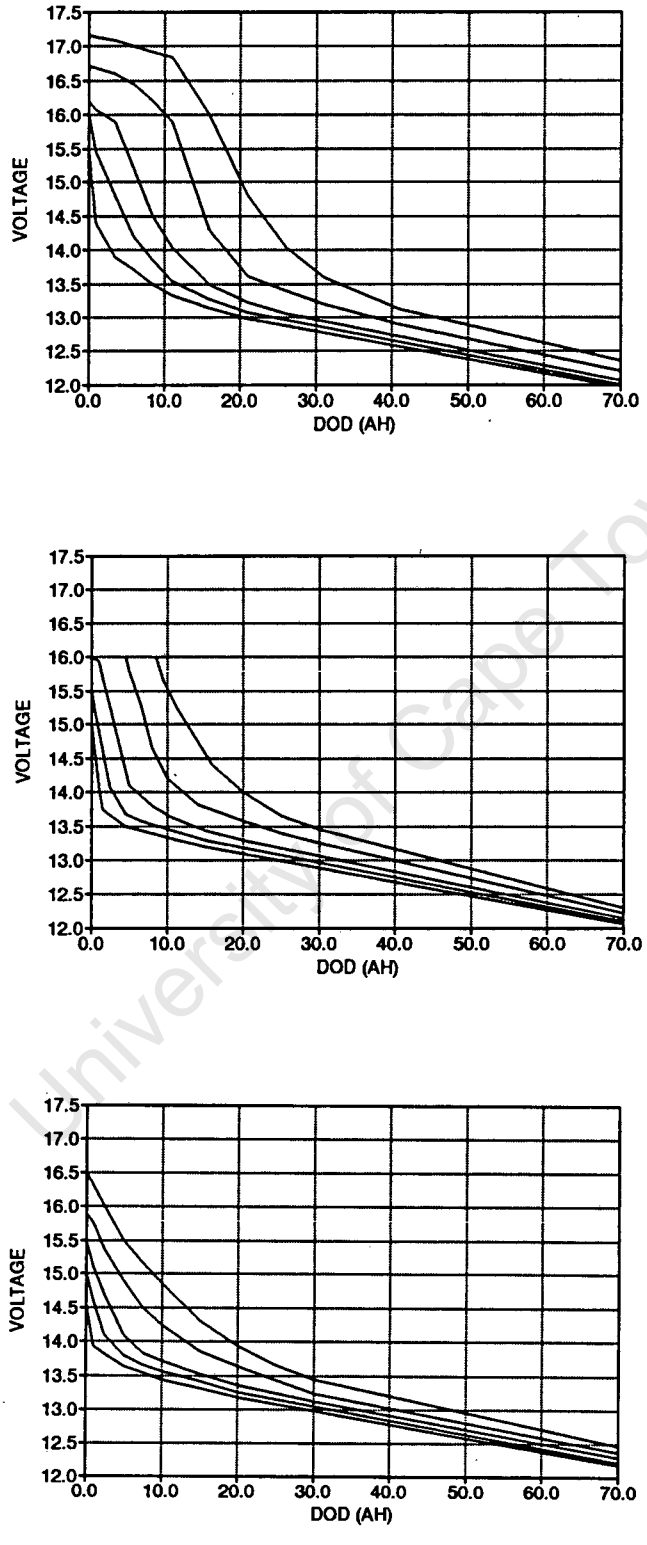

Figure 7.45 Compensated charging curves at a) 0°C, b) 18°C, c) 35°C. Charging rates used were 10A, 5A, 2A, 1A, and 0.5A.

c) Cycling tests

Cycling tests selection

The GNB 12-5000 is designed for deep cycling in PV applications. A deep cycle full SOC test is useful to determine overcharge requirements, and a shallow cycle partial SOC test to determine experimentally the effects of partial SOC operation in the absence of stratification. The cycling tests are described in Section 6.2.7. All cycling tests were conducted at 20°C. The 10A capacity before the tests was 75Ah.

Shallow cycle partial SOC test

The battery was repeatedly cycled between 10% and 20% DOD at charge and discharge rates of C10 (10A).

Figure 7.46(a) shows the end-of-charge and end-of-discharge voltages as the test commenced. The slight decline in the end-of-discharge voltage indicates a decrease in cell capacity, and has been identified by Szymborski (1982) as being due to sulphation of the negative electrode and the possibility of slight charge inefficiencies, and is typical of partial SOC operation in lead-acid batteries. The slight increase in end-of-charge voltage is attributed to the formation of hard lead sulphate which is difficult to charge, resulting in elevated end-of-charge potentials. Hard sulphation of positive plates is reversible while the negatives show a strong capacity loss.

The short term effect of sulphation on battery performance is shown in Figure 7.46(b) by the gradual and continuing drop in the Wh cycle efficiency, and further sulphation is likely. Long term undercharging will result in irreversible sulphation.

It is calculated from the charging curves that very little gassing occurs, so capacity losses are therefore not due to gassing losses. The available capacity after 28 cycles was determined to be 57Ah (10A, 18°C), representing a loss of 17Ah or 0.6Ah per cycle due only to the physical phenomena. Szymborski (1982) has

determined that the rate of decay of capacity is related more to the time spent in the discharged state than the cycling rate.

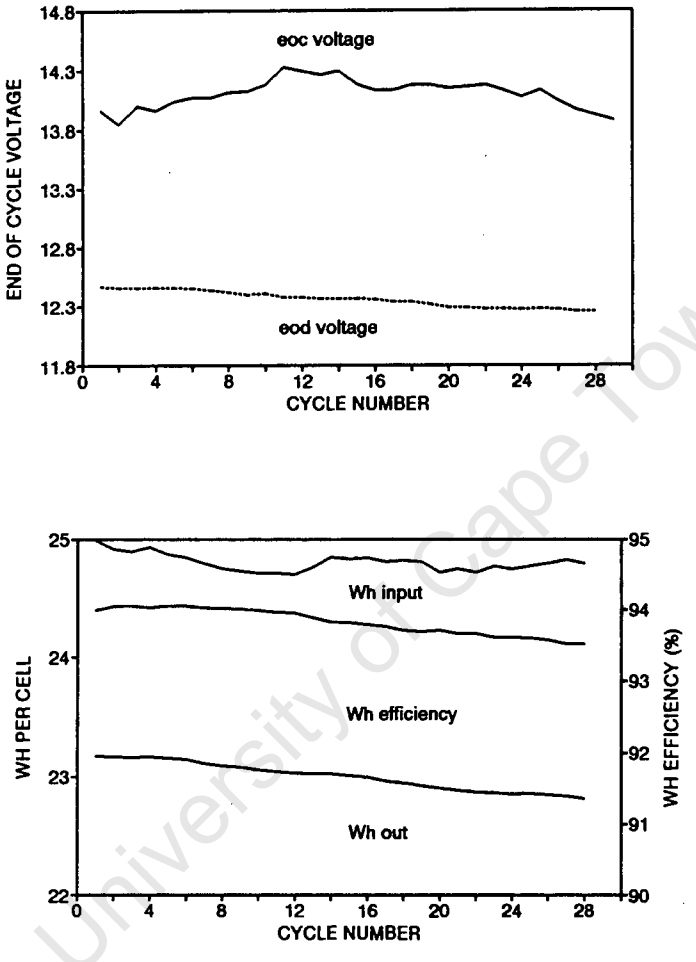

Figure 7.46 Shallow cycle partial SOC test. a) end-of-cycle conditions, b) Wh cycle efficiencies.

Deep cycle full SOC test

The battery was repeatedly cycled between a fully charged state and 45% DOD. The discharge rate was C10 (10A). The battery was recharged at 2.43V/cell, with a current limit of C10, and an overcharge limit of 15% (6.75Ah/cycle) for a maximum of 8 hours per cycle.

Figure 7.47(a) shows the steady end-of-charge current and end-of-discharge voltages as the test progressed. The end-of-charge current is very low, indicating a fully charged battery. During the charging cycles only 48Ah could be returned to the cell in the allowed time, ie only 3Ah of overcharge. This at first seems like too little overcharge for deep cycling, but confirmation can be obtained from the charging curve (Figure 7.41) which shows that at 2.43V/cell only 1Ah is required to overcome inefficiencies. 2Ah are therefore used in overcharge and equalisation. Examination of the charging profiles (Figure 7.47(b)) obtained from the first and last charge cycles shows absolute coincidence, and therefore no physical effects during the 10 cycles. The charging profile also shows the excellent self-regulating nature of the battery which restricts charging current to 0.7A at 2.43V/cell once the battery is full.

The efficient self-regulating or pinching by the battery during charging is characteristic of the gassing curve, which is to a high degree dependant on the high polarisation potential of the lead-calcium-tin negative electrode. (Compare gassing curve with the WILLARD 774).

The watt-hour efficiency for this controlled cycling was stable at 86%.

Capacity at end of cycle tests

The (C10) cell capacity at the end of the partial SOC test was 57Ah to 10.5V. After boost charging and equalisation the cell recovered full capacity. The temporary loss in capacity due to reversible sulphation is therefore 17Ah during the partial SOC test, or 0.66Ah/cycle.

The cell capacity after the deep cycling test was 83Ah (10A, 25°C), or 78Ah at 20°C ie an increase in capacity of 3Ah. The increase is probably due to the cycling in a mild operating regime.

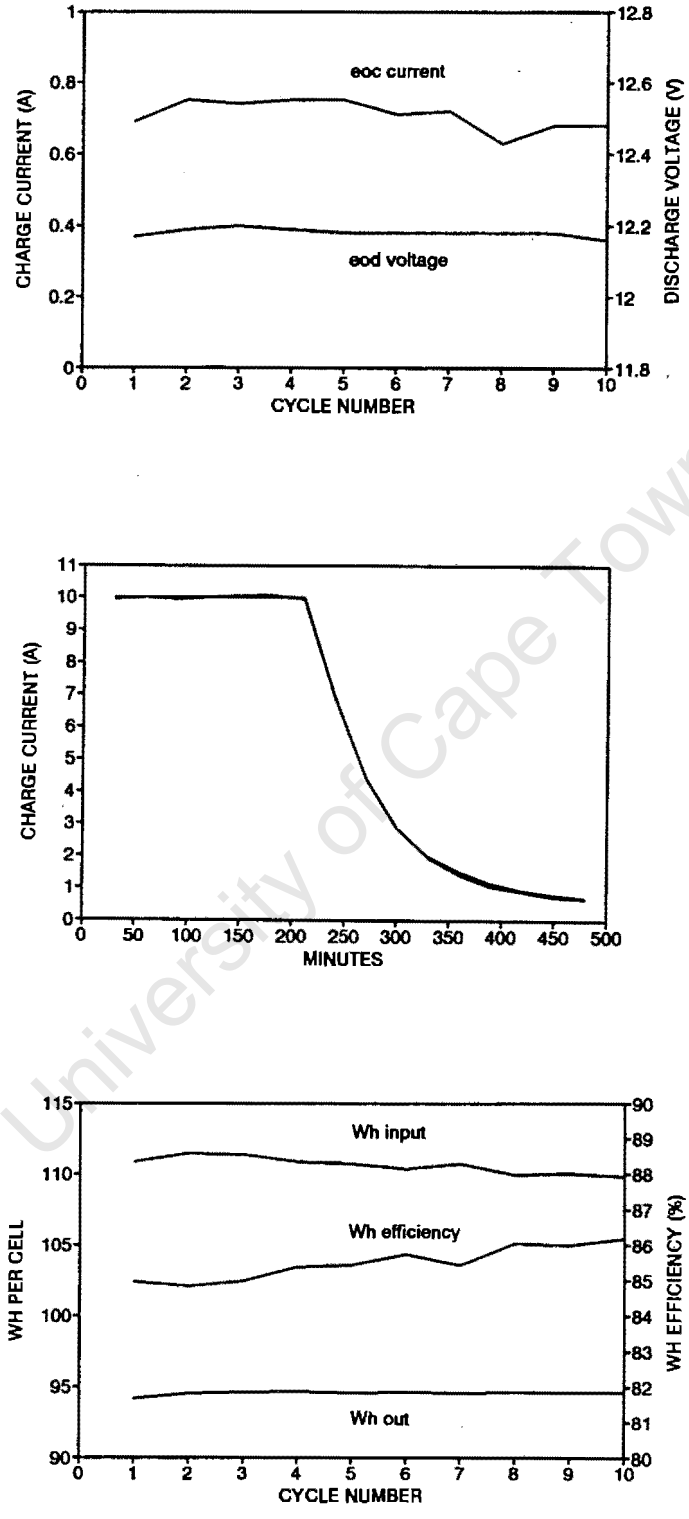

Figure 7.47 Deep cycle full SOC test. a) end-of-cycle conditions, b) charging profiles, c) Wh cycle efficiencies.

H20 Consumption

The accumulated overcharge during the cycling tests was minimal, and water loss could not easily be measured because of the sealed nature of the batteries, and the difficulty in detecting the very small weight changes. It can be deduced from the gassing curves and the pressure curve that as the charge voltage was maintained below 16.0V, no venting occurred and therefore there was no water loss.

Charging current and voltage requirements

Charging requirements for the GNB 12-5000 revolve around keeping the cell pressure below the venting point yet away from the partial SOC regime if possible. The pressure limitation requires restricting the gassing current, which may be indicated by the cell voltage if temperature compensation is used. The gassing current limit is 2A. If the voltage (gassing current) is too high then the cell may vent and become dried out and useless in a very short while. If the charging voltage is too low then the self-regulating nature of the battery will prevent recharging within a reasonable time, resulting in partial SOC operation. Overcharge requirements are minimal as the battery is by nature very efficient, and 3Ah per cycle should be sufficient for most deep cycle application, while for shallow cycling 1Ah would be sufficient.

7.4.5 Sizing and Selection:considerations in PV applications

1) Optimise battery life by choosing 40% daily DOD.
2) Charge the battery at a voltage which allows sufficient time for recharging of the battery, with some overcharge, but do not exceed the 2A gassing current. Partial SOC operation is far less problematic than for flooded electrolyte batteries as stratification is eliminated, but the deleterious effects of hard sulphation can not be ignored.
3) Control pressure inside the battery, which could cause venting, water loss and permanent damage. This is easily accomplished by charge voltage regulation. If the charge voltage is maintained below 15V then no temperature compensation of the charge regulator is required.

4) Consider using the self-regulating nature of the battery to full advantage. This can be accomplished by using the battery without a regulator with a well matched PV array, but is also subject to several other constraints (Section 3.14.1). Particularly, the cell venting pressure should not be exceeded. This battery remains a prime candidate for self-regulation provided matching of the panel and battery with the load avoids cell venting and overdischarge.

7.5 DELCO 1250 TRUCK/UPS BATTERY

7.5.1 General Information

Data summary

Capacity: C_{20} = 105Ah; C_{100} = 115Ah
Voltage: 12V
Application: UPS/float charge applications

Description: Flat plate 12V power pack. Vented with flooded electrolyte, in black casing. Essentially a modified SLI design, with thicker plates. Lead-calcium negative and positive grids. Internal optical SG hydrometer for instant SOC indication.

See Appendix D5 for manufacturer's data sheet.

Costing

Cost: R280 per battery (@ 23/10/1990)
Wh cost: R0.22/Wh
Wh value: R2.78/kWh over battery life, assuming 800 cycles at 10% DOD, the optimum DOD. These figures are based on approximate data. (See Section 7.5.3 for detailed discussion of life cycle data, and Section 7.5.4(c).)

7.5.2 Physical

Physical construction

Dimensions:	height, width, length:	238.8 x 172 x 330.2mm
	height over terminal:	360mm
	mass:	26.9kg
Plates:	design:	15 flat plates/cell
		8 positives, 7 negatives[11]
	pos. active material:	111.5g, 1.11mm thick
	neg. active material:	120.5g, 1.14mm thick
	active block mass:	2.464kg/cell
Grid:	positive:	lead-calcium, 57.9g, 1.19mm thick
	negative grid	lead-calcium, 38.0g, 0.99mm thick
	grid mass:	0.729kg/cell
Dry mass:	17.18kg	
Electrolyte:	SG:	1.270 @ 27°C
	volume:	6.38l[12]
	mass:	8.1kg
Wet mass:	25.28kg	
Gas venting:	No vent caps, but single sintered glass gas escape. As far as the user is concerned, the battery is maintenance-free.	
Casing:	black plastic	
SOC indicator:	optical hydrometer,	located in cell number 2 only
Terminals:	Two types are available.	
	model 1251:	conventional lead post
	models 1250 and 2000:	stainless stud type (M10 316 stainless nuts and washers not provided)

11 It is conventional for the number of negative plates to be equal the number of positive plates plus one.

12 The DELCO 2000 Photovoltaic battery is identical in all respects, except that is contains additional (unspecified amount) electrolyte, but of lower SG.

Active mass utilisation coefficients

(Calculated)

	Active mass	Electrolyte	SG @ end of test
Capacity @ 100% utilisation	199Ah	133Ah	1.000
utilisation @ nominal capacity (105Ah)	53%	78%	1.072
utilisation @ 100hr rate (115Ah)	58%	86%	1.050
utilisation @ opt. DOD (11Ah @ 10% DOD)	5.8%	8.6%	1.260

Under normal operation, the SG of the electrolyte will limit capacity, as well as resulting in higher internal resistances which reduce efficiencies.

7.5.3 Basic Operating Data Available

Charging requirements and limits

(following deep discharge cycling)
fast charge: 50A for 1½ hours (50% of C20)
slow charge: 5A for 20 hours (5% of C20)
Equalising charge: 2.7A or 3.0% of C20
with the proviso that the voltage in all cases is less than 13.8V at 30°C in float applications.

Discharge curves

Complete discharge curves are available, from 1A to 100A.

Life cycle data

Delco Remy enclose unconventional cycle life curves with the comprehensive battery literature. The curves show cycle life, till 50% capacity loss, vs DOD on a log-log scale. (The conventional format is to show life till 20% capacity loss on a semi-log scale). By their own admission, Delco have extrapolated the life cycle data from some experimental results. It is debatable which of the log-log and semi-log model extrapolations is valid for this battery (see comprehensive discussion Section 3.12.). The semi-log and log-log models are compared in Figure 7.48. In one case the semi-log model is based on the 10% DOD (2000 cycles) and 50% DOD (150 cycles) points, in the other case the 20% DOD (800 cycles) and the 50% DOD points are common. The log-log model is very much more optimistic at low DOD's, and the range of cycle lives suggested by the different models at low DOD's is cause for concern. The optimum DOD is equally uncertain. The manufacturer's model would indicate that cycle life approaches infinity as DOD decreases. The semi-log models suggest that optimal DOD is in the range 20-30%. Basing an estimate on all three curves, a conservative guess for optimal DOD might be in the region of 10% DOD, for cycling to a loss of capacity of 50%. (See Figure 7.49.)

It is desirable to know the expected battery life to 20% loss of capacity. Several attempts were made to correct for this using models. Fortunately Delco released an unofficial correction, which is once again shown as a log-log model (Figure 7.50), with the corresponding semi-log models. The curves show the cycle life on this basis to be more comparable to similar batteries. The suggested optimum DOD is again around 10-20%, with considerable uncertainty involved at lower DOD (Figure 7.51). The gains in effective Ah resulting from the log-log model cannot match the potential deficits of the semi-log models, and it is safest to select the shallowest DOD at which disagreement is least, say 10% to 20% DOD. Lead-calcium batteries perform more optimally at shallow DOD if all else is equal.

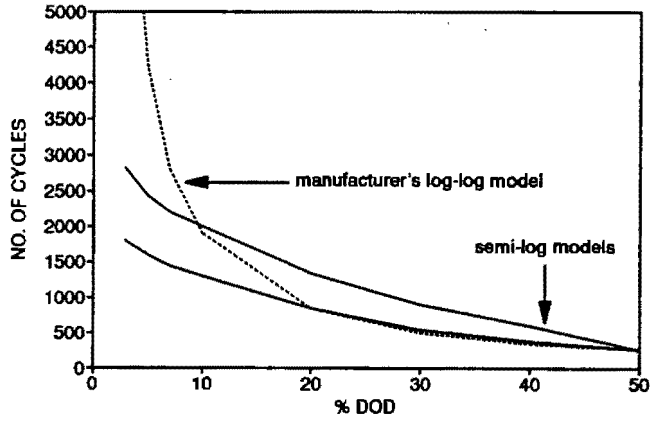

Figure 7.48 Life cycle curves to 50% loss of capacity.

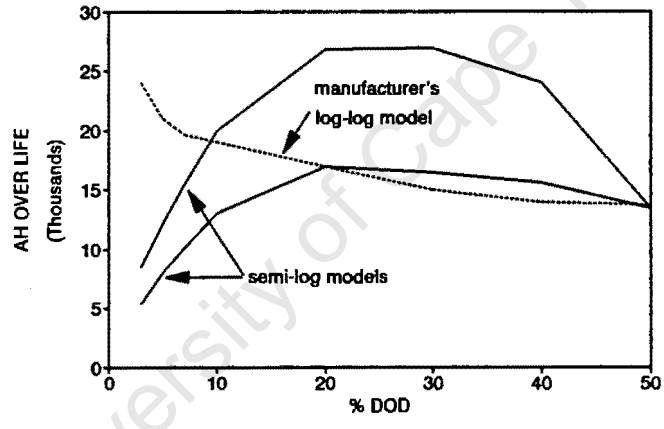

Figure 7.49 Effective Ah over the battery life, to 50% loss in capacity.

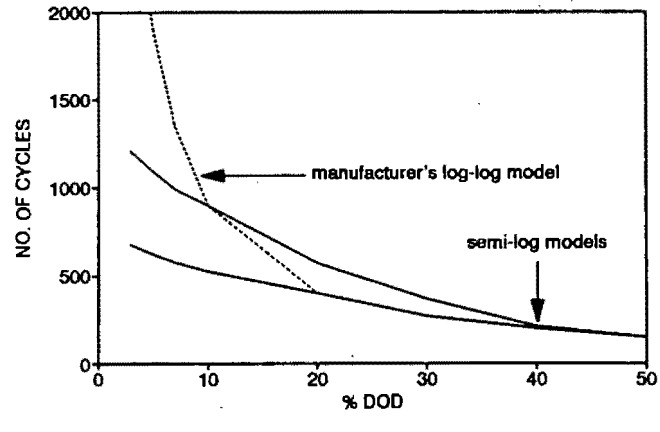

Figure 7.50 Life cycle curves to 20% loss of capacity.

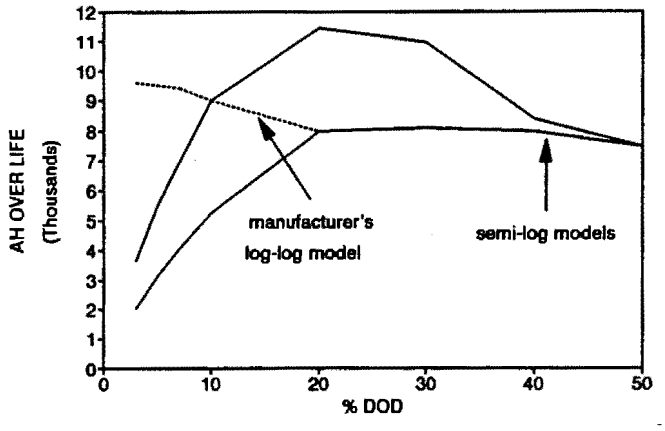

Figure 7.51 Effective Ah over the battery life, to 20% loss in capacity.

Extent of data from manufacturer

Data Quality:
Considerable data is available for the Delco 2000, which is for all intents the same battery as the Delco 1250, though it contains more electrolyte, estimated as insufficient to affect significantly battery performance. (The batteries are specified as the same mass). Data quality is mostly Grade A2 for the Delco 2000, or grade B (performed by the manufacturer in-house on the specific battery).

Data as purchased:

- Standard discharge curves were provided (20°C). (Grade A2)
- Freezing point vs DOD (calculated)
- Capacity vs discharge current (Grade A2)
- Self-discharge vs temperature (Grade A2)
- SG and open circuit voltage vs DOD (calculated)
- Maximum float charge voltages (calculated)
- Expected electrolyte life vs charge voltage (calculated)
- Expected cycle life vs DOD to 50% loss of capacity (see Cycle life discussion) (Grade A2, B)

Additional data on request by personal communication:

- Plate masses, (dry and wet), overall masses and dimensions
- Corrected life cycle data: to 20% loss of capacity (Grade C)
- Test procedures used by Delco Remy

See Appendix D5 for manufacturer's data sheet.

7.5.3 Test results and discussion

Two Delco 1250 batteries were purchased. These are referred to as 1250A and 1250B.

The Delco 1250 normally does not require water addition for the duration of its operational life, and therefore no external filler caps are provided. No convenient method exists for SG measurement. The optical hydrometer located above cell 2 can be removed and SG measurements taken of that cell only, but it is a slow and cumbersome process.

a) Capacity and discharge tests

As complete discharge curves are provided it is necessary only to verify some of the curves. Limited discharging was performed for the same reasons as the Willard LS90:

- the battery is expected to lose capacity rapidly when repeatedly deep cycled, invalidating the results of future tests,
- the capacity is expected to change rapidly with age,
- discharge curves are available and can simply be verified,
- the battery will normally operate in the shallow discharge zone only, and capacity limitations will not be encountered.

Cell 1250A, new and equalised, was discharged at 10A and 18°C to 10.5V and 88Ah were obtained. The discharge curve in the data sheet shows 95Ah at 25°C, equivalent to about 90Ah at 18°C. The battery was recharged and equalised, then discharged as before to yield 86Ah. The capacity at 0°C was determined to be

68Ah, and at 35°C to be 95Ah. (At this stage it was suspected that the run of deep discharges were beginning to curtail the battery capacity).

Cell 1250B was twice equalised at 13,8V and discharged to 10.5V at 20A and 18°C, yielding 81Ah and 78Ah. This is within 5% of the specifications, and is used as the reference capacity for this cell.

The discharge capacities for the Delco 1250's verified the capacities presented for the Delco 2000, which are accepted. The discharge curves at 25°C are shown in Figure 7.52.

It should be noted that load shedding at shallow DOD requires good knowledge of the load current. The shallow slope of the discharge curves in that region suggests that accurate load shedding may become problematic if load currents are low and variable. As a result it may be difficult to control DOD optimally in a PV environment.

The effect of temperature on capacity is shown in Figure 7.53 based on limited data, which compares with the manufacturer's estimated data.

The calculated SG vs Ah removed in Figure 7.54 is typical of SLI type batteries, and does not indicate an excess of electrolyte as is advertised in the literature for the Solar 2000.

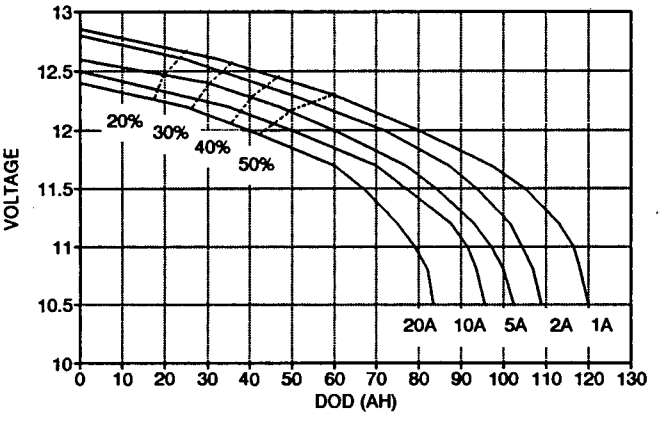

Figure 7.52 Standard discharge curves at 25°C.

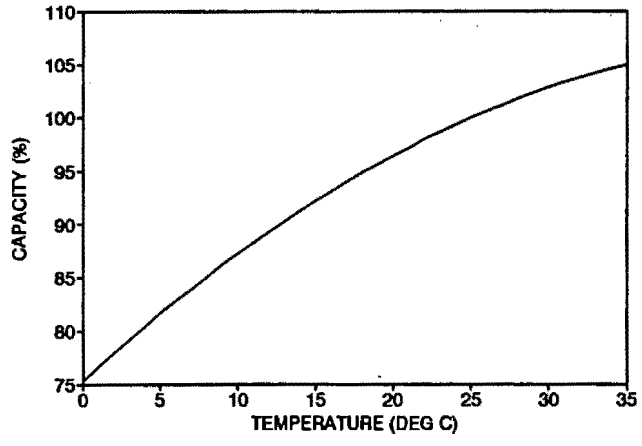

Figure 7.53 Temperature effect on capacity.

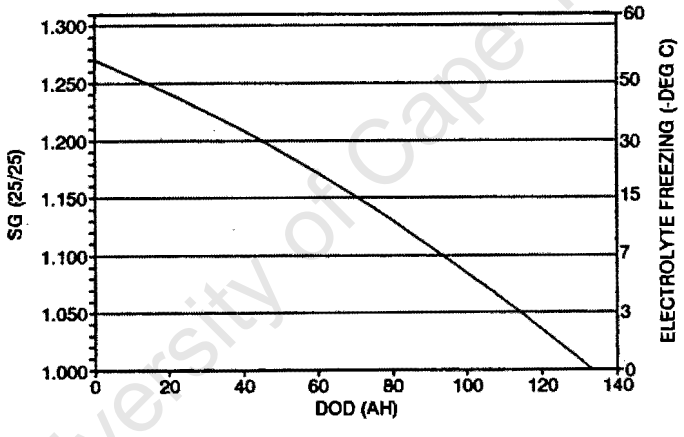

Figure 7.54 Electrolyte SG and freezing point vs Ah removed.

b] Charging tests

Charging tests were conducted as described in Section 6.2.5, on battery 1250A. Charging rates used were 10A, 5A, 2A, 1A, and 0.5A. The temperature compensated charge voltage limits used were 14.2, 13.8 and 13.5 volts at 0°C, 18°C and 35°C respectively. For the shallow cycle 1250 battery recharging was from 40% DOD.

The quasi-constant current charging curve at 18°C is shown in Figure 7.55, and indicates that charging is efficient at 13.8V and 18°C, and that no overcharge is required to reach full charge, regardless of initial DOD. This suggests that the gassing current at the recommended finishing voltage is extremely low.

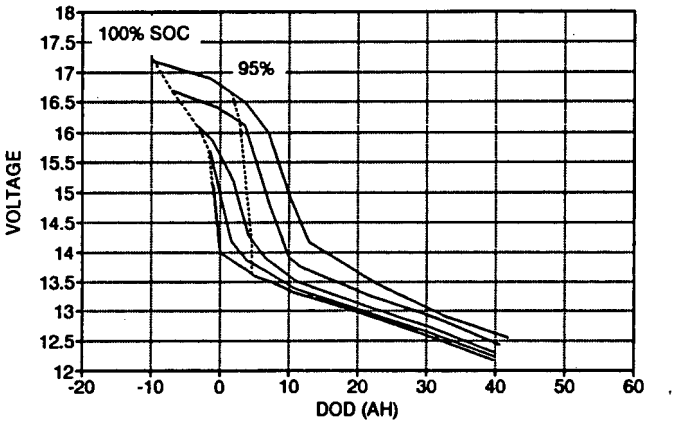

Figure 7.55 Quasi-constant current charging curve. Charging rates used were 10A, 5A, 2A, 1A, and 0.5A.

Charging efficiency was determined by the method in Section 6.2.6(vi), where the end-of-charge current is assumed to be the gassing current. The gassing current curve is in Figure 7.56. At 13.8V the battery accepts virtually no charge, and is self-regulating.

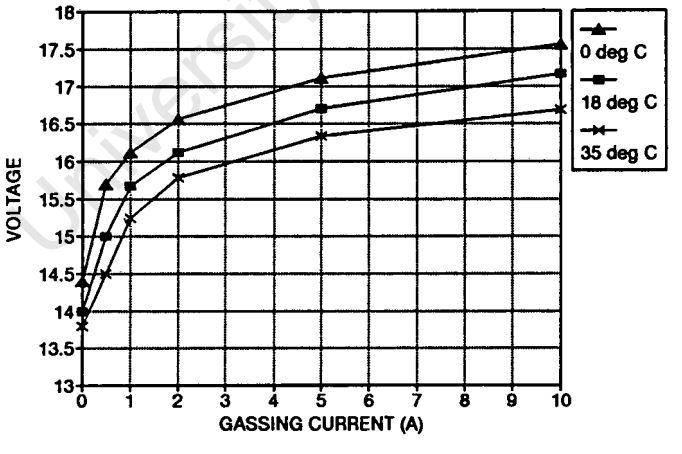

Figure 7.56 Gassing current as a function of temperature and voltage.

The charging curves after compensation for gassing and overcharge losses are shown in Figure 7.57. The end of charge voltage can be read from these curves, as well as the sensitivity of end-of-charge current to the voltage setting.

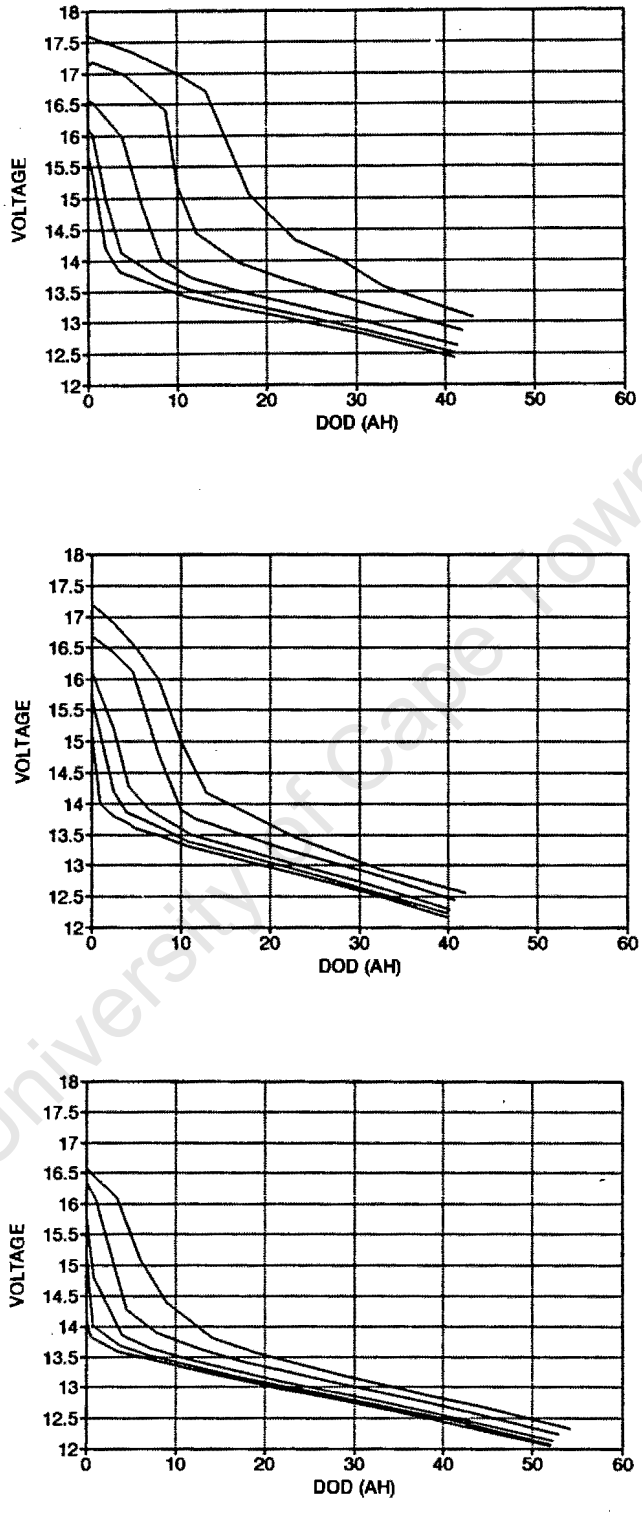

Figure 7.57 Compensated charging curves at a) 0°C, b) 18°C and c) 35°C. Charging rates are 10A, 5A, 2A, 1A, 0.5A.

c] Cycling tests

Cycling tests selection

The 1250 battery is designed only for shallow cycle applications. As previously discussed, cycle life curves suggest an optimum DOD in the region of 10% for regular cycling. A shallow cycle full SOC cycling test is required to determine whether stratification occurs, and if so the overcharge cycle to eliminate it. The test is also useful for determining the minimum charge voltage during shallow cycling, particularly since gassing in sealed vented MF batteries is to be avoided. Shallow cycling at partial SOC is a useful indicator of both stratification and cycle life limitations.

Shallow cycle full SOC Test

Battery 1250A was cycled between 100 and 90% SOC at discharge current of C10, and charge voltage of 2.37/cell, with a limiting current of C10 (10A). Overcharge was limited to 10%, and the time for charging limited to two hours.

Figure 7.58(a) shows the end-of-charge current and end-of-discharge voltage. The decreasing end-of-charge current suggests that the battery reaches and maintains a dynamic equilibrium close to 100% SOC. During the later charging cycles the Ah delivered are limited by time constraints, by the self-regulating nature of the charging curves (Figure 7.18(b)). The end-of-discharge voltage is relatively constant at 12.12V.

The watt-hour efficiency initially increased (as fewer Ah were delivered), then stabilised at 84.5% at the chosen currents.

Battery 1250B was cycled exactly as for battery 1250A for 26 cycles. The capacity at the end of the test and after equalisation was 59Ah.

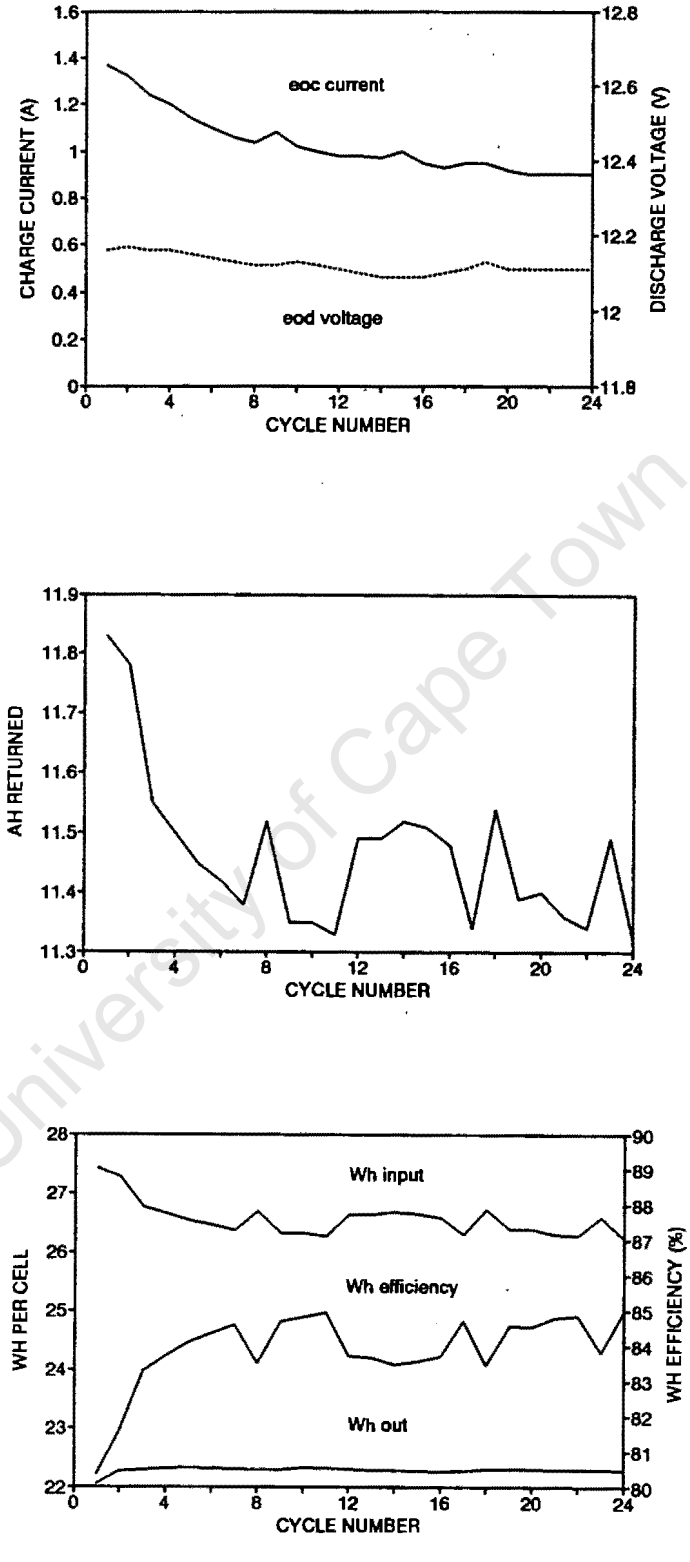

Figure 7.58 Shallow cycle full SOC test; a) end-of-cycle voltage and current, b) Ah delivered, c) Wh efficiency.

Shallow cycle partial SOC test

Battery 1250A was cycled 39 times between 90% and 80% SOC at charge and discharge rates of C10 (10A), which is below the recommended starting charge rate for the cell. Charging voltage was limited to 2.37V for safety, although the charging curves indicated that the voltage would not reach this limit.

Figure 7.59(a) shows the end-of-charge current and voltage and end-of-discharge voltages as the test commenced. The very rapid increase in the end-of-charge voltages from 13.64V in cycle 1 to 14.0V in cycle 11, followed by a jump to 14.2V in cycle 12 indicates a combination of the rapid onset of stratification and the formation of a resistive sulphate layer on the plates, together with possible single cell failure. (A practically identical rise in end-of-charge voltage was observed in this cycling test on the Willard LS90, which also has a calcium grid negative electrode, though some of these effects were identified as reversible). Szymborski (1982) has identified the rapid rise in charging voltage as due to all of the above, together with higher current densities as the calcium positive grid members fracture. The suspected irrecoverable capacity loss was verified by the end of test capacity, determined as 52Ah at 10A after 39 cycles. The end-of-test capacity showed a sudden fall of voltage typical of single cell failure. The effect of stratification/sulphation on the charging profile between cycle 1 and cycle 12 is in Figure 7.59(b).

Figure 7.59(c) maps the Wh efficiency, which eventually settled at 90.5%.

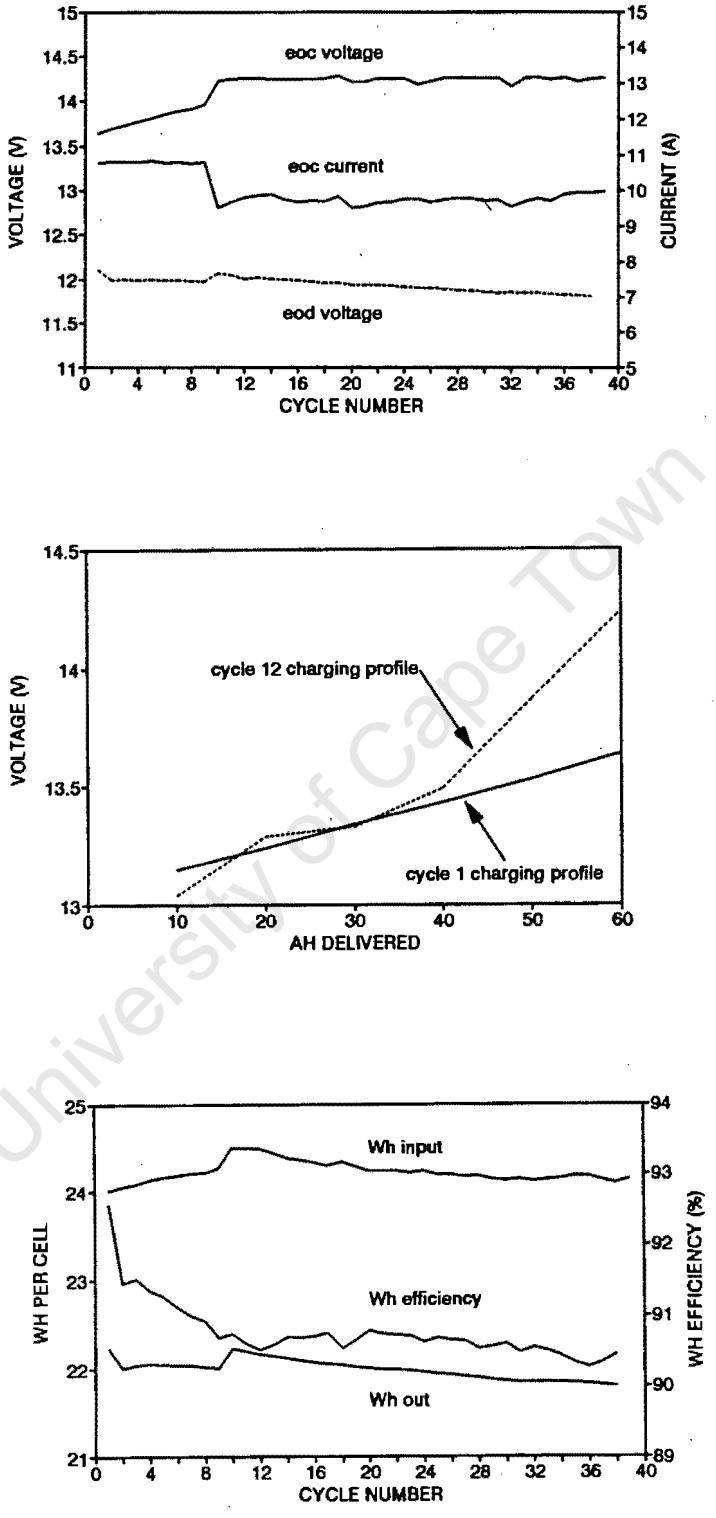

Figure 7.59 Shallow cycle full SOC test; a) end-of-cycle voltage and current, b) change in charging profile, c) Wh efficiency.

Capacity at end of cycle tests

Battery 1250A was equalised and the capacity determined at the C10 rate to be 52Ah, compared with 88Ah at the start. The drop in capacity of 36Ah (41%) seems mainly due to sulphation of both electrodes during partial SOC operation, and it is well known that calcium grid cells last longer under float polarisation than under cycling polarisation. It is probable that the cycle life curves are invalid for partial cycle operation.

The percent of useful life used can also be theoretically calculated using the manufacturer's log-log model for 20% loss of life (see earlier discussion on cycle life). The incremental wear due to:

24 cycles @ 10% DOD (900 cycles expected over battery life)
40 cycles between 10% and 20% DOD (400 life cycles expected)
4 cycles @ 100% DOD (20 cycles expected)
3 cycles to 40% DOD (200 cycles expected)

is

28/900 + 40/400 + 4/20 +3/200 = .346 or 34.6%

The capacity of battery 1250B after full cycling only was 59Ah at the 20A rate, down from the initial capacity of 80Ah. After a further 24 hours on float charge at 14.5V the capacity remained at 59Ah, or a permanent 26% loss in capacity. After a 2nd equalisation the capacity was 56Ah.

The incremental calculated wear due to:

26 cycles @ 10% DOD (900 cycles expected over battery life)
2 cycles to 80% DOD (50 cycles expected)
1 cycles to 100% DOD (20 cycles expected)

is

26/900 + 2/50 + 1/20 = .119 or 11.89%

These limited life cycle tests show that the Delco 1250 performed below expectations during both full and partial shallow cycling. While poor partial SOC cycling may be expected for calcium grid cells, near optimal performance is expected for shallow full cycles with float charge. The small samples used cannot

be used to make statistically valid modifications to the life cycle curves, but further investigation is certainly justified.

H20 Consumption

Very little overcharge was applied to the batteries during testing, and water loss was expected to be minimal. At no time was the SOC indicator coloured yellow. (Yellow indicates excessive loss of electrolyte and possible plate exposure).

Delco presents a curve of electrolyte life vs charge voltage which presumably correlates loss of electrolyte with voltage. A calculation based on the experimental gassing curves compares charging voltage with years of electrolyte life and with centimetres of (estimated) electrolyte above the plates. Three centimetres is considered the maximum possible. The calculated electrolyte life is considerably less than specified. The difference could be due to variation in gassing current, in excess electrolyte volume, or in the gas recovery rate.

In the Delco battery the gases from all the cells accumulate in a mixing chamber, where some recombination occurs. Recombined condensate trickles back to the electrolyte reservoirs, while excess gas escapes to atmosphere through a single vent. After many cycles, the centre cells may accumulate more of the recombined electrolyte than the others. However, these cells are likely to gas more, as their insulated central positions will probably result in higher temperature operation. The location of the optical hydrometer on the cell two probably indicates electrolyte levels within a reasonable average of all the cells.

Charging Current and Voltage Requirements

The main considerations are to prevent loss of electrolyte and to prevent stratification, and to operate the battery in float mode (under voltage controlled charging) for most of the time, as partial SOC operation is so damaging.

The charge voltage should allow use of the self-regulating nature of the battery (see Section 3.14.1), but should also allow some gassing to mix the electrolyte.

The manufacturer recommends a float voltage of 14.3V at 20°C, which would provide less than 0.25A of gassing, but also minimise electrolyte loss.

7.5.5 Sizing and selection: considerations in PV applications

1) Optimise battery life by allowing only shallow daily DOD, and avoid partial SOC operation at all costs as it is battery life limiting.
2) Avoid excess gassing, which could enhance corrosion of the thin SLI type grids, as well as consuming H_2O which cannot be replaced.
3) Minimise electrolyte stratification and the possibility of negative electrode failure by operating in float charge regime for as much time as possible. Long float charge cycles are required as the gassing current is negligible at the recommended charge voltage.
4) Consider using the self-regulating nature of the battery to full advantage. The rapid rise in voltage of the charge curves make the Delco 1250 a possible candidate battery for self-regulating PV systems. Practical application will require careful combination with a self-regulating PV panel. This will facilitate float charge operation. However, in most self-regulating systems overcharge of the battery can occur and should be avoided by considering factors discussed in Section 3.14.1.

7.6 COMPARATIVE DISCUSSION

The five batteries have been discussed individually in some detail. This section compares, in much less detail, the main performance characteristics of the batteries.

7.6.1 Initial Costs

The batteries examined are approximately the same nominal ampere-hour capacity, 100Ah, yet their prices range considerably for the different battery types.

Table 7.1 Wh energy costs

	Cost (R)	nominal Ah	nominal V	kWh of capacity	R/Wh Capacity
774	294	90	12	1.08	.27
RMT108	400	108	4	.43	.93
LS90	364	90	12	1.08	.34
GNB 12-5000	660	93	12	1.12	.59
DELCO 1250	280	105	12	1.26	.22

The cost (R) and R/Wh capacity figures reflect the initial costs of the battery only. These vary considerably. The available capacity during normal use also differs according to the type. However, the main costs are the lead costs, then labour costs for special processes, and the costs of special chemical processes. Table 7.2 shows the comparative costs per mass of lead (approximated by the dry mass of the cell) as the electrolyte is relatively cheap.

Table 7.2 Cost per kilogram of lead

	Cost (R)	dry mass (kg)	R/kg
774	294	17.7	16
RMT108	400	14.7	27
LS90	364	17.7	21
GNB 12-5000	660	±17.7	37
DELCO 1250	280	17.2	16

The conventional flat plate flooded electrolyte batteries cost about R16-R20 per dry kg. The tubular RMT108 costs R27/kg, and this increment is probably a reflection of the cost of the labour intensive tubular manufacturing process. The GNB 12-5000 cost of R37/kg is a reflection of the advanced technology used; absorbed electrolyte, sealed recombination and proprietary Pb-Ca-Sn processes on the negative grid; as well as the cost of importing the battery. The Delco 1250 is surprisingly low cost for an imported battery. Table 7.2 shows that the active mass utilisation seems to be a reasonable basis for comparison. Overall, you pay for what you get in terms of manufacturing costs. Lifetime R/kWh costs are discussed later.

7.6.2 Charging Parameters

Gassing curves

Gassing current/voltage is fundamental to determining charging regimes for batteries in PV applications, where gassing is in most cases required yet must be restricted.

The gassing curves of the five batteries can be divided into two distinct groups, those with calcium negative plates and those with antimony negatives. The

gassing curves at 18°C are in Figure 7.60. The modified RMT108 gassing curve is shown adjusted for utilisation coefficient (nominal capacity divided by capacity if active materials were completely used), so that the batteries experience the same current density. (Current density is used in the theoretical determination of gassing overvoltage). The RMT108 and 774 curves are closely related. These batteries gas heavily at 15.5V, while the calcium grid cells gas mildly at 15.5V.

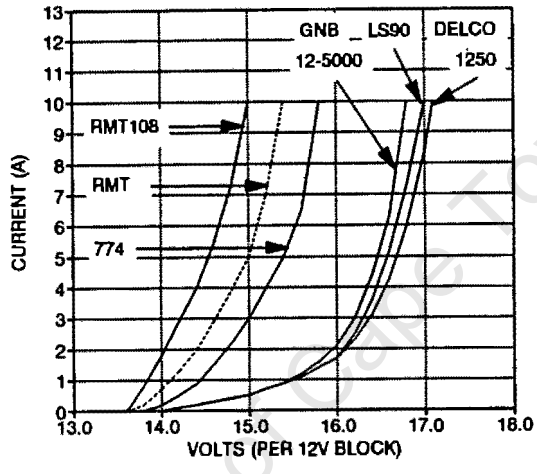

Figure 7.60 Gassing curves at 18°C for the five batteries. The dashed line represents the RMT curve adjusted for utilisation coefficient.

Table 7.3 shows the change in gassing current with temperature at the recommended charging voltages. This represents a situation where the charge voltage is held constant by an uncompensated charge regulator while the battery temperature varies. The RMT108 is most susceptible to uncontrolled gassing if the charge voltage is not compensated for temperature. Table 7.3 also shows the change in gassing current with temperature ($\Delta A/\Delta T$) in the vicinity of 1A gassing current, and the temperature coefficient ($\Delta V/\Delta T$) of voltage required to keep gassing at that level. Temperature compensation coefficients are not the same for all batteries, and should ideally be set specifically for each battery.

Table 7.3 Gassing and charge regulator variation with temperature

	V_{ch} recom. @ 18°C	I_g	ΔA/ΔT (0-35°C)	Voltage at I_g=1A @18°C	ΔA/ΔT (0-35°C)	ΔV/ΔT (0-35°C)
774	14.2	0.75	0.75	14.5	1.5	0.7
RMT108	14.2	1.5	5	14.0	3	1.2
LS90	13.8	0	0	15.5	1.5	1.8
GNB 12 -5000	14.4	0.25	1	15	1.5	0.5
DELCO 1250	14.3	0.25	0	15.7	1.5	0.8

Clearly some batteries gas only slightly at the recommended charge voltages. The reason for the low recommended voltages in these batteries is primarily to limit water loss in the maintenance free designs, which cannot be topped up, as once the electrolyte level has dropped to the level of the plates, plate exposure prematurely ends battery life. The selection of a low charge voltage represents a trade-off between maintenance free operation and reduced battery life due to prolonged electrolyte stratification in the anticipated cycling regimes caused by insufficient gassing. Cycle performance is discussed in Section 7.6.4. The theory does not indicate that any chemical damage could occur to the plates at elevated gassing voltages, but instead states explicitly that antimony-free cells perform optimally in the gassing regime.

Water loss

Gassing and overcharge affect water loss and maintenance as described above. Table 7.4 shows the estimated time between water replacement maintenance (or end of battery life for the MF LS90 at 0.5A gassing current) if the battery is charged continuously at the recommended voltage, as well as the reduced maintenance period if the temperature is increased without charge voltage compensation.

Table 7.4 Maintenance intervals

	V_{ch} recom. at 18°C	Reserve electrolyte (ml)	Hours of charge at 18°C	Hours of charge at 35°C
774	14.2	176	698	460
RMT108	14.2	304	300	150
LS90	13.8	176	no gassing	no gassing
LS90	15.0 (0.5A)	176	1047	523
GNB 12-5000	14.4	NA	no H_20 loss	no H_20 loss
DELCO 1250	14.3	180	2142	1071

7.6.3 Discharge Parameters

The batteries are all of similar nominal capacities, but these are at different discharge rates. The capacities at 10A and 2A discharges at 18°C are in Table 7.5. Included is the capacity of the RMT108 after the current has been corrected by the active mass utilisation coefficient. The capacity is still well above the comparable capacities for flat plate cells. This difference is probably attributable to the large excess electrolyte, which means that the electrolyte volume itself does not limit capacity. The role of the electrolyte is more clearly indicated by the temperature variation of capacity, which shows the change in capacity between 18°C and 0°C as a percent. The typical flooded electrolyte figures show changes of -20% over the range, while the RMT108 with the large electrolyte reservoir shows only a -15% change. The starved electrolyte GNB 12-5000 shows a large -37% change, emphasising the retarded electrolyte transport properties at reduced temperatures.

Table 7.5 Capacity variation with temperature

	Capacity at 10A (Ah)	Capacity at 2A (Ah)	% change in capacity (18-0°C)
774	79	91	-20%
RMT108	140	180	-15%
RMT108 (adjusted)	100 (23A)	160 (5A)	-15%
LS90	79	91	-20%
GNB 12-5000	75	89	-37%
DELCO 1250	95	91	-18%

7.6.4 Cycle Performance

There are three main concerns in discussing cycle performance: depth of discharge, partial SOC operation or complete cycling, stratification and sulphation. Energy efficiency is interesting only if the battery is capable of sustained operation in the cycling regime under consideration.

The cycling tests showed that the antimony grid flooded cells (774 and RMT108) can operate in either deep or shallow full cycles, that stratification and reversible sulphation occur, but can be prevented or reversed by relatively short spells of overcharge at the recommended charge voltages. The cells gas easily, but as the gassing is damaging to the grids (especially for the flat plate 774) it is probably optimal to avoid stratification and subsequent requirement for gassing where possible.

These cells can also operate at partial SOC if the resulting stratification and sulphation is subsequently reversed through gassing. Prolonged partial SOC operation will eventually lead to deep rooted stratification and irreversible hard sulphate formation.

The cyclic energy efficiency is very dependent on the average amount of overcharge per cycle. The overcharge requirements lead to reduced energy efficiencies.

The antimony positive, calcium heat treated ternary negative, absorbed electrolyte cell (GNB 12-5000) can operate in almost any regime cycling provided that the cell internal pressure does not exceed the venting pressure. This cell does not stratify, but the negative electrode is susceptible to hard sulphation at partial SOC cycling, though this is reduced by proprietary processes used during manufacture. The high coulombic efficiency facilitates regular top-of-charge cycle overcharge for cell equalisation and recovery from sulphation. Cycle efficiency can be high, since mixed stage charging is minimised by the self-regulating nature of the charging curves at the recommended voltage.

The conventional calcium negative grid, antimony positive LS90, and the calcium grid Delco 1250 performed very poorly under (shallow) partial SOC operation, losing capacity permanently within thirty cycles. This has been identified as breakdown of the negative electrode under cyclic polarisation. The batteries operate well under full cycling provided that they are also under slight overcharge for most of the cycle. Stratification of these cells is a problem, as the gassing currents are so low at the recommended charge voltages as to be ineffective in the short term. Long term overcharge polarisation is required to recover from stratification.

7.6.5 Cycle Life

Cycle life is one of the most important parameters in costing batteries for PV systems. However, there is considerable uncertainty in the cycle life estimates for the batteries tested, whether based on manufacturers' data or on data for similar batteries.

The cycle life data additionally may apply to very specific conditions, and not to the type of operating regimes encountered in some PV applications. The experimental results have shown that the untreated calcium negative grid batteries in general responded exceptionally (and unexpectedly) poorly to partial state of charge operation.

Figure 7.61 shows the estimated cycle life curves for the batteries tested.

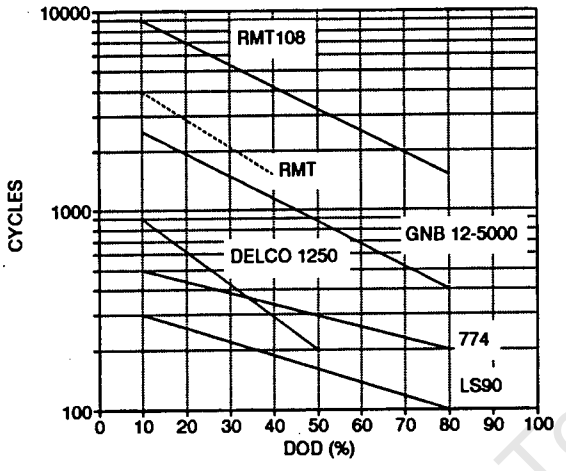

Figure 7.61 Estimated cycle life curves for the five batteries. The dashed line represents the RMT curve adjusted for utilisation coefficient.

The RMT108 has by far the highest cycle life expectancy, but this is primarily a reflection of the low utilisation coefficients. The cycle life adjusted for the utilisation coefficient shows that under similar utilisation the life expectancy is closer to the GNB 12-5000. The high life expectancy of the GNB 12-5000 at high utilisation is the result of the manufacturing process and technology employed, although it appears that this technology has not yet made cycle life gains over the more conservative tubular designs. It is possible that the GNB 12-5000 could withstand prolonged partial SOC operation for longer than the RMT108. The 774 cycle life is moderate, as expected of a conventional antimony battery, with good deep cycle performance. The Delco 1250 cycle life estimates are questionable. The slope of its curve, and that of the LS90 are dissimilar, although theory and practical experience suggest similar failure modes and preference for similar operating regimes. Similarly sloped curves are expected. Delco 1250 cycle life is probably closer to the LS90 than indicated.

The estimated optimum operating DOD and number of cycles expected for each battery is shown in Table 7.6. The same uncertainties surrounding cycle life estimates apply to the calculated figures in Table 7.6. The total energy stored over the battery life is shown for the expected number of complete cycles between the

optimum DOD and the fully charged state. The overall cost of that stored energy provides an indication of the value of the battery. (Only the initial costs are considered, maintenance and other costs are ignored). The expected battery life in years assumes one cycle per day.

It is important to stress that cycle lives are based on manufacturers' data (where possible), and there are considerable limitations in the adequacy and reliability of this data. The Delco 1250 figure is considered ambitious. The stored energy costs are intended for approximate comparisons only. The PV system costs and balance of system requirements, and resultant losses in system efficiency when sizing to provide suitable operating regimes for the different batteries may alter the comparative costs. In small PV systems, component choices may be limited to discrete size increments, which can introduce a further cost factor.

Table 7.6 Stored energy cost and battery value

	Cost (R)	DOD (%)	Cycles	Stored energy (kWh)	Energy cost (R/kWh)	Life (years)
774	294	50	300	162	1.81	1
RMT108	400	40	4000	691	0.58	10
LS90	364	20	300	65	5.62	1
GNB 12-5000	660	40	1300	580	1.14	3.5
DELCO 1250	280	10	800 500[13]	101 63	2.78 4.44	2.5 1.5

13 The cycle life is most probably less than the 800 cycles claimed. 500 cycles at 10% is used for comparison.

7.6.6 Conclusions

There is no straight forward answer to the question, "Which battery is best for PV applications?".

The answer is complex principally because there is great variety in PV installations, and the relative performances of PV systems using battery storage are strongly dependent on the operating environment. The differences may be minor for similarly designed systems in close proximity, but the simple analysis in Chapter 2 has demonstrated how two installations designed for the same site can present fundamentally different battery operating environments. No one battery will work in all PV systems, let alone perform optimally.

Factors which strongly influence battery operating environment in a stand-alone PV system include

a) site-dependent weather (primarily solar irradiation, and to a lesser extent ambient temperature), and variability in weather over different time scales (days to months) (Cowan,1990);
b) load energy demand profiles, again over different timescales, in relation to (a);
c) the design loss of power probability of a system, reflecting system energy capacity in relation to (a) and (b);
d) the design choice amongst array/battery combinations capable of satisfying (c);
e) the maximum battery DOD allowed, and load shed regulator settings;
f) the relation between maximum and average depths of discharge which is partly a function of (c) and (d);
g) charge regulator control.

System design decisions will largely determine the range of requirements placed upon the batteries and thus influence choice of battery type and sizing of battery capacity. System sizing and battery choice will in turn affect aspects such as the ratio between capital and running costs, maintenance frequency and the predictability of battery performance (all of which could be design constraints).

Factors affecting battery choice

Realising that different battery chemistries and designs have different operational preferences the system designer must come to terms with the design features that affect these preferences.

Special attention should be given to:

1) matching the expected cycle regime with a battery of suitable design and grid chemistry;
2) effective charge and discharge regulation within the expected cycle regime to minimise the onset of long term grid corrosion, stratification or sulphation;
3) temperature compensation of charge and discharge regulation for expected battery operating temperature;
4) array requirements to provide sufficient energy for overcoming inefficiencies in the battery.

Some practical examples of concerns might be:

Immobilised electrolyte batteries perform better than flooded electrolyte batteries in a partial SOC regime, but prolonged partial SOC operation will also be detrimental in the long term.

Calcium and non-antimonial grid batteries are sometimes proposed to reduce maintenance requirements. Under controlled charging they demonstrate low water consumption. If overcharged they will consume as much water as other batteries overcharged by the same ampere-hours. But since they are usually cycled in shallow regimes they do not require the same amount of overcharge. Batteries must be matched with suitable regulators.

For deep cycling applications, the lowest life cycle battery costs appear to come from tubular batteries, but capital costs tend to be high and it is important that the array can source sufficient current to overcome self-discharge, charge inefficiencies and stratification limitations.

The battery selected as being technically most suitable may not be the best choice on economic grounds.

For example, high initial battery cost may discourage use of some battery types; selection of batteries with lower energy efficiencies or more demanding charging requirements may increase costs elsewhere in the system; attempts to minimise initial costs of array and batteries can lead to decreased battery lifetimes and increased running costs.

In order to select an optimal trade-off between economical capital costs and economical running costs over the lifetime of a system, it is desirable to be able to predict running costs with a degree of certainty. Uncertainty in predicting battery lifetime is increased if batteries are not operated within fairly conservative cycling regimes. For this reason it is advisable to apply battery design data cautiously, even where operating conditions are similar to the cycling conditions under which the data was obtained. Extra caution is warranted if operating conditions may deviate significantly form test conditions.

Uncertainties remaining

PV system sizing is a statistical problem because of uncertainties in solar irradiance and system interaction with often uncertain load profiles. Battery cycling regimes in PV systems are therefore also statistical in nature and subject to uncertainties. Complete battery data covering all possible operating conditions will probably never be available. The combination of incomplete battery performance data and highly variable operating regimes leads to considerable uncertainties in determining the impact of technical choice on system life cycle costs.

Battery performance characterisation itself has a statistical aspect due to variations amongst batteries of the same model. The data generated in this project has a non-statistical basis as time did not permit repetitive testing to statistically validate the data. However it is doubtful whether this limitation is a major contributor to uncertainty, relative to other sources of uncertainty, except perhaps in cases where batteries degraded during testing.

However, with regard to life cycle data, tremendous uncertainties still exist. Causal linkages between operating regimes and cycle life can be established (this has been a primary motivation for documenting the battery theory in Chapter 3), but there is a dearth of information describing the magnitude of the effects of external variables on cycle life.

The empirical battery characterisation data from this study can be used in PV system simulation programs to explore the long-term cycling conditions of specific batteries in specific PV systems. This will be a step towards greater predictability of battery lifetimes in PV systems and identification of system design parameters affecting battery life. However considerable ground would need to made in modelling battery degradation and failure modes in order to achieve more definitive understanding.

For most installations a high priority in designing systems to minimise costs is to understand with some certainty what the longer term effects of a particular design and sizing will be. This chapter has endeavoured to remove some initial uncertainties by providing comparative data concerning the principal problems with batteries in small PV systems, namely continuous undercharging, partial state-of-charge operation, stratification and sulphation; overcharging, gassing, charge voltage temperature compensation and stratification elimination; and primary implications for cycle life estimation and costing.

This data should already be useful for selection of batteries for specific PV applications.

CHAPTER 8

CONCLUSIONS AND RECOMMENDATIONS

The main objective of this study was to determine accurate empirical data for locally available batteries which could be used in photovoltaic systems, and to present this data in a format directly applicable to PV system designers.

Secondly, the experimental battery data and gains made in understanding battery performance were intended to contribute to the accuracy of PV system simulation methods being developed at EDRC. PV system simulation tools provide an effective way of evaluating and optimising system design options. Modelling battery behaviour is a vital but presently problematic component in simulating PV systems with battery storage.

8.1 LITERATURE REVIEW

Battery theory and research literature has been extensively reviewed from the viewpoint of understanding battery behaviour in PV systems. Theory and existing research were presented to provide background for the concerns and test methods used in the present study. Existing models of battery performance were discussed.

The review was essential for understanding major mechanisms which determine battery behaviour. In particular the examination of polarisation and overpotential theory has enabled development of time efficient methods of battery charge curve determination and charge efficiency measurement. The review of macro and micro-processes provided insight into failure modes specific to certain generic battery types in PV operating regimes.

Batteries in stand-alone PV systems are generally subject to particular operating conditions such as low charging currents and variable depths of discharge. In the light of such requirements and theories of battery performance, innovative designs for specialist PV-compatible batteries were described. Methods of battery charge

regulation, which should be adapted to battery performance characteristics and operating conditions, were assessed.

8.2 BATTERY TESTING FACILITY AND TEST METHODS

A major interim objective of this project was the design, development and construction of specialised test equipment to collect empirical battery data relevant to photovoltaic applications. A microcomputer-controlled battery testing unit was developed which is capable of variable charge and load cycling, automated data capture and PV emulation.

The unit consists of a 3kW (50A, 60V) programmable power supply and a 1.8kW (30A, 60V) programmable electronic load, both constructed in house, controlled through analog-digital converters by customised software.

The test software supports conventional battery testing as well as PV system emulation. In the latter case, solar irradiation data, characteristic PV curves and load data are input, and the software-controlled power supply is able to emulate the PV array to determine and display the battery and array operating points.

The system has operated almost continually for 24 hours per day for more than one year without serious or prolonged down time. The primary limitation of the test-unit is the inability to test and monitor more than one string of batteries at any time. (The software could be readily adapted, but for each additional battery string another power supply and load are required.) This cost based limitation reduced the scope for statistical testing of batches of batteries and required thorough and efficient utilisation of the test-unit.

A range of lead-acid batteries was selected to cover the generic types most often used in PV applications in Southern Africa. Because of the long test periods required, care was taken to obviate unnecessary overlap or redundancy.

Prior to data collection, the literature on testing methods was extensively searched to establish suitable experimental techniques for particular batteries.

A short and elegant method of determining charge curves was developed. This method entails periodically and incrementally varying the battery charging current over a suitable range, and maintaining the incremented current till the battery charge voltage stabilises. The stabilised voltage is taken as one point on the charge curve and points of constant current can be combined to form the charging curve.

Instantaneous charging efficiencies were determined by monitoring gassing rates, and quasi-constant current charging curves were generated by correcting the experimental charging curves for the charging inefficiencies indicated by the gassing curves.

Good agreement with conventional constant current charging curves has been obtained. The innovative method permitted the collection of battery charging data in a range of low charging currents applicable to PV operating conditions. Such data are rarely available from battery manufacturers and would take an impractically long time to collect by conventional constant current charging methods.

Other experiments conducted on the selected batteries included discharge tests and capacity determination at various temperatures. Cycling tests developed by Sandia National Laboratories were used to charge/discharge the batteries in typical PV system state-of-charge regimes and these tests provided comparative information on charge acceptance rates and overcharge requirements. Temporary and reversible capacity losses caused by stratification, and permanent capacity losses leading to battery failure, were also monitored through the cycling tests.

8.3 TEST RESULTS

The five types of lead-acid battery were:

1) conventional calcium alloy positive and negative grids, flat plate, flooded electrolyte, vented casing (the Delco 1250 was selected)

2) low antimony alloy positive grid, conventional calcium negative grid, flat plate, flooded electrolyte, vented casing (Willard Vantage selected)

3) low antimony alloy positive grid, heat treated calcium negative grid, flat plate, immobilised absorbed electrolyte, sealed casing with O_2 cycle gas recombination. (GNB Mini-Absolyte selected)

4) antimony alloy positive and negative grids, flat plate, flooded electrolyte, vented casing. (Willard 774 selected)

5) antimony alloy positive and negative grids, tubular plate, flooded electrolyte, vented casing. (Raylite RMT tubular cells selected)

Selenium grid alloy cells and gelled electrolyte batteries were not represented amongst the batteries tested, owing to problems of availability or cost.

The data collected in this project is already of practical use for PV system designers. In some cases the information generated is the only relevant performance information available for a particular battery, in other cases it complements manufacturers' data but which is in a form that would otherwise not be directly applicable for the PV system designer.

The comparative data provided indications of the differences between the generic battery types. The main advantages and disadvantages of the generic battery types in a PV application are summarised below.

Table 8.1

SUMMARY OF GENERIC BATTERY TYPES

Battery Type	Advantages	Disadvantages	Comments
conventional calcium positive and negative grids, flat plate, flooded electrolyte, vented casing	maintenance free in specified voltage range. low gassing rate.	poor partial cycle life. poor full cycle life. electrolyte stratification.	poor cycle performance, suitable for float charge with occasional shallow cycle. requires basic uncompensated voltage regulator to prevent fatal H_2O loss. low initial cost, high operating cost, though may require large PV array to ensure float charge operation.
low antimony alloy positive grid, conventional calcium negative grid, flat plate, flooded electrolyte, vented casing	maintenance free (but may require H_2O addition in 2nd half of life). low gassing rate. moderate cycle life.	poor partial cycle life. electrolyte stratification difficult to eliminate once set in.	suitable only for shallow cycling. requires only basic regulator to prevent H_2O loss. moderate initial cost, high operating cost.
low antimony alloy positive grid, heat treated calcium negative grid, flat plate, immobilise absorbed electrolyte, sealed casing with O_2 cycle gas recombination	totally maintenance free in specified voltage range. low gassing rate. good cycle life at deep and shallow, full and partial SOC[1]. no electrolyte stratification problems.	high temperature coefficient of capacity. higher grid corrosion during gas recombination. imported technology.	suitable for any operating regime, provided gassing is controlled. requires basic voltage regulator. high initial cost, moderate operating cost.

Continued

Continued

Battery Type	Advantages	Disadvantages	Comments
antimony alloy positive and negative grids, flat plate, flooded electrolyte, vented casing	moderate cycle life at deep and shallow full and partial SOC[1]. easy recovery from stratification. excellent cycle life at deep and shallow full SOC[1].	moderate gassing rate and gassing temperature dependence. high maintenance requirements. possible electrolyte freezing at deep discharges and low temperatures. electrolyte stratification.	moderate cycle performance at deep cycle, float charge is best avoided. gassing must be controlled to prevent H_2O loss and fatal grid corrosion. temperature compensated voltage regulator preferred. low initial cost, high operating cost.
antimony alloy positive and negative grids, tubular plate, flooded electrolyte, vented casing	good deep and shallow cycle life at partial SOC[1] if regularly equalised. easy recovery from stratification. can withstand substantial overcharge.	moderate gassing rate and temperature coefficient of gassing. moderate-high maintenance requirements. electrolyte stratification requires overcharge. higher charging currents required. lower cycle efficiency.	good deep full cycle performance. gassing must be controlled and ensured to eliminate stratification. temperature compensated voltage regulator desirable. high initial cost, low operating cost.

Note [1]. Partial state of charge operation implies prolonged periods of undercharge, while full state of charge operation implies frequent overcharge.

Besides providing valuable empirical data for the generic battery types this project has investigated the areas of battery modelling, charge and load shed regulation requirements and battery selection for PV system sizing. The main conclusions from these laboratory based investigations are outlined below.

8.4 BATTERY MODELLING

Two fairly distinct concerns in assessing or simulating battery performance in PV systems are ways of modelling electrical performance characteristics and ways of modelling battery lifetime degradation.

For operating conditions typical of the PV environment, battery electrical characteristics are most accurately represented by interpolating between empirical data points rather than fitting known models. The latter tend to be inaccurate at the low current densities typical of PV systems. It is suggested that battery charge efficiency can most effectively be modelled as a function of the charge voltage determined from the empirical data interpolation. This hypothesis is based on the non-linear overpotential variation indicated by the Bultler-Volmer equation.

Empirical battery performance data from the present study has been used to establish database battery models in the PVPRO photovoltaic simulation program (Geerdts and Eberhard,1990).

Battery life modelling provides the only theoretical means for predicting battery lifetimes in a range of PV system configurations. However, present battery life models remain ambiguous and uncertain even when applied to normal battery failure modes associated with incremental wear. Incremental wear models have been employed in this study for approximate estimations, but the estimates are presented with caution. Premature failure due to inappropriate operating conditions is not at all well modelled due to a deficiency of reliable statistical data describing the specific failure modes associated with particular operation hazards for particular types of battery.

Available models for incremental wear have been used in conjunction with battery characterisation data and PV simulation software, but tentatively, and there is clearly scope for further work in developing and implementing adequate battery life models. More accurate predictions of battery lifetime, according to system design parameters, battery selection and regulation, and long-term operating conditions are of considerable interest to PV system designers.

8.5 CHARGE AND LOAD SHED REGULATORS

Battery lifetime depends critically on optimal regulation. It is rarely possible to operate satisfactorily for sustained periods without charge and discharge regulation.

There are several modes of charge regulation, most of which control the battery charging voltage. Regulator voltage settings must take account of battery type and operating temperatures. With some batteries it is advisable to use temperature compensating regulators, particularly where the battery temperature varies over an appreciable range. The battery temperature compensation coefficient depends on the battery type.

Overdischarge protection is based most often on the battery operating voltage. However, the approximate discharge current must also be known if load shedding is to occur anywhere above 50% depth-of-discharge, since the cut-off voltage is a strong function of discharge current. Locally available loadshedding units which respond only to battery voltage could be ineffective in maintaining the desired maximum depth of discharge in shallow cycling regimes. For load shedding at deeper discharges the current is not as critical.

The battery drop-out voltage is relatively insensitive to temperature during shallow cycling. Beyond 50% depth-of-discharge, however, voltage is strongly affected by battery temperature. For regular deep-cycling, therefore, some temperature compensation on the load shed should be provided.

The design, configuration and control algorithms of the regulator and load shed units should be selected to complement the operational requirements of the battery in the PV system. Not only should the charge and discharge control settings be adjustable, but also the temperature (and discharge current) compensation. The regulating units should be matched with the system design as a whole, so that the battery is adequately protected against overcharge or deep discharge even following regulator or load shed unit failure.

Optimal regulator design therefore requires detailed knowledge of battery characteristics in a PV environment, and this factor has been an important motive for the present research.

8.6 PV SYSTEM SIZING

The main aims, priorities and trends in PV system sizing for low cost developments are to minimise the lifetime costs of the system to make it as affordable as possible. One approach is to size the system accurately so that is just meets the load demand requirements. Loss of power probability methods provide an elegant means of sizing and comparing systems that just meet this need at selectable availability levels.

There is a range of PV/battery combinations that can satisfy the selected loss of power probability and specified load demand. The choice of PV/battery combination will influence the effective average battery depth-of-discharge, frequency of cycling, extent and frequency of overcharge. Together these have a strong determining influence on the battery life, and hence system life cycle costs. Current PV system sizing methods do not provide systematic means for taking these effects into account.

The results of the present project in conjunction with PV system simulation and sizing software can provide insight into the variable nature of the operating parameters and enable more accurate estimation of battery life.

Costing

Although PV systems generally require relatively little maintenance, there remains a balance between capital costs and operation and maintenance costs.

Minimising the installed cost of a system does not necessarily lead to minimised operating costs. Conversely, minimising operating costs will usually result in higher installed costs.

Operating costs are primarily affected by the type of battery selected, and its lifetime. Obviously the battery should be suited to the prevalent operating

regimes. A comparative discussion of the performance characteristics of the batteries tested in this project provides some guidance in the selection of appropriate battery types.

8.7 RECOMMENDATIONS

For most installations a high priority in designing systems to minimise costs is to understand with some certainty what the longer term effects of a particular design and sizing will be. This project has endeavoured to remove some initial uncertainties by providing comparative data concerning the principal problems with batteries in small PV systems. Recommended areas for future work focus are detailed below.

Battery modelling

While electrical performance of batteries in good condition can be well modelled using empirical data collected in the laboratory, (this applies to charge/discharge curves and charge efficiency), electrical degradation can not be well modelled because neither sufficient empirical data nor adequate electrical degradation models exist. Electrical degradation models should be investigated in conjunction with battery life models.

Battery life models are uncertain even when based only on normal failure modes associated with incremental wear. There is clearly scope for further work in developing adequate cycle life and degradation models incorporating possible hazards and failure modes expected from specific batteries in PV operating environments. Data and theory from this project can provide an initial basis for identifying such failure modes.

Battery testing

Further categories of generic battery types available for PV applications in South Africa should be electrically characterised based on the existing procedures to provide additional comparative performance data. Selenium alloy grid batteries and gel electrolyte batteries should be specifically included. Additionally, a full variety of specialist photovoltaic batteries should be tested.

Useful performance and life cycle data should be accumulated by cycling batteries in PV regimes using the cycling tests developed by Sandia National Laboratories, described in Section 6.2.7. This data will assist model development.

Manufacturers should provide cycle life data together with detailed test procedures used, especially for batteries for which cost effectiveness is dependent on long cycle life. It would also be beneficial if manufacturers routinely supplied more complete electrical performance characteristics.

Regulation and control

Charge voltage regulation has been identified as an area of particular weakness that is closely associated with the battery in PV systems. Potential exists for characterisation of locally available charge controllers to provide system design information and for PV system simulation. These controllers should be suitably grouped for use with generic battery types.

In future, designers of locally manufactured regulators should be informed by the improved battery performance data now becoming available.

A. References and Bibliography

Alzieu J, Koechlin N, Robert J, (1987). Internal Stress Variations in Lead-Acid Batteries During Cycling, *Journal Electrochemical Society*, 1987, 134(8A), 1881-4.

Anderson D J et al, (1981). *Solar Energy Battery Storage*, Final Report, BDM/A-81-058-TR, BDM Corporation

Arco Solar, (1982). *SASY-B PV System Sizing Package for Stand-alone Systems with Batteries*, Arco Solar Inc.

Baikie P E, (1972). Effect of Temperature and Current Density on the Capacity of Lead-Acid Battery Plates. *Electrochim.Acta*, 1972, 17, 839.

Bechtel National,(1980). *Handbook for Battery Storage in Photovoltaic Power Systems*, Bechtel National Inc.

BDM,(1983). *Lead-Acid Battery Model*, Final Report, BDM/A-82-175-TR, BDM Corporation.

Bode H,(1977). *Lead-Acid Batteries, The Electrochemical Society Series*, Wiley-Interscience, NY.

Borchers M L, (1988). *A Decision Making Tool for Assessing Grid Electrification versus Stand-Alone Power Supply Options for Remote Areas.* Unpublished M.Sc.(Eng) thesis, Energy Research Institute, University of Cape Town.

Borden C S, Volkmer K, Cochrane E H, Lawson A C, (1984). *Stand-Alone Flat-Plate Photovoltaic Power Systems: system sizing and life-cycle costing for federal agencies*, JPL Publications 84-37, Pasedena, CA. Jet Propulsion Laboratories.

Bower W, (1988). Evaluation of Stand-Alone Inverters for Remote Applications. *Electrochemical Society Proceedings*, Symposia on Stationary Energy Storage, 1988, 327-345.

Bower W, Dunlop J, Maytrott C, (1990). *Performance of Battery Charge controllers.* An Interim Test Report, FSEC-PF-204-90, Florida Solar Energy Center.

Burke A F, (1984). Laboratory tests of Electric Vehicle Batteries. *Power Sources for Electric Vehicles.* McNicol & Rand (ed), Elsevier.

Canadian Standards Association, (1989). *Characterisation of Storage Batteries for Photovoltaic Applications.* Canadian Standards Association.CAN/CSA-F382-M89.

Calder S M, (1985). *Effects of Charging Regimes on Lead-Acid Batteries.* ILZRO Project No. LE-344, International Lead Zinc Research Organization, Progress Report No. 2, January - June 1985.

Cataldo R L, (1978). Responses of Lead-Acid Batteries to Chopper-Controlled Discharge. *13th Intersociety Energy Conversion Engineering Conference, Proceedings,* 1978, 764-8.

Cataldo R L and Thomas R D, (1981). Laboratory Evaluation of a Pilot Cell Battery Protection System for Photovoltaic Applications. *16th Intersociety Energy Conversion Engineering Conference, Proceedings,* 1981, 689-694.

Chapman R N, (1987). *Sizing Handbook for Stand-Alone Photovoltaic Storage Systems.* Internal Report Sand-87-1087, Sandia National Laboratories, Alberqueque, NM.

Chapman R N and Chamberlin J L, (1989). *Sizing and Selection of Batteries for Stand-alone Photovoltaic Systems.* Internal Report SAND-89-2134C, Sandia National Laboratories, Alberqueque, NM, 1989.

Clifford J E and Thomas R E, (1982). *Study of Battery Accelerated Testing Techniques.* Final Report, SAND-82-7049, Sandia National Laboratories, Alberqueque, NM, 1982.

Cowan W D, (1990). A Critical-Run Loss of Power Probability Method for Sizing Stand-Alone Photovoltaic Systems With Battery Storage. *Energy and the Environment into the 1990's - 1st World Renewable Energy Conference,* A A M Sayigh (ed), Pergamon Press, Oxford.

Davis M, (1990). *POWERCOST 2.0, A Decision Making Tool for Assessing Grid Electrification versus Stand-Alone Power Supply Options for Remote Areas.* Energy for Development Research Centre, Energy Research Institute, University of Cape Town.

Delco, (1979). Delco Remy data package for heavy duty freedom batteries

DeLuca W H, Biwer R L, Yao N P, (1981). Effects of Constant-Current/Constant-Voltage Cahrge Parameters on Lead-Acid Traction Cell Performance. *16th Intersociety Energy Conversion Engineering Conference, Proceedings*, 1981, 674-679.

Eggers M, (1984). A Long-Life Deep Cycle Tubular Lead-Acid Battery. *18th Intersociety Energy Conversion Engineering Conference, Proceedings*, 1984, 868-874.

Enochs J S, Meighan R M, Fleischmann C W, Boden D P, (1984). Nonantimonal Lead-Acid Batteries for Cycling Applications. *18th Intersociety Energy Conversion Engineering Conference, Proceedings*, 1984, 850-856.

Facinelli W A, (1983). Modelling and Simulation of Lead-Acid Batteries for Photovoltaic Systems. *17th Intersociety Energy Conversion Engineering Conference, Proceedings*, Orlando, 1983, 4, 1582-88.

Fry M G, (1973). Precision DC Power Supplies. *Intersociety Energy Conversion Engineering Conference, Proceedings*, 1973, 332-50.

Fry M G, (1970). Magnetic Power Supply Practice since Oxford. *International Conference on Magnetic Technology, Proceedings*, 1970, 1261-74.

Geerdts P C and Eberhard AA, (1990). PVPRO, A New Computer Simulation Model for Stand-alone Photovoltaic Systems. *Energy and the Environment into the 1990's - 1st World Renewable Energy Conference*, A A M Sayigh (ed), Pergamon Press, Oxford.

Gerald C F, (1978). *Applied Numerical Analysis.* 2nd edition, Addison-Wesley Publishing, California.

Grieve W, (1987). Developments in Stationary Maintenance-Free Lead-Acid Batteries. *Journal of Power Sources*, 1987, 378-86.

Gu H, (1989). The Distribution of Voltage Losses Among Components of a Battery. *Journal of Applied Electrochemistry*, 1989, 19, 505-11.

Hewlett-Packard, (1989). *DC Power Supply Catalog with Electronic Loads*. Hewlett-Packard

Hill R J, (1989). Hydrogen and Order-disorder in PbO_2 in Lead-Acid Positive Plates. *Journal of Power Sources*, 1989, 25(4), 313-20.

Horowitz P and Hill W, (1980). *The Art of Electronics*. 1st edition, Cambridge University Press, New York.

Hughes M, Barton R T, Karunathilaka S, Hampson N A, (1986). The Estimation of the Residual Capacity of Sealed Lead-Acid Cells using the Impedance Technique. *Journal of Applied Electrochemistry*, 1986, 16, 555-64.

Hyman E A, (1977). *Phenomenological Cell Modelling*. Report RD77-1, PSE&G Research Corporation, Newark, NJ

IEC, (1967). Publication No. 254, International Electrochemical Commission.

IEEE P1013, (1990). *Recommended Practice for Sizing Lead-Acid Batteries for Photovoltaic Systems*. Institute of Electronic and Electrical Engineers, February 1990.

Jensen J and Tofield B C, (1981). Advanced Batteries for Energy Storage. *International Conference on Energy Storage, Proceedings*, Brighton, April 29-May 1 1981.

Klinger J, Yao N P, Cook G M, (1980). Simplified Computer Modelling of Battery Behaviour under Various Load Profiles. *Electrochemical Society, Proceedings*, May 11-16, 1980.

Kuiper A C J, Einerhand R E F, Visscher W, (1989). Computer Controlled Testing of Batteries. *Computers in Chemistry*, 1989, 13(1), 69-73.

Kuhn D J, (1988). Photovoltaic systems - Battery Sizing and Selection, *Electrochemical Society, Proceedings*, Symposium on Stationary Energy Storage, 1988, 394-99.

Kurokawa K, Nozaki K, Tani T, Akai Y, Sekiguchi H, (1987). A Photovoltaic Power Generating System Provided with Redox Flow Battery. *International Solar Energy Society*, Solar World Congress, Hamburg 13-18 Sept, 1987

Lakeman J B, (1989). Real-time Charge Efficiency Monitoring and On-charge Gas Evolution in Tall Lead-acid Traction Cells. *Journal of Power Sources*, 1989, 27(2), 155-65.

Lander C W, (1981). *Power Electronics*. 1st edition, McGraw-Hill, Maidenhead.

Langley P R, (1990). *Evaluation of Solar Regulators*. ESKOM Internal Report TRR/E/90/002, Project no. E/90/C3010/I, Electricity Supply Commission, South Africa.

Lasnier F and Gan Ang T, (1988). *Solar Photovoltaic Handbook*. 1st edition, Asian Institute of Technology, Bangkok.

Liebenov C, (1897). *Elektrochem.Z*. 3, p71.

Liesgang T C, Johnson S J, Hafen D P, (1988). Dynamic Perrformance Battery Model. *Intersociety Energy Conversion Engineering Conference*, 1988, 23(2), 439-41.

Lindstrom O, (1970). Structure of Wetted Porous Gas Diffusion Electrodes. *Journal Electrochemical Society*, 117.

Maja M and Penazzi N, (1989). Sealed Gas Recombining Lead-Acid Batteries - analysis of real systems. *Journal of Power Sources*, 1989, 25(3), 229-38.

Mantel C L, (1970). *Batteries and Energy Systems*. McGraw-Hill,1970

Mahato B K and Bullock K R , (1987). A New Gelled Electrolyte Lead-Acid Battery for Deep-Discharge Applications. *Progress in Batteries & Solar Cells*, 1987, 6, 136-139.

Matsui T, (1987). Portable Type Optical Hydrometer for Lead-Acid Batteries. *Progress in Batteries and Solar Cells*, 1987, 6, 130-132.

Matsumoto J H, Collins G, Hwang W C, (1984). Applicability of Accelerated Testing. *19th Intersociety Energy Conversion Engineering Conference, Proceedings*, 1984, 303-305.

Maycock P, (1990). Lecture on PV, Solar Energy Society of South Africa PV Workshop, Pretoria, June 1990.

Miller J F, Mulcahey T P, (1988). Evaluation of Advanced Lead-Acid Batteries Developed for Load Levelling Applications. *Electrochemical Society Proceedings*, Symposia on Stationary Energy Storage, 1988, 63-70.

Millner A R & Kaufman D L, (1984). Microprocessor Control of Photovoltaic Systems. *18th Intersociety Energy Conversion Engineering Conference*, Proceedings, 1984, 422-427.

Morris G J, (1988). *Performance Evaluation of Photovoltaic and Diesel Electricity Generating Applications in the Kruger National Park*. Unpublished M.Sc.(Eng) thesis, Energy Research Institute, University of Cape Town.

Pavlov D, (1984). Aqueous Electrolyte Batteries-Lead-Acid. *Power Sources for Electric Vehicles*. McNicol and Rand (ed), Elsevier, 1984.

Peukert W, (1897). On the Dependence of Capacity on Discharge Current in Lead Storage Batteries. *Elek.Z*, 1897, 18, 287.

Rahnmanai H, Ijichi K, Claused N A, Lundorff O, (1984). Microprocessor Based Autonomous Nickel-Hydrogen Battery Management System. *18th Intersociety Energy Conversion Engineering Conference, Proceedings*, 1984, 400-405.

Rand D A J, Barret D, Frost M T, Hamilton J A, Harris K, Moresby J F (1980). ILZRO Project No. LE-290, International Lead Zinc Research Oranization, Progress Report No. 2, December 1979 - July 1980.

Rand D A J, (1984). Overview of Candidate Battery Systems. *Power Sources for Electric Vehicles*. McNicol and Rand (ed), Elsevier, 1984.

Rausenbauch, H S, (1980). *Solar Cell Array Design Handbook*. 1st edition, Van Nostrand Reinhold, New York.

Roberge P R and Beaudoin R, (1989). Voltage Noise Measurements on Sealed Lead-Acid batteries. *Journal of Power Sources*, 1989, 27(2), 177-86.

Shepherd C M, (1965). Design of Primary and Secondary Cells II, An Equation Describing Battery Discharge. *Journal Electrochemical Society*, 1965, 112, 657.

Shimizu K,(1987). Lead-Acid Batteries for Solar Photovoltaic Systems. *Journal Power Sources*, 1987, 19(2-3), 211-12.

Sieger H N, (1981). Effect of Depth of Discharge on Near-Term Batteries. *Intersociety Energy Conversion Enginering Conference*, 1981, 16, 102-110.

Smith G, (1964). *Storage Batteries*. 2nd ed, Pitman, London.

Solar Energy Research Institute, (1984). *Basic Photovoltaic Principles and Methods*. Von Nostrand Reinhold Co, New York.

Szymborski J, (1982). *Maintenance-Free Deep-Discharge Lead-Acid Battery for Photovoltaic Applications*. Sandia National Laboratories Contractor Report SAND-82-7026, April 1982.

Tiedmann W H and Newman J, (1978). Mathematical Modeling of the Lead-Acid Cell. *Journal Electrochemical Society*, 1978, 125(8).

Thaller L H,(1981). Sythenthetic Battery Cycling. *Intersociety Energy Conversion Engineering Conference*, 1981, 16, 667-673.

Thaller L H, (1983). Expected Cycle Life vs. Depth of Discharge Relationships of Well-Behaved Single Cells and Cell Strings. *Journal Electrochemical Society*, May 1983, 986-990.

Tuphorn H, (1987). Gel Type Batteries for Solar Applications. *Progress in Batteries & Solar Cells*, 1987, 6, 145-149.

Waaben S, Moskowitz I, Federico J, Dyer C, (1985). Computer modelling of Batteries from Non-linear Circuit Elements. *Journal Electrochemical Society*, Electrochemical Science and Technology, June 1985, 1356-62.

Williams A T, (1989). *Off-Grid Small Power Supply Options for Rural Areas*. Final Report, GEN 130, Energy Research Institute, University of Cape Town.

Wood J R and Crutchen J L, (1980). *Handbook for Battery Energy Storage in Photovoltaic Power Systems*. Final Report, SAND-80-7022.

Varma R, Tomczuk Z, Kazadi S, Yao N P, (1989). Stibine and Arsine Generation from a Lead-acid Cell during Charging under a Utility Load-levelling Duty Cycle. *Journal Applied Electrochemistry*, 1989, 19, 10-18.

Vinal G W, (1955). *Storage Batteries*. Wiley, New York, 1955.

Verardo A E, Butler P C, Bush D M, Miller D W, (1981). Testing Batteries for Photovoltaic Power Systems. *16th Intersociety Energy Conversion Engineering Conference, Proceedings*, 1981, 680-684.

Voss, E and Huster G, (1967). The Effect of Depth of Discharge on the Cycle Life on Positive Lead Acid Plates. *29th Mtg AGARD prop and Energ Panel*, Belgium.

Zmood R B, McCluskey T A, Rand D A J, Baldsing W G A, Hill R J, (1988). Re mote-Area Domestic Power Supplies: Simulated Load Profiles for Battery Testing. *Electrochemical Society Proceedings*, Symposia on Stationary Energy Storage, 1988, 375-93.

B1. Life Cycle Costing

For renewable energy systems there are two major cost components: usually a high capital outlay and the lower operating costs. Comparison with conventional energy supply options is difficult unless the systems are compared on a cost per unit energy basis over the system lifetime.

Net present value methods (NPV) discount all money to be spent in the future to the present value. The NPV of the project indicates the project life cycle cost. The unit energy cost is the NPV divided by the total energy produced over the system lifetime.

$$NPV = I_{t=0} + \sum [\, I_t \, x \, (1 + i/100)^{-t} \,]$$

where

NPV = net present value of the project at time $t=0$
$I_{t=0}$ = expenditure at time $t=0$
I_t = expenditure at time t
i = real interest rate

Energy cost = NPV/total energy produced

The life cycle costs and the unit energy cost for the systems analyzed in Chapter 2 are shown in Appendix B2.

TYPICAL SUPPLIER SYSTEM
Life Cycle Costing

Base Case Assumptions

Interest rate (%)	5
Battery life (years)	10
System life (years)	20
Panel (Wp)	325
Battery size (Ah)	540
Daily load (Wh)	1000

A deep cycle antimony battery is used. Daily DOD is 15%, with no seasonal element. Expected life is ten years under these mild conditions. Battery cost is R581 for a 2V 540Ah cell.

Panel cost is R20/W_p.

The daily load of 1000Wh/day is actually a nighttime only load, so that 100% of the energy is cycled through the battery.

The ARCO sizing program showed 5 days of autonomy.

LIFE CYCLE COSTING: Variation with battery life

Battery life (years)	3	5	10	15
Capital Costs				
panel	6480	6480	6480	6480
battery	3488	3488	3488	3488
balance of systems	344	344	344	344
TOTAL	10302	10302	10302	10302
O & M Costs				
Battery replacement	11642	7081	3111	1510
Maintenance	1956	1956	1956	1956
TOTAL	13598	9037	5067	3466
Life Cycle Cost (R)	**23900**	**19339**	**15369**	**13768**
Energy cost (c/kWh)	**525**	**424**	**337**	**302**

LOW-COST PV SYSTEM
Life Cycle costing

Base Case Assumptions

Interest rate (%)	5
Battery life (years)	2
System life (years)	20
Panel (Wp)	41
Battery size (Ah)	200
Daily load (Wh)	200

An automotive battery is used. Daily DOD is 5%, with seasonal DOD of 20%. Expected life is two years under these conditions. Battery cost is R250 for a 12V 100Ah cell.

Panel cost is R20/W_p.

The daily load of 200Wh/day is actually a nighttime only load, so that 100% of the energy is cycled through the battery.

LIFE CYCLE COSTING: Variation with battery life

Battery life (years)	1	2	3	4
Capital Costs				
panel	820	820	820	820
battery	500	500	500	500
balance of systems	47	47	47	47
TOTAL	1387	1387	1387	1387
O & M Costs				
Battery replacement	5832	2845	1735	1353
Maintenance	292	292	292	292
TOTAL	6124	3137	2027	1645
Life Cycle Cost (R)	**7511**	**4524**	**3414**	**3032**
Energy cost (c/kWh)	**916**	**552**	**416**	**370**

BATTERY SIZING CONSIDERATIONS IN STAND-ALONE PHOTOVOLTAIC SYSTEMS

Introduction

A full treatment of battery sizing in PV systems is outside the scope of the present study. In fact a primary aim of this study was to obtain initial battery data suitable for use in computer simulation modelling which is necessary in order to assess detailed implications of array and battery sizing in relation to load and climatic conditions.

At this stage, however, it may nonetheless be helpful to refer briefly to two common stages in sizing batteries for PV systems. The first stage concerns estimating the available battery storage required to provide a certain reliability of power supply from the specified system. The second entails checking factors which constrain battery sizing choices, taking into account factors such as maximum allowable depth of discharge, temperature effects and charge rates. Present PV sizing methods typically treat these as two distinct stages, but the discussion which follows will show that they are interrelated, and that considerable knowledge of battery operating environment and characteristics is needed to make optimal choices.

PV System Sizing by Loss of Power Probability Methods

A wide variety of methods of sizing the major components of a PV system are in use, ranging through rules of thumb, amp-hour methods through to statistical loss of power probability (LOPP) methods. In contrast to many rule of thumb PV sizing techniques, the LOPP method attempts to size systems for a specified loss of system availability over the entire year. The LOPP method is attractive as it provides a basis for comparing the performance of systems sized using this technique, and in principle should lead to more exact determination of system sizing for particular applications.

Major developments in LOPP techniques include methods put forward by Borden et al (1984) and Chapman (1987). These are discussed in Borchers (1989) together with recent advances by Cowan (1990).

For a given daily load demand and for a given geographical site there is a range of PV/battery size combinations that will satisfy a specified LOPP, say 0.01. This means that the system will be able to supply the given load demand 99% of the time, on average over a duration of a several years at the particular site. Usually one of the range of PV/battery combinations has the lowest levelised life cycle cost (LCC) and is said to be the most cost effective power supply option over the specified payback period. The life cycle costing includes estimates of battery replacement costs, system maintenance costs and other relevant parameters (Morris,1988).

Now as an illustration, consider a hypothetical system located in the Northern Transvaal, designed to support a 180W daily load with a specified LOPP of 0.01. The method of Cowan (1990) embodied in the POWERCOST sizing program developed at EDRC (Borchers,1989; Davis,1990) yields a range of PV and battery combinations, and is shown in Figure 1. The solid line in the figure is the locus of points satisfying the LOPP requirements. The options range from large panel, small battery systems to small panel, large battery systems. A system configuration above the line is "oversized", and one beneath or to the left is "undersized". The oversized system will provide for more than the required energy demand at the specified LOPP and is an under-utilised installation. The undersized system will not support the required LOPP.

Consider again the options that exactly satisfy the given LOPP. The choice of PV/battery combination will determine the effective battery depth of discharge (DOD), frequency of cycling, extent and frequency of overcharge. Together these have a strong deterministic effect on the battery life.

South African economic conditions and current PV module pricing tends to favour the option with the smallest PV panel requirement, practically regardless of the resultant battery size. This skewness is a result of the high module prices compared to batteries.

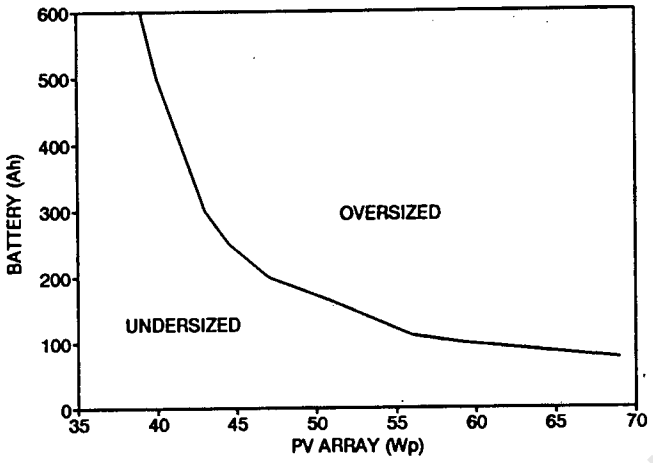

Figure 1 PV Array/Battery combinations satisfying: load=180W/day, LOPP=0.01, DOD=20%, site location Pretoria; using the method of Cowan (1990).

It is quite possible that a purely cost based selection is in contradiction to guidelines for battery sizing specified by manufacturers. In particular, PV charging currents may be less than the optimum current for the battery, (IEEE,1990). Subjecting the battery to unfavourable operating conditions is likely to shorten its projected life considerably. Compensation for decreased battery life under unfavourable conditions is not included in most sizing programs.

The LOPP methods, like most sizing procedures, do not provide insight into the dynamic operating parameters of the system. For instance, the battery depth of discharge range is not easily pre-defined or predicted, and cannot obviously be related to cycle life. There is scope for incorporating such improvements to current methods, but simulation is required to gain more reliable understanding of such dynamics.

The main considerations for selecting a battery when sizing a PV system with battery storage are illustrated by means of an example.

Sizing Example

Site description

The site under consideration is in Pretoria, South Africa. The load is of a domestic nature, typically 180Wh/day throughout the year, and is drawn at night times only. Appliances are restricted to a few lights and a television set. Nominal system voltage is to be 12V.

LOPP sizing

Detailed historical weather data are available for Pretoria, including insolation, wind speeds and ambient temperatures, so the LOPP method is an appropriate method for determining the basic PV array/battery combinations that will provide the load. The loss of power probability acceptable for domestic loads is usually taken to be 1% or 0.01. Figure 2 shows the range of array/battery combinations satisfying the LOPP for the given load in Pretoria. At this stage, the battery capacities indicated by the sizing are the raw required capacities unadjusted for DOD or any other parameters.

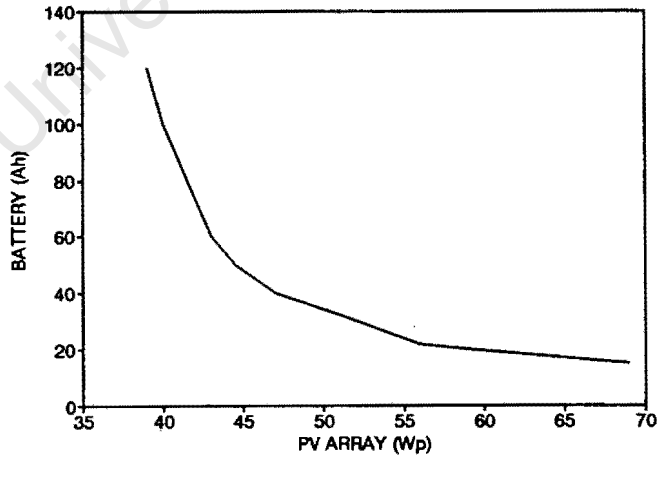

Figure 2 PV Array/Battery combinations satisfying: load=180Wh/day, LOPP=0.01, DOD=100%, system voltage =12V, site location Pretoria; using the method of Cowan (1990).

Battery size selection

Each PV application can present the designer with requirements that are specific to that application. The battery requirements are usually considered to ensure reliable performance. Different batteries have different operating parameters, and battery that performs exceptionally well in one application may perform poorly in another.

In this example only flooded, vented, tubular antimony grid cells are considered. They are suited to low discharge currents typical of domestic systems. They can withstand considerable overcharge and often have large electrolyte reservoirs to minimise maintenance requirements. They also have can have long life at deep daily discharges.

Selecting the battery size requires determining which point on the LOPP curve provides the most suitable operating regime once the battery has been derated and checked for several factors. Systematic methods for appropriate derating and checking procedures have recently been published by Chapman (1989) and IEEE (1990). The most important considerations drawn from these are summarised as follows:

CRITERIA

1) operation within the voltage window required by the load. Certain loads (motors and inverters) have maximum and minimum voltage requirements, particularly during startup when high currents are drawn.
2) normal and maximum discharge currents less than the maximum discharge rate for the battery.

3) maximum depth-of-discharge (MDOD). Manufacturers usually specify a DOD which should not be exceeded at any cost. For calcium grid batteries the maximum is typically 40%, for deep cycle tubular 80% is common. The adjustment is applied to the raw required capacity.
4) maximum daily dod (MMDOD). The daily depth of discharge contributes towards the determination of battery cycle life. This

adjustment is applied to the maximum daily load (Ah), though there is uncertainty attached to the optimum DOD.

5) end-of-discharge (eod) voltage detectable by load-shed device.
6) temperature variation of eod voltage. If the system requires accurate load shed protection, then the rate of voltage change at the load shed should be easily detectable, and the temperature effects should be small. If accurate regulators are not available, then some sizing adjustment may be required.

7) SG at end-of-discharge (eod).
8) freezing point at eod, compared with minimum temperature.
9) temperature correction for capacity at minimum temperature.

10) Capacity correction for end-of-life factor. The rate of change in available capacity at end-of-life is high. The raw required capacity is adjusted is adjusted by the factor equal to the percent of original capacity available at end-of-life.
11) Self-discharge rate included in load. Antimony batteries have high relatively discharge rates, which contribute significantly to the load if battery capacity is very large relative to the array.

Maximum array current at end-of-charge voltage and maximum array current compatible with:
13) End-of charge voltage, and temperature variation. The PV array should be capable of providing sufficient voltage to float the battery (at least) even when array temperatures are high and the battery is fully charged. Effect of battery temperature on the end-of-charge voltage may be important.
14) Equalising charge rate. The array must provide at least sufficient current to equalise the battery.
15) Finishing charge rate. Suitable for finishing charge.
16) Maximum charge rate. The maximum charging rate should not be exceeded, and is usually array limited.

17) Sufficient gassing provided to prevent stratification. This is crucial for most flooded electrolyte batteries, particular tall tubular. The amount

of gassing required will depend heavily on whether partial state of charge operation occurs.

These factors should be considered when selecting battery/array points on the LOPP curve, to get the actual battery size required and to check that criteria for suitable charge/discharge regimes are not violated.

The approach usually adopted follows. The raw required battery capacity from the LOPP method should be separately derated for:

MDOD
MMDOD
end-of-life factor
maximum charge current
maximum discharge current

The maximum of these capacities provides the derated capacity, which is then further derated for temperature to provide the required capacity. The results should again be re-checked against operational requirements numbered above, to ensure that the following are resolved:

1) maximum charge rate
2) overcharging
3) undercharging
4) high rate discharge
5) electrolyte freezing
6) self-discharge
7) electrolyte reserve/maintenance period

Some of these require knowledge of operating parameters not provided by sizing.

For this example the specifications and laboratory data of the RMT108 are used. The data sheet and derating is shown in Tables 1 and 2. In most cases the depth-of-discharge is limiting. In the case of the RMT108 the charging current may be critical, and should be at least 3% of the capacity to ensure should ensure stratification prevention. The LOPP curves showing the raw and the required

battery capacity are shown in Figure 3. The 3% and 7% charging current lines are also shown, based on the maximum current delivered from the panel at 800Wm^{-2} at 45°C. Typical average currents would be lower.

Table 1 Battery data sheet for derating

MDOD (%)	60
MMDOD (%)	40
maximum charge rate (A)	15% of C_{10}
finishing charge rate (A)	7% of C_{10}
equalising charge rate (A)	3% of C_{10}
maximum discharge rate (A)	15% of C_{10}
end-of life factor (% of C_{10} when life is over)	80
self discharge (% / month)	2
temperature correction (@ 10°C)	0.92
SG when discharged to MDOD	1.22
freezing point when discharged to MDOD (°C)	-30

Table 2 Derating of raw required battery capacity

LOPP array size (Wp)	69	59	52	47	43	39
LOPP raw battery size (Ah)	15	20	32.3	40	60	120
Array I_{max} (at 800Wm^{-2} & 45°C)	3.94	3.37	3.91	2.69	2.46	2.23
Array I_{eq} (@ regulator 13,8V)	3.68	3.14	2.72	2.50	2.30	2.08
Battery I_{eq} (minimum required)	(1.21)	(1.21)	(1.74)	(2.16)	(3.24)	(6.48)
Derating of raw capacity						
1) adjust for MDOD	25.0	33.3	53.8	66.7	100.0	200.0
2) adjust for MMDOD	37.5	37.5	37.5	37.5	37.5	37.5
3) adjust for end-of life	18.8	25.0	40.4	50.0	75.0	150.0
4) adjust for max charge	32.9	28.1	24.3	22.4	20.5	18.6
5) adjust for max discharge	23.3	23.3	23.3	23.3	23.3	23.3
Derated capacity [maximum of 1) to 6)]	37.5	37.5	53.8	66.7	100.0	200.0
Adjust capacity for temperature	40.5	40.5	58.1	72.0	108.0	216.0

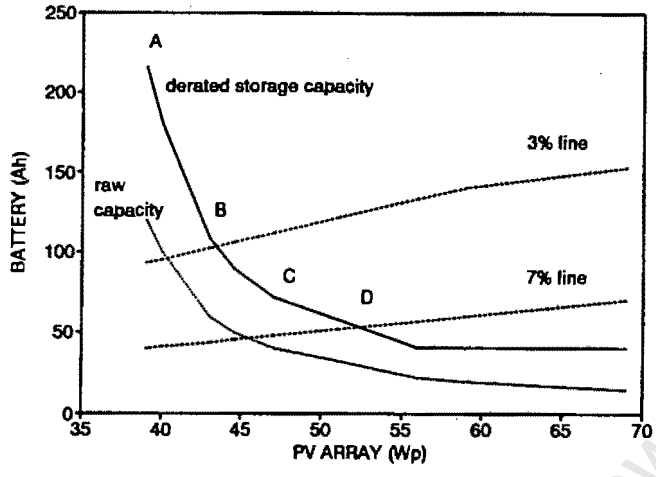

Figure 3 Adjusted LOPP curve after battery derating.

DOD determination

One could simply select the option with optimum cost from Figure 3. Unfortunately the cost is directly related to the battery cycle life, which is in turn determined by the operating conditions. For long life batteries like tubular cells it is important that conditions are moderate, otherwise the long life may well not be achieved. Here system simulation can be of value. PVPRO (Geerdts,1990) was used to determine DOD profiles employing empirical data for the battery gained from results presented in Chapter 7. The simulated DOD profiles of four systems selected from the LOPP curve are shown in Figure 4. The systems are shown on the LOPP curve and array and battery sizes tabulated below. The effect of PV array/battery ratio on DOD profile is clearly demonstrated. As the array becomes smaller, the period of extended partial SOC operation increases, and the battery becomes less likely to be fully charged at all. Even if the cycle life projected by battery models were the same for cases A,B,C and D, cases A and B would be seriously stratified after one year, which could be irreversible and probably life limiting. There is some scope for controlling and increasing gassing by adjusting the charge regulator set points.

Table 3 Array and battery sizes used in simulations

	Array (W_p)	Battery (Ah)
Case A	39	216
Case B	43	110
Case C	47	72
Case D	52	58

Charge regulator settings and gassing determination

Daily Ah overcharge can also be easily determined from simulation. The Ah overcharge for the four cases already simulated is shown in Figure 5. The peak daily array currents obtained are also shown. The regulator voltage in the simulations is set at 2.3V/cell (13.8V), and is not temperature compensated.

The overcharge is, as expected, highly seasonal. A single figure for measuring the overcharge following the period of partial SOC operation might be the mean daily overcharge divided by the battery capacity. This figure is called the daily overcharge percent. The effect on daily overcharge percent of resetting the charge voltage to 2.42V/cell (14.5V) is illustrated in Figure 6. For case A, the regulator has almost no effect, while for case D overcharge is almost uncontrollable.

Cases B and C provide optimum overcharge and the ability to tune the system after installation. Cases B and C correspond with the equalise and finishing rates recommended by the battery manufacturer.

Sizing to alter the effect of regulator and battery

From the simulations it is clear that the battery in case C may be in danger of being overcharged during regulator failure (depending on the regulator design), and that the regulator is of prime importance. The normally ideal and mild

operating parameters experienced by the battery make its response predictable, and its likelihood of premature failure during normal regulator operation is low. But the regulator in system C is critical, and failure of the regulator to regulate will be disastrous. A series regulator, which shuts down completely on failure may be the most appropriate choice. The heavy duty cycle of the regulator could indeed accelerate its failure.

System B hardly requires a charge regulator, but the sizing of the system results in a battery that is highly stressed and often in a partial state-of-charge. Premature deterioration of the battery is the most likely failure route.

The relative stresses on the battery and regulator can be adjusted by altering the panel/battery ratio in the sizing procedure. No quantitative data is available however, so it is purely a matter of engineering judgement.

Costing

In principle the system with the lowest life cycle cost should be optimum. But determining the life cycle cost brings many external parameters into play, each with considerable uncertainty attached. There is uncertainty in component life, in system usage, and in costing factors such as interest rates and escalation.

The simulations of the sizing options for this system present evidence that cases A and D are totally impractical options. The battery is almost certain to suffer in the short to medium term. Practical sizing would select be somewhere between cases B and C, preferably located at the economic optimum.

Costing of small PV systems is further prone to errors in discretisation of components. For instance, the optimum battery size may be 90Ah, but the available tubular batteries are 72 and 108Ah. A similar predicament occurs for panel selection, so optimisation is not linear, but rather stepwise. Discretisation of components will alter system performance parameters. The choice of components sizes and relative costs will depend on the system suppliers. Panel prices may vary linearly with size, but tubular battery costs are non-linear for small sizes.

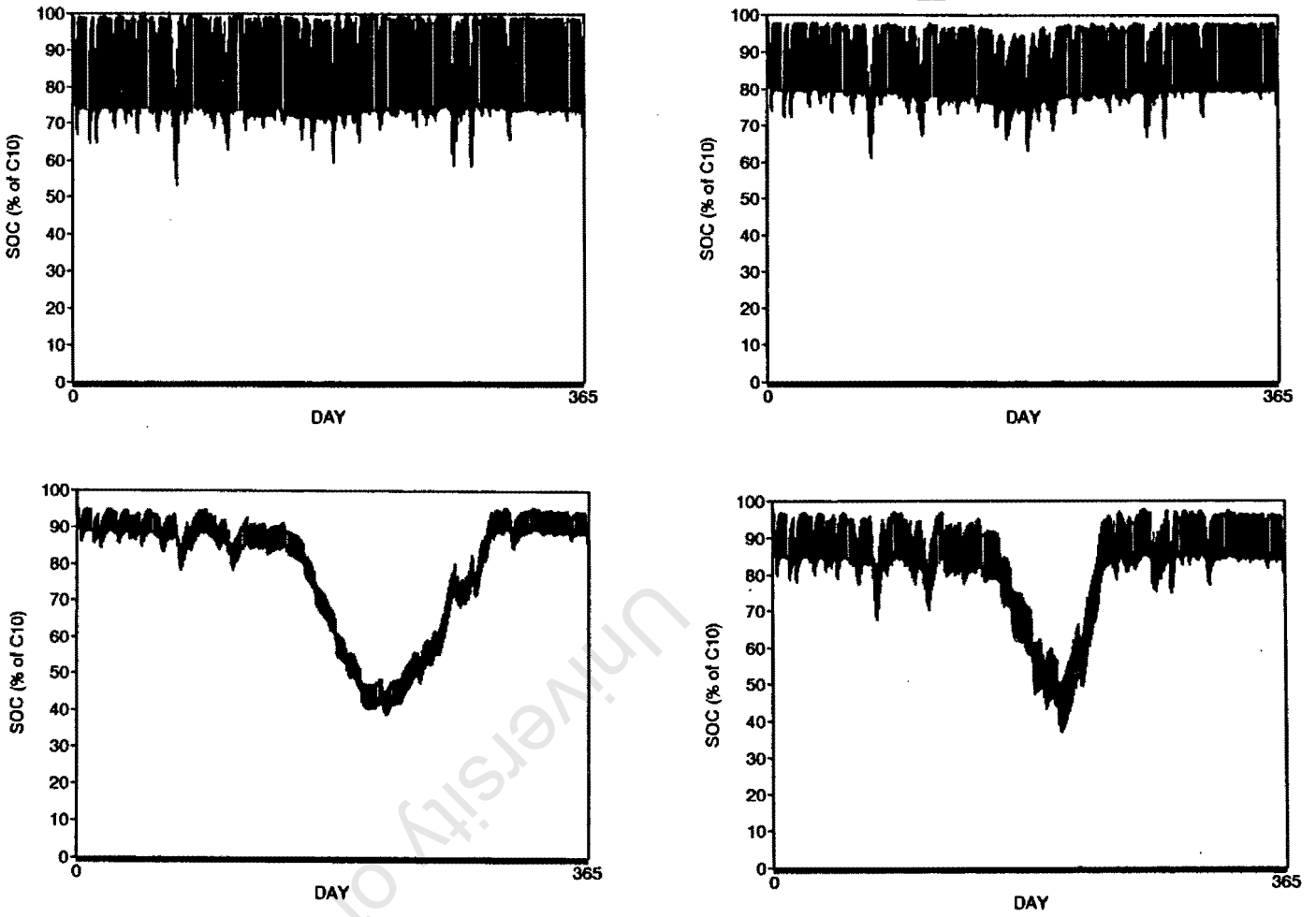

Figure 4 DOD profiles for the four cases under consideration. (Clockwise A, B, C, D)

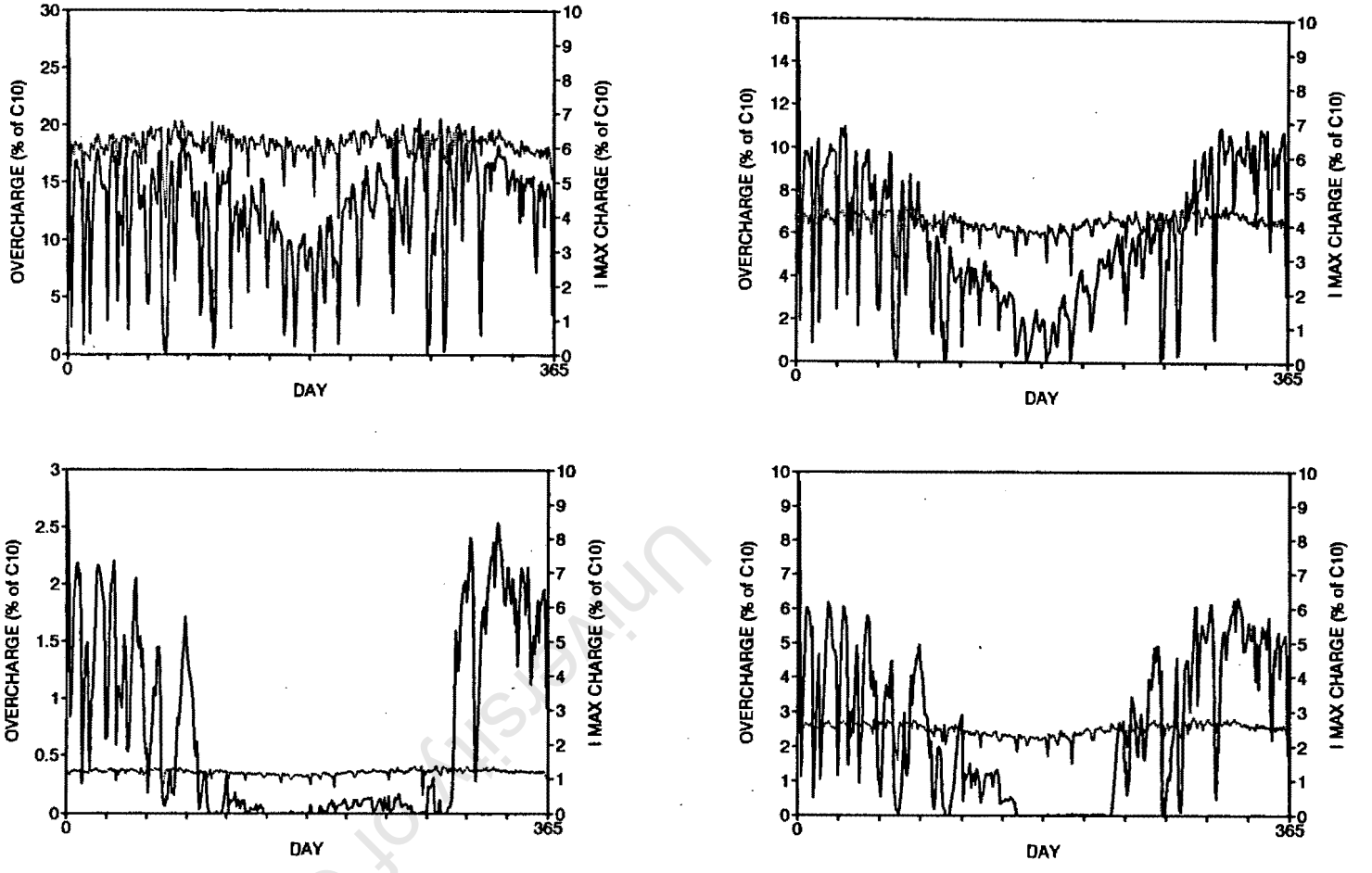

Figure 5 Daily overcharge profile for cases A,B,C and D.
Charge regulator setting = 13.8V. Dashed line represents charging current.

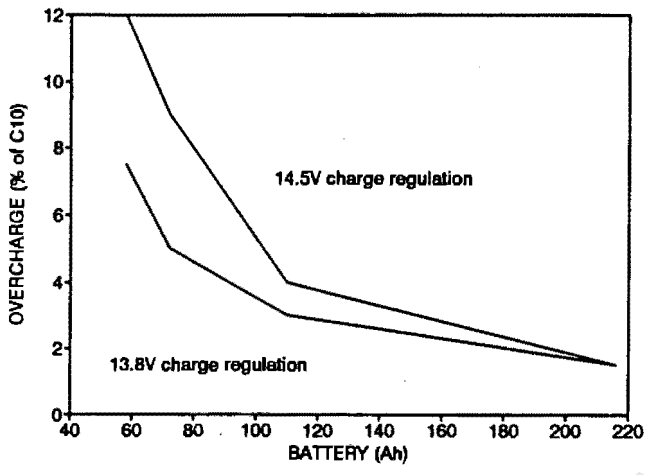

Figure 6 Daily overcharge percent for cases A,B,C and D, showing effect of charge regulator setting.

D. Manufacturers' Battery Data

This appendix contains the data provided by the manufacturers for the batteries tested. The batteries are:

- Willard 774
- Raylite RMT108
- Willard LS90
- GNB Mini-Absolyte 12V-5000
- Delco 1250

In addition, data for the specialist PV batteries discussed in Section 3.13 are appended. These batteries are:

- BP Solar P-series Tubular Cells
- Sonnenschein A600 Solar Battery

D1. WILLARD 774

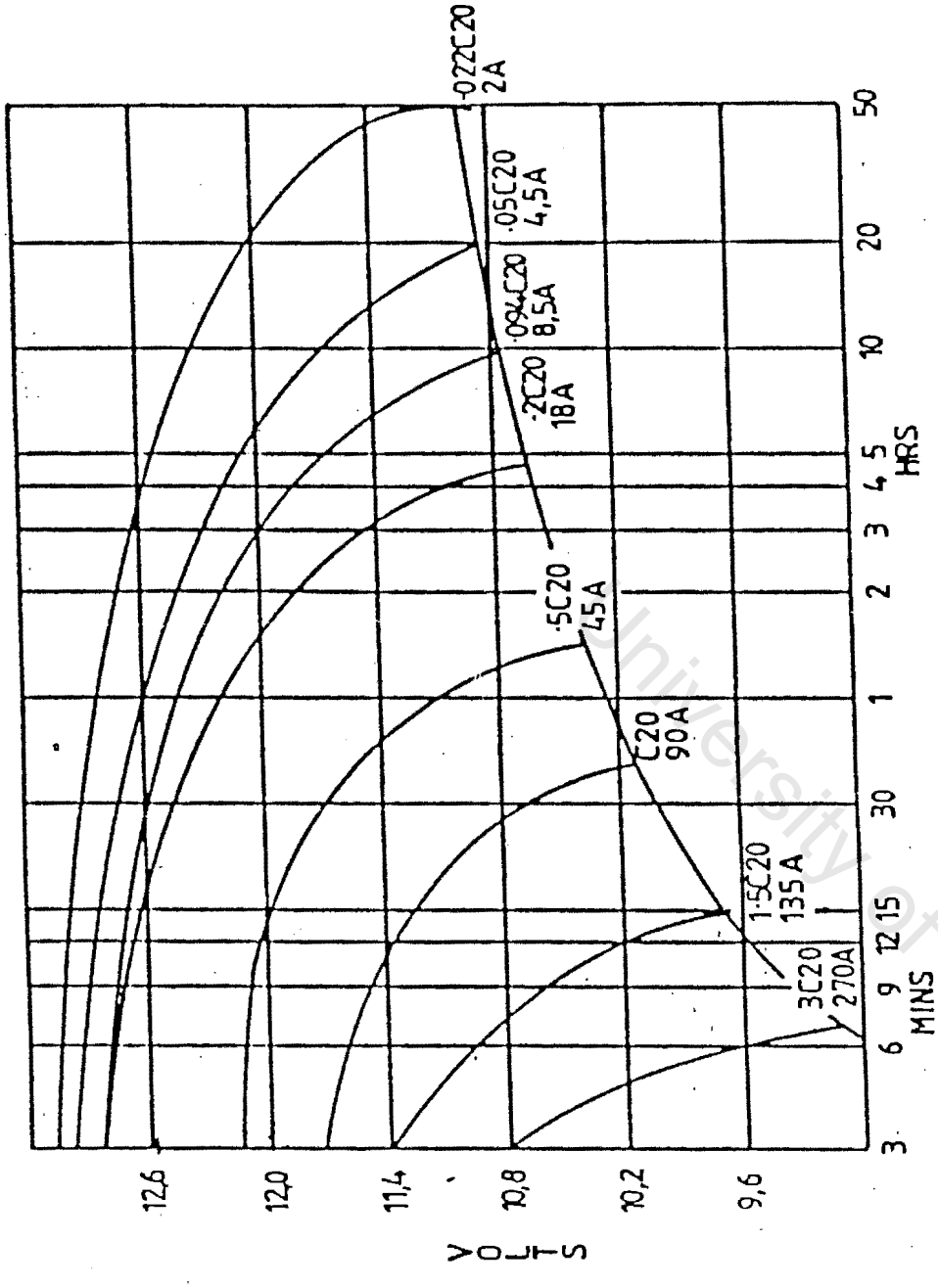

D2. RAYLITE RMT108

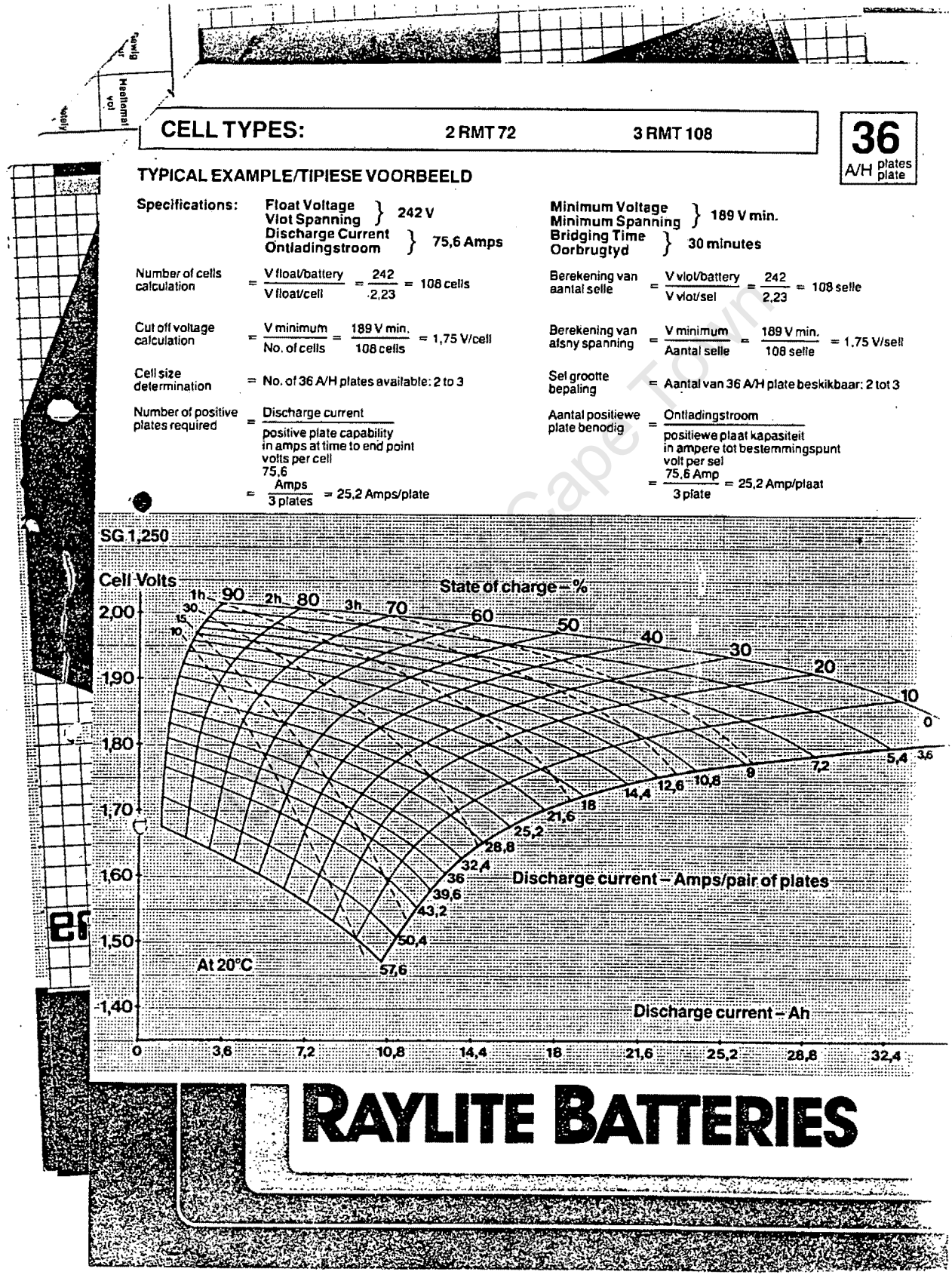

D2. RAYLITE RMT108

Raylite noodkragselle	Kapaasiteit A/uur	Ontladingstyd uur	Ontladingstroom amp	Finale spanning	Laaistroom Begin amp	Laaistroom Eindig amp	Ampereuur per pos. plaat (10 uur)	Afmetings van sel Lengte Breedte Hoogte	Hoogte bo battery-klem	Sel Droog	Gewig Suur alleen	Heeltemal vol
Raylite Standby Power Cells	Capacity A/Hrs.	Discharge Time Hrs.	Discharge Current Amps	Final Voltage	Charging Current Start. Amps.	Charging Current Finish. Amps.	Ampere-Hrs./ Pos. Plate (10 Hr)	Length Width Height/ Cell mm	Height Over Terminal	Dry Cell Kg	Weight Acid Only Kg	Completely Filled Kg
4V 2 RMT 72	72 62 54	10 5 3	7,2 12,4 16	1,85 1,81 1,78	10	5	36	130 208 312	360	11	5,1	17,1
4V 3 RMT 108	108 93 81	10 5 3	10,8 18,6 27	1,85 1,81 1,78	15	7,5	36	180 208 312	360	14,7	8,5	23,2

Typical arrangement – double row double tier stand / Tipiese rangskikking – dubbel-ry stapelstaander	A	B	C	D	E	F	G	H	I	J	K	L
4V-2RMT 72	1 180	70	70	677	1 130	850	312	1 480	207	122	130	16
4V-3RMT 108	1 200	70	70	677	1 130	850	312	1 480	207	122	180	16

Typical arrangement – single row double tier stand / Tipiese rangskikking – enkel-ry stapelstaander	A	B	C	D	E	F	G	H	I	J	K	L
4V-2RMT 72	1 180	70	70	370	1 130	850	312	1 480	207	122	130	16
4V-3RMT 108	1 200	70	70	370	1 130	850	312	1 480	207	122	180	16

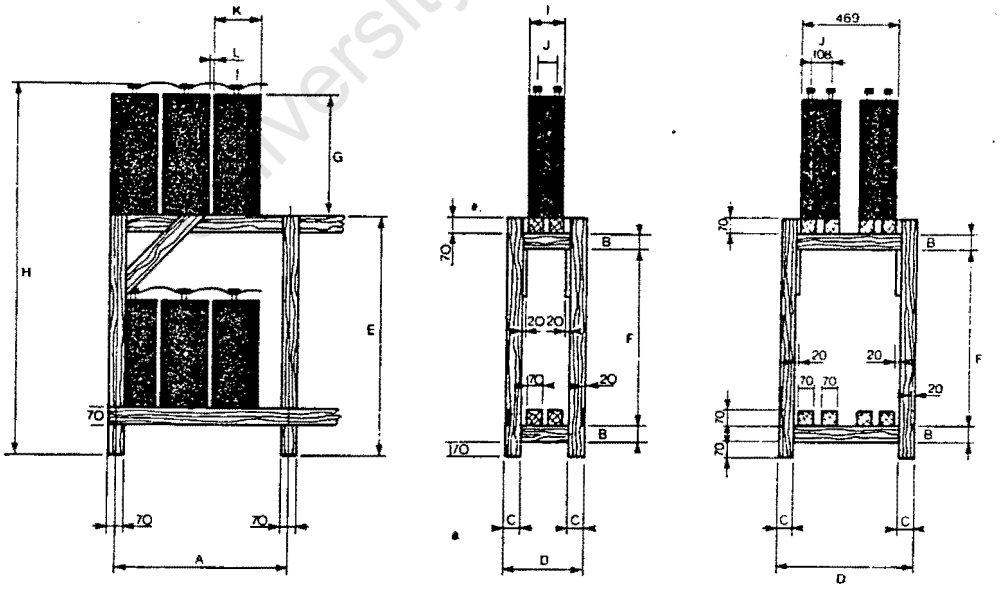

Dimensions in Millimetres Afmetings in Millimeter

D2. RAYLITE RMT108

Raylite noodkragselle	Kapasiteit A/uur	Ontladingstyd uur	Ontladingstroom amp	Finale spanning	Laaistroom		Ampereuur per pos. plaat (10 uur)	Afmetings van sel Lengte Breedte Hoogte	Hoogte bo batterykiem	Sel Droog	Gewig Suur sleen	Heelemal vol
					Begin amp	Eindig amp						
Raylite Standby Power Cells	Capacity A/Hrs	Discharge Time Hrs.	Discharge Current Amps	Final Voltage	Charging Current Start. Amps.	Finish. Amps.	Ampere Hrs./ Pos. Plate (10 Hr)	Length Width Height/ Cell mm	Height Over Terminal	Dry Cell Kg	Weight Acid Only Kg	Completely Filled Kg
6V 1 RMT 15	15 13,5 12	10 5 3	1,5 2,7 4	1,83 1,81 1,79	2,1	1,0	15	102 155 265	265	5,4	2	7,4
6V 2 RMT 30	30 27 24	10 5 3	3 5,4 8	1,83 1,81 1,79	4,2	2,1	15	153 156 230	265	8,5	3	11,5
6V 3 RMT 45	45 40,5 36	10 5 3	4,5 8,1 12	1,83 1,81 1,79	6,3	3,1	15	211 156 265	265	11,5	5,8	17,3
6V 4 RMT 60	60 54 48	10 5 3	6 10,8 16	1,83 1,81 1,79	8,4	4,2	15	265 156 265	265	14,6	6,7	21,3
4V 2 RMT 72	72 62 54	10 5 3	7,2 12,4 16	1,83 1,81 1,79	10	5	36	130 208 312	360	11	8,1	17,1
4V 3 RMT 108	108 93 81	10 5 3	10,8 18,6 27	1,83 1,81 1,79	15	7,5	36	180 208 312	360	14,7	8,5	23,2
3 RST 150	150 126 113	10 5 3	15 25,2 37,6	1,82 1,79 1,78	23	11	50	103 206 355	435	13	5	18
4 RST 200	200 168 150	10 5 3	20 33,6 50	1,82 1,79 1,78	30	14	50	103 206 355	435	14,2	4,8	19
5 RST 250	250 210 188	10 5 3	25 42 62,6	1,82 1,79 1,78	38	18	50	124 206 355	435	16,7	6,1	22
6 RST 300	300 252 225	10 5 3	30 50,4 75	1,82 1,79 1,78	45	21	50	145 205 355	435	19,6	7,3	26,9
5 RST 350	350 303 263	10 5 3	35 60,6 87,7	1,81 1,79 1,77	53	25	70	124 206 471	551	22,3	8,6	30,9
6 RST 420	420 363 315	10 5 3	42 72,6 105	1,81 1,79 1,77	63	29	70	145 206 471	551	26,2	10,3	36,5
7 RST 490	490 424 368	10 5 3	49 84,8 122,7	1,81 1,79 1,77	74	34	70	166 206 471	551	30,2	12,2	42,2
6 RST 600	600 519 450	10 5 3	60 103,8 150	1,80 1,78 1,76	90	42	100	145 208 646	726	36,3	14,7	51
7 RST 700	700 606 525	10 5 3	70 121,2 175	1,80 1,78 1,76	105	49	100	210 191 646	726	42,8	21	63,8
8 RST 800	800 692 600	10 5 3	80 138,4 200	1,80 1,78 1,76	120	56	100	210 191 646	726	47,6	19,8	67,2
9 RST 900	900 779 675	10 5 3	90 155,8 225	1,80 1,78 1,76	135	63	100	210 233 646	726	53,9	25,8	79,7
10 RST 1 000	1 000 865 750	10 5 3	100 173 250	1,80 1,78 1,76	150	70	100	210 233 646	726	58,9	24,4	83,3
11 RST 1 100	1 100 952 825	10 5 3	110 190,4 275	1,80 1,78 1,76	165	77	100	210 275 646	726	65,7	30,7	96,4
12 RST 1 200	1 200 1 038 900	10 5 3	120 207,6 300	1,80 1,78 1,76	180	84	100	210 275 646	726	70,7	29,3	100
11 RST 1 375	1 375 1 189 1 031	10 5 3	137,5 237,8 343,6	1,80 1,78 1,76	206	96	125	210 275 771	851	78,2	30,7	107,2
12 RST 1500	1 500 1 297 1 125	10 5 3	150 259,4 375	1,80 1,78 1,76	225	105	125	210 275 771	851	78,6	31,5	110,1
13 RST 1 625	1 625 1 405 1 218	10 5 3	162,5 281 406	1,80 1,78 1,76	244	114	125	212 397 771	851	85,4	34,5	119,9
14 RST 1 750	1 750 1 513 1 312	10 5 3	175 302,6 437,3	1,80 1,78 1,76	263	123	125	212 397 771	851	92,3	37,4	129,7
15 RST 1 875	1 875 1 621 1 406	10 5 3	187,5 324,4 468,6	1,80 1,78 1,76	281	131	125	212 397 771	851	99,2	40,4	139,6
16 RST 2 000	2 000 1 730 1 500	10 5 3	200 346 500	1,80 1,78 1,76	300	140	125	212 397 771	851	105,1	43,3	149,4
17 RST 2 125	2 125 1 838 1 593	10 5 3	212,5 367,6 531	1,80 1,78 1,76	319	149	125	212 487 771	851	117,1	50,2	167,3
18 RST 2 250	2 250 1 946 1 687	10 5 3	225 389,2 562,3	1,80 1,78 1,76	338	158	125	212 487 771	851	128,0	57,2	185,2
19 RST 2 375	2 375 2 054 1 781	10 5 3	237,5 410,8 593,6	1,80 1,78 1,76	356	166	125	212 487 771	851	138,9	64,2	203,1
20 RST 2 500	2 500 2 162 1 875	10 5 3	250 432,4 625	1,80 1,78 1,76	375	175	125	212 487 771	851	149,8	71,2	221,0

D3. WILLARD LS90

PERFORMANCE

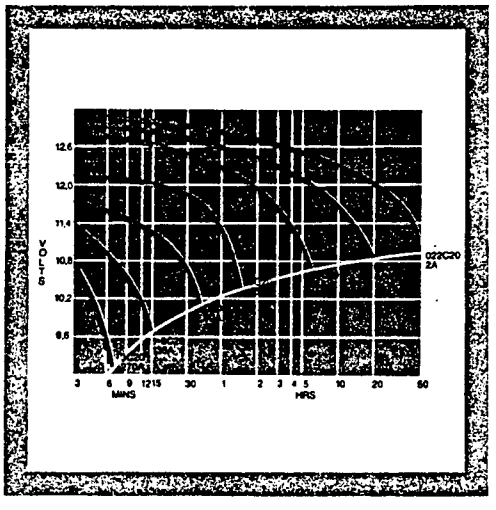

The Willard LS90 is designed for a variety of standby applications.
Calculation Methods: The following example is designed to illustrate the method of determining the number of LS90 batteries required for a specific requirement.

Application — U.P.S.

Sample of specifications
- Invertor of load — 45 kVA
- P.F. — 0,8
- Minimum Voltage — 300
- Duty Period — 15 Minutes
- Invertor Efficiency — 90%
- Maximum Voltage — 430V

Step 1 – Convert kVA to kW

$$= \frac{45 \times 0{,}8 \times 100\%}{90}$$

$$= 40 \text{ kW}$$

Step 2 – Convert kW to load in Amperes

$$= \frac{40 \times 1000}{300}$$

$$= 133 \text{ A}$$

Step 3 – By reference to the above discharge graph a constant current of 135 A is available for 15 minutes down to 9,8 Volts per battery.

Step 4 – Determine number of batteries

$$\frac{\text{Minimum System Voltage}}{\text{Minimum Battery Voltage}}$$

$$= \frac{300V}{9{,}8V} = 30{,}6 \text{ or } 31 \text{ x } 12 \text{ V LS90 batteries}$$

Step 5 – Check recharge capability of system voltage

$$\frac{\text{Maximum System Voltage}}{\text{Number of Batteries}}$$

$$= \frac{430}{31} = 13{,}87 \text{ or } 2{,}31 \text{ V/cell}$$

NB: Recommended Float Voltage at 25°C is 13,62 or 2,27 V/cell

APPLICATIONS

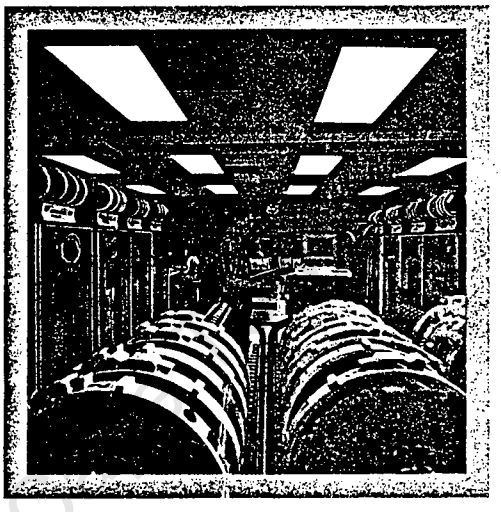

The Willard LS90 Maintenance Free battery provides ideal standby power for the following applications (Capacity 90 Ah):

- *Microwave Communications Systems*
- *Hydro Coal and Atomic Power Stations*
- *Emergency lighting supplies*
- *Diesel Starting*
- *Earth-Satellite Stations*
- *Railway signalling and substations*
- *PABX Systems*
- *Uninterruptible Power Supply Systems (U.P.S.)*
- *Radio Communication Equipment.*

Principal Advantages Versus Nickel Cadmium

Before the LS90 was introduced, lead acid batteries already had many advantages over Nickel Cadmium batteries. Now, the superior quality intrinsic to the LS90 Maintenance Free battery makes it the sensible choice for standby applications.

D4. GNB MINI-ABSOLYTE 12V-5000

RE-SOURCE™
Mini-***ABSOLYTE***™
Photovoltaic Battery

Mini - ***ABSOLYTE***™ *TYPE 12-5000*

Available in 12 volt units, GNB's Mini-***ABSOLYTE***™ battery provides the same quality, features and benefits as the tried and proven large ***ABSOLYTE II*** ® batteries – in a space saving, compact, power efficient mini-module. Cost saving, lightweight, transportable and totally maintenance-free, Mini-***ABSOLYTE***™ batteries are designed for a variety of applications including shallow or deep discharge cycling. Ideal for small power and portable installations, the Mini-***ABSOLYTE***™ battery line is the most cost effective and long lived battery of its class, with a design cycle life of more than 1200 shallow cycles.

Completely sealed maintenance free battery incorporating GNB's patented ***ABSOLYTE***® Technology.

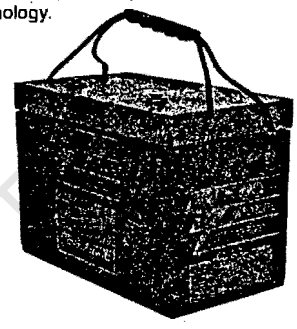

Specifications

Container and cover:	Foam polypropylene
Separators:	Spun glass microporous matrix
Safety Vent:	5 PSI (± 2 psi) self-resealing
Self Discharge:	1.0% per month after stabilizing
Terminals:	Heavy duty integral copper inserts
Charge Voltage:	2.25-2.45 VPC
Positive Plate:	Special hybrid alloy
Negative Plate:	Lead Calcium
Life:	500 cycles @ 80% DOD 800 cycles @ 50% DOD 1200 cycles @ 20% DOD

Recognizing the ever-increasing value and importance of renewable energy obtained from the sun and the wind, GNB has developed the RE-SOURCE line of lead-acid batteries that are ideally suited for use with photovoltaic or other renewable energy systems.

GNB has responded to this need by developing unique deep-cycle batteries. Because of cost, availability and reliability, photovoltaic-powered installations are being used more and more for telecommunications, railroads signals, irrigation pumps, cathodic pipeline, bridge protection and village electrification.

Innovative Features

Sealed
- Never requires watering
- Spillproof and leakproof
- No gases escape during normal charging
- Explosion resistant
- Operates at low internal pressure
- Increased operating safety

Immobilized Electrolyte
- Extended partial state of charge operation (at reduced capacities)
- Freezing tolerated
- Minimizes need for equalization

Patented Hybrid Alloy
- Deep cycle capability
- Long Life
- Low self discharge rate

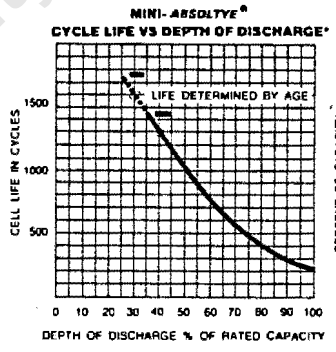

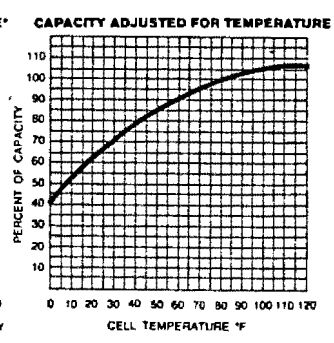

Physical Characteristics

Type	Overall Dimensions: Length in	Length mm	Width in	Width mm	Height in	Height mm	Weight: Net Ea. Lbs	Net Ea. kg
12-5000	12.75	324	6.78	173	8.47	216	63	29

Electrical Performance

Type	Nom VDC Per Cell	AH Capacity to 1.75 VPC: 8 Hr	24 Hr	48 Hr	100 Hr
ABSOLYTE 12-5000	12	85	93	96	100

Accessories

Intercell connectors (if required), installation and operating instructions, stainless steel bolts and lock washers matched to copper insert post threads, rope handle.

Please Note: Batteries are shipped at 90% of their final capacity. Designed capacity will be achieved after cycling. GNB reserve the right to change the design and specifications without notice.

D5. DELCO 1250

DELCO HIGH-CYCLE HEAVY-DUTY FREEDOM BATTERY

Description

Delco Heavy-Duty High-Cycle Freedom batteries are maintenance-free, 12-volt design combining both cranking and cycling abilities in a single power source.

Features

True maintenance-free design eliminates watering and regular service. Heavy-duty construction and wrought lead-calcium grid resist vibration, shock, overcharge, heat, and thermal runaway. Special chemistry and plate formulation for extra life, extra reserve and extra cycling capability in moderate depth discharge. High-impact polypropylene case and cover permanently assembled by heat sealing. Low self-discharge permits long storage life. Standard size for simplified stocking and mounting flexibility. Built-in test hydrometer, Liquid-Gas separator, and flame arrester protection. Available with sealed top terminals and stainless steel connecter stud or standard SAE tapered posts.

Application

Recommended for heavy-duty applications where extra life and reserve capacity is needed to carry the entire electrical load for short periods. Delco 1150 and 1151 are suited for heavy trucks in P&D, car carrier or short-haul service and for emergency vehicles, buses, marine and off-road equipment, recreational vehicle auxiliary power, and trolling motors. For energy storage system use, photovoltaic or other stationary applications, Delco 2000 offers special electrolyte and other features not offered in vehicle batteries.

Specifications

Voltage: 12-volt

Maximum Ambient Temperature:
Continuous—52°C (125°F)
Intermittent—77°C (170°F)

Mounting: Top retainer

Performance: See table

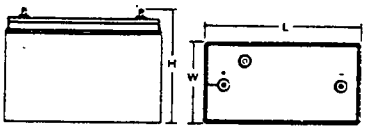

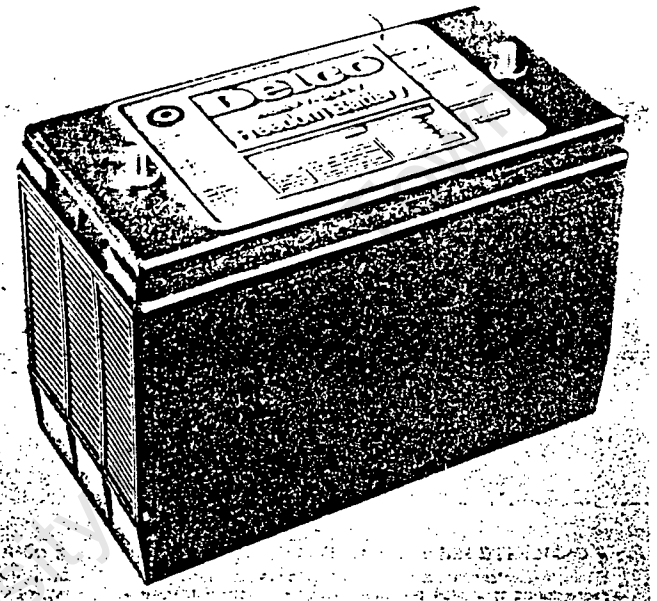

BCI Group Size	Cold Cranking Amps @ 0°F (−18°C) 30-sec. 7.2V	Reserve Capacity Minutes @ 80°F (27°C) 25A, 10.5V	Maximum Dimensions			Approx Weight Lb (kg)	Type Terminal	DR Model Number	Replacement Part Number
			Length in. (mm)	Width in. (mm)	Height in. (mm)				
31	580	180	13.0 (330.2)	6.8 (172.0)	9.4 (238.8)	60 (26.9)	Top Stud	514	1150
31	580	180	13.0 (330.2)	6.8 (172.0)	9.4 (238.8)	60 (26.9)	Top Post	8195	1151
31	Amp-Hour Rate (100-hr) 105		13.0 (330.2)	6.8 (172.0)	9.4 (238.8)	60 (26.9)	Top Stud	860	2000

D5. DELCO 1250

DELCO HIGH-CYCLE MAINTENANCE-FREE HEAVY-DUTY FREEDOM BATTERY

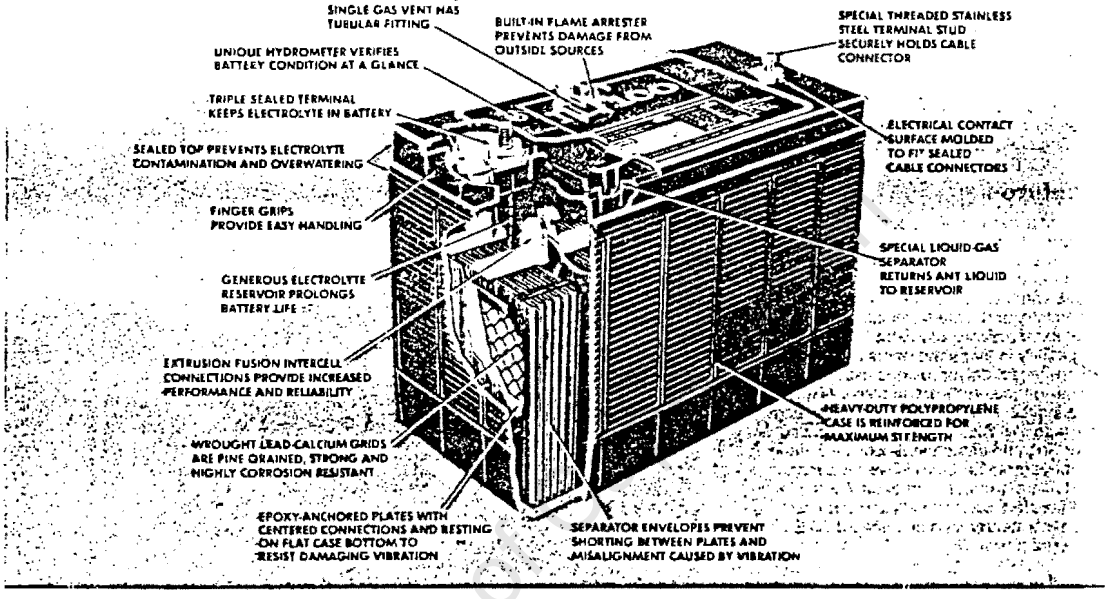

■ INCREASED SERVICE LIFE

Eliminating water filler caps prevents electrolyte contamination, overwatering or damage to internal elements. Vibration-resistant construction—with center lug connections, epoxy-anchored plates resting on flat case bottom, and separator envelopes—help prevent damage in rugged use. Eliminating antimony from the plates cuts gassing, resists overcharge, heat and thermal runaway. Unique grid design with wrought alloy means less internal corrosion, more efficient current conductivity for more power and more life. Generous electrolyte reserve, factory checked for purity and specific gravity, is sealed in to last the service life of the battery. The result is a battery that, when properly applied, provides real maintenance-free performance for long periods without service and inspection.

■ HIGH CRANKING POWER

Delco High-Cycle, rated at 580 CCA, packs plenty of power for faster starts with large diesels. A four battery complement provides 2320 CCA, with nearly 1000 minutes reserve capacity. Thus, the Delco High-Cycle can provide substantial advantages in power, performance and electrical hook-up.

■ SIMPLIFIED STOCKING AND STORAGE

Delco High-Cycle can be fitted to almost any installation where cycling is expected. Two or more can be used in series, parallel or parallel-series to meet the cranking/cycling needs of the application and engine. Plus, the battery comes fully activated, charged and ready to go. Antimony-free plates reduce self-discharge and increase wet storage life to a year or more in vehicle uses. This eliminates trickle charging, activation and acid handling.

■ LONG CYCLING LIFE

Until now, batteries were either designed for cranking use—with high power output for short periods of time—or they were designed for cycling use—long, steady drains, followed by recharge. Now, with the new plate design and maintenance-free technology, the Delco High-Cycle offers both. The plates resist deterioration in cycling use...where conventional battery plates rapidly wear out or warp, shed and eventually short out. Standard tests show the High-Cycle to have about 75% greater cycling life than our best heavy-duty maintenance-free cranking battery and more than three times the life of our popular Freedom battery when used in cycling applications.

■ REDUCED MAINTENANCE

Delco High-Cycle Heavy-Duty Freedom batteries never need water or checking for water. Antimony-free plates cut electrolyte loss from gassing. The special vent design with Liquid-Gas separator helps keep electrolyte inside the battery. Cover has no filler caps to allow electrolyte spill, splash and spew. Sealed terminal design stops corrosion of terminals and cables, eliminates regular cleaning.

■ MOUNTING FLEXIBILITY

In addition to combining cranking and cycling properties, there are no routine service requirements with Delco High-Cycle. So, it offers new possibilities in mounting. Batteries can be relocated to reduce harmful vibration. This also can permit savings on cables and mounting hardware, from better use of available space, or allow larger size fuel tanks.

Delco Remy
DIVISION OF GENERAL MOTORS
ANDERSON, INDIANA 46011

DP 1000

D5. DELCO 1250

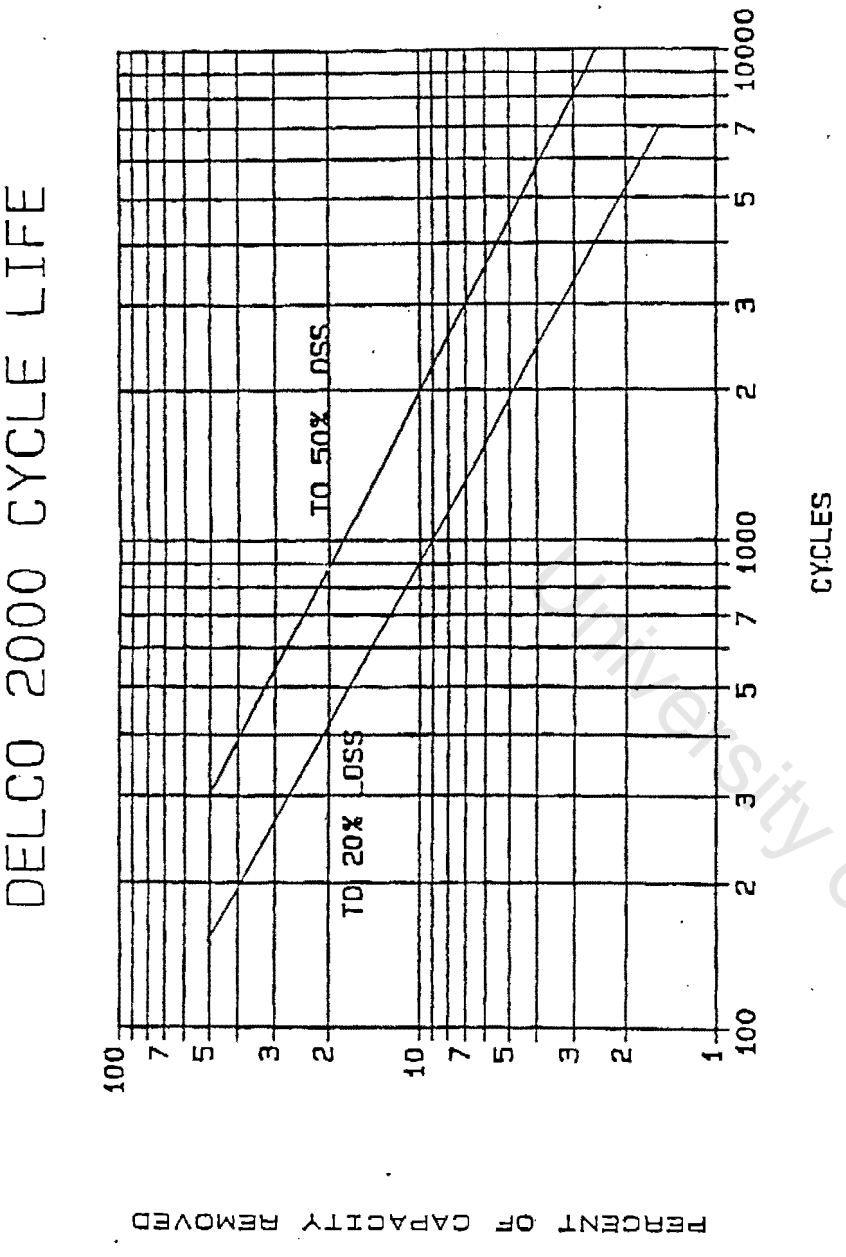

D5. DELCO 1250

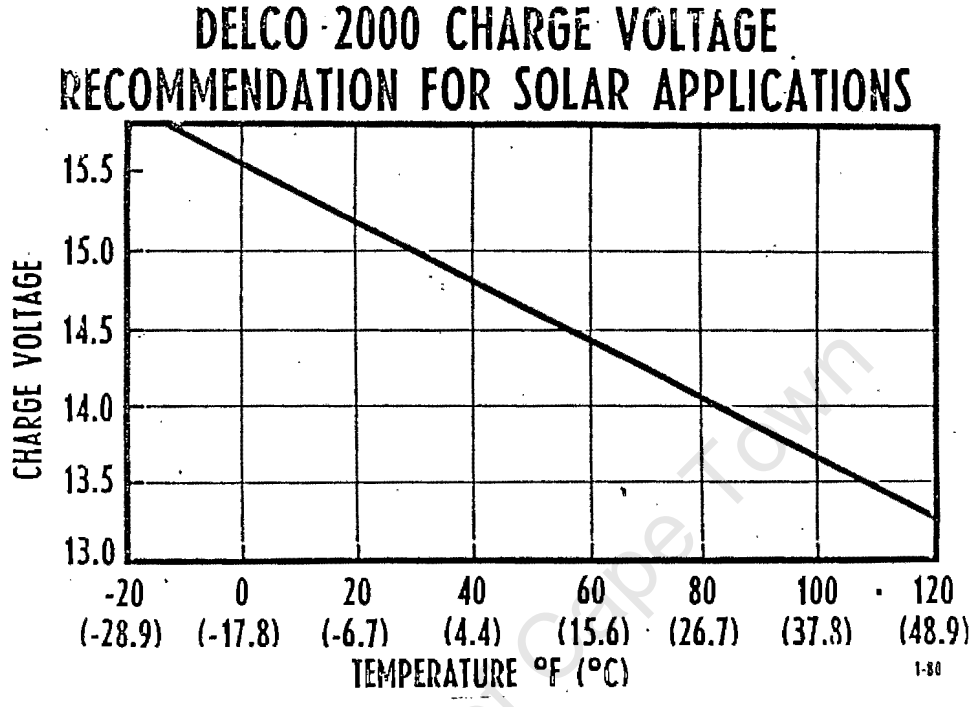

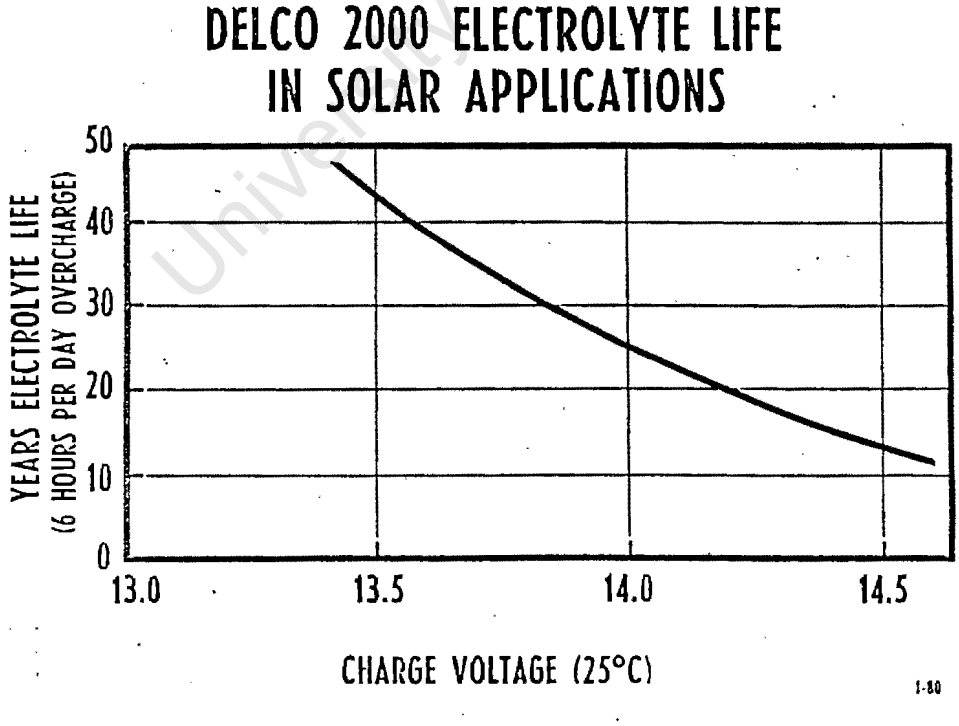

D5. DELCO 1250

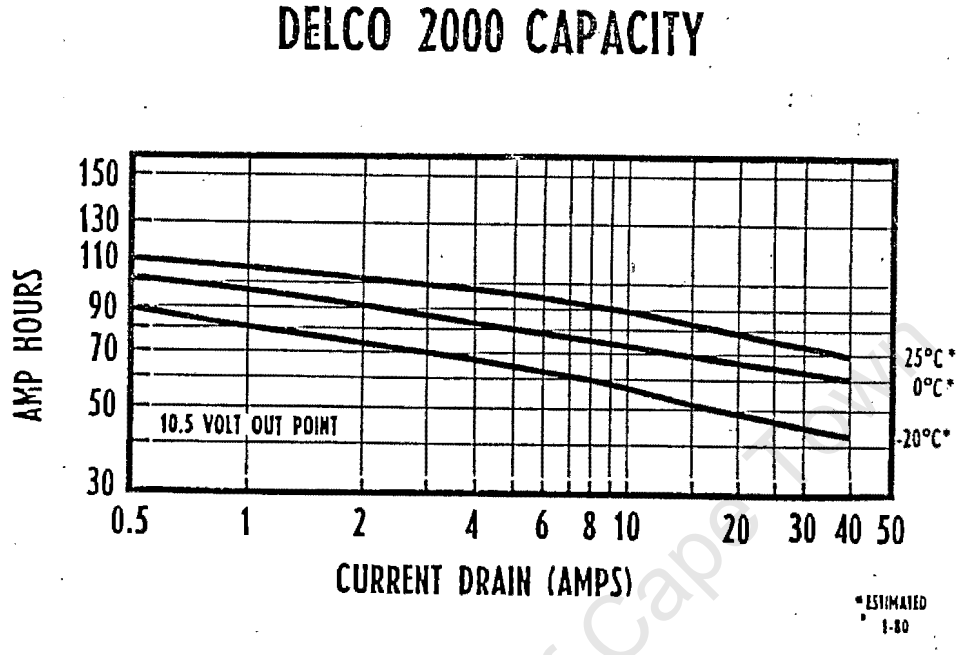

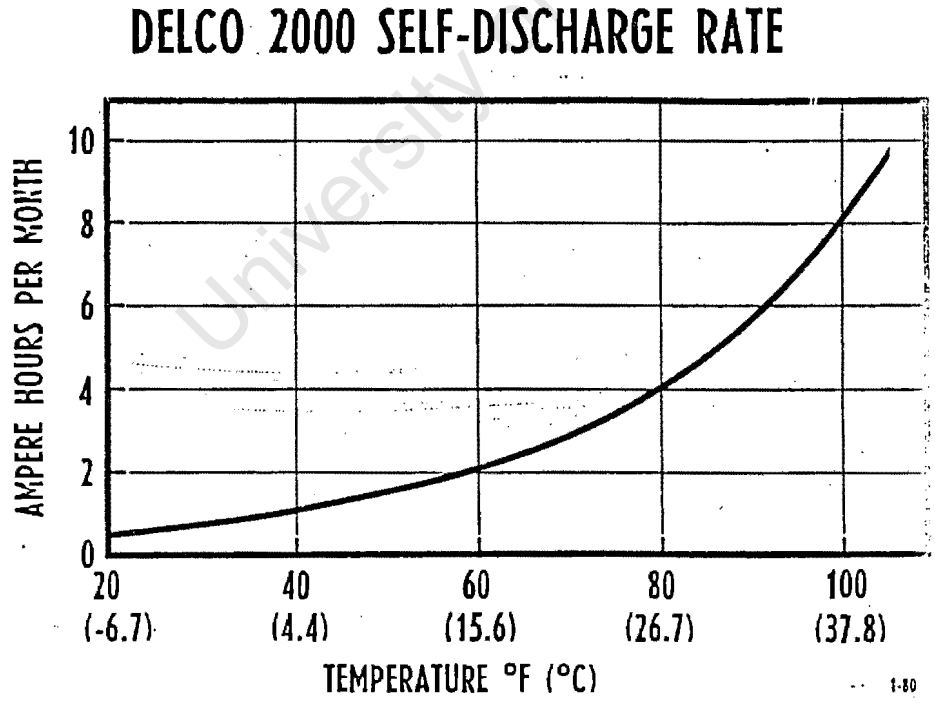

D5. DELCO 1250

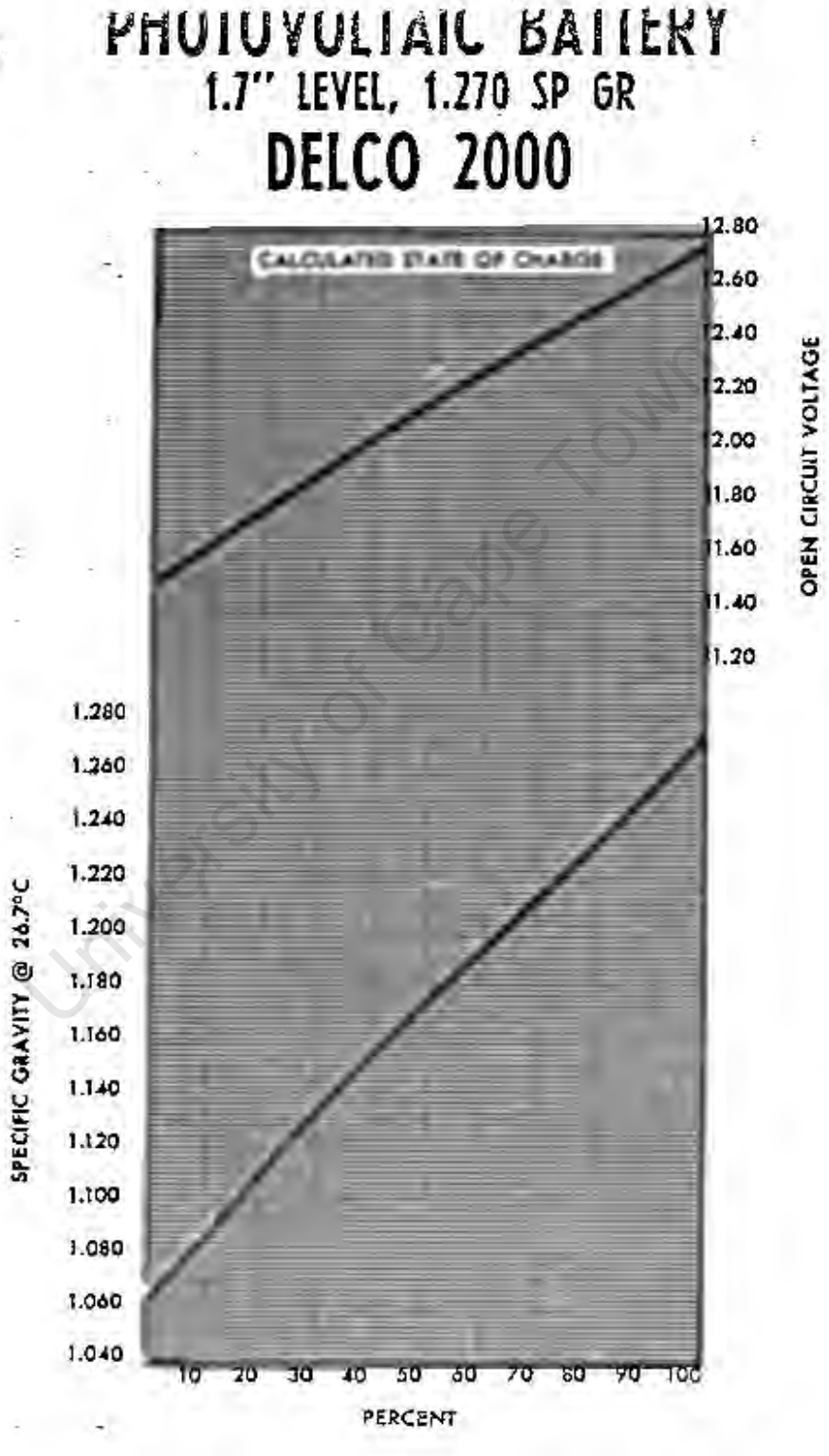

D5. DELCO 1250

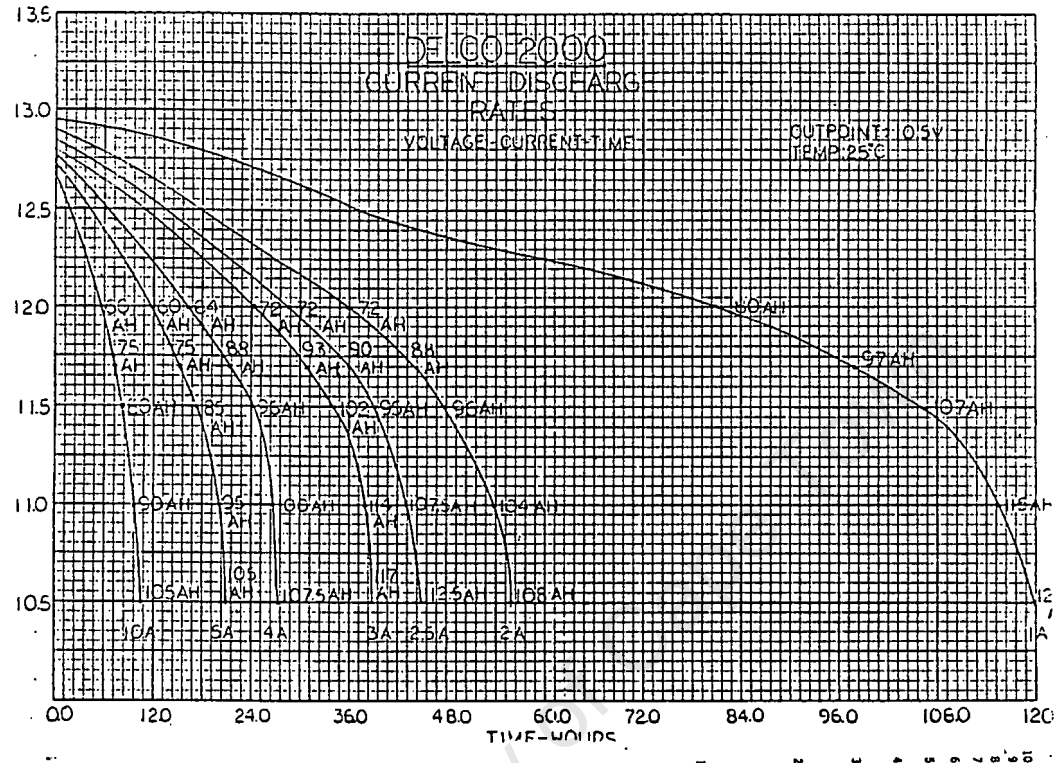

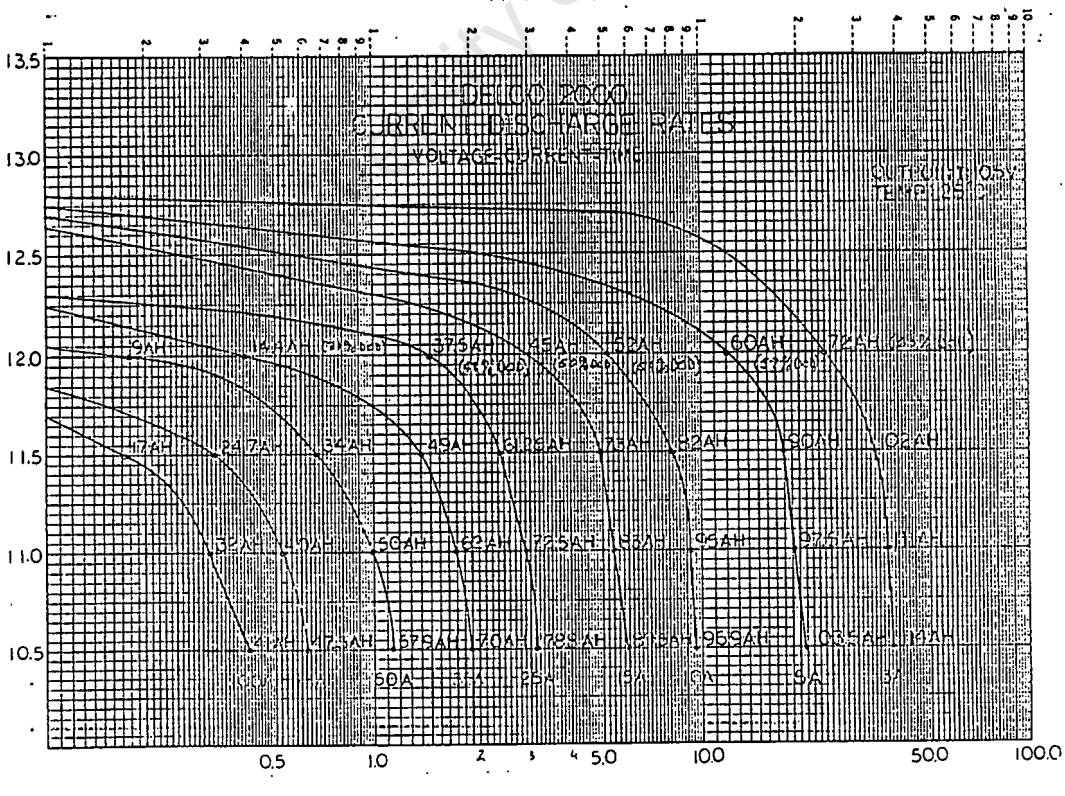

D6. BP SOLAR LUCAS P-SERIES

Technical Specification

All battery capacities are measured at 25°C, to an end voltage of 1.8 volts per cell, specification to ±10%.

Battery Type	Battery Volt	Capacity (Ah)					Dimensions (mm)			Weight (kg)	
		10 hr	25 hr	50 hr	100 hr	120 hr	Length	Width	Height	Wet	Dry
12P58	12	35	42	49	58	61	272	205	379	33.5	20
12P108	12	65	78	92	108	113	380	205	379	50	29
12P157	12	94	114	133	157	165	380	205	379	56.5	37.5
6P207	6	124	150	176	207	217	272	205	379	37.5	23
6P363	6	218	263	309	363	381	380	205	379	56.5	36.5
2P425	2	255	308	361	425	446	124	206	500	23.5	14.5
2P566	2	340	410	481	566	594	166	206	500	31.5	19
2P641	2	385	465	545	641	673	166	206	500	33	21
2P779	2	467	565	662	779	818	191	210	675	46.5	26
2P886	2	532	642	753	886	930	191	210	675	49	29
2P987	2	592	716	839	987	1036	191	210	675	51	31.5
2P1101	2	661	798	936	1101	1156	233	210	675	60.5	35.5

Larger capacities are obtainable by connecting like cells in parallel, higher voltages are obtainable from connecting like cells in series.

Performance Characteristics Charging efficiency (up to 60% state of charge) 97%.
Cycle life – to 10% discharge 7200 cycles (20 years estimated life)
– to 50% discharge 3000 cycles (8 years estimated life)
– to 75% discharge 1500 cycles (4 years estimated life)

In typical photovoltaic applications the P-series battery cell gives a minimum life expectancy of 10-12 years.

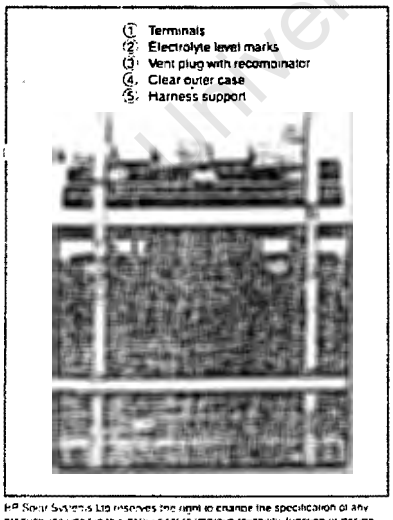

BP Solar Systems Ltd reserves the right to change the specification of any products included in this data sheet to improve reliability, function or design

Maintenance

The specialist design of the P-series battery ensures minimal maintenance. Typical field maintenance at yearly intervals involves cleaning all electrodes and topping up with distilled water.

Equipment Supply

The P-series battery cells are supplied either wet charged, or dry charged (acid supplied separately) complete with flexible insulated terminal interconnectors, pole caps and fasteners. Batteries can be supplied with flame arrestors or a catalytic vent plug recombinator system upon request. (A recombinator fits into the battery vent plug and catalytically recombines the oxy-hydrogen gas evolved during boost charging back to water. This optional system reduces battery maintenance interval to 3-4 years. recombinators are available to fit 2, 6, and 12 volt nominal cells).

As a systems supplier BP Solar recommend the use of specially designed GRP battery boxes or steel battery racks to facilitate cell storage with the optimal system configuration.

Ancillary equipment includes on-site installation/ maintenance kit consisting, apron, gloves, faceshield, thermometer hydrometer, funnel water container, eye wash kit, and de-ioniser exchange column.

D6. BP SOLAR LUCAS P-SERIES

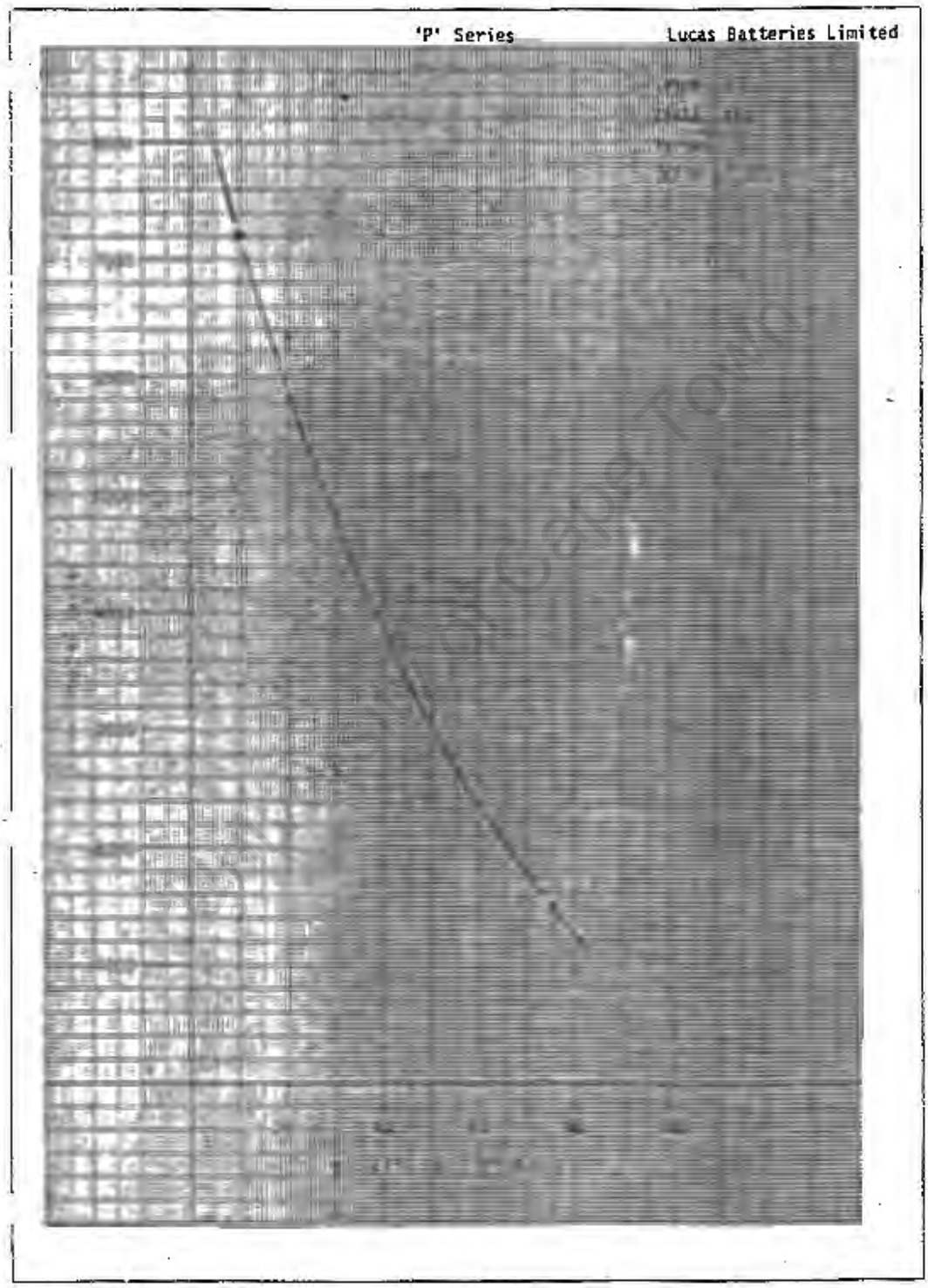

D6. BP SOLAR LUCAS P-SERIES

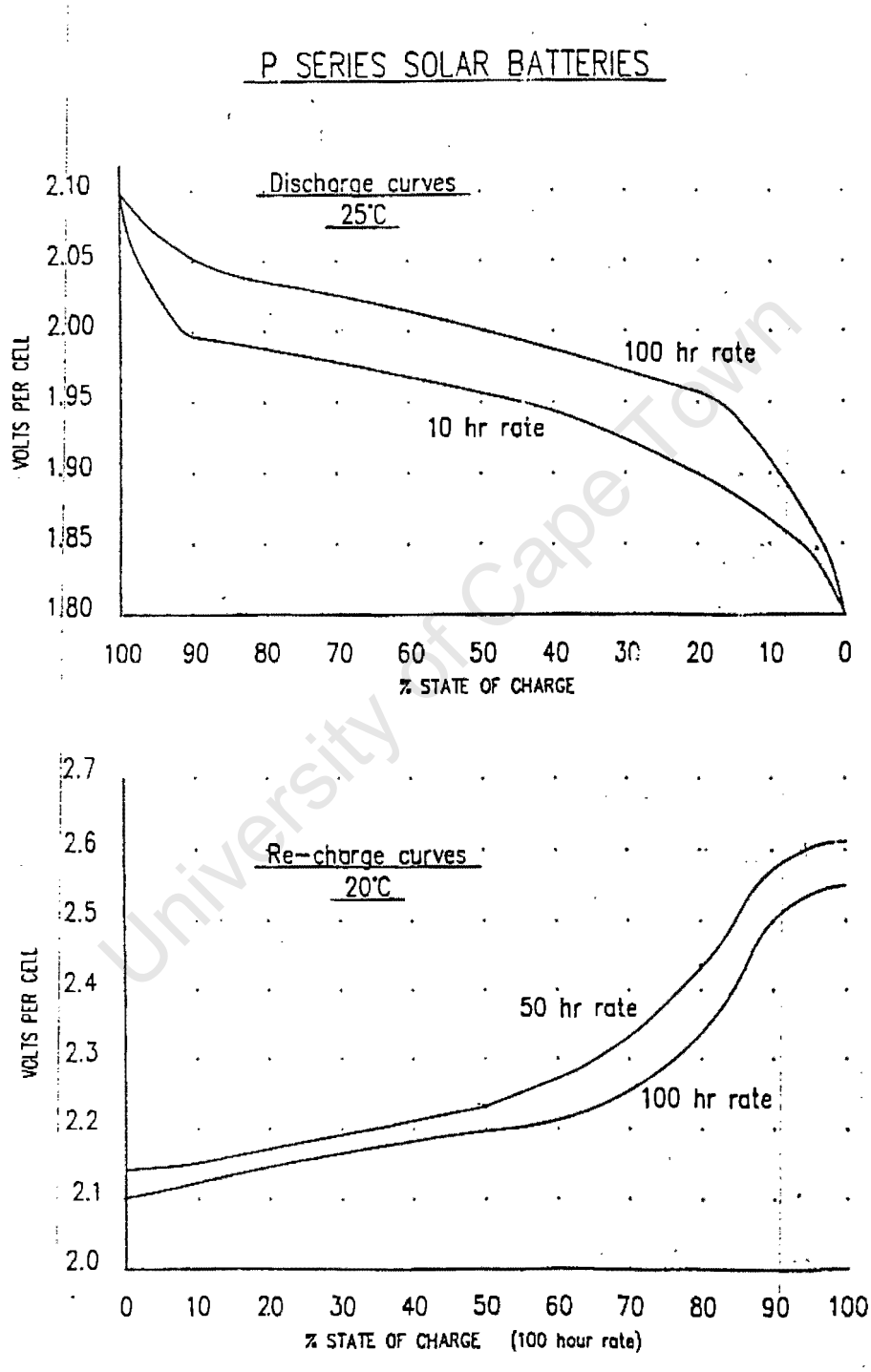

D7. SONNENSCHEIN A600 SOLAR

Sonnenschein Batteries

Sonnenschein

dryfit A600 solar

– The battery for alternative energy sources.

Alternative energy sources are always of interest where mains power is not available at the end of a plug.

It has long been known that man could obtain power from the wind, the water or the sun. For solar energy to be used in electrical applications, it has to be stored. Sonnenschein, in their A 600 solar battery – a further development from the A 600 industrial battery – have produced the ideal battery for solar energy storage. Since the efficiency of solar energy is dependent on the intensity and duration of solar radiation, it is used primarily in hot areas.

The maintenance-free A 600 solar battery has been designed for this specific purpose. Experience has shown that the conventional battery, with its regular maintenance requirement, is frequently the weak point in an installation, since in many cases service personnel are either untrained, or simply not available.

The A 600 solar battery has an exceptionally long, maintenance-free life, despite exposure to a stringent cyclic load, a higher charge voltage, during heavily concentrated energy supply (e.g. midday solar peak), and high ambient temperatures.

Similarly unaffected by these are the following properties of the A 600 solar battery:

- low self-discharge rate
- leakproof
- deep discharge proof
- cycle resistant
- suitable for high and low ambient temperatures.

The A 600 solar battery may, for example, be used:

- to store energy from solar panels, wind and wave generators
- to supply buoys, drilling platforms, radio and television relay transmitters and irrigation plants
- in pipeline monitoring stations

Battery construction

- Plates
  The A 600 battery is fitted with positive tubular and flat negative grid plates.

  The positive plate mass is surrounded by a porous, extremely strong plastic jacket – the tube. Sonnenschein tubes have an exceptionally high retention capacity, giving long life even in cyclic operation. The lead cores are die cast in a special antimony-free alloy. Microporous plastic separators are fitted between the different polarity plates.

- Electrolyte
  The electrolyte is contained in a thixotropic gel, its composition and amount especially designed for cyclic loads. The density of the acid, 1.2 kg/l, is suitable for the high ambient temperatures expected to occur, hence attack by corrosion is extremely low. The large electrolyte reserve ensures that the specific gravity value of the acid remains high during discharge allowing the cell to be used at temperatures down to – 20 °C.

- Cases
  The cell cases are made of SAN, a high-grade acid-resistant plastic.

  The cases and cover are sealed, and are completely leak proof.

  The newly developed terminal bushing and pressure relief valve provide an airtight seal for the cell, preventing ingress of any atmospheric oxygen.

- Connection
  The individual cells, rated at 2 volts each, are interconnected by maintenance-free threaded connectors (tapered cone).

D7. SONNENSCHEIN A600 SOLAR

Sonnenschein Batteries

Sonnenschein

Type	Plates per cell	Rated capacity C_{10} Ah	Dimensions Length Width Height Height over terminal mm	Overall length = case + gap mm	Discharge capacity Ah	Discharge time h	Discharge current A	Weight kg	Number of terminals
2/90	2	90	105 208 360 420	115	40 57 70 90 108 140	1 3 5 10 20 100	40 19 14 9 5.4 1.4	14	2
3/130	3	130	147 208 360 420	155	62 90 108 130 160 206	1 3 5 10 20 100	62 30 21.6 13 8 2.06	19	2
3/190	3	190	147 208 475 535	155	85 120 150 190 228 290	1 3 5 10 20 100	85 40 30 19 11.4 2.9	25	2
3/270	3	270	147 208 650 710	155	120 165 210 270 320 420	1 3 5 10 20 100	120 55 42 27 16 4.2	34.0	2
4/360	4	360	193 212 650 710	220	160 222 280 360 432 550	1 3 5 10 20 100	160 74 56 36 21.6 5.5	47	4
5/450	5	450	235 212 650 710	220	200 279 350 450 540 695	1 3 5 10 20 100	200 93 70 45 27 6.95	57	4
6/540	6	540	277 212 650 710	220	240 333 420 540 648 830	1 3 5 10 20 100	240 111 84 54 32.4 8.3	67	4
6/680	6	680	277 212 800 865	220	306 420 530 680 820 1050	1 3 5 10 20 100	306 140 106 68 41 10.5	83	4

D7. SONNENSCHEIN A600 SOLAR

Sonnenschein Batteries

Sonnenschein

dryfit A 600 solar discharge curves

The following diagram shows the voltage curve for various load currents.

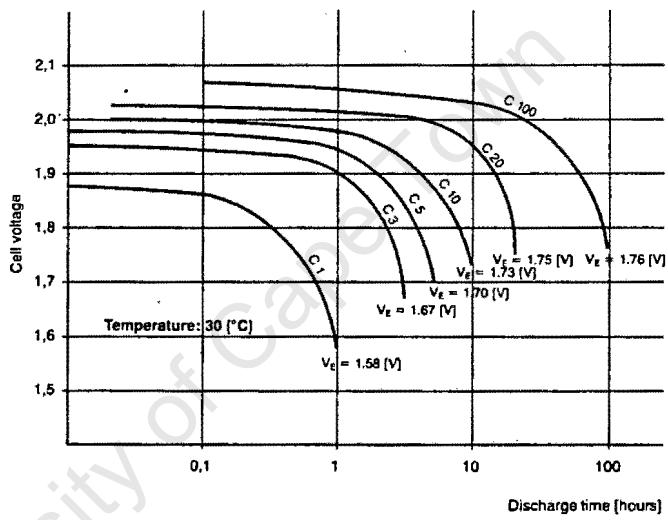

Low self-discharge rate

The A 600 solar battery has an extremely low rate of self-discharge. The primary energy is thus almost exclusively available for the load, since little energy is required to compensate for battery losses. It is therefore possible to span even relatively long periods of use with a low energy supply.

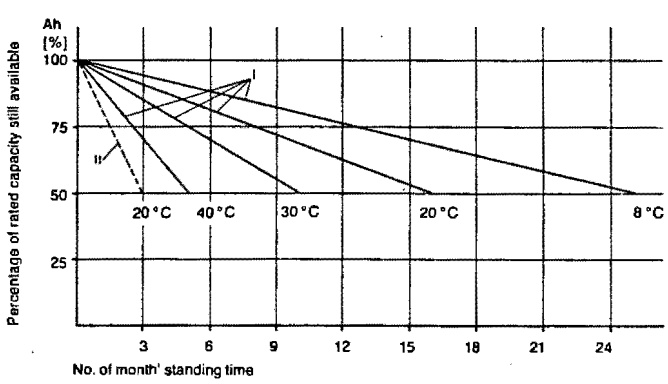

Fig. 2
A 600 solar battery self-discharge at various temperatures compared with a conventional standard lead-acid battery.
I = A 600 solar battery
II = Standard lead-acid battery

D7. SONNENSCHEIN A600 SOLAR

Sonnenschein Batteries

Sonnenschein

Charger

The Sonnenschein solar charger is recommended as the ideal charging system for A 600 solar batteries. It provides optimum utilisation of the energy supplied, hence a long battery life. If other chargers are used, the charge voltage must be matched to the radiation and load profile.

Based on the rated value, the charge voltage must be adjusted to temperature variations as shown in fig. 3.

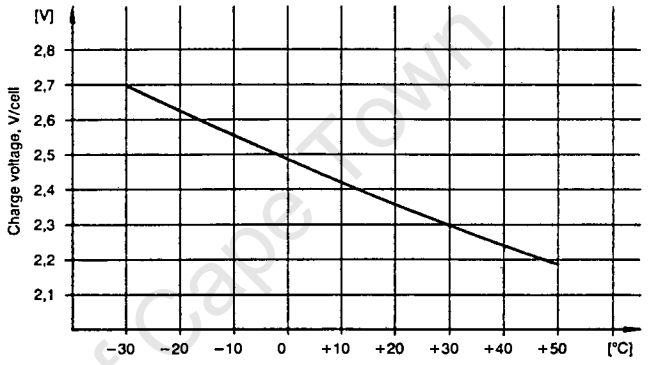

Fig. 3
Charge voltage as a function of temperature

Capacity curve and temperature profile

Temperature, of cource, affects the battery capacity. The graph and table show the capacity curves and discharge cut-off voltages for various load currents.

Ambient temperatures outside the range −20 °C to +50 °C should be avoided.

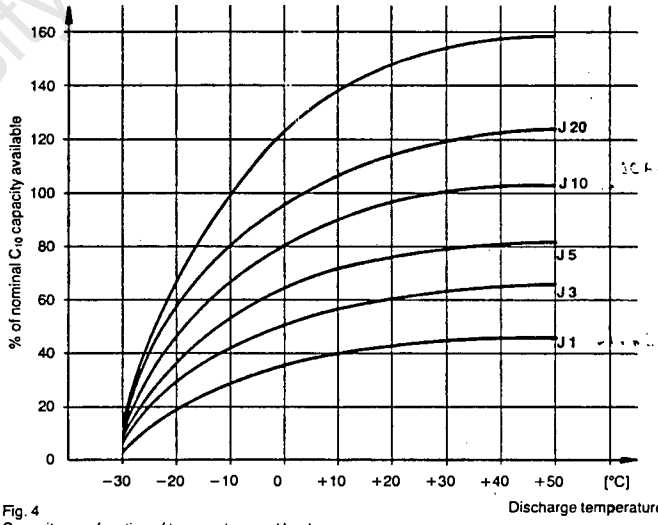

Fig. 4
Capacity as a function of temperature and load

Discharge temperature		−20 °C	0 °C	+30 °C	+50 °C
Discharge current	I_1	1.39	1.45	1.58	1.61
	I_3	1.53	1.58	1.67	1.68
	I_5	1.59	1.63	1.70	1.72
	I_{10}	1.66	1.68	1.73	1.75
	I_{20}	1.72	1.73	1.75	1.77
	I_{100}	1.74	1.75	1.76	1.77

Fig. 5
Discharge cut-off voltage as a function of temperature and load (V per cell)

E1. Heatsinking of 2N3442 Transistors

(An experimental determination)

Six 2N3442 transistors are mounted on 50cm length of heavy duty aluminium heatsink. The total heat that can be dissipated by the heatsink and the transistors is determined experimentally, since the heat transfer coefficient from the heatsink to the air (R_{h-a}) cannot be otherwise determined.

For each transistor:

- the junction to case resistance, R_{j-c} = 1.51°C/W
- and the case to heatsink resistance, R_{c-h} = 0.14°C/W
  (if heatsink compound is used).

For the six transistors mounted on the heatsink the overall heat transfer network is

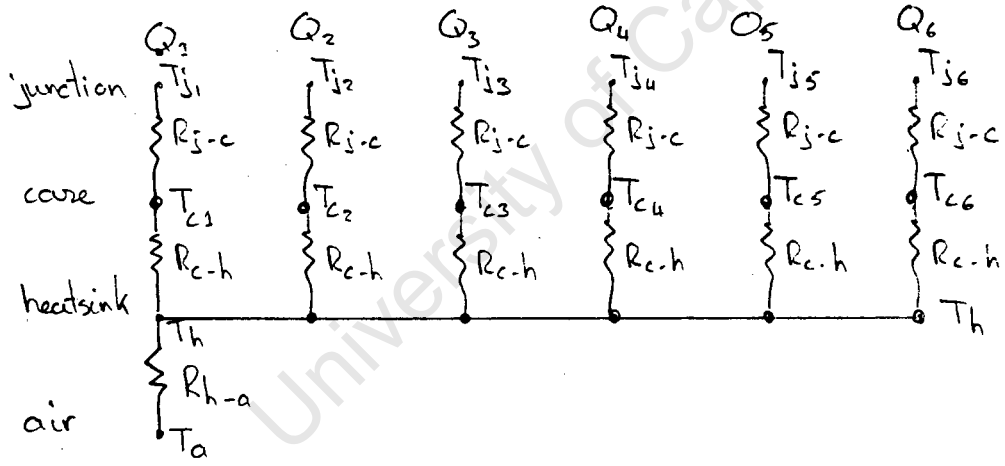

The heatsink is assumed to be at uniform temperature, since all transistors (Q1 to Q6) carry the same current.

The circuit can be Thevenised to

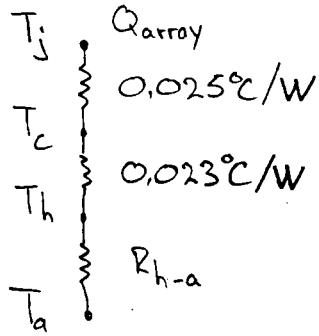

Method

By discharging a battery through the six transistor heatsink array and measuring power dissipation vs heatsink temperature (T_h), for a known air temperature (T_a). Steady state is assumed.

Sample Calculation

At 24V and 7.5A discharge rate through the array, the total power dissipation (P) is 180W. The power in each transistor (P_{tran}) is 30W.

T_a = 20°C, and T_h = 64°C at steady state.

now

$$R_{h\text{-}a} = (T_h - T_a)/ P = (64 - 20)/180 = 0.244°C/W$$

$$T_j = T_a + (R_{h\text{-}a} + R_{h\text{-}c} + R_{j\text{-}c}) * P = 112°C$$

T_c is assumed equal to T_h

From the power derating curve in the specifications, the maximum power per transistor (P_{max}) at T_c of 64°C is 90W.
30W is clearly within limits, and T_j < 200°C as required.

Results

The experimental results are shown in Table 1 for T_a = 20°C.

E2. Frequency Compensation for Electronic Load

The lead-lag circuit used for frequency compensation is shown below.

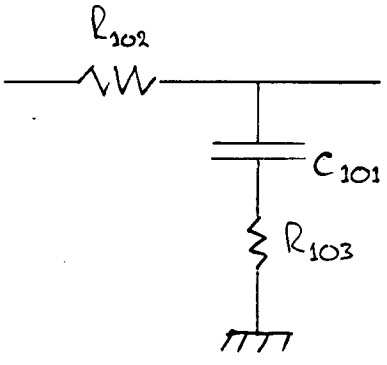

The circuit locates one pole and one zero, enabling interacting poles to be separated. The frequencies of the pole and zero are:

$$f_{zero} = \frac{1}{R_{103}\, C_{101}} = 30kHz$$

$$f_{pole} = \frac{1}{(R_{102}+R_{103})\, C_{101}} = 2.24kHz$$

If C_{101} *is chosen as* 1µF then:

$f_{zero} = 30 \times 10^3 = 1/(2\Pi \times 0.1 \times 10^{-6} \times R_{103})$

→ R_{103} = 53Ω (use 56Ω)

$f_{pole} = 2.24 \times 10^3 = 1/(2\Pi(R102+56)\ 0.1 \times 10^{-6})$

→ R_{102} = 654Ω

E3. LC Filter Design

Assume that the SCR AC input voltage is $60V_{rms}$ at 50Hz. The second harmonic is the major harmonic, with a maximum of $V_{2rms} = 38V_{rms}$, and a frequency of 100Hz. If the second harmonic is successfully filtered then the contributions from the remaining harmonics is likely to be insignificant.

The inductance ,L, required to attenuate the signal by -20dB at 100Hz (and zero at 10Hz) is given by

$$L=\frac{1}{4\pi^2 f^2 C}$$

where C is the capacitance.

For capacitance of 10000uF, the inductance required is 25.3mH.

The impedance of the inductance at 100Hz is

$$X_L=25.3\times10^{-3}\times2\pi\times100Hz$$

The output current ripple due mainly to the second harmonic is given by

$$I_{rmsripple}=\frac{V_{2rms}}{X_L}=1.7A_{rms}$$

The peak ripple is given by

$$I_{maxripple}=\sqrt{2}\times I_{rmsripple}=2.4A_{max}$$

This calculation can be repeated for several sizes of capacitor, to determine inductance and performance for fixed output voltage specifications. The results are shown in both tabular and graphical format. The most cost effective option is a 20000uF capacitor and a 12.6mH inductor.

Table 3 LC filter cost vs performance optimisation

OPTION NUMBER	1	2	3	4
Capacitance (uF)	10000	20000	30000	40000
Inductance (mH)	25.3	12.6	8.4	6
$I_{rms\ ripple}$ (A)	1.7	3.4	5.1	7.1
$I_{max\ ripple}$ (A)	2.4	4.8	7.2	10
Capacitor cost[1] (R)	39	78	117	156
Inductor cost[2] (R)	280	140	115	110
Total cost (R)	319	218	232	266

[1] Source: Hamrad Electronics [2] Source: Powerform Transformers

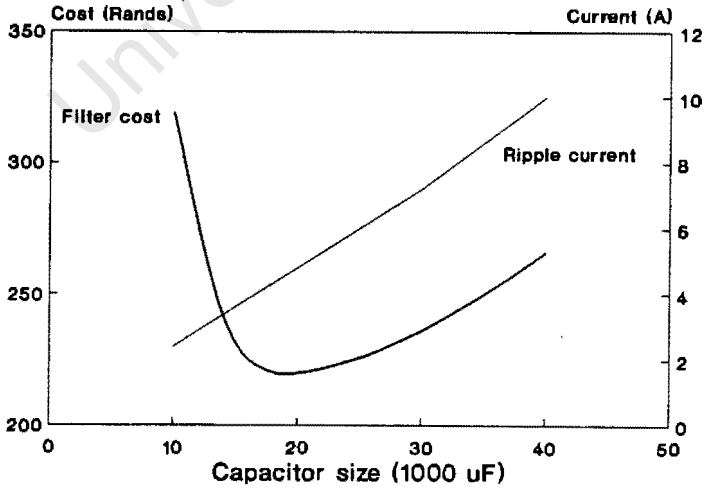

Figure 1 Graphical display of the tabular optimisation

E4. Transistor Array SOAR and Current Gain

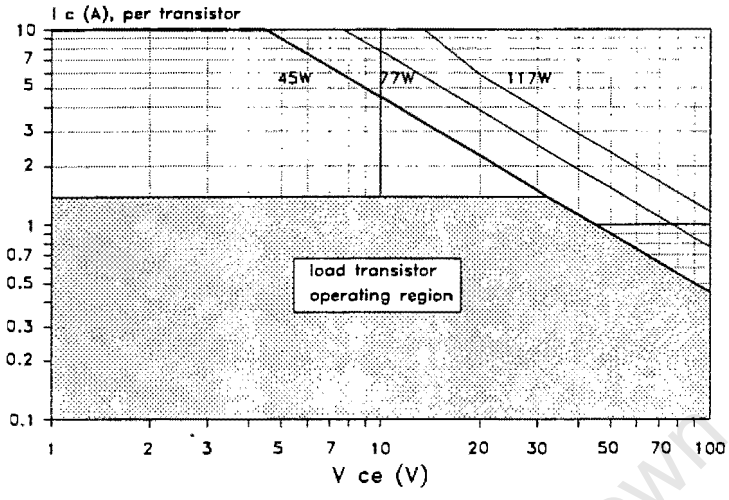

Figure 2 Load transistor operating region

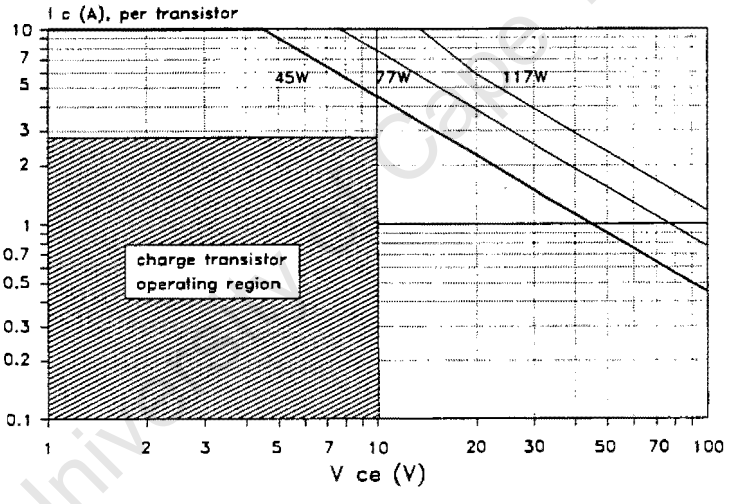

Figure 3 Power supply transistor operating region

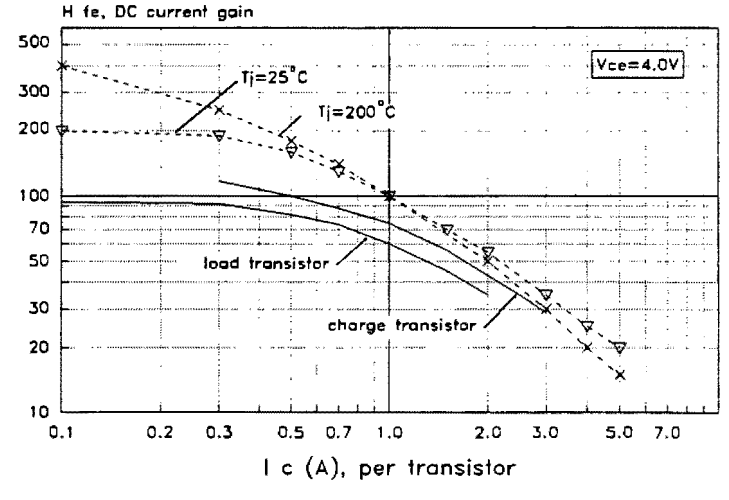

Figure 4 Current gain of load and power supply transistor arrays

E5. Program Data Flow

The data flow and sequence of the control software is outlined. Subroutine names appear in parentheses.

Mainprogram (Mainprog)

open files for input and output
define PV system (PVdefine)
read the input file (ReadNextOutputs)
adjust load current (LoadCurr)
adjust power supply current (PVCurr)
read the data channels (ReadAllChannels)
start the internal timer
default to numeric display (DisplayNumeric)
enable menu use

repeat
    repeat
        wait for operator input
    until 1 minute has elapsed

    execute timed routine (Timed)
until test finished

close all files
end

Timed Routine (Timed)

```
    disable menu use
    read the data channels (ReadAllChannels)
    generate derived data (SumChannelData)

    if operating cycle ended or termination criteria satisfied
        read the input file (ReadNextOutputs)
        write the data to disk
    elseif log interval
        write the data to disk

    if loadmode = CC
        then adjust load current (LoadCurr)
    elseif loadmode = RC
        then adjust load current (LoadShedSimulator)

    if PSmode = CC
        then adjust PS current (PVCurr)
    elseif PSmode = CV
        then adjust PS voltage (PVVolt)
    elseif PSmode = PV
        then find PV operating point (PVsim)

    read the channels (ReadALLChannels)

    if displaymode = numeric
        then display numeric format (DisplayNumeric)
    elseif displaymode = graphic
        then display graphic format (DisplayGraphic)
    elseif displaymode = Control
        then display operator control format (  )

    enable menu
end
```

Adjust load current (LoadCurr)

```
    Output the digital current
    Read the current
    repeat
        adjust digital
        output digital current
        read current
    until current within tolerance or specified iterations
end
```

Adjust PS current (PVCurr)

```
    Output the digital current
    Read the current
    repeat
        adjust digital
        output digital current
        read current
    until current within tolerance or specified iterations
end
```

Adjust PS voltage (PVVolt)

```
    Repeat
        Solve for the required current using battery operating line (  )
        adjust the PS current (PVCurr)
        read the voltage and current (MeasurePVOutputs)
        update battery operating line (GetBatteryLine)
    until voltage within tolerance or specified iterations
end
```

Find PV operating point (PVsim)

Repeat
Solve for the operating point using Newtons Method on the battery operating line and PV operating curve (SolvePVPoint)
Adjust the operating point if voltage regulator is present (RegulatorSimulator)
adjust the PS current (PVCurr)
read the battery voltage and current (MeasurePVOutputs)
update battery operating line (GetBatteryLine)
until voltage within tolerance or specified iterations
end

Display graphic format (DisplayGraphic)

Scan the output file for logged data (ScanDataForGraph)
Add new points to the graph array (AddPointsToArray)
Set up the axes (SetUpGraph)
Plot (PlotGraph)
end

E6. Electrical Component Data

This appendix contains manufacturers' technical specifications for the following components:

LM-358	dual op-amp
2N-3442	NPN power transistor
TIP-31C	NPN low power transistor
MTM-15N45	N-channel enhancement mode Mos-FET
MJ-802	PNP power transistor
AEG B2-250-30Si	power diode bridge
AEG TT45N-200K	power SCR block

Shimaden Temperature Controller

National Semiconductor

Operational Amplifiers/Buffers

LM158/LM258/LM358, LM158A/LM258A/LM358A, LM2904 Low Power Dual Operational Amplifiers

General Description

The LM158 series consists of two independent, high gain, internally frequency compensated operational amplifiers which were designed specifically to operate from a single power supply over a wide range of voltages. Operation from split power supplies is also possible and the low power supply current drain is independent of the magnitude of the power supply voltage.

Application areas include transducer amplifiers, dc gain blocks and all the conventional op amp circuits which now can be more easily implemented in single power supply systems. For example, the LM158 series can be directly operated off of the standard +5 V_{DC} power supply voltage which is used in digital systems and will easily provide the required interface electronics without requiring the additional ±15 V_{DC} power supplies.

Unique Characteristics

- In the linear mode the input common-mode voltage range includes ground and the output voltage can also swing to ground, even though operated from only a single power supply voltage.
- The unity gain cross frequency is temperature compensated.
- The input bias current is also temperature compensated.

Advantages

- Eliminates need for dual supplies
- Two internally compensated op amps in a single package
- Allows directly sensing near GND and V_{OUT} also goes to GND
- Compatible with all forms of logic
- Power drain suitable for battery operation
- Pin-out same as LM1558/LM1458 dual operational amplifier

Features

- Internally frequency compensated for unity gain
- Large dc voltage gain 100 dB
- Wide bandwidth (unity gain) 1 MHz (temperature compensated)
- Wide power supply range:
  - Single supply 3 V_{DC} to 30 V_{DC}
  - or dual supplies ±1.5 V_{DC} to ±15 V_{DC}
- Very low supply current drain (500μA) — essentially independent of supply voltage (1 mW/op amp at +5 V_{DC})
- Low input biasing current 45 nA_{DC} (temperature compensated)
- Low input offset voltage 2 mV_{DC} and offset current 5 nA_{DC}
- Input common-mode voltage range includes ground
- Differential input voltage range equal to the power supply voltage
- Large output voltage swing 0 V_{DC} to V^+ − 1.5 V_{DC}

Connection Diagrams (Top Views)

Metal Can Package

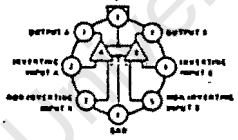

Order Number LM158AH, LM158H, LM258AH, LM258H, LM358AH or LM358H
See NS Package H08C

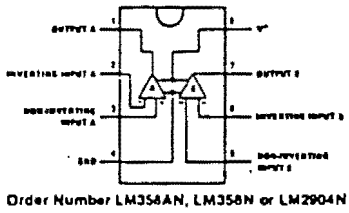

Order Number LM358AN, LM358N or LM2904N
See NS Package N08B

Schematic Diagram (Each Amplifier)

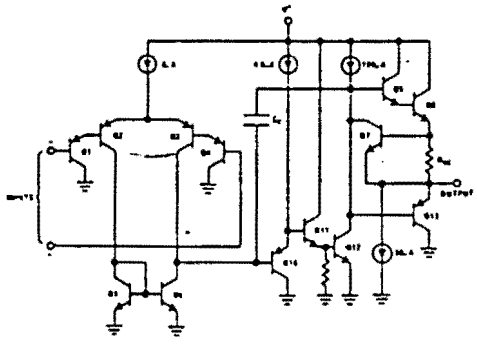

MOTOROLA

2N3442
2N4347

HIGH-POWER INDUSTRIAL TRANSISTORS

NPN silicon power transistors designed for applications in industrial and commercial equipment including high fidelity audio amplifiers, series and shunt regulators and power switches.

- Low Collector-Emitter Saturation Voltage –
  $V_{CE(sat)}$ = 1.0 Vdc (Max) @ I_C = 2.0 Adc – 2N4347
- Collector-Emitter Sustaining Voltage –
  $V_{CEO(sus)}$ = 120 Vdc (Min) – 2N4347
  140 Vdc (Min) – 2N3442
- Excellent Second-Breakdown Capability

5.0 AND 10 AMPERE

POWER TRANSISTORS
NPN SILICON

120, 140 VOLTS
100, 117 WATTS

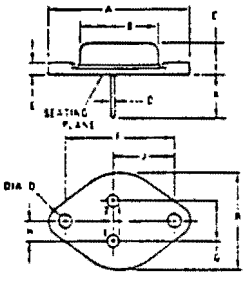

STYLE 1:
PIN 1. BASE
2. EMITTER
CASE COLLECTOR

DIM	MILLIMETERS MIN	MILLIMETERS MAX	INCHES MIN	INCHES MAX
A	–	39.37	–	1.550
B	–	21.08	–	0.830
C	6.35	7.62	0.250	0.300
D	1.65	1.09	0.038	0.043
E		3.43		0.135
F	26.90	30.40	1.059	1.197
G	10.67	11.18	0.420	0.440
H	5.33	5.59	0.210	0.220
J	16.64	17.15	0.655	0.675
K	11.18	12.19	0.440	0.480
Q	3.84	4.09	0.151	0.161
R		26.67	–	1.050

Collector connected to case

CASE 11-01
(TO-3)

*MAXIMUM RATINGS

Rating	Symbol	2N4347	2N3442	Unit
Collector-Emitter Voltage	V_{CEO}	120	140	Vdc
Collector-Base Voltage	V_{CB}	140	160	Vdc
Emitter-Base Voltage	V_{EB}	7.0		Vdc
Collector Current – Continuous Peak	I_C	5.0 10	10 15**	Adc
Base Current – Continuous Peak	I_B	3.0 8.0	7.0 –	Adc
Total Power Dissipation @ T_C = 25°C Derate above 25°C	P_D	100 0.57	117 0.67	Watts W/°C
Operating and Storage Junction Temperature Range	T_J, T_{stg}	–65 to +700		°C

THERMAL CHARACTERISTICS

Characteristic	Symbol	2N4347	2N3442	Unit
Thermal Resistance, Junction to Case	$R_{\theta JC}$	1.75	1.5	°C/W

*Indicates JEDEC Registered Data.
**This data guaranteed in addition to JEDEC registered data.

ELECTRICAL CHARACTERISTICS (T_C = 25°C unless otherwise noted)

Characteristic		Symbol	Min	Max	Unit
OFF CHARACTERISTICS					
Collector-Emitter Sustaining Voltage (I_C = 200 mAdc, I_B = 0)	2N4347	$V_{CEO(sus)}$	120	–	Vdc
	2N3442		140	–	
Collector Cutoff Current		I_{CEO}			mAdc
(V_{CE} = 100 Vdc, I_B = 0)	2N4347		–	200	
(V_{CE} = 140 Vdc, I_B = 0)	2N3442		–	200	
Collector Cutoff Current		I_{CEX}			mAdc
(V_{CE} = 125 Vdc, $V_{BE(off)}$ = 1.5 Vdc)	2N4347		–	2.0	
(V_{CE} = 140 Vdc, $V_{BE(off)}$ = 1.5 Vdc)	2N3442		–	5.0	
(V_{CE} = 120 Vdc, $V_{BE(off)}$ = 1.5 Vdc, T_C = 150°C)	2N4347		–	10	
(V_{CE} = 140 Vdc, $V_{BE(off)}$ = 1.5 Vdc, T_C = 150°C)	2N3442		–	30	
Emitter Cutoff Current (V_{BE} = 7.0 Vdc, I_C = 0)	2N4347, 2N3442	I_{EBO}	–	5.0	mAdc
ON CHARACTERISTICS (1)					
DC Current Gain		h_{FE}			–
(I_C = 2.0 Adc, V_{CE} = 4.0 Vdc)	2N4347		15	60	
(I_C = 5.0 Adc, V_{CE} = 4.0 Vdc)	2N4347		10	–	
(I_C = 3.0 Adc, V_{CE} = 4.0 Vdc)	2N3442		20	70	
(I_C = 10 Adc, V_{CE} = 4.0 Vdc)	2N3442		7.5	–	
Collector-Emitter Saturation Voltage		$V_{CE(sat)}$			Vdc
(I_C = 2.0 Adc, I_B = 200 mAdc)	2N4347		–	1.0	
(I_C = 5.0 Adc, I_B = 0.83 Adc)	2N4347		–	2.0	
(I_C = 10 Adc, I_B = 2.0 Adc)	2N3442		–	5.0	
Base-Emitter On Voltage		$V_{BE(on)}$			Vdc
(I_C = 2.0 Adc, V_{CE} = 4.0 Vdc)	2N4347		–	2.0	
(I_C = 5.0 Adc, V_{CE} = 4.0 Vdc)	2N4347		–	3.0	
(I_C = 10 Adc, V_{CE} = 4.0 Vdc)	2N3442		–	5.7	
DYNAMIC CHARACTERISTICS					
Current-Gain – Bandwidth Product (2)		f_T			kHz
(I_C = 0.5 Adc, V_{CE} = 4.0 Vdc, f_{test} = 50 kHz)	2N4347		200	–	
(I_C = 2.0 Adc, V_{CE} = 4.0 Vdc, f_{test} = 40 kHz)	2N3442		80	–	
Small-Signal Current Gain		h_{fe}			–
(I_C = 0.5 Adc, V_{CE} = 4.0 Vdc, f = 5.0 kHz)	2N4347		40	–	
(I_C = 2.0 Adc, V_{CE} = 4.0 Vdc, f = 1.0 kHz)	2N3442		12	72	

*Indicates JEDEC Registered Data

NOTES: 1. Pulse Test: Pulse Width = 300 μs, Duty Cycle ≤ 2.0%.

2. $f_T = |h_{fe}| \cdot f_{test}$

FIGURE 1 – POWER DERATING

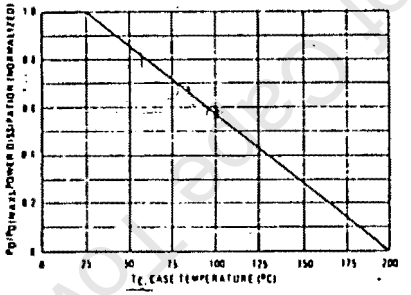

2N3442, 2N4347

ACTIVE REGION SAFE OPERATING AREA INFORMATION

FIGURE 2 – 2N3442

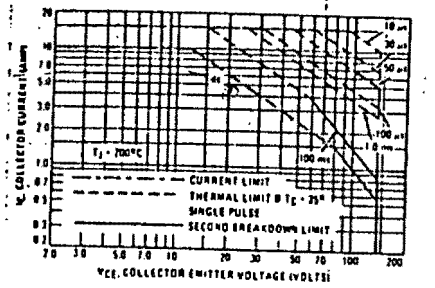

FIGURE 3 – 2N4347

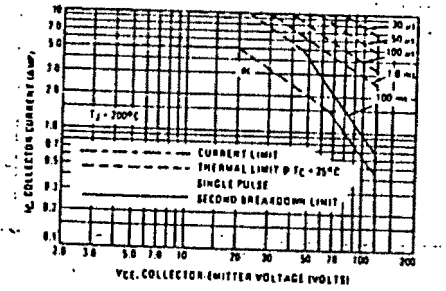

There are two limitations on the power-handling ability of a transistor: average junction temperature and second breakdown. Safe operating area curves indicate I_C-V_{CE} limits of the transistor that must be observed for reliable operation, i.e., the transistor must not be subjected to greater dissipation than the curves indicate.

The data of Figures 2 and 3 is based on $T_{J(pk)}$ = 200°C; T_C is variable depending on conditions. At high case temperatures, thermal limitations will reduce the power that can be handled to values less than the limitations imposed by second breakdown.

FIGURE 4 – DC CURRENT GAIN

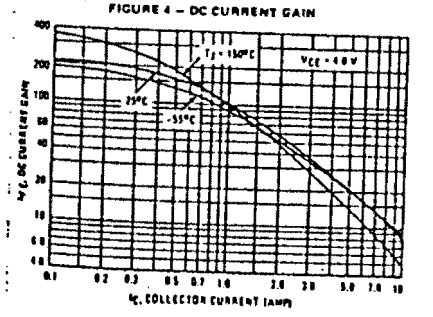

FIGURE 5 – COLLECTOR SATURATION REGION

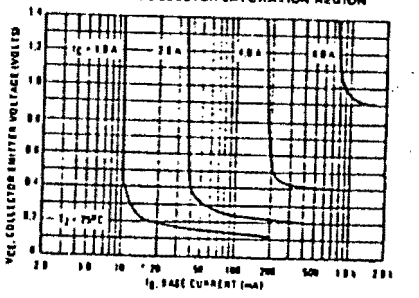

NPN PNP

TIP31 TIP32
TIP31A TIP32A
TIP31B TIP32B
TIP31C TIP32C

MOTOROLA

COMPLEMENTARY SILICON PLASTIC POWER TRANSISTORS

. . . designed for use in general purpose amplifier and switching applications.

- Collector-Emitter Saturation Voltage –
  $V_{CE(sat)}$ = 1.2 Vdc (Max) @ I_C = 3.0 Adc
- Collector-Emitter Sustaining Voltage –
  $V_{CEO(sus)}$ = 40 Vdc (Min) – TIP31, TIP 32
  = 60 Vdc (Min) – TIP31A, TIP32A
  = 80 Vdc (Min) – TIP31B, TIP32B
  = 100 Vdc (Min) – TIP31C, TIP32C
- High Current Gain – Bandwidth Product
  f_T = 3.0 MHz (Min) @ I_C = 500 mAdc
- Compact TO-220 AB Package
- TO-66 Leadform Also Available

3 AMPERE POWER TRANSISTORS COMPLEMENTARY SILICON

40 60 80 100 VOLTS
40 WATTS

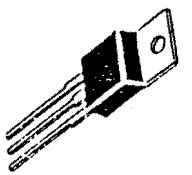

*MAXIMUM RATINGS

Rating	Symbol	TIP31 TIP32	TIP31A TIP32A	TIP31B TIP32B	TIP31C TIP32C	Unit
Collector-Emitter Voltage	V_{CEO}	40	60	80	100	Vdc
Collector-Base Voltage	V_{CB}	40	60	80	100	Vdc
Emitter-Base Voltage	V_{EB}	5.0				Vdc
Collector Current - Continuous / Peak	I_C	3.0 / 5.0				Adc
Base Current	I_B	1.0				Adc
Total Power Dissipation @ T_C = 25°C / Derate above 25°C	P_D	40 / 0.32				Watts / W/°C
Total Power Dissipation @ T_A = 25°C / Derate above 25°C	P_D	2.0 / 0.016				Watts / W/°C
Unclamped Inductive Load Energy (1)	E	32				mJ
Operating and Storage Junction Temperature Range	T_J,T_{stg}	-65 to +150				°C

THERMAL CHARACTERISTICS

Characteristic	Symbol	Max	Unit
Thermal Resistance, Junction to Case	$R_{\theta JC}$	3.125	°C/W
Thermal Resistance, Junction to Ambient	$R_{\theta JA}$	62.5	°C/W

(1) I_C = 1.8 A, L = 20 mH, P.R.F. = 10 Hz, V_{CC} = 10 V, R_{BE} = 100 Ω.

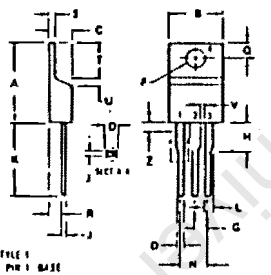

STYLE 1
PIN 1 BASE
2 COLLECTOR
3 EMITTER
4 COLLECTOR

DIM	MILLIMETERS MIN	MILLIMETERS MAX	INCHES MIN	INCHES MAX
A	14.60	15.75	0.575	0.620
B	9.65	10.29	0.380	0.405
C	4.06	4.82	0.160	0.190
D	0.64	0.89	0.025	0.035
F	3.61	3.73	0.142	0.147
G	2.41	2.67	0.095	0.105
H	2.79	3.93	0.110	0.155
J	0.36	0.55	0.014	0.022
K	12.70	14.27	0.500	0.562
L	1.14	1.39	0.045	0.055
N	4.83	5.33	0.190	0.210
Q	2.54	3.04	0.100	0.120
R	2.04	2.79	0.080	0.110
S	1.14	1.39	0.045	0.055
T	5.97	6.48	0.235	0.255
U	0.00	1.27	0.000	0.050
V	1.14	-	0.045	-
Z	-	2.03	-	0.080

CASE 221A-02
TO-220AB

ELECTRICAL CHARACTERISTICS (T_C = 25°C unless otherwise noted)

Characteristic		Symbol	Min	Max	Unit
OFF CHARACTERISTICS					
Collector-Emitter Sustaining Voltage (1) (I_C = 30 mAdc, I_B = 0)	TIP31, TIP32	$V_{CEO(sus)}$	40	–	Vdc
	TIP31A, TIP32A		60	–	
	TIP31B, TIP32B		80	–	
	TIP31C, TIP32C		100	–	
Collector Cutoff Current (V_{CE} = 30 Vdc, I_B = 0)	TIP31, TIP31A, TIP32, TIP32A	I_{CEO}	–	0.3	mAdc
(V_{CE} = 60 Vdc, I_B = 0)	TIP31B, TIP31C, TIP32B, TIP32C		–	0.3	
Collector Cutoff Current (V_{CE} = 40 Vdc, V_{EB} = 0)	TIP31, TIP32	I_{CES}	–	200	μAdc
(V_{CE} = 60 Vdc, V_{EB} = 0)	TIP31A, TIP32A		–	200	
(V_{CE} = 80 Vdc, V_{EB} = 0)	TIP31B, TIP32B		–	200	
(V_{CE} = 100 Vdc, V_{EB} = 0)	TIP31C, TIP32C		–	200	
Emitter Cutoff Current (V_{BE} = 5.0 Vdc, I_C = 0)		I_{EBO}	–	1.0	mAdc
ON CHARACTERISTICS (1)					
DC Current Gain (I_C = 1.0 Adc, V_{CE} = 4.0 Vdc)		h_{FE}	25	–	–
(I_C = 3.0 Adc, V_{CE} = 4.0 Vdc)			10	50	
Collector-Emitter Saturation Voltage (I_C = 3.0 Adc, I_B = 375 mAdc)		$V_{CE(sat)}$	–	1.2	Vdc
Base-Emitter On Voltage (I_C = 3.0 Adc, V_{CE} = 4.0 Vdc)		$V_{BE(on)}$	–	1.8	Vdc
DYNAMIC CHARACTERISTICS					
Current Gain – Bandwidth Product (2) (I_C = 500 mAdc, V_{CE} = 10 Vdc, f_{test} = 1 MHz)		f_T	3.0	–	MHz
Small-Signal Current Gain (I_C = 0.5 Adc, V_{CE} = 10 Vdc, f = 1 kHz)		$\lvert h_{fe} \rvert$	20	–	–

(1) Pulse Test: Pulse Width ≤ 300 μs, Duty Cycle ≤ 2.0%.
(2) $f_T = \lvert h_{fe} \rvert \cdot f_{test}$

FIGURE 1 – POWER DERATING

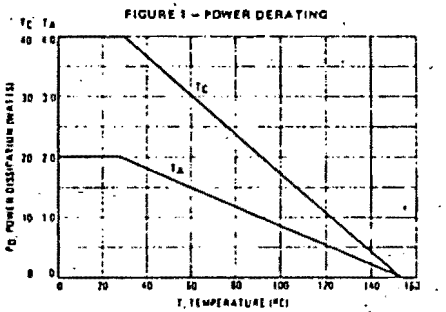

FIGURE 2 – SWITCHING TIME EQUIVALENT CIRCUIT

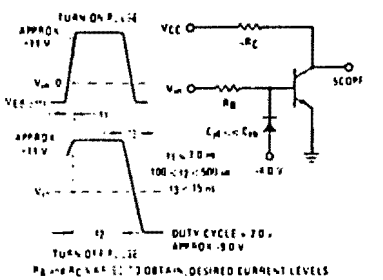

FIGURE 3 – TURN-ON TIME

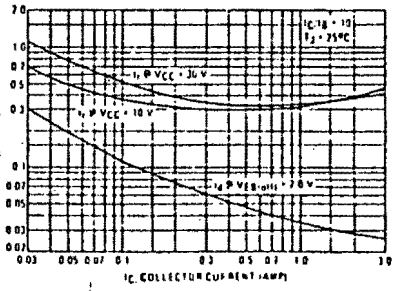

MOTOROLA
SEMICONDUCTOR
TECHNICAL DATA

Designer's Data Sheet

Power Field Effect Transistor

N-Channel Enhancement-Mode Silicon Gate TMOS

MTM15N45
MTM15N50

TMOS

TMOS POWER FETs
15 AMPERES
$r_{DS(on)}$ = 0.4 OHM
450 and 500 VOLTS

These TMOS Power FETs are designed for high voltage, high speed power switching applications such as switching regulators, converters, solenoid and relay drivers.

- Silicon Gate for Fast Switching Speeds — Switching Times Specified at 100°C
- Designer's Data — I_{DSS}, $V_{DS(on)}$, $V_{GS(th)}$ and SOA Specified at Elevated Temperature
- Rugged — SOA is Power Dissipation Limited
- Source-to-Drain Diode Characterized for Use With Inductive Loads

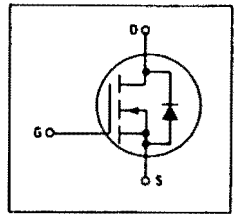

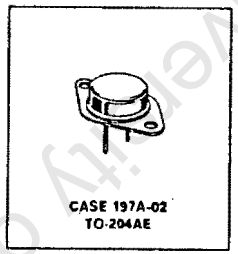

CASE 197A-02
TO-204AE

MAXIMUM RATINGS

Rating	Symbol	MTM 15N45	MTM 15N50	Unit
Drain-Source Voltage	V_{DSS}	450	500	Vdc
Drain-Gate Voltage (R_{GS} = 1 MΩ)	V_{DGR}	450	500	Vdc
Gate-Source Voltage — Continuous — Non-repetitive ($t_p \leq 50\ \mu s$)	V_{GS} V_{GSM}	±20 ±40		Vdc Vpk
Drain Current — Continuous — Pulsed	I_D I_{DM}	15 65		Adc
Total Power Dissipation @ T_C = 25°C Derate above 25°C	P_D	250 2		Watts W/°C
Operating and Storage Temperature Range	T_J, T_{stg}	−65 to 150		°C

THERMAL CHARACTERISTICS

Thermal Resistance — Junction to Case — Junction to Ambient	$R_{\theta JC}$ $R_{\theta JA}$	0.5 30	°C/W
Maximum Lead Temperature for Soldering Purposes, 1/8" from case for 5 seconds	T_L	275	°C

ELECTRICAL CHARACTERISTICS (T_C = 25°C unless otherwise noted)

Characteristic		Symbol	Min	Max	Unit
OFF CHARACTERISTICS					
Drain-Source Breakdown Voltage (V_{GS} = 0, I_D = 0.25 mA)	MTM15N45 MTM15N50	$V_{(BR)DSS}$	450 500	— —	Vdc
Zero Gate Voltage Drain Current (V_{DS} = Rated V_{DSS}, V_{GS} = 0) (V_{DS} = 0.8 Rated V_{DSS}, V_{GS} = 0, T_J = 125°C)		I_{DSS}	— —	0.2 1	mAdc
Gate-Body Leakage Current, Forward (V_{GSF} = 20 Vdc, V_{DS} = 0)		I_{GSSF}	—	100	nAdc
Gate-Body Leakage Current, Reverse (V_{GSR} = 20 Vdc, V_{DS} = 0)		I_{GSSR}	—	100	nAdc
ON CHARACTERISTICS*					
Gate Threshold Voltage (V_{DS} = V_{GS}, I_D = 1 mA) T_J = 100°C		$V_{GS(th)}$	2 1.5	4.5 4	Vdc
Static Drain-Source On-Resistance (V_{GS} = 10 Vdc, I_D = 7.5 Adc)		$r_{DS(on)}$	—	0.4	Ohm
Drain-Source On-Voltage (V_{GS} = 10 V) (I_D = 7.5 Adc) (I_D = 15 Adc, T_J = 100°C)		$V_{DS(on)}$	— —	6 5.8	Vdc
Forward Transconductance (V_{DS} = 15 V, I_D = 7.5 A)		g_{FS}	4	—	mhos
DYNAMIC CHARACTERISTICS					
Input Capacitance	(V_{DS} = 25 V, V_{GS} = 0, f = 1 MHz) See Figure 11	C_{iss}	—	3000	pF
Output Capacitance		C_{oss}	—	500	
Reverse Transfer Capacitance		C_{rss}	—	200	
SWITCHING CHARACTERISTICS* (T_J = 100°C)					
Turn-On Delay Time	(V_{DD} = 25 V, I_D = 0.5 Rated I_D R_{gen} = 50 ohms) See Figures 9, 13 and 14	$t_{d(on)}$	—	60	ns
Rise Time		t_r	—	180	
Turn-Off Delay Time		$t_{d(off)}$	—	450	
Fall Time		t_f	—	180	
Total Gate Charge	(V_{DS} = 0.8 Rated V_{DSS}, I_D = Rated I_D, V_{GS} = 10 V) See Figure 12	Q_g	110 (Typ)	160	nC
Gate-Source Charge		Q_{gs}	50 (Typ)	—	
Gate-Drain Charge		Q_{gd}	60 (Typ)	—	
SOURCE DRAIN DIODE CHARACTERISTICS*					
Forward On-Voltage	(I_S = Rated I_D V_{GS} = 0)	V_{SD}	1.1 (Typ)	1.4	Vdc
Forward Turn-On Time		t_{on}	Limited by stray inductance		
Reverse Recovery Time		t_{rr}	1200 (Typ)	—	ns
INTERNAL PACKAGE INDUCTANCE					
Internal Drain Inductance (Measured from the contact screw on the header closer to the source pin and the center of the die)		L_d	5 (Typ)	—	nH
Internal Source Inductance (Measured from the source pin, 0.25" from the package to the source bond pad)		L_s	12.5 (Typ)	—	

*Pulse Test: Pulse Width ≤ 300 μs, Duty Cycle ≤ 2%.

TYPICAL ELECTRICAL CHARACTERISTICS

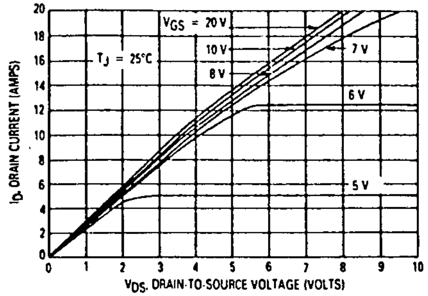

Figure 1. On-Region Characteristics

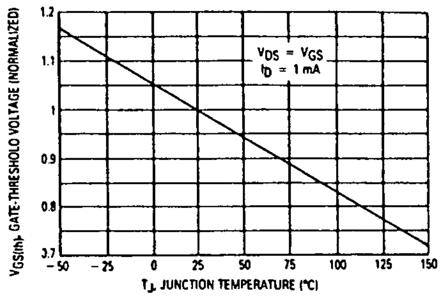

Figure 2. Gate-Threshold Voltage Variation With Temperature

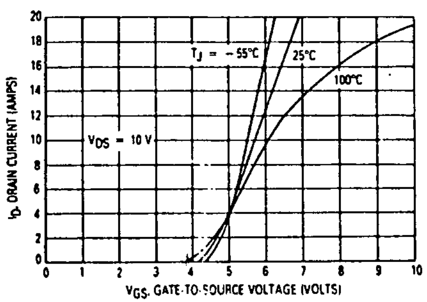

Figure 3. Transfer Characteristics

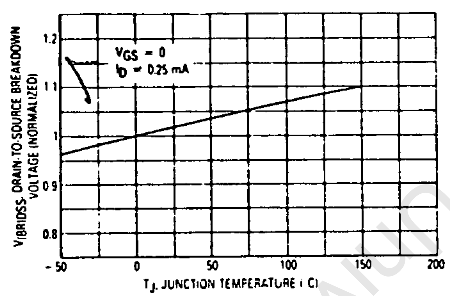

Figure 4. Breakdown Voltage Variation With Temperature

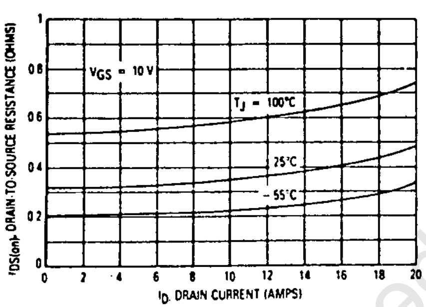

Figure 5. On-Resistance versus Drain Current

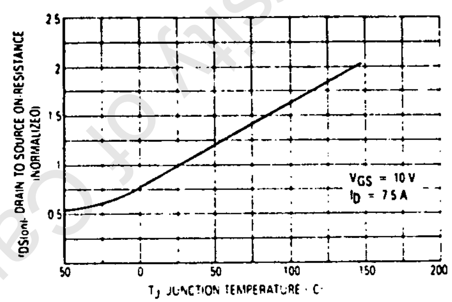

Figure 6. On-Resistance Variation With Temperature

SAFE OPERATING AREA INFORMATION

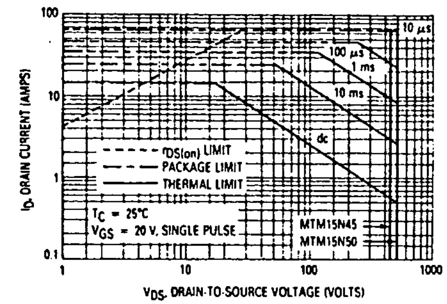

Figure 7. Maximum Rated Forward Biased Safe Operating Area

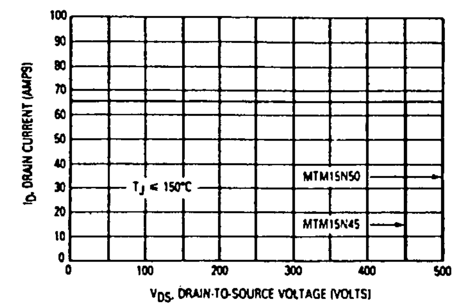

Figure 8. Maximum Rated Switching Safe Operating Area

FORWARD BIASED SAFE OPERATING AREA

The FBSOA curves define the maximum drain-to-source voltage and drain current that a device can safely handle when it is forward biased, or when it is on, or being turned on. Because these curves include the limitations of simultaneous high voltage and high current, up to the rating of the device, they are especially useful to designers of linear systems. The curves are based on a case temperature of 25°C and a maximum junction temperature of 150°C. Limitations for repetitive pulses at various case temperatures can be determined by using the thermal response curves. Motorola Application Note, AN569, "Transient Thermal Resistance-General Data and Its Use" provides detailed instructions.

SWITCHING SAFE OPERATING AREA

The switching safe operating area (SOA) of Figure 8 is the boundary that the load line may traverse without incurring damage to the MOSFET. The fundamental limits are the peak current, I_{DM} and the breakdown voltage, $V_{(BR)DSS}$. The switching SOA shown in Figure 8 is applicable for both turn-on and turn-off of the devices for switching times less than one microsecond.

The power averaged over a complete switching cycle must be less than:

$$\frac{T_{J(max)} - T_C}{R_{\theta JC}}$$

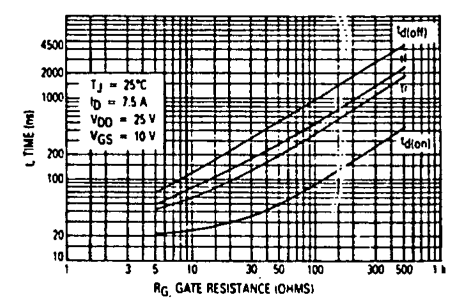

Figure 9. Resistive Switching Time Variation versus Gate Resistance

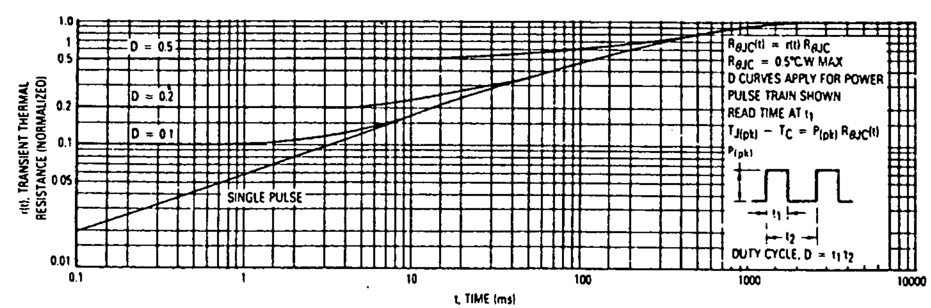

Figure 10. Thermal Response

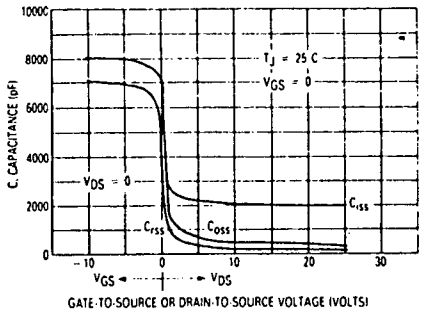

Figure 11. Capacitance Variation

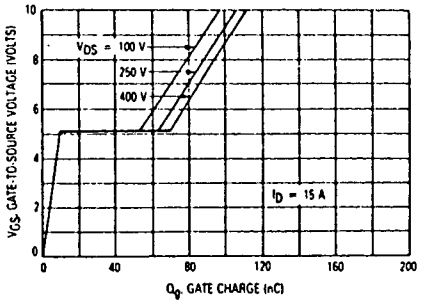

Figure 12. Gate Charge versus Gate-to-Source Voltage

RESISTIVE SWITCHING

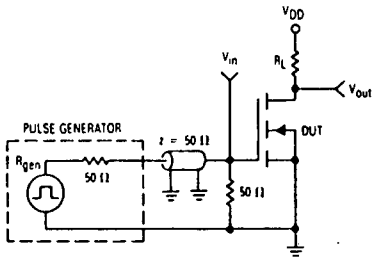

Figure 13. Switching Test Circuit

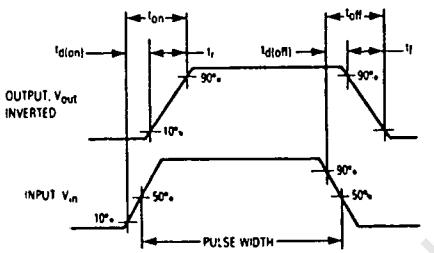

Figure 14. Switching Waveforms

OUTLINE DIMENSIONS

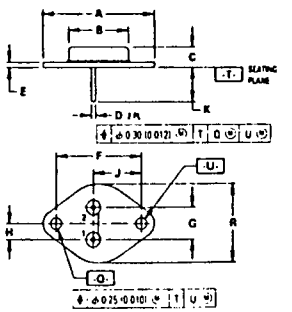

DIM	MILLIMETERS MIN	MAX	INCHES MIN	MAX
A	38.35	39.37	1.510	1.550
B	19.31	21.08	0.760	0.830
C	6.35	9.25	0.250	0.325
D	1.45	1.60	0.057	0.063
E	1.53	1.77	0.060	0.070
F	30.15 BSC		1.187 BSC	
G	10.92 BSC		0.430 BSC	
H	5.46 BSC		0.215 BSC	
J	16.89 BSC		0.665 BSC	
K	11.18	12.19	0.440	0.480
Q	3.84	4.19	0.151	0.165
R	25.15	26.67	0.990	1.050
U	3.84	4.19	0.151	0.165

NOTES
1. DIMENSIONING AND TOLERANCING PER ANSI Y14.5M, 1982.
2. CONTROLLING DIMENSION: INCH.

STYLE 3
PIN 1. GATE
2. SOURCE
CASE: DRAIN

CASE 197A-02
TO-204AE

Gleichrichterbrücken
Rectifier bridges
Ponts redresseurs

Typ Type	V_{RRM} V		I_{FSM} t = 10ms t_j = $t_{j\max}$ A	I_{FAVM} Last,Load Charge: R / C A	$t_{j\max}$ °C	G g	Maßbild Outline Figure
B 40 C 800,...D,...D1,...SD	100	40	50	0,9/0,8	125	1	103 D : 104 D1: 105 SD: 106
B 80 C 800,...D,...D1,...SD	190	80					
B 125 C 800,...D,...D1,...SD	300	125					
B 250 C 800,...D,...D1,...SD	600	250					
B 380 C 800,...D,...D1,...SD	900	380					
B 40 C 1000	100	40	50	1,2/1	125	1	103
B 80 C 1000	190	80					
B 125 C 1000	300	125					
B 250 C 1000	600	250					
B 380 C 1000	900	380					
B 40 C 1500	100	40	100	1,6/1,5	125	1	103
B 80 C 1500	200	80					
B 125 C 1500	300	125					
B 250 C 1500	600	250					
B 380 C 1500	900	380					
B 40 C 1500/1000 Si C	100	40	65	1,2/1	150	2	107
B 80 C 1500/1000 Si C	200	80		1,8/1,5*			
B 125 C 1500/1000 Si C	300	125					
B 250 C 1500/1000 Si C	600	250					
B 380 C 1500/1000 Si C	900	380					
B 40 C 3700/2200 Si C	100	40	80	2,7/2,2	150	18	108
B 80 C 3700/2200 Si C	200	80		4,8/3,7*			
B 125 C 3700/2200 Si C	300	125					
B 250 C 3700/2200 Si C	600	250					
B 380 C 3700/2200 Si C	900	380					
B 40 C 5000/3300 Si C	100	40	250	4/3,3	150	18	108
B 80 C 5000/3300 Si C	200	80		6/5 *			
B 125 C 5000/3300 Si C	300	125					
B 250 C 5000/3300 Si C	600	250					
B 2 40/ 35-10 Si	100	40	160	5/4	150	20	109
B 2 80/ 70-10 Si	200	80		7,5/6,5*			
B 2 125/110-10 Si	300	125					
B 2 250/220-10 Si	600	250					
B 2 30/ 25-30 Si	75	30	280	10/9	175	100	110
B 2 60/ 52-30 Si	150	60		17/15**			
B 2 125/110-30 Si	300	125					
B 2 250/225-30 Si	700	250					
B 2 380/340-30 Si	1100	380					
B 2 500/450-30 Si	1500	500					
B 6 30/ 38-40 Si	75	30	280	13/12	175	150	111
B 6 60/ 78-40 Si	150	60		24/22**			
B 6 125/165-40 Si	300	125					
B 6 250/330-40 Si	700	250					
B 6 380/500-40 Si	1100	380					
B 6 500/670-40 Si	1500	500					

*) Kühlblech 200 cm² **) Kühlblech 400 cm²

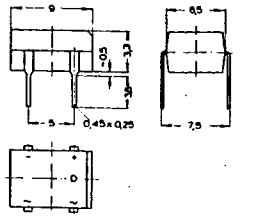

104

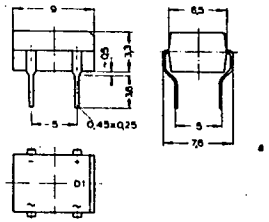

105

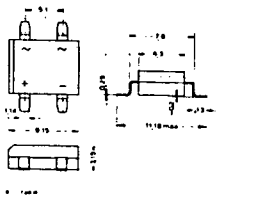

106

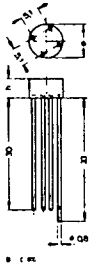

	◆	h
B .. C 800, B .. C 1000	8,2	5,1
B .. C 1500	9,5	7,1

103

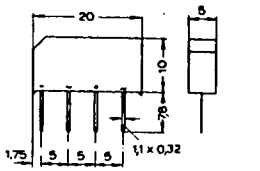

107

Powerblocks für netzgeführte Stromrichter
Power modules for line commutated converters
Modules surmoulés pour applications secteur

TT..N - Vollgesteuerte Kompaktbausteine/Fully controlled power modules/Modules surmoulés à 2 thyristors
TD..N / DT..N - Halbgesteuerte Kompaktbausteine/Half controlled power modules/Modules surmoulés mixtes

Typ Type	V_{DRM} V_{RRM}	I_{TRMSM}	I_{TSM} t_p = 10ms t_{vj} = t_{vjmax} 45°C		$\int i^2dt$ t_p = 10ms t_{vj} = t_{vjmax} 45°C		I_{TAVM}/I_C	$V_{T(TO)}$	r_T	$(di/dt)_{cr}$	$(dv/dt)_{cr}$	t_q	V_{GT}	I_{GT}	R_{thJC}	R_{thCK}	t_{vjmax}	M	G	Maßbild Outline Figure
	V	A	A	A	A^2s	A^2s	A/°C	V	mΩ	A/µs	V/µs	µs	V	mA	°C/W	°C/W	°C	Nm	g	
TT 18 N TD 18 N DT 18 N	400 800 1200 600 1100 1400 1600*	40	350	390	0,61 x10³	0,76 x10³	25/60 18/65	1,1	18	100	C = 400 F = 1000	50	2,5	150	1,2	0,2	125	4	160	47
TT 25 N TD 25 N DT 25 N	400 800 1200 600 1100 1400*	50	460	520	1,06 x10³	1,35 x10³	32/68 25/85	1,05	11	100	C = 400 F = 1000	60	2,5	150	0,92	0,2	125	4	160	47
TT 31 N ● TD 31 N DT 31 N	400 1100 1600* 600 1200 800 1400	50	680	780	2,3 x10³	3,04 x10³	48/50 31/85	0,95	6,4	100	C = 400 F = 1000	60	2,0	150	0,8	0,16	125	4	200	47
TT 32 N ■	1100 1400 1200 1600*	75	620	700	1,92 x10³	2,45 x10³	48/52 32/85	1	7,5	120	C = 400 F = 1000	120	1,4	120	0,72	0,16	125	4	160	48
TT 36 N TD 36 N DT 36 N	200 800 1400* 400 1100 600 1200	80	850	980	3,6 x10³	4,8 x10³	51/60 36/85	1	6,2	120	C = 400 F = 1000	60	2,5	150	0,65	0,18	125	4	200	47
TT 45 N TD 45 N DT 45 N	800 1200 1600* 1100 1400	100	1000	1200	5 x10³	7,2 x10³	63/59 45/85	0,85	4,7	150	C = 400 F = 1000	120	1,4	120	0,6	0,16	125	4	160	48
TT 46 N TD 46 N DT 46 N	200 800 1400 400 1100 1600* 600 1200	100	1000	1150	5 x10³	6,6 x10³	64/61 46/85	0,95	4,5	120	C = 400 F = 1000	60	2,5	150	0,55	0,18	125	4	160	47
TT 56 N TD 56 N DT 56 N	200 800 1400 400 1100 1600* 600 1200	100	1350	1500	9,1 x10³	11,25 x10³	64/74 56/85	0,9	3,5	120	C = 400 F = 1000	80	2,5	150	0,52	0,18	125	4	200	47
TT 60 N TD 60 N DT 60 N	400 1100 1600* 600 1200 800 1400	120	1400	1550	9,8 x10³	12 x10³	76/68 60/85	0,8	3,4	150	C = 400 F = 1000	120	1,4	120	0,39	0,1	125	4	200	48
TT 75 N TD 75 N DT 75 N	400 800 1200 600 1100 1400*	150	1700	1950	14,4 x10³	19 x10³	95/70 75/85	0,85	2,6	150	C = 400 F = 1000	180	1,4	120	0,37	0,08	125	4	250	48
TT 86 N TD 86 N DT 86 N	600 1200 1800* 800 1400 1100 1600	160	1800	2050	16,2 x10³	21 x10³	102/69 86/85	1	3,5	150	C = 400 F = 1000	150	1,4	150	0,39	0,1	140	4	200	49
TT 95 N TD 95 N DT 95 N	400 1100 1500* 600 1200 800 1400	150	1700	1950	14,4 x10³	19 x10³	95/85	0,85	2,6	150	C = 400 F = 1000	200	1,4	120	0,33	0,08	140	4	250	48
TT 106 N TD 106 N DT 106 N	600 1200 1800* 800 1400 1100 1600	180	2000	2250	20 x10³	25,3 x10³	115/78 106/85	0,9	2,6	150	C = 400 F = 1000	150	1,4	150	0,23	0,06	140	6	430	49
TT 121 N TD 121 N DT 121 N	1100 1600 1200 1800* 1400	200	2350	2600	27,6 x10³	33,8 x10³	128/81 121/85	0,85	2	150	C = 400 F = 1000	180	1,4	150	0,23	0,06	140	6	430	50
TT 131 N TD 131 N DT 131 N	400 1100 600 1200 800 1400*	220	3200	3600	51,2 x10³	64,8 x10³	141/80 131/85	0,85	1,5	150	C = 400 F = 1000	180	1,4	150	0,17	0,04	125	m.:6 el.:12	430	50
TT 142 N ● TD 142 N DT 142 N	400 1000 1600* 600 1200 800 1400	230	4100	4800	84 x10³	115 x10³	142/85	0,9	1,1	150	C = 400 F = 1000	200	2,0	200	0,13	0,04	125	m.:6 el.:12	310	51
TT 150 N ●	1800 2400 2000 2600* 2200	350	4000	4500	80 x10³	101 x10³	223/54 150/85	1,2	1,3	60	C = 400 F = 1000	300	2,0	200	0,13	0,04	125	m.:6 el.:12	800	52
TT 162 N ● TD 162 N DT 162 N	400 1000 1500* 600 1200 800 1400	260	4400	5200	97 x10³	135 x10³	162/85	0,85	0,95	150	C = 400 F = 1000	200	2,0	150	0,13	0,04	125	m.:6 el.:12	310	51
TT 170 N TD 170 N DT 170 N	400 1100 1600 600 1200 1800* 800 1400	350	4600	5200	106 x10³	135 x10³	223/68 170/85	0,95	1,0	150	C = 400 F = 1000	250	2,0	200	0,17	0,04	125	m.:6 el.:12	800	52
TT 210 N TD 210 N DT 210 N	400 1100 1600 600 1200 1800* 800 1400	410	5800	6600	168 x10³	218 x10³	261/73 210/85	1	0,85	150	C = 400 F = 1000	200	2,0	200	0,13	0,04	125	m.:6 el.:12	800	52

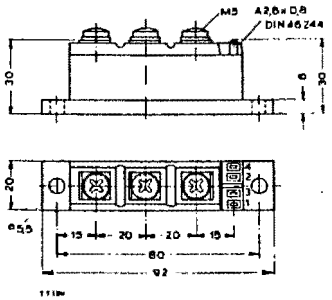

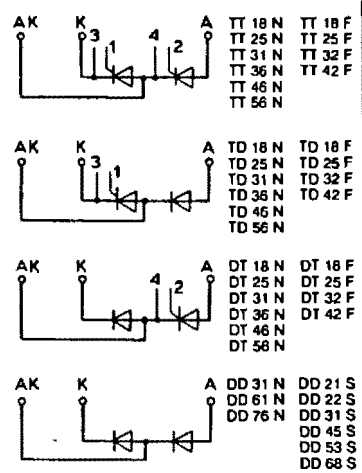

Innerer Aufbau: Lötkontakt
Internal construction: solder contact
Structure interne: contact soudé
Innere Isolation / Internal insulation / Isolation interne Al_2O_3

47

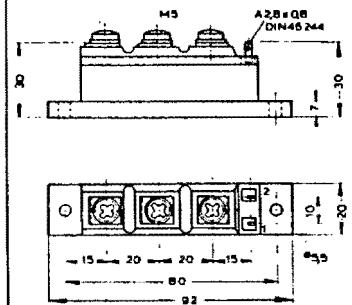

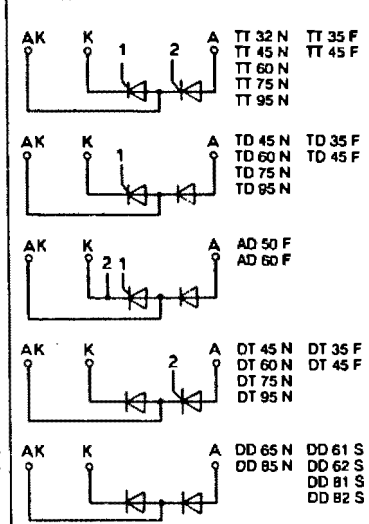

Innerer Aufbau: Druckkontakt
Internal construction: pressure contact
Structure interne: contact pressé
Innere Isolation / Internal insulation / Isolation interne BeO [1]

48

Digital Controller
OPERATING INSTRUCTIONS
3-Position Control (Coding No. 3)

Digital Indicating Series SR10

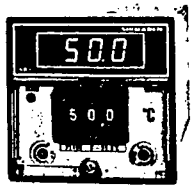

Analog Deviation Series SR11

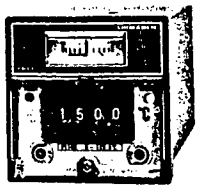

1. SPECIFICATIONS

SR10 Indicating Accuracy	±(0.5% + 1-digit) of measuring range
SR11 Deviation Range	±10% of measuring range (vs. setting range)
Thermocouple External Resistance Tolerable Range	100 Ω maximum
Cold Junction Temperature Compensation Range	5~45°C (thermocouple input only)
Burn-Out Circuit	Standard (thermocouple input only)
R.T.D. Resistance Tolerable Range	5 Ω maximum/wire
Operating Ambient Temperature & Humidity	−10~+50°C, 90% RH maximum
Power Consumption	Approx. 4 VA
Insulation Resistance	500 V DC 20 MΩ minimum between input terminal and power supply terminal 500 V DC 20 MΩ minimum between power supply terminal and earth terminal
Dielectric Strength	One minute at 500 V AC between input terminal and earth terminal One minute at 1000 V AC between power terminal and earth terminal

2. ORDERING CODE & SPECIFICATIONS

Ordering Code Nos.			Specifications
SR10			Digital Indicating Controller
SR11			Analog Deviation Indicating Controller
Inputs	−1		Thermocouple (T J E K R)
	−2		R.T.D. (Pt100 RTD Amperage 2 mA)
	−3		Voltage (0~10 mV DC)
	−4		Current (4~20 mA DC)
	−0		Others (Please consult.)
Control Mode		1	Proportioning
		2	On/Off (2-position), Control output 1 : Not available
		3	3-position, Control output 1 & P : Not available
		4	On/Off + upper/lower alarm, − Drive −
		5	P.I.D.
Control Outputs		Y	Contact, 240 V AC 3 A/resistive load and 1 A/inductive load
		1*	Current, 4~20 mA DC, Load resistance 600 Ω max.
		P	SSR voltage, 15 V DC 20 mA max.
		X	Others (Please consult.)
Control Alarms		−00	Non-alarm
		−01	Lower alarm
		−02	Upper alarm
		−04	Lower alarm with standby mode
		−05	Upper alarm with standby mode
		−63	Upper/Lower alarm
		−66	Upper/Lower alarm with standby mode
Analog Output			0 Not provided
			3 Voltage 0~10 mV DC
			9 Others (Please consult.)
Power Supply			11 100~110 V/200~220 V AC ±10%, 50/60 Hz
			12 110~120 V/220~240 V AC ±10%, 50/60 Hz
			99 Others (Please consult.)

Note: No alarm function is available on the models of On/Off + Upper/Lower, Contact output PID and SSR voltage output PID

3. EXTERNAL DIMENSIONS & PANEL CUTOUT

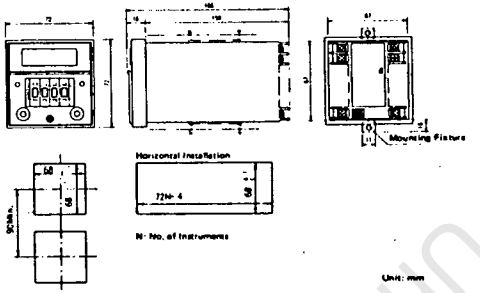

4. INSTALLATION

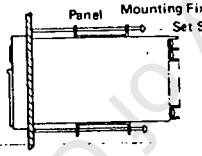

1) Prepare a panel cutout of 68 (H) x 68(W) mm wide on the panel.
2) Insert the unit to the panel cutout and fasten with the mounting fixtures.
3) The ambient conditions shall be:

a. Free from corrosive gasses and dusty atmosphere,
b. Within −10~+50°C ambient temperature and under 90% RH humidity,
c. Away from direct sunlight and radiant heat from electric ovens.

5. NAMES & FUNCTION

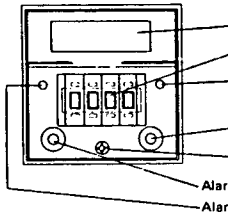

Note: Since this device is plug-in type the chassis can be pulled out in the state of with wiring.
Be sure to cut off the line power before loosing screw & pulling out the chassis.

Temperature and Humidity Control Instruments
SHIMADEN CO.,LTD.
Head Office Factory 2-30-10, Kitamachi, Nerima-ku, Tokyo 176 Japan
Phone (03) 931-9111 Telex 02722778 SDCL J

6. WIRING

The dimension of terminal screw(s) is 3.5 mm diameter and 8.0 mm length.
Prepare terminal connection of 7.2 mm max. outer diameter.

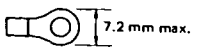

1. Wiring for Input Circuit
   a) Thermocouple Input Type:
      Confirm the type of thermocuople and lead wire.
      Then, connect properly to (+) & (−) terminals as shown below.
   b) R.T.D. Input Type:
      Connect properly RTD (Pt100 Ω) to (A), (B), (B) terminals as shown below.
   c) Current & Voltage Input Type:
      Be sure to confirm the (+) & (−) polarity of the input terminals.
2. Wiring for Power Supply
   Refer to the figures below.

■ Contact Output

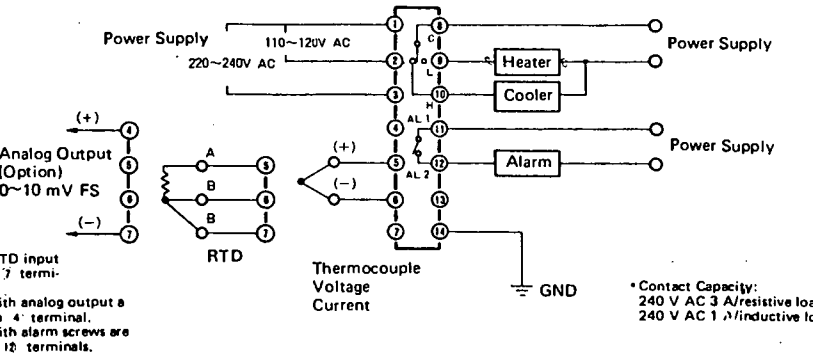

* On the models of RTD input with analog output 7 terminal is common.
* On the models of with analog output a screw is provided on 4 terminal.
* On the models of with alarm screws are provided on 11 & 12 terminals.

* Contact Capacity:
  240 V AC 3 A/resistive load
  240 V AC 1 A/inductive load

7. OPERATION

After installation and wiring start operation as below.
a) Set the digital setting switch(es) to the value required.
b) Turn on the power supply and confirm if the control lamp lights.
c) Set the neutral zone variable resistor (NZ, 1~20%FS) to the value required in the application.

8. CONTROL OUTPUT CONFIGULATIONS

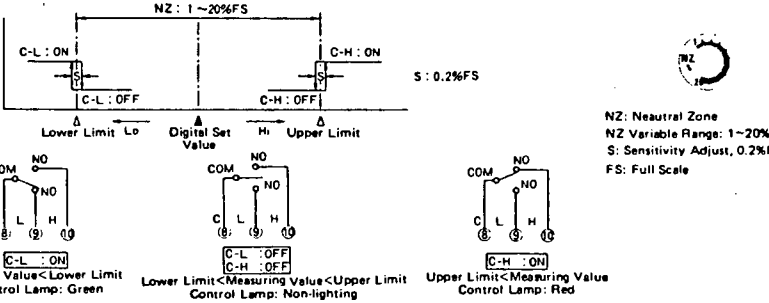

9. ALARMS

■ Alarm Action

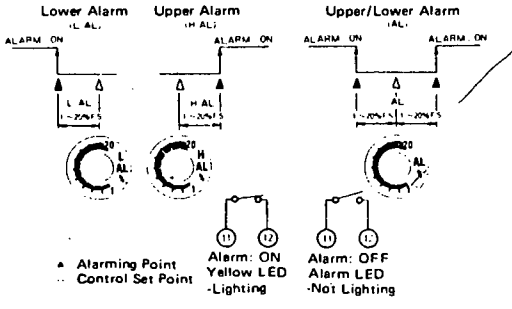

■ Alarm Specifications
Alarm Setting: By front variable resistors (L AL)−Lower Alarm, (H AL)−Upper Alarm and (AL)−Upper/Lower Alarm
Alarm Range: 1~20% variable vs. control set value
Alarm Sensitivity: 0.2%FS fixed
Alarm Output: Contact 240 V AC 3 A/resistive load & 1 A/inductive load
Alarm Indication: By front yellow LED lighting

■ Upper/Lower alarm is an alarm mode of upper & lower symmetric setting vs. control setpoint. Alarm output from upper & lower limit is from the same alarm relay and same contact. No identification of from upper or lower is available by relay contact output.

■ Alarm with standby mode is an alarming system that upper, lower or upper/lower alarms will not function until the temperature has been in the non-alarming area once after the power source applied.